DESIGN AND IMPLEMENTATION OF ONLINE ESTIMATION BASED BACKSTEPPING CONTROLLER FOR DC-DC BUCK CONVERTERS

TOUSIF KHAN N

DESIGN AND IMPLEMENTATION OF ONLINE ESTIMATION BASED BACKSTEPPING CONTROLLER FOR DC-DC BUCK CONVERTERS

A
Thesis Submitted
in Partial Fulfilment of the Requirements
for the Degree of

DOCTOR OF PHILOSOPHY

By
TOUSIF KHAN N

Department of Electronics and Electrical Engineering
Indian Institute of Technology Guwahati
Guwahati - 781 039, Assam, India.
November 2017

Certificate

This is to certify that the thesis entitled "**DESIGN AND IMPLEMENTATION OF ON-LINE ESTIMATION BASED BACKSTEPPING CONTROLLER FOR DC-DC BUCK CONVERTERS**", submitted by **Tousif Khan N** (10610229), a research scholar in the *Department of Electronics and Electrical Engineering, Indian Institute of Technology Guwahati*, for the award of the degree of **Doctor of Philosophy**, is a record of an original research work carried out by him under my supervision and guidance. The thesis has fulfilled all requirements as per the regulations of the Institute and in my opinion has reached the standard needed for submission. The results embodied in this thesis have not been submitted to any other University or Institute for the award of any degree or diploma.

Dated:
Guwahati.

Prof. Chitralekha Mahanta
Dept. of Electronics and Electrical Engg.
Indian Institute of Technology Guwahati
Guwahati - 781039, Assam, India.

Dedicated

to

My beloved parents

Mr. Nizam Ali Khan and *Mrs. Farhath Unnisa*

Acknowledgement

First and foremost, I am grateful to Almighty for having guided me through the righteous path and bestowed on me to complete this Ph.D thesis successfully.

I take this opportunity to express my deepest gratitude and heartfelt thanks to my thesis supervisor Prof. Chitralekha Mahanta for her incisive expertise, consistent guidance and supportive nature. Her sincere dedication, accessibility and keen attention to minor details in my research have provided immense motivation to me. I must acknowledge her kindness, patience and extreme diligence in correcting all my manuscripts. I am highly indebted to my doctoral committee chairman Dr. Praveen Kumar for his constructive criticism and useful comments in enhancing the quality of work. My deep appreciation and sincere thanks to him for granting me the access to experimental facility at *Electrical Machines Research Laboratory* which helped me in physical realization of proposed control schemes on time. I owe a debt of gratitude to other members of my doctoral committee, Dr. Indrani Kar and Dr. Praveen Tripathy for devoting their precious time in evaluating the progress of my research. Their critique and quality inputs counseled on timely basis have been of a great help to me.

I wish to offer my sincere respect to the Director of the institute, Prof. Gautam Biswas for the enlightening discussions at different occasions and his encouragement to excel. Also, my admiration to other faculty members and staff from the *Department of Electronics & Electrical Engineering* who have been kind and cooperative during my tenure at IIT Guwahati.

I am thankful to the Ministry of Human Resource Development (MHRD) and University Grants Commission (UGC), Government of India for providing me the necessary fellowship grants to peruse the Ph.D programme.

A special thanks and admiration to the person, I share a strong bond of friendship with, my dear friend Arghya Chakravarty! Thank you for having stood beside me against all odds and being there for me in both difficult and good times during my stay. Your consistent encouragement and faith in my abilities have helped me immensely to overcome the challenges and finally led to the successful completion of this thesis.

This journey would not have been complete without the love and affection of my dear friends Sandeep R, Jyoti Prakash Medhi & his family, Rahul Soni, Vaneet Yadav, Jitender Meena, Hanif Ahmed Choudhry, Abu Mostako, Rahul Sanal, Mohd. Imran, Nawab Alam, Mohsin Khan, Palashuddin Sheikh, Vibhuti Kumar, Jasvindar Singh, Ankit Bansal, Ajaz Ahmad Dar, Faishal Khan, Sami Al-Issa and Ali Jraisheh. Also, my acknowledgment to my old college friends James Vajinath, Arif Shariff and Nayeem Mohammed for their unconditional support and confidence in my worthiness.

I thank my colleagues and friends from Control & Instrumentation Laboratory, who have made this

journey a truly learning and joyful experience. Among them my appreciation to Dr. Sanjoy Mondal, Dr. Bajarangbali, Dr. Dola Govind Pradhan, Dr. Ezhil Reena Joy, Y. V. Karteek, Mridul K. Malakar, Saurabh Pandey, Gautam Rituraj, Reshmi N. C. and Suman Roy.

Last but definitely not the least, I do not find words to describe the extent of debt I owe to my family. The unlimited sacrifices and relentless hardwork of my parents have been truly motivating and been a consistent source of encouragement to me. The unmatched love and patience of my elder brothers and sisters, Ayub Khan, Summaiya Khan, Zakiya Khan, Asma Khan, Mohsin Khan and their lovely children Late Tayeeb, Uznain, Momin, Huma, Saqlain, Faiza, Huda, Danish, Adeeba and Yusuf have been undeniable, without whom my dreams would not have taken a shape.

Abstract

DC-DC buck converters belong to the class of complex and time varying variable structure systems. These are primarily employed to obtain an uninterrupted lower level of DC voltage at the output end from a DC input voltage source. However, the output voltage tracking in these converters is significantly sensitive to unanticipated load disturbances, parametric uncertainties and input voltage fluctuations. In this thesis, a few backstepping based adaptive control methodologies have been proposed for the robust output voltage control in DC-DC buck converters with immunity to external disturbances, matched and mismatched uncertainties. The effect of an uncertain load on the converter has been compensated by incorporating online parameter adaptation, which estimates the load disturbance. The proposed adaptive law ensures overall closed loop stability of the DC-DC buck converter satisfying Lyapunov stability criterion. Performance of the proposed controller is evaluated over a wide range of operating points. Further, the designed adaptive backstepping control (ABSC) methodology is extended and validated on a DC-DC buck converter driven permanent magnet DC (PMDC)-motor system, wherein the problem of angular velocity tracking is addressed under a wide range of load torque disturbances. In order to improve the transient performance of output tracking with backstepping control method, a neural network based learning scheme is developed for a faster and more accurate estimation of the uncertain load. A single layer Chebyshev neural network (CNN) based adaptive backstepping control technique is proposed for output regulation in DC-DC buck converters. Such a methodology circumvents the drawbacks faced by the ABSC in its application to DC-DC buck converters. Further, the proposed CNN based ABSC offers decreased computational complexity and fast learning. The proposed approach is improved by using a Hermite neural network (HNN) in the backstepping framework for quicker and closer estimation of unknown load parameters. This HNN based ABSC results in a faster rejection of load perturbations, thereby delivering a superior control mechanism. Although the proposed neuro-adaptive schemes yield a bound and asymptotic load estimation, yet guaranteeing the exactness of estimation is analytically difficult. Therefore, a disturbance observer based backstepping control scheme is proposed for output voltage tracking in DC-DC buck converters. The disturbance observers exactly estimate the uncertainties encountered during the converter operation in finite time. In addition to rapidity and exactness, such a time bounded estimation based control scheme enhances the output transient and steady state performances over a wide operating range. Finally, a current sensorless adaptive control approach is proposed to overcome challenges faced in measuring current in practical applications. The adaptive control schemes proposed in this thesis have been validated through extensive simulation and experimentation in laboratory. The experimental results support the theoretical propositions.

Contents

List of Figures

List of Tables

Nomenclature

ABSC	Adaptive backstepping control
AC	Alternating current
ADRC	Active disturbance rejection control
ADC	Analog to digital converter
ATSMC	Adaptive terminal sliding mode control
BSC	Backstepping control
CCM	Continuous conduction mode
CLF	Control Lyapunov function
CNN	Chebyshev neural network
CT	Current transformer
DAC	Digital to analog converter
DC	Direct current
DCM	Discontinuous conduction mode
DSP	Digital signal processor
EMI	Electromagnetic interference
ESO	Extended state observer
FTDO	Finite time disturbance observer
FTOBSC	Finite time observer based backstepping control
FTCO-ABSC	Finite time current observer based adaptive backstepping control
FTS	Finite time stable
GDC	Gate drive circuit
HNN	Hermite neural network
IAE	Integral absolute error
NN	Neural network
PI	Proportional integral
PID	Proportional integral derivative
PWM	Pulse width modulation
PMDC	Permanent magnet direct current
RBFNN	Radial basis function neural network
SMC	Sliding mode control
SPDT	Single pole double throw
VSC	Variable structure control

List of Symbols

E	DC Power supply voltage
L	Buck inductor
C	DC capacitor
D	Power diode
R	Resistive load
S_w	Power electronic switch
v_r	Reference output voltage
v_o	Output voltage
i_L	Inductor current
i_C	Capacitor current
i_R	Resistive load current
r_L	Inductor resistance
k	Duty ratio
f_s	Switching frequency
t_s	Settling time
P_u	Peak undershoot
P_o	Peak overshoot
M_p	Maximum peak
Δv_o	Peak to peak ripple in output voltage
R_a	Armature resistance
L_a	Armature inductance
B	Viscous friction coefficient
J	Moment of inertia
K_e	Back electromotive force (EMF) constant
K_t	Torque constant
i_a	Armature current
v_a	Armature voltage
τ_L	Load torque
ω	Angular velocity
ω_r	Reference angular velocity
u	Averaged control input
u_s	Switched control input

List of Publications

Refereed International Journals

1. **Tousif Khan Nizami**, Arghya Chakravarty and Chitralekha Mahanta, "Neuro-Adaptive Backstepping Control for Cascaded Buck Converter PMDC Motor Combination", *Control Engineering Practice, Elsevier*, Volume 58, January 2017, Pages 78-87.

2. **Tousif Khan Nizami** and Chitralekha Mahanta, "An intelligent adaptive control of DC-DC buck converters", *Journal of the Franklin Institute, Elsevier*, Volume 353, Issue 12, August 2016, Pages 2588-2613.

3. **Tousif Khan Nizami**, Arghya Chakravarty and Chitralekha Mahanta, "Analysis and Experimental Investigation into a Finite Time Current Observer Based Adaptive Backstepping Control of Buck Converters", *Journal of the Franklin Institute, Elsevier*, revision under review.

4. **Tousif Khan Nizami**, Arghya Chakravarty and Chitralekha Mahanta, "Finite Time Exact Compensation of Uncertainties in DC-DC Buck Converters", *IEEE Transactions on Control Systems Technology* , under review.

Conference

1. **Tousif Khan Nizami**, Arghya Chakravarty and Chitralekha Mahanta, "A Fast Learning Neuro Adaptive Control of Buck Converter driven PMDC Motor: Design, Analysis and Validation", 20^{th} *IFAC World Congress, (IFAC WC 2017)*, France, 9-14 July 2017.

2. **Tousif Khan Nizami** and Chitralekha Mahanta," Fast Neuro-Adaptive Control of DC-DC Buck Converters: Design and Implementation", *Power and Energy Conference at Illinois (PECI)*, University of Illinois, USA, 23-24 February 2017.

3. **Tousif Khan Nizami** and Chitralekha Mahanta, "A Single Layer Hermite Neural Network Based Direct Adaptive Control of DC-DC Buck Converter, 3^{rd} *International Conference on Soft Computing & Machine Intelligence (ISCMI 2016)*, Dubai, UAE, 23-25 November 2016.

4. Arghya Chakravarty, **Tousif Khan Nizami** and Chitralekha Mahanta "Real Time Implementation of an Adaptive Backstepping Control of Buck Converter PMDC-Motor Combinations", *Indian Control Conference (ICC)*, 4-6 January 2017.

5. **Tousif Khan Nizami** and Chitralekha Mahanta, "Single Layer Type II Chebyshev Neural Network Based Adaptive Backstepping Control of DC-DC Buck Converter", *IEEE India International Conference INDICON*, 16-18 December 2016, pp. 1-6.

6. **Tousif Khan Nizami**, Arghya Chakravarty and Chitralekha Mahanta, "Finite time current observer based adaptive backstepping control of buck converters", *IEEE India International Conference INDICON*, 17-20 December 2015, pp. 1-6.

7. **Tousif Khan Nizami** and Chitralekha Mahanta, "Adaptive backstepping control for DC-DC buck converters using Chebyshev neural network," *IEEE India Conference INDICON*, 11-13 December 2014, pp. 1-5.

8. **Tousif Khan Nizami** and Chitralekha Mahanta, "Adaptive Chebyshev Neural Network Based Speed Control of Buck Converter Fed DC Motor", *Third National Symposium on Advances in Control & Instrumentation*, BARC, India, 24-26 November 2014.

1

Introduction

Contents

1.1 Evolution of DC-DC Power Conversion

Electric power supply is the principal entity behind realization of any electrical circuits and systems. Irrespective of their function in either analog or digital domain, these circuits necessarily require a reliable and efficient energy source for their operations. Among the two existing forms of electrical energy, namely, the direct current (DC) and the alternating current (AC), the DC power finds wide use in numerous applications in the field of telecommunication, instrumentation, medical electronics, aerospace, defence and power transmission.

Ever since the fundamental innovations in DC systems by Thomas Alva Edison in 1880, DC rectification and modulation method have remained central to various utilities. During the initial years, DC power conversion primarily resorted to the use of vacuum tube technology in delivering a desirable level of voltage from an AC source. The rectification stage was subsequently followed by filtering of the voltage at the output end. Nonetheless, the vacuum tube technology supported very low current density and featured a high ripple content in the DC voltage. Additionally, the output voltage was inconsistent or rather unregulated, making it inappropriate for DC power operated electrical and electronic systems. Much later in 1967, integrated series regulators were developed which eventually became popular as *linear power supplies* (LPS). Such a classical DC power generation method involved AC transformer, AC-DC rectifier and a voltage regulator in its assembly. Although the entire circuit is nonlinear, yet the term '*linear*' is used in the perspective of linear amplifier based output filter design. The transistors in LPS operate under active region and dissipate large amount of heat due to the voltage drop while high current flows through the collector-emitter junction, thereby causing substantial power loss and a very low energy efficiency. Even though they characterize low level of noise and find better suitability in audio applications, yet their critical limitations of huge size, heavy weight and high cost make them infeasible for use in portable electronic devices. Moreover, LPS are incapable in catering to the need of obtaining higher DC output voltages in reference to the source and are irrelevant in specific operations.

In tandem to these aforementioned developments, the advancements in power semiconductor technology led to the invention of low cost reliable power switches exhibiting fast switching response. This proved to be instrumental in building an energy efficient switched mode power supply which gradually gained popularity. Its impact on electrical technology was phenomenal, replacing conventional linear voltage supplies with switched mode power supplies giving rise to enhanced efficiency, light weight, compactness and comparably lower cost. Such a modern DC conversion system primarily includes DC-DC converters, wherein the rectified input voltage is fed to the DC-DC converter circuits for obtaining specific voltage levels.

The primary objective in DC-DC converters is to transfer the energy among different DC circuits functioning at specific voltage and current levels. This process of energy transfer is performed by temporarily storing the energy from the input source in a particular operating mode, followed by releasing it in the other operational mode of the converter. Thus, one level of DC input voltage is converted to another level of average DC output voltage at the load end. Meanwhile, the converter being ideal, is expected to consume no energy. Any consumption of energy in the converter interface amounts to direct power loss in the overall supply system. Typically, converters render high input-output conversion

efficiency in the range of 85% − 90%. As per the intended applications, the three basic non-isolated topologies of DC-DC converters are buck, boost and buck-boost converters. Buck converters step down the DC voltage, boost converters step up the DC voltage and buck-boost converters perform both stepping up and stepping down of the DC voltage depending on the requirement.
Within the family of switched power electronic circuits, DC-DC buck converters are well acclaimed in utilities wherein it is required to deliver lower voltages like 3.3V, 5V, 12V, 36V, 170V and 220V. Alternatively, it may be argued that voltage divider circuits can be employed to obtain lower magnitude DC voltages with respect to the input source. Although such circuits seem to be more appropriate for extremely low power and multiple DC voltage requirements, they usually suffer from serious issues of inefficiency due to power wastage in addition to complete loss of both line and load regulation. Undoubtedly, DC-DC buck converters are found to acquire an important place among all classes of existing DC step down regulators.

1.2 DC-DC Buck Converters

The objective of DC-DC buck converters is to convert a higher level of DC input voltage to a lower level of filtered average output DC voltage at the load end. They belong to the class of variable structure non-smooth systems and operate either under continuous conduction mode (CCM) or discontinuous conduction mode (DCM), depending on the flow of current through the inductor coil. Pertaining to their utility in large scale industrial systems, DC-DC buck converters find extensive usage in various practical applications [1–6] , which include battery charging, switched mode power supply in electronic devices, DC servo drives, electric transportation system, data communication, advanced telecommunication, medical instruments, process control and robotics. In such applications,

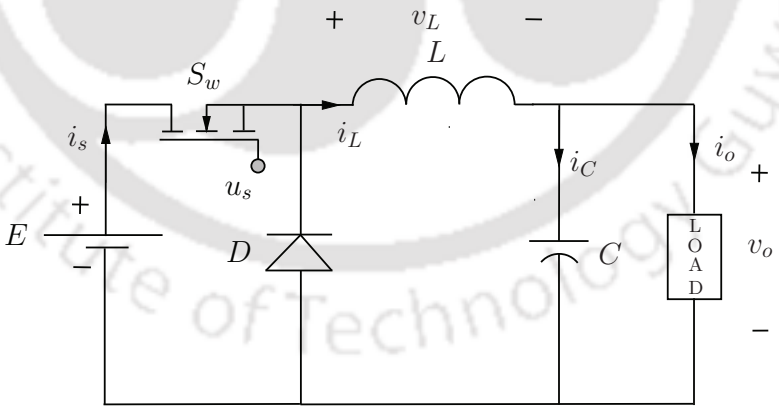

Figure 1.1: Circuit of DC-DC buck converter

the converter is required to deliver an efficient ripple free, reliable and robust output voltage regulation along with a satisfactory response of the inductor current. Apart from the converter efficiency which primarily depends on its design, the performance of the DC-DC buck converter is mainly attributed to the transient and steady-state response of the output state. The transient response is essentially

governed by the choice of adopted control mechanism, while the steady-state response depends on the topology, selection of circuit parameters and operational switching frequency of the DC-DC buck converter.

Circuit topology of the DC-DC buck converter [1] is presented in Figure 1.1. It consists of a DC voltage source E, a power semiconductor switch S_w, a power semiconductor diode D, filter inductor L, filter capacitor C and an external load. Further, u_s is the switching signal representing the position of the switch S_w. Hence, $u_s = 0$ denotes that S_w is open and $u_s = 1$ denotes that S_w is closed. The instantaneous currents through the inductor L and load are denoted by i_L and i_o with the output voltage across the load being represented as v_o. The instantaneous values of source current, capacitor current and voltage drop cross the inductor are denoted as i_s, i_C and v_L respectively. Moreover, the gate voltage required to turn on and turn off the switch S_w is termed as v_g. The switch S_w operates with a switching frequency f_s and a variable duty ratio k. The working of CCM DC-DC buck converter

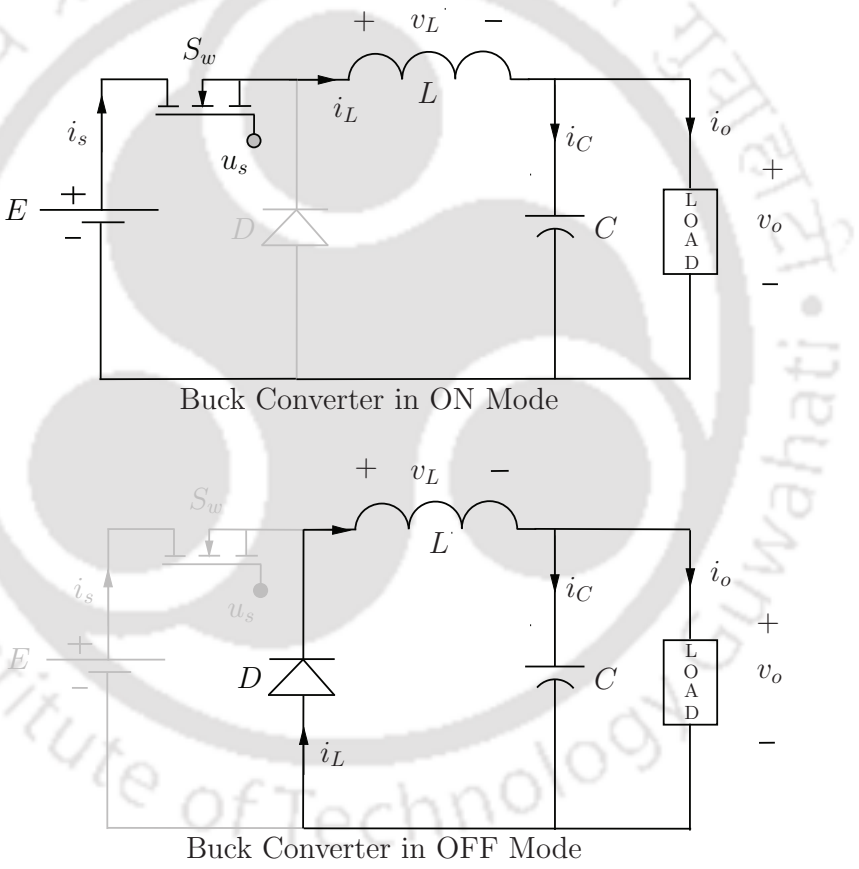

Figure 1.2: Modes of DC-DC buck converter

during ON and OFF mode of the switch is shown in Figure 1.2. During ON time period of the switch S_w, the diode D is in blocked state and the input DC source E supplies voltage to the DC-DC buck converter. During OFF time period of the switch S_w, the diode D is in conduction state which permits the flow of unidirectional current through the inductor L. Thus the energy stored in the inductor in the previous mode drives the converter load in OFF mode. In this way, the average output voltage V_a

generated across the load is lesser than the input voltage source E. Under the assumption of DC-DC buck converter operation in CCM and the load drawing a constant load current i_o, the waveforms [1] of relevant voltages and currents are illustrated in Figure 1.3. It is known that efficiency of a DC-DC buck converter largely depends on the circuit parameter design. Therefore, in order to design the circuit parameters, relevant electrical laws are discussed below. Referring to Figure 1.2 and applying the fundamental Faraday's law of electromagnetic induction, the voltage drop across the inductor L is obtained as,

$$v_L = L\frac{di_L}{dt}. \tag{1.1}$$

During ON time period of the switch S_w, the rise of inductor current is witnessed to be linear from I_1 to I_2 in the time interval t_1. Applying Kirchhoff's voltage law yields,

$$E - V_a = L\frac{I_2 - I_1}{t_1} = L\frac{\Delta I}{t_1} \tag{1.2}$$

where V_a is the average output voltage. The time interval t_1 can be represented through

$$t_1 = \frac{\Delta IL}{E - V_a}. \tag{1.3}$$

Similarly, during the descent of inductor current from I_2 to I_1 in the time interval t_2 yields,

$$-V_a = -L\frac{\Delta I}{t_2} \tag{1.4}$$

or rather the time interval t_2 can be written as

$$t_2 = \frac{\Delta IL}{V_a} \tag{1.5}$$

where $\Delta I = I_2 - I_1$ is the ripple current in the inductor L. Equating (1.2) and (1.4) for ΔI yields,

$$\Delta I = \frac{(E - V_a)t_1}{L} = \frac{V_a t_2}{L}. \tag{1.6}$$

It is known that $t_1 = kT$ and $t_2 = (1 - k)T$, where T is the switching period. Therefore, using this information, the average output voltage V_a can be expressed as,

$$V_a = E\frac{t_1}{T} = kE. \tag{1.7}$$

Assuming a lossless circuit and using (1.7), the relation between the average input current I_s and average output current I_a can be derived as

$$I_s = kI_a. \tag{1.8}$$

Further, the switching period T can be obtained as,

$$T = \frac{1}{f_s} = t_1 + t_2 = \frac{\Delta IL}{E - V_a} + \frac{\Delta IL}{V_a} \tag{1.9}$$

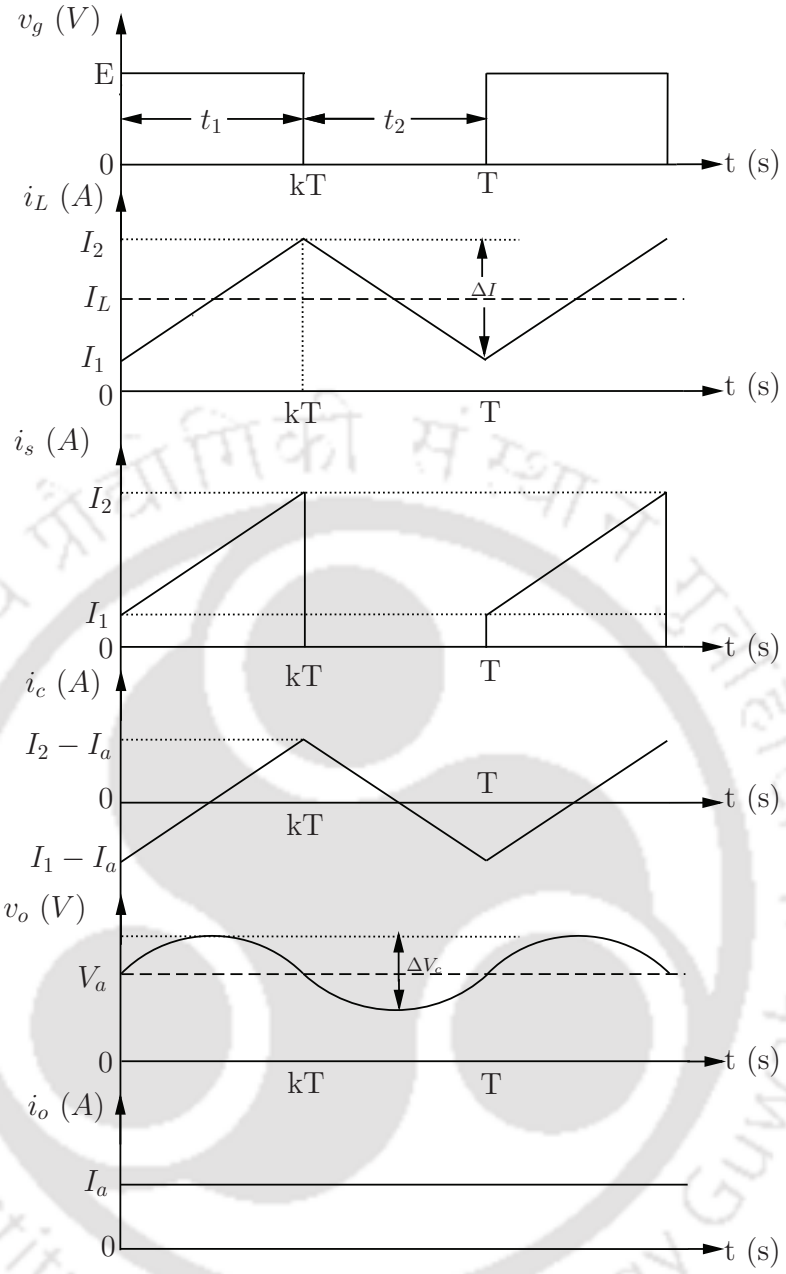

Figure 1.3: Voltage and current waveforms of DC-DC buck converter under CCM

$$T = \frac{\Delta ILE}{V_a(E - V_a)} \tag{1.10}$$

provides the relationship between inductor ripple current, input voltage, switching frequency, duty ratio and the inductor. Again,

$$\Delta I = \frac{V_a(E - V_a)}{fLE} \tag{1.11}$$

$$L = \frac{Ek(1-k)}{\Delta I f}. \tag{1.12}$$

Next, using Kirchhoff's current law $i_L = (i_C + i_o)$ and assuming negligible load ripple current Δi_o yields $\Delta i_L = \Delta i_C$. Moreover, the average value of capacitor current I_C flowing for $(t_1/2 + t_2/2) = T/2$ duration can be deduced as $I_C = \Delta I/4$. The instantaneous voltage across capacitor C is given by

$$v_C(t) = \frac{1}{C}\int i_C dt + v_C(0) \tag{1.13}$$

and the peak-to-peak ripple voltage across the capacitor is found as

$$\Delta v_C = v_C(t) - v_C(0) = \frac{1}{C}\int_0^{T/2} \frac{\Delta I}{4} dt = \frac{\Delta I}{8fC}. \tag{1.14}$$

Substituting the value of ΔI from (1.11) in (1.14) yields

$$\Delta v_C = \frac{V_a(E - V_a)}{8LCEf^2} \tag{1.15}$$

$$C = \frac{Ek(1-k)}{8L\Delta v_C f^2} \tag{1.16}$$

In the above derivations, (1.7) defines the input-output voltage relation under ideal lossless condition in the converter. Further, (1.12) and (1.16) define the design requisites of L and C in terms of other specifications of DC-DC buck converter circuit parameters. Therefore, by appropriate selection of circuit parameters and switching frequency the DC-DC buck converter can be designed for a desired level of nominal steady state performance.

1.3 Control Issues in DC-DC Buck Converters

In order to maintain a regulated output voltage with satisfactory transient and steady-state responses, the DC-DC buck converter is generally equipped with a closed loop feedback control mechanism. The design and synthesis of an efficient controller for DC-DC buck converters have to take into account the following challenges;

- ***Parametric uncertainties***: Uncertainties arising out of modelling errors, time varying magnetic characteristics of the inductor due to a large magnetic flux density originating from ferromagnetic core, stray inductance present in the connecting wires and cables, parasitic capacitance appearing in the switching devices. Uncertainties like parasitic capacitance and stray inductance lead to oscillations in every switching cycle. In addition affects of component ageing and the temperature rise also add to the parametric uncertainty. [7].

- ***Supply voltage fluctuations:*** Variations in input voltage from sources such as battery and sudden power surges and spikes in supply voltage are major concerns. In real time, the internal resistance, series inductance in power source and load also add to parasitics, causing modeling errors and power loss.

- ***Load disturbances:*** Highly unanticipated abrupt disturbances occurring in the external load cause drastic affect on the nominal operation of the converter.
- ***Bandwidth restrictions:*** The bandwidth of switching frequency is restricted by an upper bound to remain well within the permissible thermal limits and switching losses. Moreover, the switching frequency is constrained by a lower bound for maintaining an acceptable output voltage ripple.
- ***Safe operation:*** Most of the applications expect a safe operation of the converter, while imposing a limit on the peak value of inductor current during transient periods. This is specially to avoid inductor saturation and damage to the switching components.
- ***Sensor and noise issues:*** Imperfections in the voltage and current measurement devices and unwarranted noise intrusion manipulate the input feedback signal.
- ***Practical implementation:*** Simplicity in controller design and its feasibility in real-time scenarios are vital design requirements.
- ***Fast Transient behaviour and satisfactory response:*** Above all, almost all the applications demand smooth and fast transient characteristics under start-up with acceptable overshoot values as well as satisfactory steady-state response during the entire operation of the converter.

In the light of all the aforementioned issues, the DC-DC buck converter dynamics exhibit a complex nonlinear structure affected by time varying perturbations, exogenous disturbances and parametric uncertainties [8, 9], which pose challenges in the design of an effective controller reliable for output voltage tracking.

1.4 Literature Review

The objective of a controller is to maintain stability and a desirable performance even in presence of intrinsic and extrinsic disturbances. An accurate mathematical model describing the exact dynamic characteristics of the system is an essential pre-requisite for designing an efficient and robust control system. As discussed in the preceding section, occurrence of parametric uncertainties is inevitable in DC-DC buck converters. Hence, accurate estimation of parameters including the knowledge of instantaneous load change is highly essential for designing an appropriate control input to achieve a robust output voltage regulation.

On the basis of parametric and non-parametric uncertainty estimation, two types of model identification approaches for DC-DC converters have been reported in literature [10–12]. Estimation of non-parametric uncertainties usually involves spectral and correlation analysis methods to obtain the frequency response of the system, without taking parametric modelling into account [10–12]. In this method, the duty cycle of the DC-DC converter is perturbed with a frequency rich input signal. Thereafter, the Fourier transform techniques are utilized to find frequency response curves. The frequency

response reveals the intrinsic behavior of the system. Nevertheless, such a method requires the system to operate in an open loop mode without involving any closed loop regulation, while consuming considerable amount of time and may not be feasible in practice [13, 14]. In [15], an identification technique for obtaining system dynamics without running it in open loop mode is proposed. In [16], using maximum length pseudo random binary sequence (PRBS) [12], the Fourier amplitude spectrum is developed. The technique is straight forward for implementation purpose. However, its use is restricted to obtaining frequency domain response only.

On the contrary, the methods for estimation of parametric uncertainties are purely based on the mathematical model of the system. An accurate model leads to better parameter approximations although at the cost of increased complexity. Some of these methods [10, 17] are recursive least squares (RLS) method, subspace method, and maximum likelihood estimation method. Although RLS is a deterministic approach suitable for online applications, yet they are not very appropriate for low cost and low power consuming systems due to intense computational complexity. In [13], a limit cycle oscillations (LCO) based scheme for online parameter estimation is proposed. Measurement of amplitude and frequency of oscillation in the output state assists in finding the system parameters [18]. Nonetheless, the method results in lower estimation accuracy [19]. In [20], a hybrid method is proposed by combining both parametric and non-parametric identification schemes for designing a digital controller. However, due to increased complexity, this method is better suited for offline estimation problems. Majority of these methods involve significant amount of signal processing, leading to increased implementation cost in real-time. Under the maximum likelihood based output error method [21, 22], the estimation is achieved by continuously tuning the model parameters in response to the output of the actual system, until there is a close match between the actual system and the model under consideration. Kalman filter [23] based approaches have emerged as a celebrated technique for parameter estimation in a wide range of engineering problems across the globe. In such estimation methods, although the convergence of estimation error is proven theoretically, the controllers demand parameter convergence at the fastest possible rate in order to deliver an effective and timely control action.

The choice of an appropriate control mechanism for DC-DC buck converters is vital to realize the desired control objective. In linear controllers, a small-signal model of nonlinear system is derived based on the method of linearization at a specific operating point. Thereafter, proceeding with the transfer function model, the controllers are designed using conventional control techniques [24]. These linear controllers include proportional-integral (PI)/proportional-integral-derivative (PID) [25–27] controllers which handle static disturbances only. A near-satisfactory steady state response can be obtained by adjusting the frequency domain curves like Bode plot to achieve the necessary gain margin, phase margin and crossover frequencies. Besides, time domain based root locus approach can be adopted to improve the transient performance of the output signal [28]. These linear controllers are popular mainly because of their simplicity, clear functionality and ease of implementation. It must be emphasized that the small-signal model varies with the change in operating point of the converter. Such a technique provides a low frequency approximation of the entire converter and neglects the discontinuous effect produced due to the switching behavior in the actual dynamical system. Alternatively, some works in the direction of optimal gain search PI/PID controller through bio-inspired evolution-

ary optimization can be found in [29,30], wherein the wisdom inherited from nature is utilized for an optimal selection of controller parameters. These are offline methods and provide near-satisfactory response around a certain fixed operating point and lead to complications in presence of uncertain converter parameters. The sudden injection of disturbances influencing the converter leads to changes in the operating point and eventually causes chaotic behavior and poor dynamic response often resulting in instability [31–33].

Large-signal model based schemes for DC-DC buck converters have evolved in the recent past. One-cycle control (OCC) [34] is one nonlinear control method where the output voltage tracking error is made to converge to near-zero, by producing the appropriate duty cycle through the method of integration. However, this method faces difficulty in obtaining an efficient control response when significant non-idealities exist in the system and hence integration process contributes to an imprecise control action.

With increasing interests in modern control techniques, Sliding mode control (SMC) [35–38] has emerged as a popular nonlinear technique in recent decades. The SMC possesses a simple structure and its control is inherently discontinuous in nature. Although the SMC offers immunity towards matched uncertainties, it does not ensure complete robustness in the output tracking in presence of the mismatched uncertainty. In addition, the high frequency operation in the SMC is a serious concern as its implementation may lead to an excessive switching loss and electromagnetic interference (EMI).

Backstepping control (BSC) [39–42] is a powerful control technique for stabilizing a large class of nonlinear systems providing a promising transient performance. These controllers are developed through a systematic and recursive design framework, eliminating the restrictions of matching condition on system uncertainties. In BSC, the asymptotic stabilization of the full system dynamics is guaranteed through the design of virtual controllers stabilizing each of the lower dimensional sub-systems using consecutive control Lyapunov functions followed by the final control law. Further, unlike SMC based strategies, the control law in BSC is smooth and continuous. Lately, neural networks have emerged as an alternative technique to control the uncertain time varying systems [43]. The potential of such methods lies in their strong ability to approximate the unknown dynamics of the system. Neural networks can be trained in both offline and online modes for the purpose of estimation. Lately, by exploiting the merits of linguistic reasoning and neural learning, fuzzy neural network based methods have been proposed for power converters [44, 45].

A few other control methods reported in the literature include passivity based control [46], hierarchical control [47], $\mathcal{H}_\infty$ based control [48] and flatness-based control [49].

1.5 Research Motivation

In the context to output voltage tracking problem in DC-DC buck converters, the control strategies can be broadly classified under two types: voltage-mode control (VMC) and current-mode control (CMC) [50], based on the type of feedback error loops. The VMC DC-DC buck converter consists of a single feedback loop driven directly by the output voltage error. Although the VMC offers simplicity in implementation, yet disturbance at the input voltage cannot be detected unless it is reflected on the output.

On the contrary, the CMC is a multiple loop feedback structure utilizing the inductor current in addition to the voltage error dynamics to produce a fast dynamical response. With respect to DC-DC buck converters, disturbances arising at the input voltage will initially result in change in the inductor current slope prior to its impact on the output. However, when this real-time information is fed to the controller through a current sensing mechanism, an almost constant volt-second balance is obtained by appropriate rectification of the pulse width modulation (PWM) signal operating the power semiconductor switch. This makes the DC-DC buck converter less sensitive to the input voltage perturbations [51]. In this way, the CMC inherently prevents the use of an extra input voltage sensor to curb the input fluctuations and subsequently the additional loop delay appearing due to the input voltage sensor is avoided. Furthermore, the CMC is instrumental in providing automatic protection against over-current and short-circuit arising in the converter due to abrupt eventualities, thereby enhancing the converter's reliability. It may be noted that in DC-DC buck converters the inductor current is a function of the load current. Therefore, any load current perturbations will also be taken into account with the inductor current sensing. Hence, it can be anticipated that for DC-DC buck converters, the control methodology involving a two loop feedback mechanism of output voltage and inductor current sensing has better suitability and offers multiple benefits while attaining the objective of output voltage regulation.

In this direction, the inherent benefits of backstepping control (BSC) make it suitable for DC-DC buck converter control operation with the following useful features. Since the state-space averaged model of the DC-DC buck converter can be represented in strict-feedback form, the BSC method can be directly applied to it. The systematic, step-by-step and recursive control Lyapunov function (CLF) based controller design framework guaranteeing asymptotic error convergence in each of the sub-systems, ease in physical realization and successful rejection of linearly parameterized matched and mismatched uncertainties make backstepping an appealing control technique. In addition, the BSC avoids cancellations of some useful nonlinearities present in the system, which may help to improve the transient performance. Moreover, the BSC design requires a full-state feedback involving both voltage and current sensing loops and hence meets the requirements of a reliable converter operation. However, for an accurate computation of the control law, it necessarily requires the exact state-space model of the converter. Furthermore, the unavailability of precise parametric knowledge leads to a stable, yet unsatisfactory transient response. Additionally, the load current disturbance in the BSC yields steady-state error in the output voltage.

Motivated by such challenges present in the backstepping control method for DC-DC buck converter control, efforts have been made in this thesis to develop appropriate robust control methodologies based on backstepping technique with online adaptation mechanism for estimating uncertainties affecting the system. The main aim of the thesis is to improve the transient response of the output using online adaptation to estimate the unknown load. Attempts are made to ensure a satisfactory reliable performance of the converter at wide range of operating points caused by fluctuations in the input voltage supply, parametric uncertainties and load current disturbances.

The contributions of this thesis are enumerated and briefly discussed in the following section.

1.6 Contributions of the Thesis

The contributions made under each chapter of the thesis are highlighted below.

(i) Firstly, exploiting the system structure, an adaptive backstepping control (ABSC) method is developed for the DC-DC buck converter feeding a resistive load. The ABSC method has been investigated on a laboratory made hardware prototype by subjecting the DC-DC buck converter to unanticipated disturbances over a wide range. This has unveiled some of the major beneficial attributes of the ABSC regarding its application to DC-DC buck converters. Furthermore, the issue of angular velocity control in DC-DC buck converter driven permanent-magnet DC (PMDC)-motor system with varying load torque is addressed using the ABSC scheme on the experimental set-up fabricated in the laboratory.

(ii) An orthogonal recursive polynomial based single layer Chebyshev Neural Network (CNN) with online learning in conjunction with the adaptive backstepping control is proposed. Using this proposed method, a fast approximation of the parametric uncertainty is realized which eventually renders better transient performance of the output voltage. Further, the proposed CNN based ABSC method is used to control angular velocity of a DC-DC buck converter driven PMDC motor subjected to sudden variations in load torque.

A rapid adaptation in accordance with the unanticipated varying load enables better control prospects of output voltage in both start-up and load transients. In order to enhance the speed of uncertainty estimation a Hermite Neural Network (HNN) based ABSC technique is proposed.

(iii) A finite time exact uncertainty estimation based backstepping controller is proposed to estimate and reject unknown parametric uncertainties and load changes. This method attains a time bound exact determination of the uncertainty and unlike conventional adaptive backstepping control, the scheme does not need persistence of excitation condition for convergence of the estimation error to the origin. The proposed controller is experimentally validated.

(iv) To mitigate the ill effects of measurement noise and time delay in the control loop, a finite time current observer based adaptive backstepping control is proposed. The proposed control methodology utilizes the structure of the system dynamics. Hardware realization of the proposed controller supplements theoretical propositions.

1.7 Organization of the Thesis

This thesis is organized as follows.

- **Chapter 2:** This chapter starts with a brief introduction on the backstepping control method and its application to the problem of DC-DC buck converter. The adaptive backstepping controller is designed next for DC-DC buck converter fed resistive load and PMDC-motor load. The proposed control method is simulated and verified via experimental validation on a laboratory prototype.

- **Chapter 3:** In this chapter, a Chebyshev neural network (CNN) with adaptive learning is proposed for estimation of the unknown load. A backstepping controller is integrated with the CNN to achieve the desired output tracking in the presence of unanticipated load and input disturbances. The developed control scheme has also been applied to the problem of angular velocity tracking in a DC-DC buck converter fed PMDC motor load and the simulation and experimental results obtained are quite promising. A Hermite neural network (HNN) based backstepping control law to enable a faster estimation of the unknown load is proposed next.

- **Chapter 4:** In the previous chapters, the load estimation error is bounded or at the most asymptotically stable to the origin. Further, there is no design freedom on the time of estimation convergence. Therefore, to increase the degrees of freedom in control design and to exactly estimate the parametric uncertainties within a stipulated time, a finite time disturbance observer based backstepping controller is proposed. A rigorous stability analysis follows the proposed control design. Both simulation and experimental studies are conducted to investigate the efficacy of the proposed control scheme.

- **Chapter 5:** This chapter proposes a current sensorless adaptive backstepping controller for DC-DC buck converters. A finite time current observer is used in the adaptive backstepping control, wherein the unknown current is treated as a disturbance term in the voltage tracking error dynamics. Such a control scheme alleviates the drawbacks of measurement noise and delay in the control loop inherent in the sensor, which otherwise adversely affect the tracking performance. The proposed controller promises a better output voltage regulation besides being robust to uncertainties. This novel design methodology ia validated experimentally.

- **Chapter 6:** In this chapter, conclusions from the research work are drawn and the scope for future research is outlined.

2

Adaptive Backstepping Control of DC-DC Buck Converters

Contents

2.1 Introduction

The merits of backstepping control method motivated active research for developing it as an adequate adaptive control strategy [52–56]. However, very few works related to DC-DC buck converter [57–63] can be found in the literature in this regard. In 1995, H. Sira-Ramirez et al. first presented the preliminary results on adaptive backstepping control of DC-DC converters [64]. In 2003, H. El Fadil et al. [62] demonstrated on simulation platform, the effectiveness of adaptation in the controller, by framing adaptive laws to estimate unknown converter parameters. In 2007, Li-kui Yi et al. [60] proposed adaptive backstepping in combination with sliding mode control to operate DC-DC buck converters. Their work was examined with numerical results. Nevertheless, the controller response with wide range of load uncertainty has not been investigated there. Fan Liping et al. [59] proposed an integrated control algorithm by combining adaptive backstepping and terminal sliding mode control (TSMC), where a fast settlement of initial transients was achieved. However, the influence of the proposed control on the dynamic behavior of the inductor current during start-up and disturbances has not been investigated there. In addition, the efficacy of the suggested method has not been validated through experiments on wide range of converter operating points. In 2011, Salimi M. et al. [57] designed backstepping control by taking into account the effect of parasitic elements and equivalent series resistance of filter inductance along with a precise modeling of power semiconductor switches. Multiple adaptive laws were framed here for estimating the varying values of load and filter components of the converter. However, the results exhibited a poor transient performance featuring significant overshoots in the output voltage and inductor current during load disturbances. This method was evaluated through simulation studies only. Later in 2013, McIntyre M. L. et al. [58] presented an adaptive backstepping control of DC-DC buck converters in presence of unknown and slowly varying load resistance. In the above design propositions, very few results pertaining to real time implementation have been reported. However, it must be noted that in reality the load change occurs abruptly and hence the assumption of slowly varying load does not always hold good. Besides, the above results mostly exhibit a slow start-up response with substantial overshoot and undershoot during the load disturbance, making the control design unsuitable for practical use.

To the best of author's knowledge, extensive and rigorous investigations into physical realization of DC-DC buck converter control through adaptive backstepping scheme have not been explored yet. Therefore, adaptive backstepping control for DC-DC buck converters (i) feeding a resistive load and (ii) driving a PMDC-motor load is investigated through extensive simulation and experimentation. Further, in this chapter the controller response for the output alongwith all other system states is studied under widely varying operating points.

This chapter is organized as follows. Firstly, the basic control strategy involving the procedure for adaptive backstepping control (ABSC) design is explained. Thereafter, the adaptive backstepping controller design for DC-DC buck converters feeding a resistive load is presented and evaluated theoretically by conducting simulation studies. A laboratory prototype is constructed for the same and its details are explained, followed by experimentation. This ABSC method is further extended for angular velocity control of a PMDC-motor using the DC-DC buck regulator. Design, analysis and experimental studies regarding the DC-DC buck converter fed PMDC-motor control using the proposed

ABSC method are described.

2.2 Adaptive Backstepping Control Design

Adaptive backstepping [41, 52, 65–68] is a step-by-step systematic control design method. Using control Lyapunov function (CLF), the final control law is arrived at, with the closed loop system dynamics satisfying the Lyapunov stability criterion [41, 69]. The procedure involves selection of appropriate stabilizing functions of state variables in a recursive manner, to act as stabilizing pseudo-control inputs for lower dimension subsystems, obtained in the course of control design for the entire system. Each stage of adaptive backstepping control yields a new pseudo-control input, which is again expressed in terms of the previously obtained pseudo-control signal. This process is repeated until the actual control law is obtained at the final stage. Steps involved in the adaptive backstepping control algorithm are summarized below:

Let us consider a class of nonlinear systems described as follows,

$$\begin{aligned}
\dot{x}_1 &= x_2 + \boldsymbol{\Theta}^{*\mathbf{T}}\boldsymbol{\Phi}_{\mathbf{1}}(x_1) \\
\dot{x}_2 &= x_3 + \boldsymbol{\Theta}^{*\mathbf{T}}\boldsymbol{\Phi}_{\mathbf{2}}(x_1, x_2) \\
&\vdots \qquad\qquad \vdots \\
\dot{x}_{n-1} &= x_n + \boldsymbol{\Theta}^{*\mathbf{T}}\boldsymbol{\Phi}_{\mathbf{n-1}}(x_1, \ldots, x_{n-1}) \\
\dot{x}_n &= \Phi_0(\mathbf{x}) + \boldsymbol{\Theta}^{*\mathbf{T}}\boldsymbol{\Phi}_{\mathbf{n}}(\mathbf{x}) + \beta(\mathbf{x})u \\
y &= x_1
\end{aligned} \tag{2.1}$$

where $\mathbf{x} = [x_1, \ldots x_n]^T \in \mathbb{R}^n$, $u \in \mathbb{R}$ and $y \in \mathbb{R}$ are the state vector, input and output of the system respectively. Further, $\boldsymbol{\Theta}^* \in \mathbb{R}^{\mathbf{p}}$ is the unknown constant vector, $\Phi_0 \in \mathbb{R}$, $\boldsymbol{\Phi}_{\mathbf{i}} \in \mathbb{R}^{\mathbf{p}}$ for $i = 1, \ldots, n$, β are smooth nonlinear known functions. It must be emphasized that (2.1) represents a class of nonlinear systems in parametric strict-feedback form. Here, the nonlinearities depend purely on those variables which are fed back to the system.

The objective of the control is to make the system output y asymptotically track a reference input signal $y_r(t)$ while ensuring overall closed loop system stability. The adaptive backstepping control (ABSC) design procedure is discussed below to serve as a primer for a clear understanding of the control methodologies proposed in this thesis. The controller is developed adopting a stepwise procedure as given below.

Step 1. Let the error variables be defined as,

$$z_1 = y - y_r \tag{2.2}$$

$$z_2 = x_2 - \dot{y}_r - \alpha_1 \tag{2.3}$$

where z_1 denotes the output tracking error and the convergence of z_1 as $\lim_{t\to\infty} z_1(t) = 0$ needs to be ensured. The dynamics of z_1 is defined as

$$\begin{aligned}\dot{z}_1 &= \dot{y} - \dot{y}_r \\ &= x_2 + \mathbf{\Theta^{*T}\Phi_1} - \dot{y}_r \\ &= z_2 + \alpha_1 + \mathbf{\Theta^{*T}\Phi_1}\end{aligned} \tag{2.4}$$

where α_1 is defined as the first virtual-control input to stabilize z_1 dynamics and is designed as

$$\alpha_1 = -c_1 z_1 - \mathbf{\hat{\Theta}^T\Phi_1}. \tag{2.5}$$

Here c_1 is a positive constant and $\hat{\mathbf{\Theta}}$ is an estimate of $\mathbf{\Theta}^*$. The first virtual control input α_1 acts as the "desired value" of x_2 in order to render the z_1 subsystem stable.
Let the first Lyapunov function be defined as

$$V_1 = \frac{1}{2}z_1^2 + \frac{1}{2}\mathbf{\tilde{\Theta}^T\Gamma^{-1}\tilde{\Theta}} \tag{2.6}$$

where $\mathbf{\Gamma}$ is a positive definite matrix and $\tilde{\mathbf{\Theta}}$ is the error in estimation, defined as $\tilde{\mathbf{\Theta}} = \mathbf{\Theta}^* - \hat{\mathbf{\Theta}}$. Using (2.4)-(2.5), the first time derivative of V_1 can be found as

$$\dot{V}_1 = z_1(-c_1 z_1 + z_2 + \mathbf{\tilde{\Theta}^T\Phi_1}) - \mathbf{\tilde{\Theta}^T\Gamma^{-1}\dot{\hat{\Theta}}} \tag{2.7}$$

$$= z_1(-c_1 z_1 + z_2) - \mathbf{\tilde{\Theta}^T}(\mathbf{\Gamma^{-1}\dot{\hat{\Theta}} - \Phi_1} z_1). \tag{2.8}$$

Let the first tuning function be defined as

$$\vartheta_\mathbf{1} = \mathbf{\Phi_1} z_1. \tag{2.9}$$

Substituting (2.9) in (2.8) yields

$$\dot{V}_1 = -c_1 z_1^2 + z_1 z_2 - \mathbf{\tilde{\Theta}^T}(\mathbf{\Gamma^{-1}\dot{\hat{\Theta}}} - \vartheta_\mathbf{1}). \tag{2.10}$$

Step 2: Herein, the next error variable z_3 is defined and subsequently forms the subsystem described by (z_1, z_2) dynamics as follows,

$$z_3 = x_3 - \ddot{y}_r - \alpha_2. \tag{2.11}$$

Taking derivative of z_2 from (2.3) and using (2.5) yields

$$\begin{aligned}\dot{z}_2 &= \dot{x}_2 - \ddot{y}_r - \dot{\alpha}_1 \\ &= z_3 + \alpha_2 - \frac{\partial \alpha_1}{\partial x_1}x_2 + \mathbf{\Theta^{*T}}\left(\mathbf{\Phi_2} - \frac{\partial \alpha_1}{\partial x_1}\mathbf{\Phi_1}\right) - \frac{\partial \alpha_1}{\partial y_r}\dot{y}_r - \frac{\partial \alpha_1}{\partial \hat{\mathbf{\Theta}}}\dot{\hat{\Theta}}\end{aligned} \tag{2.12}$$

where α_2 is the second virtual-control input designed to stabilize (z_1, z_2) systems in (2.4) and (2.12). Selecting the second virtual-control law α_2 in a manner given below would ensure stability of the

(z_1, z_2)-subsystem,

$$\alpha_2 = -z_1 - c_2 z_2 + \frac{\partial \alpha_1}{\partial x_1} x_2 - \hat{\mathbf{\Theta}}^{\mathbf{T}} \left(\mathbf{\Phi_2} - \frac{\partial \alpha_1}{\partial x_1} \mathbf{\Phi_1} \right) + \frac{\partial \alpha_1}{\partial y_r} \dot{y}_r + \frac{\partial \alpha_1}{\partial \hat{\mathbf{\Theta}}} \mathbf{\Gamma} \vartheta_{\mathbf{2}} \tag{2.13}$$

where c_2 is the positive constant and the second tuning function is $\vartheta_{\mathbf{2}}$ based on ϑ_1 as,

$$\vartheta_{\mathbf{2}} = \vartheta_{\mathbf{1}} + \left(\mathbf{\Phi_2} - \frac{\partial \alpha_1}{\partial x_1} \mathbf{\Phi_1} \right) z_2. \tag{2.14}$$

To prove the stability of (z_1, z_2)-subsystem, let the second Lyapunov function candidate V_2 be chosen as,

$$V_2 = V_1 + \frac{1}{2} z_2^2. \tag{2.15}$$

From (2.10), (2.12)-(2.14), the derivative of V_2 can be found as

$$\begin{aligned} \dot{V}_2 &= -c_1 z_1^2 + z_1 z_2 - \tilde{\mathbf{\Theta}}^{\mathbf{T}} \left(\mathbf{\Gamma^{-1}} \dot{\hat{\mathbf{\Theta}}} - \vartheta_{\mathbf{1}} \right) + z_2(-z_1 - c_2 z_2 + z_3) \\ &\quad + z_2 \hat{\mathbf{\Theta}}^{\mathbf{T}} \left(\mathbf{\Phi_2} - \frac{\partial \alpha_1}{\partial x_1} \mathbf{\Phi_1}) + z_2 \frac{\partial \alpha_1}{\partial \hat{\mathbf{\Theta}}} (\mathbf{\Gamma} \vartheta_{\mathbf{2}} - \dot{\hat{\mathbf{\Theta}}} \right) \\ &= -c_1 z_1^2 - c_2 z_2^2 + z_2 z_3 + \tilde{\mathbf{\Theta}}^{\mathbf{T}} \left(\vartheta_{\mathbf{2}} - \mathbf{\Gamma^{-1}} \dot{\hat{\mathbf{\Theta}}} \right) + z_2 \frac{\partial \alpha_1}{\partial \hat{\mathbf{\Theta}}} \left(\mathbf{\Gamma} \vartheta_{\mathbf{2}} - \dot{\hat{\mathbf{\Theta}}} \right). \end{aligned} \tag{2.16}$$

Step 3. Let the next error variable z_4 be defined as

$$z_4 = x_4 - y^{(3)} - \alpha_3 \tag{2.17}$$

where $y^{(3)}$ is the third time derivative of y. Now to deal with (z_1, z_2, z_3)-subsystem, z_3 error dynamics is required and the same is obtained by taking derivative of (2.11) and using (2.1), (2.13), (2.17) yields

$$\begin{aligned} \dot{z}_3 &= z_4 + \alpha_3 - \frac{\partial \alpha_2}{\partial x_1} x_2 - \frac{\partial \alpha_2}{\partial x_2} x_3 + \mathbf{\Theta}^{*\mathbf{T}} \left(\mathbf{\Phi_3} - \frac{\partial \alpha_2}{\partial x_1} \mathbf{\Phi_1} - \frac{\partial \alpha_2}{\partial x_2} \mathbf{\Phi_2} \right) - \frac{\partial \alpha_2}{\partial y_r} \dot{y}_r \\ &\quad - \frac{\partial \alpha_2}{\partial \dot{y}_r} \ddot{y}_r - \frac{\partial \alpha_2}{\partial \hat{\mathbf{\Theta}}} \dot{\hat{\mathbf{\Theta}}}. \end{aligned} \tag{2.18}$$

Selecting the third virtual-control input α_3 as

$$\begin{aligned} \alpha_3 &= -z_2 - c_3 z_3 + \frac{\partial \alpha_2}{\partial x_1} x_2 + \frac{\partial \alpha_2}{\partial x_2} x_3 - \hat{\mathbf{\Theta}}^{\mathbf{T}} \left(\mathbf{\Phi_3} - \frac{\partial \alpha_2}{\partial x_1} \mathbf{\Phi_1} - \frac{\partial \alpha_2}{\partial x_2} \mathbf{\Phi_2} \right) \\ &\quad + \frac{\partial \alpha_2}{\partial y_r} \dot{y}_r + \frac{\partial \alpha_2}{\partial \dot{y}_r} \ddot{y}_r + \frac{\partial \alpha_2}{\partial \hat{\mathbf{\Theta}}} \mathbf{\Gamma} \vartheta_{\mathbf{3}} + z_2 \frac{\partial \alpha_1}{\partial \hat{\mathbf{\Theta}}} \mathbf{\Gamma} \left(\mathbf{\Phi_3} - \frac{\partial \alpha_2}{\partial x_1} \mathbf{\Phi_1} - \frac{\partial \alpha_2}{\partial x_2} \mathbf{\Phi_2} \right) \end{aligned} \tag{2.19}$$

where c_3 is a positive constant. The third tuning function $\vartheta_{\mathbf{3}}$ based on $\vartheta_{\mathbf{2}}$ is defined as

$$\vartheta_{\mathbf{3}} = \vartheta_{\mathbf{2}} + \left(\mathbf{\Phi_3} - \frac{\partial \alpha_2}{\partial x_1} \mathbf{\Phi_1} - \frac{\partial \alpha_2}{\partial x_2} \mathbf{\Phi_2} \right) z_3. \tag{2.20}$$

Considering the Lyapunov function candidate V_3 to explore stability aspects of (z_1, z_2, z_3)-subsystem as

$$V_3 = V_2 + \frac{1}{2} z_3^2 \tag{2.21}$$

the first time derivative of V_3 is obtained by using (2.16), (2.18) and (2.19) as,

$$\dot{V}_3 = -c_1 z_1^2 - c_2 z_2^2 - c_3 z_3^2 + z_3 z_4 + \tilde{\mathbf{\Theta}}^{\mathbf{T}} \left(\vartheta_{\mathbf{3}} - \mathbf{\Gamma}^{-\mathbf{1}} \dot{\hat{\mathbf{\Theta}}} \right) + z_2 \frac{\partial \alpha_1}{\partial \hat{\mathbf{\Theta}}} \left(\mathbf{\Gamma} \vartheta_{\mathbf{2}} - \dot{\hat{\mathbf{\Theta}}} \right) + z_3 \frac{\partial \alpha_2}{\partial \hat{\mathbf{\Theta}}} \left(\mathbf{\Gamma} \vartheta_{\mathbf{3}} - \dot{\hat{\mathbf{\Theta}}} \right) + z_2 \frac{\partial \alpha_1}{\partial \hat{\mathbf{\Theta}}} \mathbf{\Gamma} \left(\mathbf{\Phi_3} - \frac{\partial \alpha_2}{\partial x_1} \mathbf{\Phi_1} - \frac{\partial \alpha_2}{\partial x_2} \mathbf{\Phi_2} \right) z_3. \tag{2.22}$$

Now

$$\begin{aligned} z_2 \frac{\partial \alpha_1}{\partial \hat{\mathbf{\Theta}}} \left(\mathbf{\Gamma} \vartheta_{\mathbf{2}} - \dot{\hat{\mathbf{\Theta}}} \right) &= z_2 \frac{\partial \alpha_1}{\partial \hat{\mathbf{\Theta}}} \left(\mathbf{\Gamma} \vartheta_{\mathbf{3}} - \dot{\hat{\mathbf{\Theta}}} \right) + z_2 \frac{\partial \alpha_1}{\partial \hat{\mathbf{\Theta}}} \mathbf{\Gamma} \left(\vartheta_{\mathbf{2}} - \vartheta_{\mathbf{3}} \right) \\ &= z_2 \frac{\partial \alpha_1}{\partial \hat{\mathbf{\Theta}}} \left(\mathbf{\Gamma} \vartheta_{\mathbf{3}} - \dot{\hat{\mathbf{\Theta}}} \right) - z_2 \frac{\partial \alpha_1}{\partial \hat{\mathbf{\Theta}}} \mathbf{\Gamma} \left(\mathbf{\Phi_3} - \frac{\partial \alpha_2}{\partial x_1} \mathbf{\Phi_1} - \frac{\partial \alpha_2}{\partial x_2} \mathbf{\Phi_2} \right) z_3. \end{aligned} \tag{2.23}$$

Next, substituting (2.23) into (2.22) yields

$$\dot{V}_3 = -c_1 z_1^2 - c_2 z_2^2 - c_3 z_3^2 + z_3 z_4 + \tilde{\mathbf{\Theta}}^{\mathbf{T}} \left(\vartheta_{\mathbf{3}} - \mathbf{\Gamma}^{-\mathbf{1}} \dot{\hat{\mathbf{\Theta}}} \right) + \left(z_2 \frac{\partial \alpha_1}{\partial \hat{\mathbf{\Theta}}} + z_3 \frac{\partial \alpha_2}{\partial \hat{\mathbf{\Theta}}} \right) \left(\mathbf{\Gamma} \vartheta_{\mathbf{3}} - \dot{\hat{\mathbf{\Theta}}} \right) \tag{2.24}$$

. ***Step i***: For $i = 4, \ldots, n-1$, introducing new error variables as

$$z_i = x_i - y_r^{(i-1)} - \alpha_{i-1} \tag{2.25}$$

the dynamics of each of these error variables are described by,

$$\dot{z}_i = z_{i+1} + \alpha_i - \sum_{k=1}^{i-1} \frac{\partial \alpha_{i-1}}{\partial x_k} x_{k+1} + \mathbf{\Theta}^{*\mathbf{T}} \left(\mathbf{\Phi_i} - \sum_{k=1}^{i-1} \frac{\partial \alpha_{i-1}}{\partial x_k} \mathbf{\Phi_k} \right) - \sum_{k=1}^{i-1} \frac{\partial \alpha_{i-1}}{\partial y_r^{(k-1)}} y_r^{(k)} - \frac{\partial \alpha_{i-1}}{\partial \hat{\mathbf{\Theta}}} \dot{\hat{\mathbf{\Theta}}}. \tag{2.26}$$

The virtual-control input α_i is chosen as

$$\begin{aligned} \alpha_i = &-z_{i-1} - c_i z_i + \sum_{k=1}^{i-1} \frac{\partial \alpha_{i-1}}{\partial x_k} x_{k+1} - \hat{\mathbf{\Theta}}^{\mathbf{T}} \left(\mathbf{\Phi_i} - \sum_{k=1}^{i-1} \frac{\partial \alpha_{i-1}}{\partial x_k} \mathbf{\Phi_k} \right) + \sum_{k=1}^{i-1} \frac{\partial \alpha_{i-1}}{\partial y_r^{(k-1)}} y_r^{(k)} \\ &+ \frac{\partial \alpha_{i-1}}{\partial \hat{\mathbf{\Theta}}} \mathbf{\Gamma} \vartheta_{\mathbf{i}} + \sum_{k=2}^{i-1} z_k \frac{\partial \alpha_{k-1}}{\partial \hat{\mathbf{\Theta}}} \mathbf{\Gamma} \left(\mathbf{\Phi_i} - \sum_{j=1}^{i-1} \frac{\partial \alpha_{i-1}}{\partial x_j} \mathbf{\Phi_j} \right) \end{aligned} \tag{2.27}$$

where c_i is a positive constant and $\vartheta_{\mathbf{i}}$ is the $i-th$ tuning function defined as

$$\vartheta_{\mathbf{i}} = \vartheta_{\mathbf{i-1}} + \left(\mathbf{\Phi_i} - \sum_{k=1}^{i-1} \frac{\partial \alpha_{i-1}}{\partial x_k} \mathbf{\Phi_k} \right) z_i. \tag{2.28}$$

To stabilize $(z_1, z_2, \ldots z_i)$-subsystem, the Lyapunov function V_i is selected as,

$$V_i = V_{i-1} + \frac{1}{2} z_i^2 \tag{2.29}$$

and using (2.26) the derivative of V_i can be found as

$$\dot{V}_i = -\sum_{k=1}^{i} c_k z_k^2 + z_i z_{i+1} + \tilde{\mathbf{\Theta}}^{\mathbf{T}} \left(\vartheta_{\mathbf{i}} - \mathbf{\Gamma}^{-\mathbf{1}} \dot{\hat{\mathbf{\Theta}}} \right) + \left(\sum_{k=2}^{i} z_2 \frac{\partial \alpha_{k-1}}{\partial \hat{\mathbf{\Theta}}} \right) \left(\mathbf{\Gamma} \vartheta_{\mathbf{i}} - \dot{\hat{\mathbf{\Theta}}} \right). \tag{2.30}$$

Step n: The last error variable at the n-th step is chosen as

$$z_n = x_n - y_r^{(n-1)} - \alpha_{n-1}. \tag{2.31}$$

Subsequently, the time derivative of z_n is calculated as

$$\dot{z}_n = \Phi_0 + \beta u - \sum_{k=1}^{n-1} \frac{\partial \alpha_{n-1}}{\partial x_k} x_{k+1} + \mathbf{\Theta^{*T}} \left(\mathbf{\Phi_n} - \sum_{k=1}^{n-1} \frac{\partial \alpha_{n-1}}{\partial x_k} \mathbf{\Phi_k} \right) - \sum_{k=1}^{n-1} \frac{\partial \alpha_{n-1}}{\partial y_r^{(k-1)}} y_r^{(k)} - y_r^{(n)} - \frac{\partial \alpha_{n-1}}{\partial \hat{\mathbf{\Theta}}} \dot{\hat{\mathbf{\Theta}}}. \tag{2.32}$$

Finally, the control input u is expressed as,

$$u = \frac{1}{\beta} \left(\alpha_n + y_r^{(n)} \right) \tag{2.33}$$

with

$$\begin{aligned} \alpha_n = & -z_{n-1} - c_n z_n - \Phi_0 + \sum_{k=1}^{n-1} \frac{\partial \alpha_{n-1}}{\partial x_k} x_{k+1} - \hat{\mathbf{\Theta}}^{\mathbf{T}} \left(\mathbf{\Phi_n} - \sum_{k=1}^{n-1} \frac{\partial \alpha_{n-1}}{\partial x_k} \mathbf{\Phi_k} \right) \\ & + \sum_{k=1}^{n-1} \frac{\partial \alpha_{n-1}}{\partial y_r^{(k-1)}} y_r^{(k)} + \frac{\partial \alpha_{n-1}}{\partial \hat{\mathbf{\Theta}}} \mathbf{\Gamma} \vartheta_\mathbf{n} + \sum_{k=2}^{n-1} z_k \frac{\partial \alpha_{k-1}}{\partial \hat{\mathbf{\Theta}}} \mathbf{\Gamma} \left(\mathbf{\Phi_n} - \sum_{j=1}^{n-1} \frac{\partial \alpha_{n-1}}{\partial x_j} \mathbf{\Phi_j} \right) \end{aligned} \tag{2.34}$$

where c_n is a positive constant and ϑ_n is given by,

$$\vartheta_\mathbf{n} = \vartheta_{\mathbf{n-1}} + \left(\mathbf{\Phi_n} - \sum_{k=1}^{n-1} \frac{\partial \alpha_{n-1}}{\partial x_k} \mathbf{\Phi_k} \right). \tag{2.35}$$

Now, defining the Lyapunov function at the n-th step as,

$$V_n = V_{n-1} + \frac{1}{2} z_n^2 \tag{2.36}$$

the time derivative of V_n is calculated as,

$$\dot{V}_n = -\sum_{k=1}^{n} c_k z_k^2 + \tilde{\mathbf{\Theta}}^{\mathbf{T}} \left(\vartheta_\mathbf{n} - \mathbf{\Gamma^{-1}} \dot{\hat{\mathbf{\Theta}}} \right) + \left(\sum_{k=2}^{n} z_k \frac{\partial \alpha_{k-1}}{\partial \hat{\mathbf{\Theta}}} \right) \left(\mathbf{\Gamma} \vartheta_\mathbf{n} - \dot{\hat{\mathbf{\Theta}}} \right). \tag{2.37}$$

By taking the parameter update law as $\dot{\hat{\mathbf{\Theta}}} = \mathbf{\Gamma} \vartheta_\mathbf{n}$ and its substitution in (2.37) leads to

$$\dot{V}_n = -\sum_{k=1}^{n} c_k z_k^2 < 0. \tag{2.38}$$

The negative definiteness of $\dot{V}_n$ proves the asymptotic stability of the tracking error variables z_i, $i = 1, \ldots, n$ and boundedness of parameter estimation error $\tilde{\mathbf{\Theta}}$. Thus, the control objective defined prior to the design procedure is fruitfully met. In what follows next, this technique is utilized as a potential methodology in the context of DC-DC buck converters and eventually, its benefits are realized for the application intended.

2.3 DC-DC Buck Converter with Resistive Load

The circuit of an ideal DC-DC buck converter feeding a resistive load R is shown in Figure 2.1. During the ON and OFF modes of switch S_w, the functioning of the DC-DC buck converter is illustrated in Figure 2.2. Proceeding to derive the state space model of the DC-DC buck converter, let

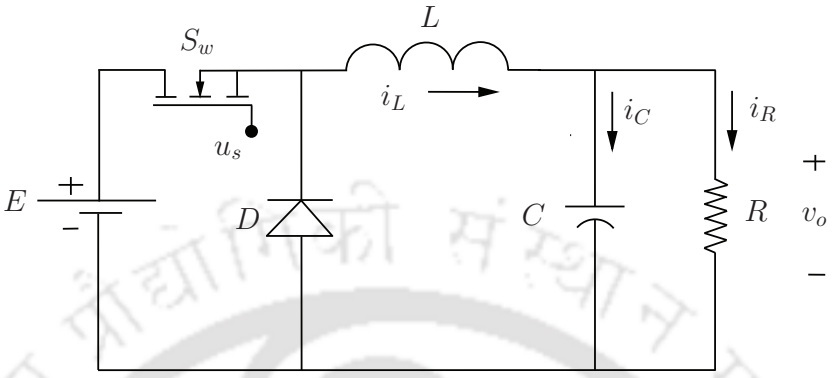

Figure 2.1: Circuit topology of DC-DC buck converter

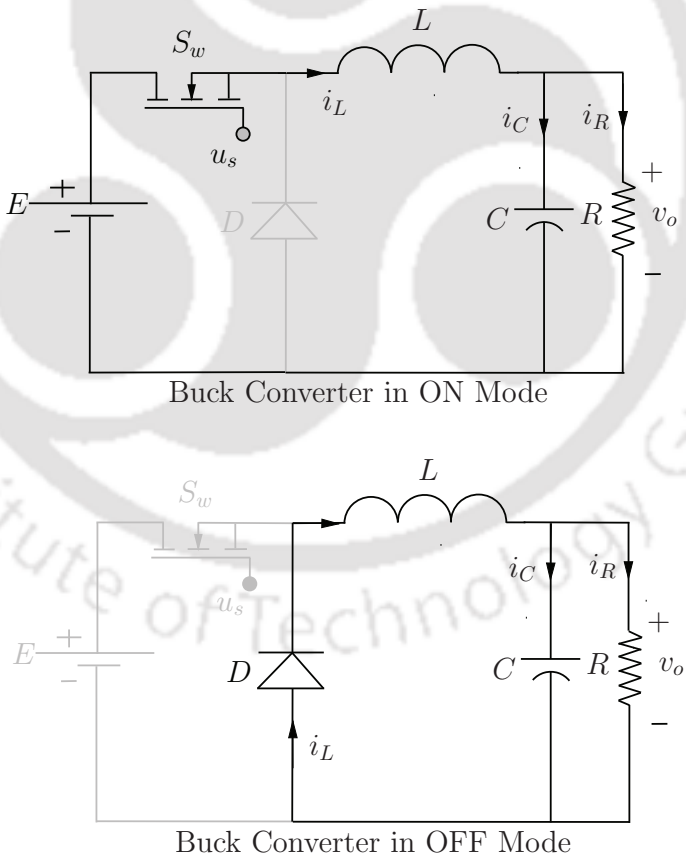

Figure 2.2: Functioning of of DC-DC buck converter

the states of the converter be defined as $x_1 = v_o$ and $x_2 = i_L$ where v_o and i_L denote the output

voltage across the load resistor R and current through the inductor L. By assuming the operation of the DC-DC buck converter in continuous conduction mode (CCM) and applying Kirchoff's voltage and current law, the state-space model is obtained as

$$\dot{x}_1 = -\frac{x_1}{RC} + \frac{x_2}{C} \tag{2.39}$$

$$\dot{x}_2 = -\frac{x_1}{L} + \frac{u_s E}{L}. \tag{2.40}$$

The model in (2.39)-(2.40) is usually referred to as *switched* DC-DC buck converter model where u_s is the switching control input signal, representing the position of the switch S_w. Further, $u_s = 0$ denotes open position of switch S_w and $u_s = 1$ denotes closed position of switch S_w.
In order to derive the feedback control law, an *average* model of the DC-DC buck converter is necessary and is obtained exactly in the same manner as described in model (2.39)-(2.40), except replacing the switched control u_s with an average control u residing within the compact set $u \in [0, 1]$ [70–72]. Hence, the state-space model is rewritten as,

$$\dot{x}_1 = -\frac{x_1}{RC} + \frac{x_2}{C} \tag{2.41}$$

$$\dot{x}_2 = -\frac{x_1}{L} + \frac{uE}{L}. \tag{2.42}$$

The above model enables us to formulate the feedback control law of DC-DC buck converters operating in CCM in order to obtain a faithful tracking of output voltage v_o around the desired DC voltage v_r with a wide range of operating points, besides yielding a promising transient performance and an acceptable inductor current response, while respecting the design constraints.

2.3.1 Adaptive Backstepping Control Design for DC-DC Buck Converters

As mentioned in the introduction, the backstepping control methodology, when applied to DC-DC buck converters, results in a control law with inherent voltage and current mode control benefits, leading to an improved output voltage tracking performance. However, in the event of unknown load change, the output voltage tracking performance may deteriorate unless a corrective action is taken online to compensate for such uncertainties. In these circumstances, adaptive control can be useful to maintain an acceptable output voltage tracking despite wide variations in load conditions. As such, an adaptive backstepping control is proposed to retain the benefits of backstepping control, at the same time to improve start up and transient performance by incorporating the traits of adaptive learning.
In (2.41), the load resistance R is assumed as an unknown quantity which often varies over time. Therefore, the term x_1/R is treated as an uncertain term and is linearly parameterized as ${\Theta^*}^T\Phi$, where Θ^* is the true value of the reciprocal of the unknown load in a particular interval of time and $\Phi = x_1$ represents the regressor. Replacing x_1/R in (2.41) with ${\Theta^*}^T\Phi$ yields

$$\dot{x}_1 = -\frac{{\Theta^*}^T\Phi}{C} + \frac{x_2}{C}. \tag{2.43}$$

Proceeding with the control synthesis, let the first error variable z_1 be defined as,

$$z_1 = x_1 - v_r \tag{2.44}$$

where v_r is the reference output voltage. Considering the second error variable as

$$z_2 = (x_2/C) - \alpha - \dot{v}_r \tag{2.45}$$

with α as the virtual-control input, the tracking error dynamics of the first z_1-subsystem are described as,

$$\dot{z}_1 = z_2 + \alpha - \frac{\Theta^{*^T}\Phi}{C}. \tag{2.46}$$

To stabilize the z_1-subsystem, the pseudo control input or rather the virtual-control is chosen as,

$$\alpha = -c_1 z_1 + \frac{\hat{\Theta}^T\Phi}{C}. \tag{2.47}$$

Hence, c_1 is the controller gain and $\hat{\Theta}$ denotes adaptive estimate of the uncertain parameter $\Theta^* = 1/R$. This leads to the dynamics of z_2, found by taking derivative of (2.45) and using (2.42), (2.47) yields

$$\dot{z}_2 = -\frac{x_1}{LC} - \sum_{k=1}^{2}\frac{\partial\alpha}{\partial x_k}\dot{x}_k - \sum_{k=0}^{1}\frac{\partial\alpha}{\partial {v_r}^{(k)}}{v_r}^{(k+1)} - \dot{\hat{\Theta}}^T\frac{\partial\alpha}{\partial\hat{\Theta}^T} + \frac{E}{LC}u. \tag{2.48}$$

Thus, (2.48) provides the direction to formulate the final control input u in such a way that it must stabilize the error variable z_2. Therefore, the final control input u is found to be

$$u = \frac{LC}{E}\left[-c_2 z_2 - z_1 + \frac{x_1}{LC} + \frac{\partial\alpha}{\partial x_1}\left(\frac{x_2}{C}\right) - \hat{\Theta}^T\frac{\partial\alpha}{\partial x_1}\frac{\Phi}{C} + \sum_{k=0}^{1}\frac{\partial\alpha}{\partial v_r^{(k)}}v_r^{(k+1)} - \frac{\partial\alpha}{\partial\hat{\Theta}}\gamma\vartheta_2(z_1, z_2)\right] \tag{2.49}$$

where c_2 is the controller gain, γ defines the adaptive rate parameter and $\vartheta_2 = \vartheta_1 + \frac{\partial\alpha}{\partial x_1}\frac{\Phi}{C}z_2$, $\vartheta_1 = -\frac{\Phi}{C}z_1$. The design procedure and the additional terminologies introduced would be clear when the stability is analyzed in the succeeding section. The unknown parameter $\hat{\Theta}$ is estimated online using the learning law

$$\dot{\hat{\Theta}} = -\frac{\gamma}{C}\left[\Phi\left(z_1 - \frac{\partial\alpha}{\partial x_1}z_2\right)\right] \tag{2.50}$$

where $\gamma > 0$ is the rate of adaptation.

2.3.2 Stability Analysis

In this section, the convergence properties of the tracking error variables are analyzed. Also, stability analysis of the adaptive law based parameter estimation and system states is conducted. The stability analysis is carried out in a stepwise procedure as follows. Firstly, the Lyapunov function V_1 is chosen as

$$V_1 = \frac{1}{2}z_1^2 + \frac{1}{2}\tilde{\Theta}^T\gamma^{-1}\tilde{\Theta} \tag{2.51}$$

where $\tilde{\Theta} = \Theta^* - \hat{\Theta} \Rightarrow \dot{\tilde{\Theta}} = \dot{\Theta}^* - \dot{\hat{\Theta}} = -\dot{\hat{\Theta}}$ since Θ^* is a constant gain. Taking time derivative of (2.51) yields

$$\dot{V}_1 = z_1 \dot{z}_1 - \tilde{\Theta}^T \gamma^{-1} \dot{\hat{\Theta}}. \tag{2.52}$$

Using (2.43)-(2.47) and (2.50) in (2.52) yields

$$\dot{V}_1 = -c_1 z_1^2 + z_1 z_2 - \tilde{\Theta}^T \left(\gamma^{-1} \dot{\hat{\Theta}} + \frac{\Phi z_1}{C} \right). \tag{2.53}$$

To avoid overparametrization, instead of finding the parameter update law as $\dot{\hat{\Theta}} = -\frac{\gamma}{C}\Phi z_1$, $\vartheta_1(z_1) = \frac{\Phi z_1}{C}$ is used. Hence,

$$\dot{V}_1 = -c_1 {z_1}^2 + z_1 z_2 - \tilde{\Theta}^T \left(\gamma^{-1} \dot{\hat{\Theta}} + \vartheta_1(z_1) \right). \tag{2.54}$$

Establishing the stability of z_2 requires defining another Lyapunov function V_2 as

$$V_2 = \frac{1}{2} z_2^2. \tag{2.55}$$

Taking the time derivative of V_2 and using (2.48) yields,

$$\dot{V}_2 = z_2 \left(-\frac{x_1}{LC} - \frac{\partial \alpha}{\partial x_1} \left(-\frac{\Theta^{*T}\Phi}{C} + \frac{x_2}{C} \right) - \sum_{k=0}^{1} \frac{\partial \alpha}{\partial {v_r}^{(k)}} y_r^{(k+1)} - \dot{\hat{\Theta}}^T \frac{\partial \alpha}{\partial \hat{\Theta}^T} + \frac{E}{LC} u \right) \tag{2.56}$$

or,

$$\dot{V}_2 = z_2 \left(-\frac{x_1}{LC} - \frac{\partial \alpha}{\partial x_1} \left(\frac{x_2}{C} \right) + \frac{\partial \alpha}{\partial x_1} \frac{\Theta^{*T}\Phi}{C} - \sum_{k=0}^{1} \frac{\partial \alpha}{\partial v_r^{(k)}} v_r^{(k+1)} - \dot{\hat{\Theta}}^T \frac{\partial \alpha}{\partial \hat{\Theta}^T} + \frac{E}{LC} u \right) \tag{2.57}$$

Further, (2.57) and (2.54) would be required for subsequent analysis of system stability. Now to prove closed loop stability of the converter under the action of the control law (2.49), the total Lyapunov function V is considered as

$$V = V_1 + V_2 = \frac{1}{2}\mathbf{z^T z} + \frac{1}{2}\tilde{\Theta}^T \gamma^{-1} \tilde{\Theta} \tag{2.58}$$

$$\begin{aligned} \dot{V} &= z_1 \dot{z}_1 + z_2 \dot{z}_2 - \tilde{\Theta}^T \gamma^{-1} \dot{\hat{\Theta}} \\ &= -c_1 z_1^2 + z_1 z_2 - \tilde{\Theta}^T \left(\gamma^{-1} \dot{\hat{\Theta}} + \vartheta_1(z_1) \right) - \frac{z_2 x_1}{LC} - z_2 \frac{\partial \alpha}{\partial x_1} \frac{x_2}{C} + z_2 \frac{\partial \alpha}{\partial x_1} \frac{\Theta^{*T}\Phi}{C} \\ &\quad - z_2 \sum_{k=0}^{1} \frac{\partial \alpha}{\partial v_r^{(k)}} v_r^{(k+1)} - z_2 \hat{\Theta}^T \frac{\partial \alpha}{\partial \hat{\Theta}^T} + \frac{E}{LC} u - \tilde{\Theta}^T \gamma^{-1} \dot{\hat{\Theta}} \end{aligned} \tag{2.59}$$

where $\mathbf{z} = [z_1 \;\; z_2]^T$ and the parameter estimation error $\tilde{\Theta} := \Theta^* - \hat{\Theta}$. On substituting u from (2.49) in $\dot{V}$ yields

$$\dot{V} = -c_1 z_1^2 - c_2 z_2^2 + \tilde{\Theta}^T \left(-\vartheta_2(z_1, z_2) - \gamma^{-1} \dot{\hat{\Theta}} \right) z_2 + \frac{\partial \alpha}{\partial \hat{\Theta}} \left(-\gamma_2 \vartheta_2(z_1, z_2) - \dot{\hat{\Theta}} \right) z_2. \tag{2.60}$$

Further, using the adaptation law $\hat{\Theta}$ from (2.50) reduces to,

$$\dot{V} \leq -c_1 z_1^2 - c_2 z_2^2 \leq - \begin{bmatrix} z_1 & z_2 \end{bmatrix} \begin{bmatrix} c_1 & 0 \\ 0 & c_2 \end{bmatrix} \begin{bmatrix} z_1 \\ z_2 \end{bmatrix} \leq 0. \tag{2.61}$$

Hence, from (2.61), $\dot{V}$ is concluded to be negative semi-definite implying closed loop asymptotic stability of $\mathbf{z}$. However, proving asymptotic stability of the tracking error vector z requires the following condition, $\dot{V} = 0 \Leftrightarrow \mathbf{z} = 0$, to be satisfied. Now from (2.61), it is found that since $c_1, c_2 > 0$, the matrix involving c_1 and c_2 is positive definite. Therefore $\dot{V} = 0$ is attained only when $\mathbf{z} = 0$. Hence, from these arguments, it is inferred that $\dot{V}$ is negative definite i.e, $\dot{V} < 0$. Therefore, the origin $(z_1, z_2) = (0, 0)$ is the only largest positively invariant set. Therefore, by LaSalle's theorem [41], the system is globally asymptotically closed loop stable. The block diagrammatic representation of the proposed control scheme is shown in Figure 2.3. However, it must be highlighted here that the gate signal fed to switch S_w as u_s is obtained by generating a discontinuous control through the PWM block using a fixed frequency triangular carrier wave V_{tri}.

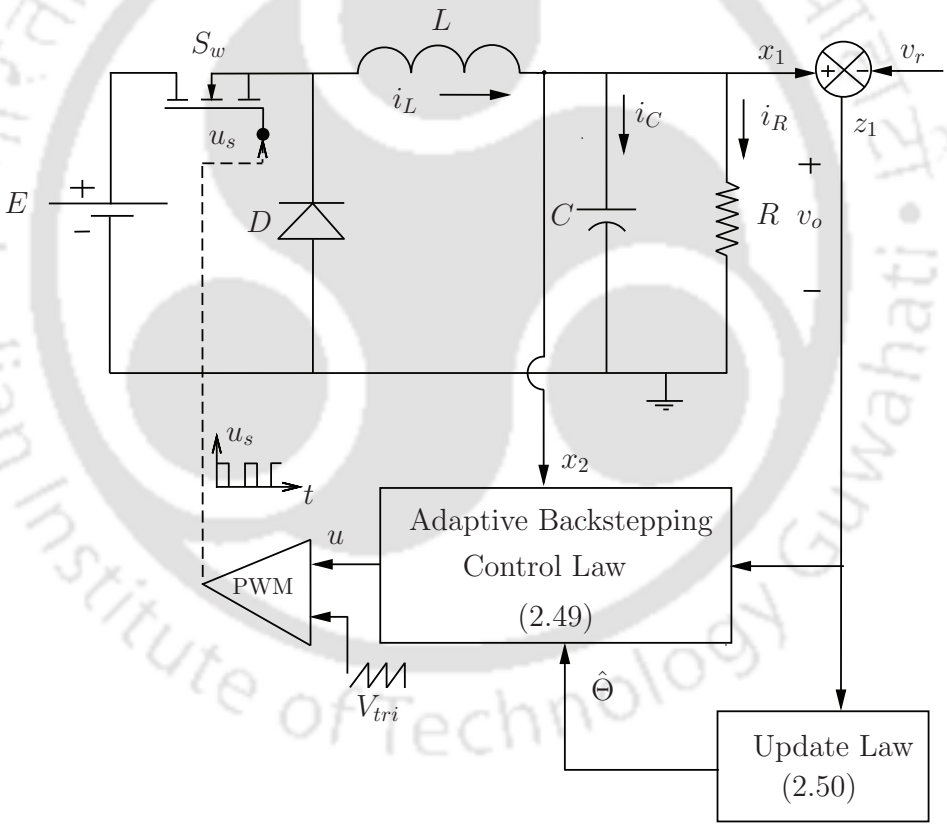

Figure 2.3: Schematic diagram of adaptive backstepping control scheme for DC-DC buck converter

2.3.3 Simulation Results and Discussion

Referring to the DC-DC buck converter in Figure 2.1, the converter parameters adopted for evaluating the control performance are given in Table 2.1.

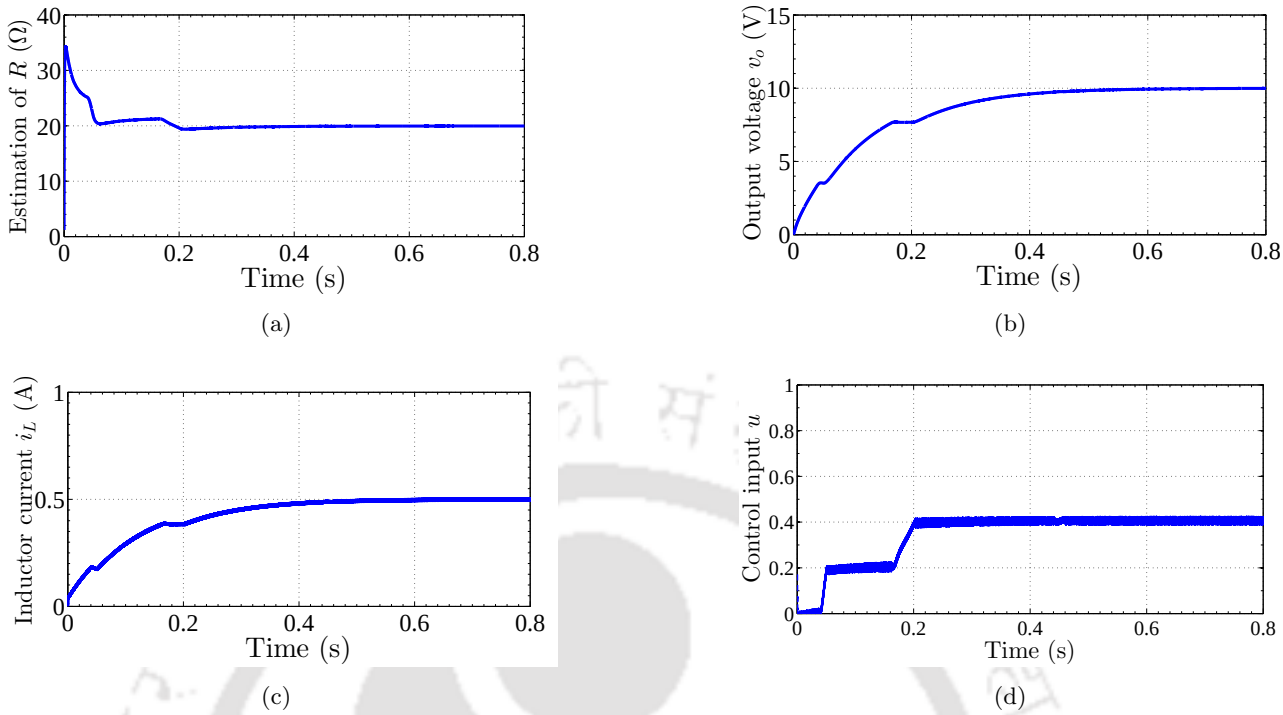

Figure 2.4: Simulated response curves of DC-DC buck converter under ABSC scheme during start-up: (a) estimation of unknown load, (b) output voltage, (c) inductor current and (d) control input.

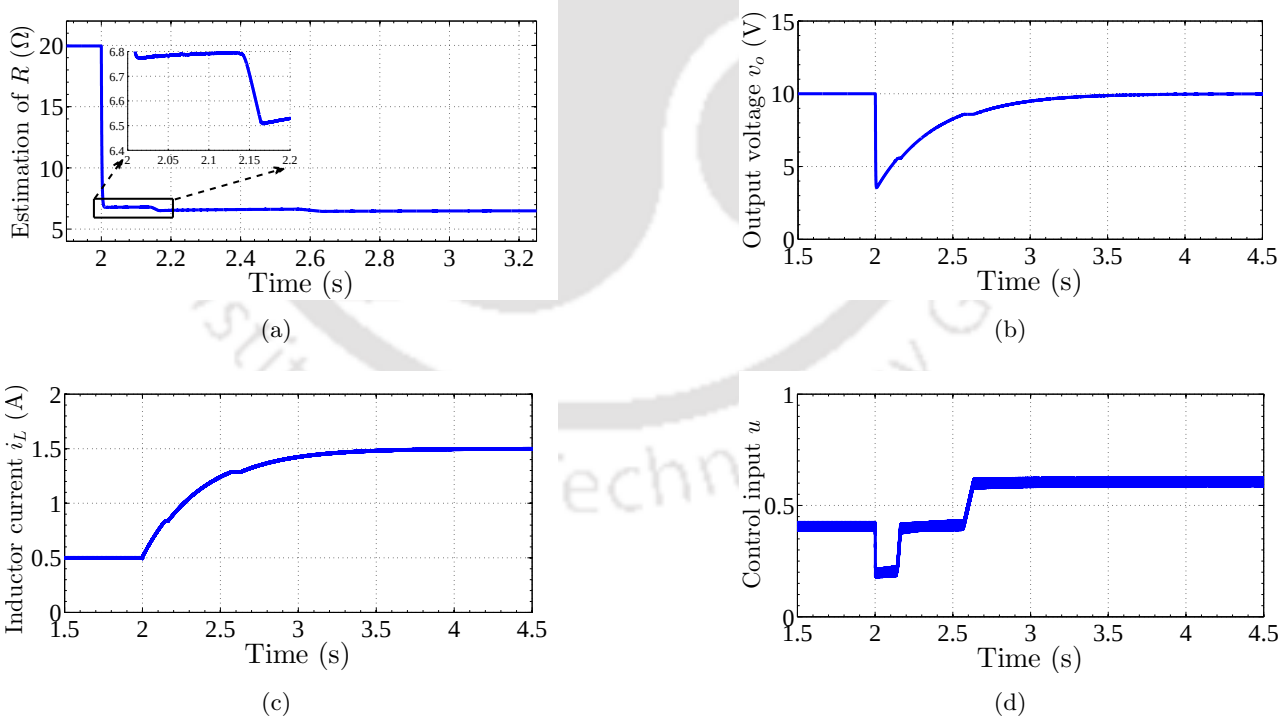

Figure 2.5: Simulated response curves of DC-DC buck converter under ABSC scheme during load resistance R change from 20Ω to 6.66Ω at $t = 2s$: (a) estimation of unknown load, (b) output voltage, (c) inductor current and (d) control input.

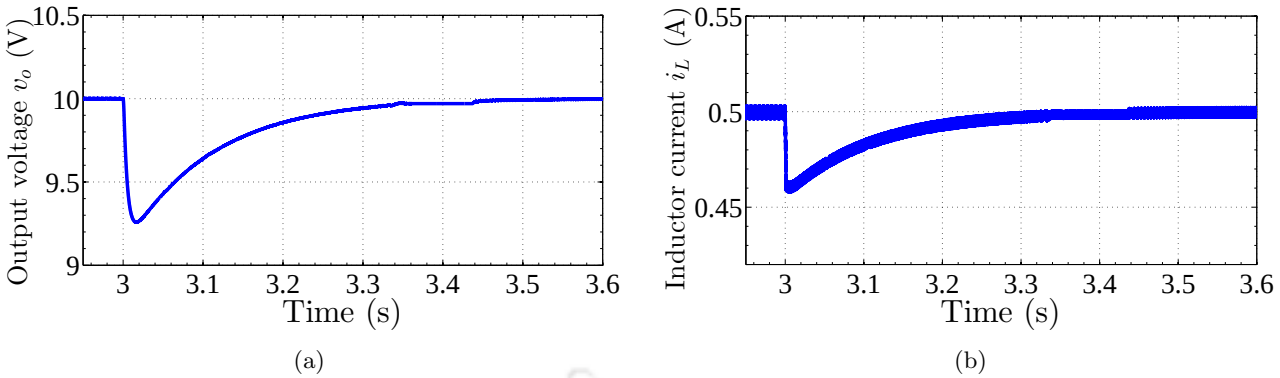

(a) (b)

Figure 2.6: Simulated response curves of DC-DC buck converter under ABSC scheme during input voltage E change from $25V$ to $17V$ at $t = 3s$: (a) output voltage and (b) inductor current.

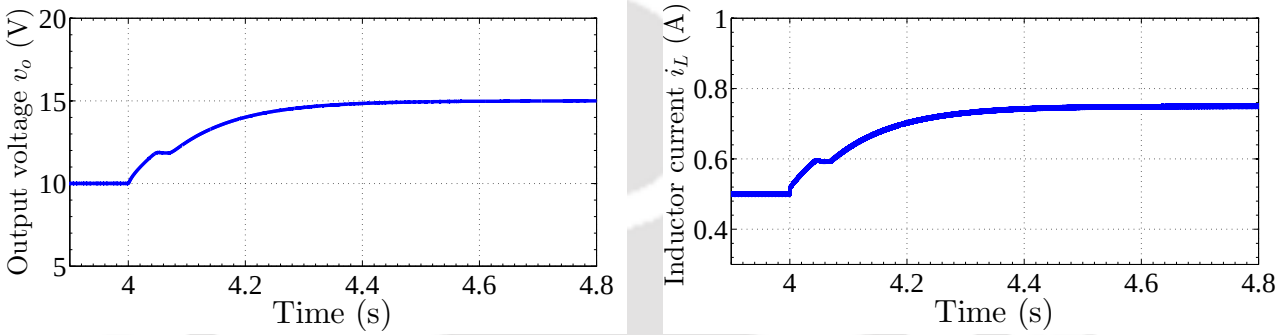

(a) (b)

Figure 2.7: Simulated response curves of DC-DC buck converter under ABSC scheme during reference voltage v_r change from $10V$ to $15V$ at $t = 4s$: (a) output voltage and (b) inductor current.

Table 2.1: Specifications of the DC-DC buck converter

Parameter	Value
Input voltage, E	$25V$
Filter inductance, L	$59mH$
Filter capacitance, C	$220\mu F$
Nominal load resistance, R	20Ω
Reference output voltage, V_{ref}	$10V$
Switching frequency, f_s	$20KHz$

Remark 1. *Ideally in the DC-DC buck converter equipped with a closed loop control mechanism, the switch S_W must remain ON till the required output voltage is obtained. Thereby, only ON-mode of the converter exists as the buck converter model during start-up. During this ON-mode, the time constant as per the converter parameters listed in Table 2.1 is found to be $\tau = 2.95ms$. Further, calculating the settling time as 5τ, an ideal settling time (t_s) is found to be $14.75ms$. Besides, it is aimed at achieving no peak overshoot/undershoot during the converter performance.*

The adaptation rate is chosen as $\gamma = 9 \times 10^{-5}$ and gain parameters are selected as $c_1 = 2200$,

$c_2 = 15$.

The efficacy of the ABSC method in regulating the DC-DC buck converter output voltage has been investigated by simulating the converter in Matlab-Simulink environment with a step size of $50\mu s$. The response of the controller during start-up is shown in Figure 2.4. The plot in Figure 2.4 (a) shows the estimation of unknown load R during start-up. It is observed that the online estimation converges to the actual value of $R = 20\Omega$ in $0.25s$ and the output voltage v_o tracks the desired reference of $10V$ in $0.45s$ as shown in Figure 2.4 (b). Subsequently the responses of the inductor current i_L and the control input u are provided in Figure 2.4 (c) and Figure 2.4 (d) respectively.

Next, the response of the ABSC method is evaluated by abruptly perturbing the load current i_R with a step disturbance. The load resistance R is changed from nominal value of 20Ω to 6.66Ω and the response obtained is shown in Figure 2.5. It can be noticed in Figure 2.5 (a) that the ABSC method successfully estimates the perturbed load value of 6.66Ω in a time span of 0.2s. Figure 2.5 (b) exhibits an undershoot of 50% in v_o prior to reaching back to its desired value of $10V$ in $1.5s$. The relevant inductor current i_L and control input u profiles are shown in Figure 2.5 (c) and Figure 2.5 (d) respectively. The inductor current i_L is observed to be a smooth profile without any overshoot.

Further, the robustness of the ABSC method is tested by subjecting the DC-DC buck converter to a step change in input voltage E from nominal $25V$ to $17V$ at $t = 3s$ as shown in Figure 2.6. The responses of v_o and i_L show a settling time of $0.5s$ to reach the desired operating point.

Lastly, the robustness of the DC-DC buck converter using the ABSC is verified by suddenly changing the desired output voltage v_r in a step manner. The reference voltage v_r is changed from its nominal magnitude of $10V$ to $15V$ and the response recorded is provided in Figure 2.7. The obtained results demonstrate the ability of the proposed ABSC control scheme in yielding a successful tracking of reference output voltage in $0.5s$.

2.3.4 Experimental Investigation

To realize the performance of adaptive backstepping control scheme in real time, a prototype of DC-DC buck converter feeding resistive load is fabricated in the laboratory. The specifications of the converter used in the experimentation is provided in Table 2.1. Prior to the discussion on experimental results, each of the hardware components utilized in the fabrication of the DC-DC buck converter and its control circuit are described for clarity.

2.3.4.1 Hardware description

The functional block diagram for implementing the ABSC control implementation for a DC-DC buck converter is shown in Figure 2.8. A prototype of DC-DC buck converters is fabricated in the laboratory as shown in Figure 2.9. Hardware components used in the experimentation process are explained briefly below.

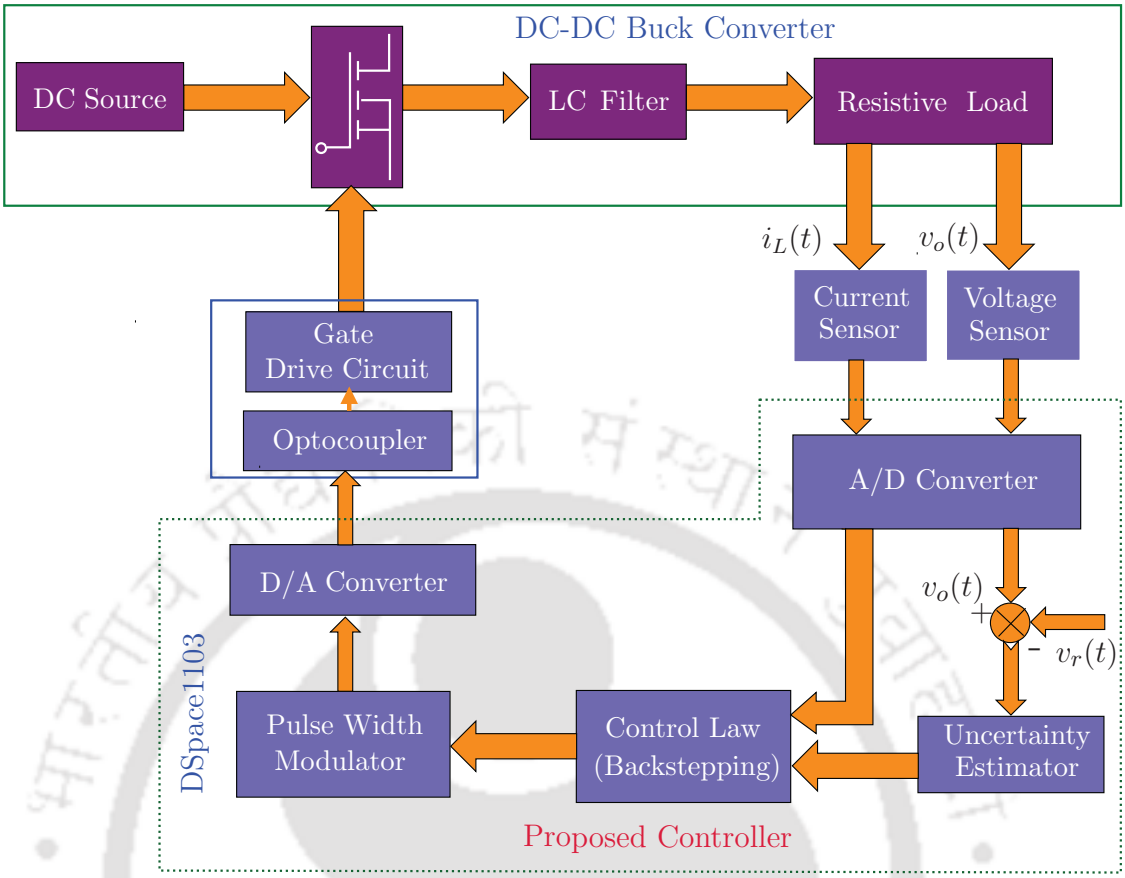

Figure 2.8: Functional block diagram of the ABSC implementation in DC-DC buck converter.

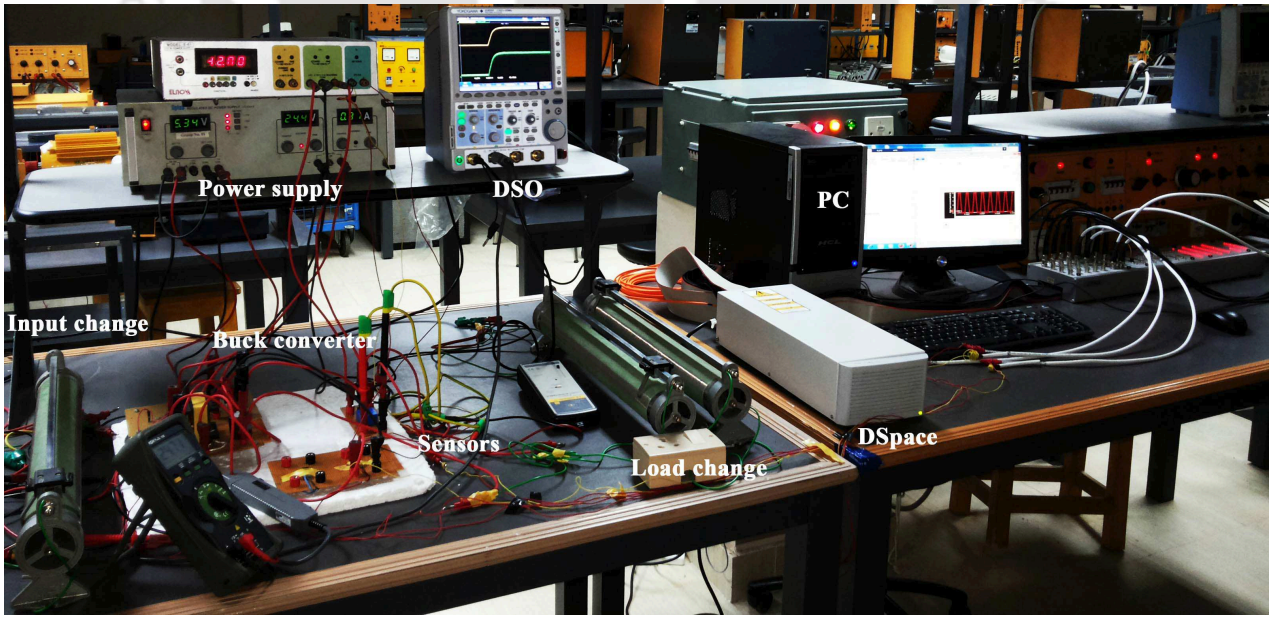

Figure 2.9: Experimental set-up of DC-DC buck converter.

DC-DC buck converter

- *Power MOSFET*: An N-Channel Power MOSFET IRFP460 is used as a control switching device in the DC-DC buck converter. It is a product of Fairchild manufacturers having a current rating of $20A$, voltage rating of $500V$ and on state Drain to Source resistance r_{DS} of 0.270Ω. It operates with a Gate to Source voltage $V_{GS} = 20V$.

- *Diode*: The diode used for freewheeling purpose is 6A4 MIC manufactured by MIC Group Rectifiers. Its maximum average forward rectified current is $6A$ and maximum repetitive peak reverse voltage is $400V$. Further, its maximum DC blocking voltage limit is $400V$.

- *Input voltage source*: Input voltage is taken from Aplab Regulated DC Power Supply. It can provide voltage in the range $0 - 32V$ with $0 - 2A$ current output. Additionally it can provide voltages $\pm 15V$ and $+5V$, which can be used to power the voltage and current sensors.

Measuring Instruments

- *Digital storage oscilloscope*: A YOKOGAWA manufactured DLM2054 with 500MHz frequency mixed signal digital storage oscilloscope is used to record the real time response. It has 4 channels for simultaneous sensing of voltage/current signals.

- *Voltage transducer*: Voltage sensor LV 25-P by LEM Manufacturer is used for sensing the output voltage across the load. It permits nominal rms primary current I_{PN} of $10mA$ and nominal rms primary voltage upto $500V$.

- *Current sensor*: For the purpose of inductor current sensing, ACS-712T from Allegro MicroSystems is utilized. This is a fully integrated, Hall effect based linear current sensor IC. It has an internal resistance of $1.2m\Omega$ during conduction. It works with a DC supply of $5V$. It offers a precise and low-offset current sensing mechanism. The Hall circuit is provided with a conduction path made of copper and it is located near the surface of the die. This helps in creating a magnetic field when there is current sensing through this copper path. This magnetic field helps in converting the current to a proportional voltage.

- *Voltage measuring probe*: A YOKOGAWA manufactured 700924 differential voltage probe is used to measure the real-time output voltage. It has frequency bandwidth of 100 MHz and maximum permissible continuous input voltage range is $1400V$ with output offset voltage of $\pm 7.5mV$.

- *Current measuring probe*: Measurement of real-time current is done by using a YOKOGAWA manufactured current probe 701932 with 100 MHz as frequency bandwidth. It allows a maximum continuous allowable input current of $30A$.

Control Equipments

The controller has been implemented using DS1103 PPC Controller board. It provides a floating point platform and facilitates an easy conversion of the control algorithm in C language for further execution in real-time.

- *DS1103 PPC controller board*: This generates an executable object code for processor. It is a single-board with comprehensive I/O and real-time processor. The controller has been simulated in Simulink and using MATLAB to DSP real-time interface the controller is executed. It uses a built-in unit of Texas Instruments DSP board TM320F240 for computation purpose. A brief mention of its peripherals is given below.
  - *TMS320F240 DSP*: It is a 16-bit fixed point digital signal processor (DSP). The analog to digital converter (ADC) can perform conversions within $6.1\mu s$. It includes the T320C2xLP Core CPU with an application memory of 32 MB.
  - *Analog to Digital Converters (ADC)*: ADCs are provided with 16 multiplexed channels equipped with 4 sample and hold circuitry. It has 8 ADC sampler channels (4 multiplexed and 4 parallel) for simultaneous sampling. Its resolution is 16-bit and requires input voltage of $\pm 10V$.
  - *Digital to Analog Converters (DAC)*: DACs are present in 8 channels with resolution of 16-bit each and output voltage range of $\pm 10V$.
  - Serial interface is available with RS232/RS422 compatibility. In this work RS 232 has been made use of.
  - Clock rate of the processor is $20MHz$.
- *Optocoupler*: It is a well known fact that the power circuitry and the control circuitry need to be isolated from each other for safety reasons. Isolation is required to prevent ground loops sharing a common return path. It is most likely that due to any fault, a high current flow from power circuit may damage the control circuitry. In this work IC HPCL-2611 is used for isolating purpose. This optocoupler works at a high speed of 10 Mbit/s. It has single-channel circuit which is optically connected to a high speed photodetector logic gate.
- *Gate drive circuit (GDC)*: In order to finally operate the power switch with PWM, the gate pulse produced by the controller needs to be processed through a gate drive circuit. The GDC assists in amplifying the control pulses from a low-power to a high-power signal thereby providing an adequate signal strength to drive the power switch S_w. Gate drive IC IR 2110 is used in this work. It is a high voltage and high speed driver. It generates a gate voltage ranging from $10V - 20V$. Besides, it produces output gate current upto $2A$. Further, it has fast turn-on and turn-off time periods typically around $120ns$ and $94ns$ respectively.

2.3.4.2 Experimental Results and Discussion

The performance of the ABSC is evaluated on the experimental prototype by first injecting the disturbances at the load end. The load resistance is suddenly changed from 20Ω to 10Ω and again brought back from 10Ω to 20Ω, as a consequence of which the load current is perturbed from $0.5A$ to $1.0A$ and again from $1.0A$ to $0.5A$. The performance exhibited by the ABSC is shown in Figure 2.10 (a). It is observed that the ABSC method takes $7s$ to track the set $10V$ with an undershoot of $5V$,

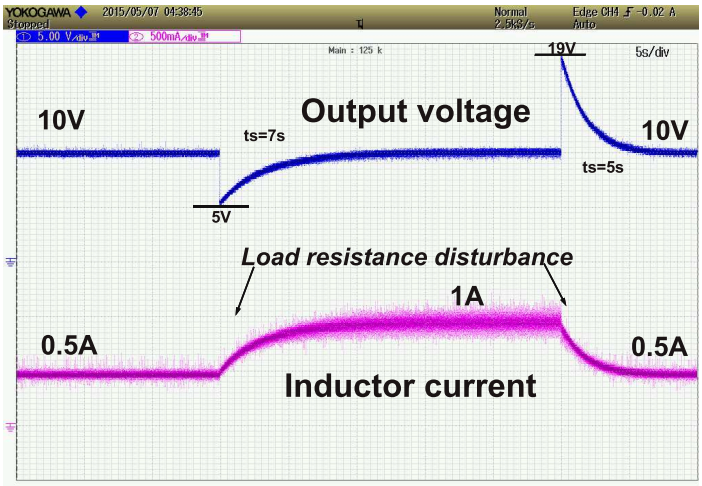

(a)

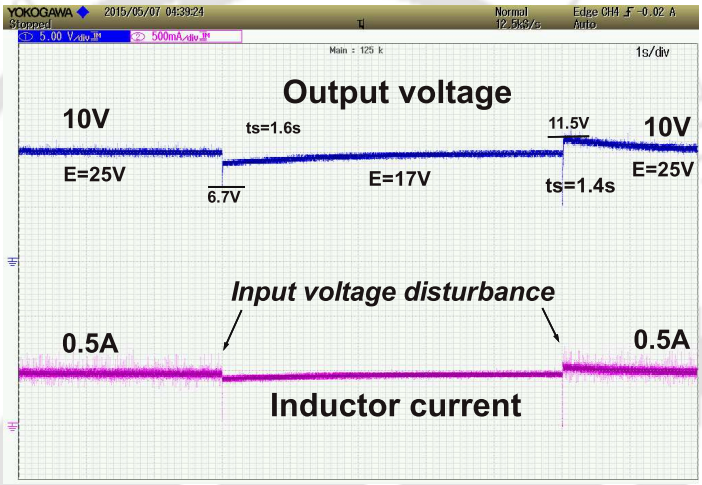

(b)

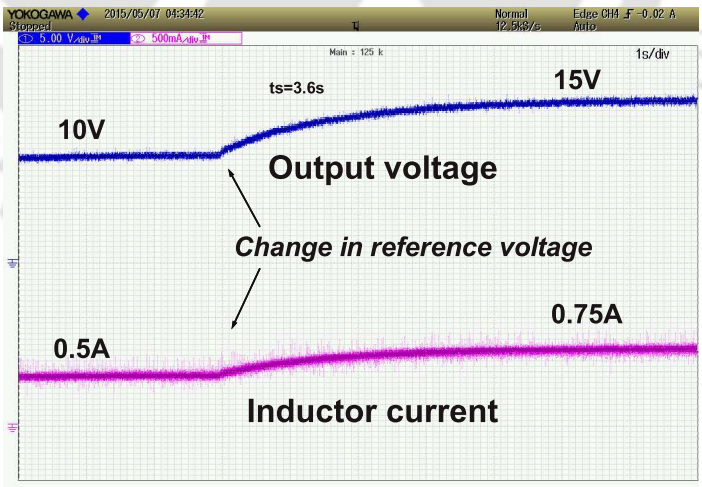

(c)

Figure 2.10: Experimental response curves of DC-DC buck converter under ABSC scheme during: (a) load resistance R change from 20Ω to 10 Ω and vice-versa (scale: x-axis; time (5s/div), y-axis: voltage (5V/div), current (500mA/div)); (b) input voltage E change from $25V$ to $17V$ and vice-versa (scale: x-axis; time (1s/div), y-axis: voltage (5V/div), current (500mA/div)); and (c) reference voltage v_r change from $10V$ to $15V$ (scale: x-axis; time (1s/div), y-axis: voltage (5V/div), current (500mA/div))

during loading from 20Ω to 10Ω. Similarly during unloading from 10Ω to 20Ω ABSC method takes $5s$ to track the set $10V$ with an overshoot of $19V$. Meanwhile the peak-to-peak voltage ripple Δv_o under nominal condition is observed to be $0.68V$. Next, for studying the effectiveness of the ABSC scheme under changes in the input voltage, a disturbance mechanism is created in the input supply by connecting a 900Ω resistance in parallel to the supply and using as a potential divider circuit. The two different input levels are achieved with the help of single pole double throw (SPDT) switch. Change in input voltage E is made from nominal $25V$ to $17V$ and again from $17V$ to $25V$, and the performance of the ABSC technique is recorded as shown in the Figure 2.10 (b). It is observed that during E change from $25V$ to $17V$ the ABSC scheme tracks the desired v_o in $1.6s$ with an undershoot in v_o upto $6.7V$. Similarly, during E change from $17V$ to $25V$ the ABSC scheme tracks the desired v_o in $1.4s$ with an overshoot in v_o to $11.5V$.
Finally, to study the response of the proposed controller under reference voltage change, the DC-DC buck converter is subjected to change in reference tracking signal from nominal $10V$ to $15V$. The results are shown in Figure 2.10 (c). It is found that the ABSC method takes $3.6s$ to track the new trajectory of $15V$.

2.4 DC-DC Buck Converter Driven PMDC Motor

Machines are used in the industries mainly as electric drives and servo control systems. Generally, such machines include DC motors, permanent magnet brushless DC motors, and AC motors which encompass a wide range of applications. Although majority of such utilities involve ac motors, yet DC machines are undoubtedly popular due to their effectiveness and flexibility in responding to the requirement of a wide range of angular velocity control. Within DC motors, there exist series and shunt excitation types used for different torque and speed requirements in numerous applications like electrical locomotives, rolling mill, double-hulled tanker, electric-powered domestic devices, goods lifts, servo control, traction, high precision digital tools and robotics.
Consistent investigations have been underway since the last few decades to improve the robustness and precision of angular velocity control in DC motors under the influence of both intrinsic and extrinsic perturbations. Basic control schemes proposed initially suggest velocity control through armature voltage by hard switching of linear regulators [73]. However, such control schemes yield unsatisfactory dynamic response of both motor current and voltage, besides high energy dissipation and larger transformer size. Later on, with the subsequent development in the field of power electronics, the advent of effective switching devices made the velocity control problem of DC motors to take an interesting turn. Owing to the fact that DC-DC converters offer lesser internal losses and exhibit higher power conversion efficiency, the choice of DC-DC buck power converter has emerged as a replacement for linear regulators in the control of DC motors. The resultant cascaded combination of DC-DC buck converter and DC-motor is a fourth order nonlinear system, wherein the filter inductance and filter capacitance associated with the DC-DC buck converter perform the task of smoothing the armature current and voltage of the DC-motor with least ripple. Therefore the drawbacks of hard switching persisting in the linear regulators are circumvented. Such an arrangement of DC-DC buck converter driven DC-motor can be well utilized in applications seeking higher efficiency, enhanced tracking

accuracy along with a precise control action, for example in machine tools, medical equipments like x-ray and tomographic systems, gas turbines, sun trackers, antenna positioning, robotics, welding equipments, air pumps, material handling equipment, mining, conditioners, computer disc drives, circuit breakers, battery operated portable devices and other residential appliances [74–77]. Thus, in order to achieve a satisfactory velocity tracking in DC motors, the power electronic switch of the DC-DC converter must be operated accordingly for required armature voltage and current regulation with the least error possible, besides guaranteeing robustness towards uncertain loads. Hence, to achieve these aforementioned design objectives, various control strategies have been proposed in literature.

The conventional approach is followed by [78], wherein a linear controller is deployed based on a linear approximation technique of the actual nonlinear system around a specific equilibrium point. The results obtained are near satisfactory, provided the mathematical modeling is accurate. However, these methods show high vulnerability for parametric perturbations and external disturbances, hence the demand for high performance is difficult to be met. In addition, their stability cannot be ensured over wide dynamical regimes. As shown in [30], artificial intelligence based tuning algorithms for PI and PID controllers are independent of the mathematical model of the plant and show good performance in presence of parameter uncertainties and external disturbances though over a limited range. Nevertheless, the real time implementation of such controllers suffers from high computational burden due to their inherent complexity.

Other recent control techniques proposed in the literature for angular velocity control include sliding mode control [37, 75], passivity based control [46], fuzzy logic based control [79], neural network (NN) based control [80], combined neuro-fuzzy control [81], hierarchical control [47], $\mathcal{H}_\infty$ based control [48], active disturbance rejection and flatness-based control [49] and backstepping control [82].

An adaptive backstepping control technique can prove to be promising in achieving the desired control objectives while guaranteeing the stability of the entire closed-loop system. Recently, the work in [83], compared the response of DC-DC buck converter DC-motor combination for angular velocity tracking under the action of both PI and traditional backstepping control. However, only the start-up response is illustrated and the effects of load torque perturbations have not been examined. Further, the results are verified only through numerical simulations. A controller based on backstepping procedure has been designed in [84]. Both adaptive and nonadaptive techniques have been presented and the results are obtained through numerical simulations. In [85], adaptive backstepping control is developed by taking parametric uncertainties into consideration. However, the investigation conducted focussed only on theoretical simulations and lacked study on physical realization of the proposed control scheme on a real time DC-DC buck converter DC-motor combination.

In the subsections to follow, the ABSC method discussed in Section 2.2 will be extended to DC-DC buck converter driven permanent magnet direct current (PMDC)-motor problem and extensive experimentation will be carried out to evaluate its performance.

2.4.1 System Description

The cascaded combination of DC-DC buck converter and PMDC-motor [47] is shown in Figure 2.11. The DC-DC buck converter acts as a regulator to adjust the armature voltage of the DC

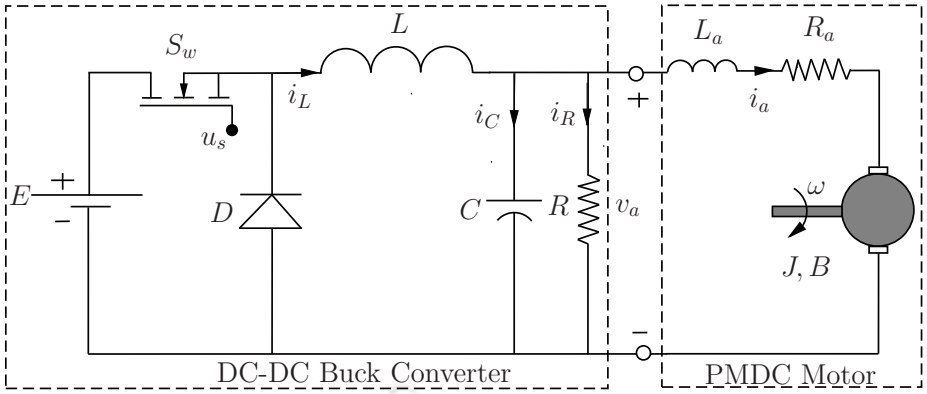

Figure 2.11: Cascaded DC-DC buck converter PMDC-motor combination.

motor in response to the desired angular speed. Therefore, the PMDC-motor acts as a dynamic load on the DC-DC buck converter. The set-up consists of a fixed input DC supply E, a power diode D, a buck inductor L, a capacitor C and resistance R across the output terminals of the DC-DC converter. Further, L_a and R_a are the equivalent inductance and resistance respectively, offered by the armature circuitry of PMDC-motor. The term ω denotes the angular velocity of the motor and the unknown load torque of the motor is represented by τ_L. Moreover, J is the combined moment of inertia of the rotor and motor load, B is the viscous friction coefficient of motor, K_e and K_t are the electromotive force constant and torque constants respectively of the PMDC-motor. Switching control input $u_s \in \mathbb{Z}_+ = \{0, 1\}$ represents the opening and closing operation of power electronic switch S_w. The operation of the circuitry is shown in Figure 2.12 and is classified under two modes depending on the position of the switch S_w working with a fixed frequency f_s and a variable duty ratio k. When the control input $u_s = 1$, the power diode D blocks the current flowing through it and the input source E supplies energy to the DC-DC buck converter PMDC-motor combination. The other mode of operation is when the control input $u_s = 0$, which leads to opening of the switch S_w. In this mode, the diode D starts conducting and E is totally disconnected from the system, thereby guaranteeing the continuity of current through the inductor L in the same direction as in the previous mode. Henceforth, the accumulation of energy in the inductor acts as a source of input voltage to drive the PMDC-motor load. Using Newton's second law of mechanics and Kirchhoff's voltage and current laws, the mathematical model [49] of the above system can be described as,

$$\left.\begin{aligned} J\frac{d\omega}{dt} &= K_t i_a - B\omega - \tau_L \\ L_a\frac{di_a}{dt} &= v_a - R_a i_a - K_e\omega \\ C\frac{dv_a}{dt} &= i_L - \frac{v_a}{R} - i_a \\ L\frac{di_L}{dt} &= uE - v_a \end{aligned}\right\} \tag{2.62}$$

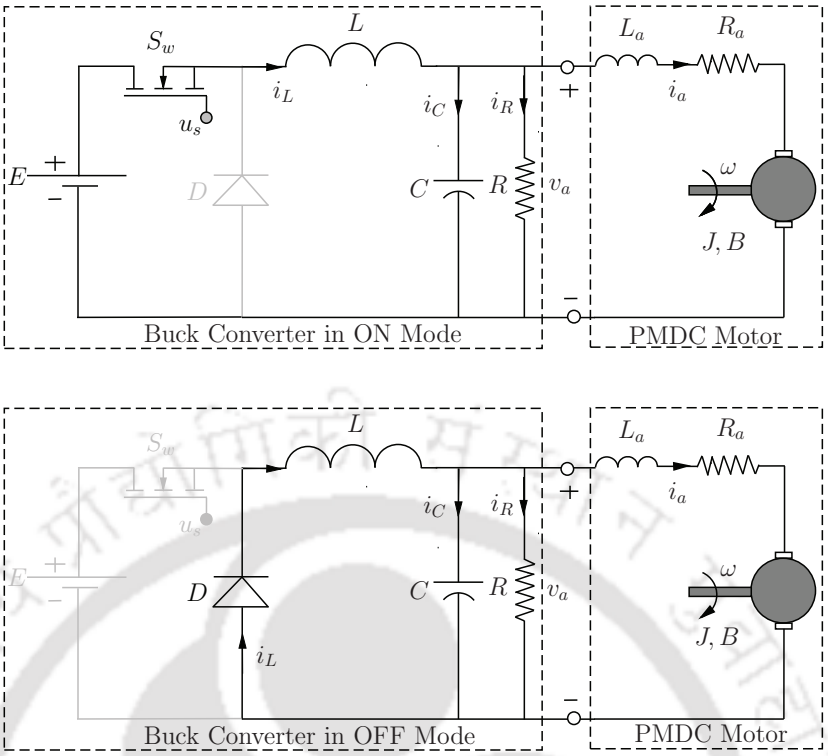

Figure 2.12: Buck converter PMDC-motor combination when: (a) S_w is ON and (b) S_w is OFF.

where i_L is the current through buck inductor L, v_a is the armature voltage and u is the unified control input. With the dynamics of the cascaded system given by (2.62), the aim is to make the angular velocity ω track a desired reference trajectory ω_r such that the tracking error asymptotically converges to zero, even in presence of the varying load torque $\tau_L(t)$ encountered at arbitrary time instants.

2.4.2 Adaptive Backstepping Control of Buck Converter Driven PMDC-Motor Load

In order to achieve the desired angular velocity tracking in PMDC-motor, by using DC-DC buck converter, an adaptive control mechanism through backstepping control is discussed in this section. Let the system states be defined as $x_1 = \omega$, $x_2 = i_a$, $x_3 = v_a$ and $x_4 = i_L$. In order to begin the controller design, let us define the operator $\mathcal{D}_y(\cdot) := \partial(\cdot)/\partial y$, $f^{(r)}$ as the $r-$th time derivative of f and the tracking error variables as,

$$\left.\begin{aligned} z_1 &= x_1 - \omega_r \\ z_2 &= \left(\frac{K_t}{J}\right) x_2 - \alpha_1 \\ z_3 &= \left(\frac{K_t}{JL_a}\right) x_3 - \alpha_2 \\ z_4 &= \left(\frac{K_t}{JCL_a}\right) x_4 - \alpha_3 \end{aligned}\right\}. \tag{2.63}$$

The unknown load term is approximated as $\tau_L = \Theta^{*^T}\Phi$ in (2.62). Further, the error terms in (2.63) are eventually stabilized, by using the intermediate virtual-control inputs α_i $(i = 1,\ 2,\ 3)$, as

$$\alpha_1 = -c_1 z_1 + (B/J)x_1 + (\hat{\Theta}^T\Phi/J) + \omega_r^{(1)} \tag{2.64}$$

$$\alpha_2 = -z_1 - c_2 z_2 + \left(\frac{K_t R_a}{JL_a}\right)x_2 + \left(\frac{K_t K_e}{JL_a}\right)x_1 + \mathcal{D}_{x_1}(\alpha_1)\left[\left(\frac{K_t}{J}\right)x_2 - \left(\frac{B}{J}\right)x_1\right]$$
$$+ \mathcal{D}_{x_1}(\alpha_1)\frac{\hat{\Theta}^T\Phi}{J} + \sum_{k=0}^{1}\mathcal{D}_{\omega_r^{(k)}}(\alpha_1)\omega_r^{(k+1)} + \mathcal{D}_{\hat{\Theta}^T}(\alpha_1)\Gamma\vartheta_2 \tag{2.65}$$

$$\alpha_3 = -z_2 - c_3 z_3 + \left(\frac{K_t}{JL_aC}\right)x_2 + \left(\frac{K_t}{JL_aCR}\right)x_3 + \mathcal{D}_{x_1}(\alpha_2)\left[\left(\frac{K_t}{J}\right)x_2 - \left(\frac{B}{J}\right)x_1\right] + \mathcal{D}_{x_1}(\alpha_2)\frac{\hat{\Theta}^T\Phi}{J}$$
$$+ \mathcal{D}_{x_2}(\alpha_2)\dot{x}_2 + \mathcal{D}_{\hat{\Theta}^T}(\alpha_2)\Gamma\vartheta_3 + \sum_{k=0}^{2}\mathcal{D}_{\omega_r^{(k)}}(\alpha_2)\omega_r^{(k+1)} - \mathcal{D}_{\hat{\Theta}^T}(\alpha_1)\Gamma\mathcal{D}_{x_1}(\alpha_2)\frac{\Phi}{J}z_2. \tag{2.66}$$

In the above mentioned virtual-control laws α_i, the terms Γ and ϑ_i denote the adaptive rate parameter and adaptive tuning function respectively. The recursive relation among tuning functions ϑ_i is defined by $\vartheta_i = \vartheta_{i-1} + w_i z_i$, wherein, $w_1 := -\Phi/J$, $w_2 := \mathcal{D}_{x_1}(\alpha_1)\frac{\Phi}{J}$ and $w_3 := \mathcal{D}_{x_1}(\alpha_2)\frac{\Phi}{J}$. The notation Θ^* is used to designate the actual value of unknown load torque parameter. In practice, this is found online as $\hat{\Theta}$ by formulating an update law using Lyapunov based adaptive learning strategy as,

$$\hat{\Theta}(t) = \hat{\Theta}(t_0) - \frac{\Gamma}{J}\int_{t_0}^{t}(\Phi(x_1(\nu))z_1(\nu) - \mathcal{D}_{x_1}(\alpha_1)z_2(\nu) - \mathcal{D}_{x_1}(\alpha_2)z_3(\nu) - \mathcal{D}_{x_1}(\alpha_3)z_4(\nu)d\nu)\,. \tag{2.67}$$

where $\Gamma > 0$ is the adaptation rate mentioned earlier. At the end the final control input $u(t)$ is derived to be,

$$u(t) = \frac{JCLL_a}{K_t E}\left[-z_3 - c_4 z_4 + \left(\frac{K_t}{JCLL_a}\right)x_3 + \left(\frac{K_t}{JL_aC}\right)x_2 + \left(\frac{K_t}{JL_aCR}\right)x_3\right.$$
$$+ \mathcal{D}_{x_1}(\alpha_3)\{\left(\frac{K_t}{J}\right)x_2 - \left(\frac{B}{J}\right)x_1\} + \sum_{j=2}^{3}\mathcal{D}_{x_j}(\alpha_3)\dot{x}_j + \sum_{k=0}^{3}\mathcal{D}_{\omega_r{}^{(k)}}(\alpha_2)\omega_r^{(k+1)}$$
$$\left.+\mathcal{D}_{\hat{\Theta}^T}(\alpha_3)\Gamma\vartheta_4 + \mathcal{D}_{x_1}(\alpha_3)\frac{\hat{\Theta}^T\Phi}{J} - \sum_{k=2}^{3}z_k\mathcal{D}_{\hat{\Theta}^T}(\alpha_{k-1})\Gamma\mathcal{D}_{x_1}(\alpha_3)\frac{\Phi}{J}\right]. \tag{2.68}$$

2.4.3 Stability Analysis

Stability of the entire DC-DC buck converter PMDC-motor combination under the action of the adaptive backstepping controller is proved by considering the dynamics of tracking errors defined from

(2.63) as follows,

$$\dot{z}_1 = -\left(\frac{B}{J}\right)x_1 - \left(\frac{\Theta^{*T}\Phi}{J}\right) + z_2 + \alpha_1 + \omega_r^{(1)} \tag{2.69}$$

$$\dot{z}_2 = -\left(\frac{K_t K_e}{JL_a}\right)x_1 - \left(\frac{K_t R_a}{JL_a}\right)x_2 + z_3 + \alpha_2 - \mathcal{D}_{x_1}(\alpha_1)\dot{x}_1 - \sum_{k=0}^{1}\mathcal{D}_{\omega_r^{(k)}}(\alpha_1)\omega_r^{(k+1)} - \mathcal{D}_{\hat{\Theta}^T}(\alpha_1)\dot{\hat{\Theta}} \tag{2.70}$$

$$\dot{z}_3 = -\left(\frac{K_t}{JL_aC}\right)x_2 - \left(\frac{K_t}{JL_aCR}\right)x_3 + z_4 + \alpha_3 - \sum_{j=1}^{2}\mathcal{D}_{x_j}(\alpha_2)\dot{x}_j - \sum_{k=0}^{2}\mathcal{D}_{\omega_r^{(k)}}(\alpha_2)\omega_r^{(k+1)} - \mathcal{D}_{\hat{\Theta}^T}(\alpha_2)\dot{\hat{\Theta}} \tag{2.71}$$

$$\dot{z}_4 = -\left(\frac{K_t}{JCLL_a}\right)x_3 + \left(\frac{K_t E}{JCLL_a}\right)u(t) - \sum_{j=1}^{3}\mathcal{D}_{x_j}(\alpha_3)\dot{x}_j - \sum_{k=0}^{3}\mathcal{D}_{\omega_r{}^{(k)}}(\alpha_3)\omega_r^{(k+1)} - \mathcal{D}_{\hat{\Theta}^T}(\alpha_3)\dot{\hat{\Theta}}. \tag{2.72}$$

Substituting (2.64)-(2.66) and the control law $u(t)$ from (2.68) into (2.69)-(2.72), the error dynamics can be written in matrix form as,

$$\begin{bmatrix}\dot{z}_1\\ \dot{z}_2\\ \dot{z}_3\\ \dot{z}_4\end{bmatrix} = \begin{bmatrix}-c_1 & 1 & 0 & 0\\ -1 & -c_2 & 1+\sigma_{23} & \sigma_{24}\\ 0 & -1-\sigma_{23} & -c_3 & 1+\sigma_{34}\\ 0 & -\sigma_{24} & -1-\sigma_{34} & -c_4\end{bmatrix}\begin{bmatrix}z_1\\ z_2\\ z_3\\ z_4\end{bmatrix} + \tilde{\Theta}^T\begin{bmatrix}-\frac{\Phi}{J}\\ \mathcal{D}_{x_1}(\alpha_1)\frac{\Phi}{J}\\ \mathcal{D}_{x_1}(\alpha_2)\frac{\Phi}{J}\\ \mathcal{D}_{x_1}(\alpha_3)\frac{\Phi}{J}\end{bmatrix} + \begin{bmatrix}0\\ \mathcal{D}_{\hat{\Theta}^T}(\alpha_1)\\ \mathcal{D}_{\hat{\Theta}^T}(\alpha_2)\\ \mathcal{D}_{\hat{\Theta}^T}(\alpha_3)\end{bmatrix}(\Gamma\vartheta_4 - \dot{\hat{\Theta}}) \tag{2.73}$$

where, $\sigma_{ij} = -\frac{\partial\alpha_{i-1}}{\partial\hat{\Theta}^T}\Gamma w_j$. In order to find the stability of (2.73), let $\mathbf{z} = [z_1\ z_2\ z_3\ z_4]^T$ and consider a positive definite, Lyapunov function is considered as

$$V(\mathbf{z}, \tilde{\Theta}, t) = \frac{1}{2}\mathbf{z^T P z} + \frac{1}{2}\tilde{\Theta}^T\Gamma^{-1}\tilde{\Theta} \tag{2.74}$$

where, $\mathbf{P} > 0$ and $\Gamma^{-1} > 0$. Taking time derivative of (2.74) and using (2.69)-(2.73), it is straightforward to prove that $\dot{V} < 0$ or $\dot{V} < -cV$, where $c = \min\{2c_i\}_{i=1}^{4}$. Hence the asymptotic stability of the tracking error dynamics is ensured.

The schematic diagram of ABSC scheme for DC-DC buck converter driven PMDC-motor is shown in Figure 2.13.

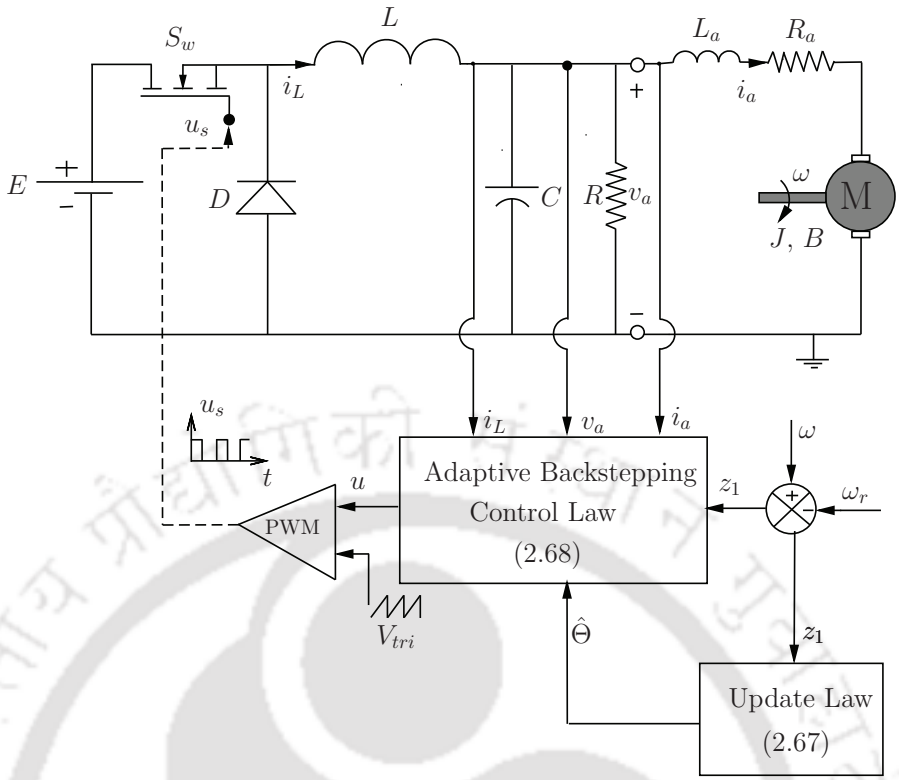

Figure 2.13: Schematic diagram of adaptive backstepping control scheme for control of DC-DC buck converter driven PMDC motor.

2.4.4 Experimental Results and Discussion

A detailed description of the equipments and components used in experimental evaluation of the control algorithm has already been provided in subsection 2.3.4.1 and the same is not reproduced here for brevity. The functional block diagram representing the realization of proposed adaptive backstepping control on DC-DC buck converter driven PMDC-motor for angular velocity tracking is shown in Figure 2.14. To investigate the performance of the adaptive backstepping control in a practical environment, a prototype of cascaded DC-DC buck converter PMDC-motor combination is fabricated in the laboratory as shown in Figure 2.15. The prototype consists of two identical PMDC-motors coupled on the same rotor shaft with a tacho-generator. One motor acts as a nominal load to the DC-DC buck converter and the other helps in generating a sudden load torque disturbance by energizing it in the opposite direction. The specifications of the practical system and the parameters associated with the proposed controller are given in Table 2.2. The stabilizing gains of the controller are selected on the basis of satisfactory static and dynamic responses and are chosen as $c_1 = 1 \times 10^7$, $c_2 = 1 \times 10^4$, $c_3 = 1 \times 10^2$ and $c_4 = 1 \times 10^2$. Further, the adaptation rate is chosen as $\Gamma = 1.1 \times 10^{-9}$.

The system of DC-DC buck converter driven PMDC-motor is subjected to the following experimental tests.

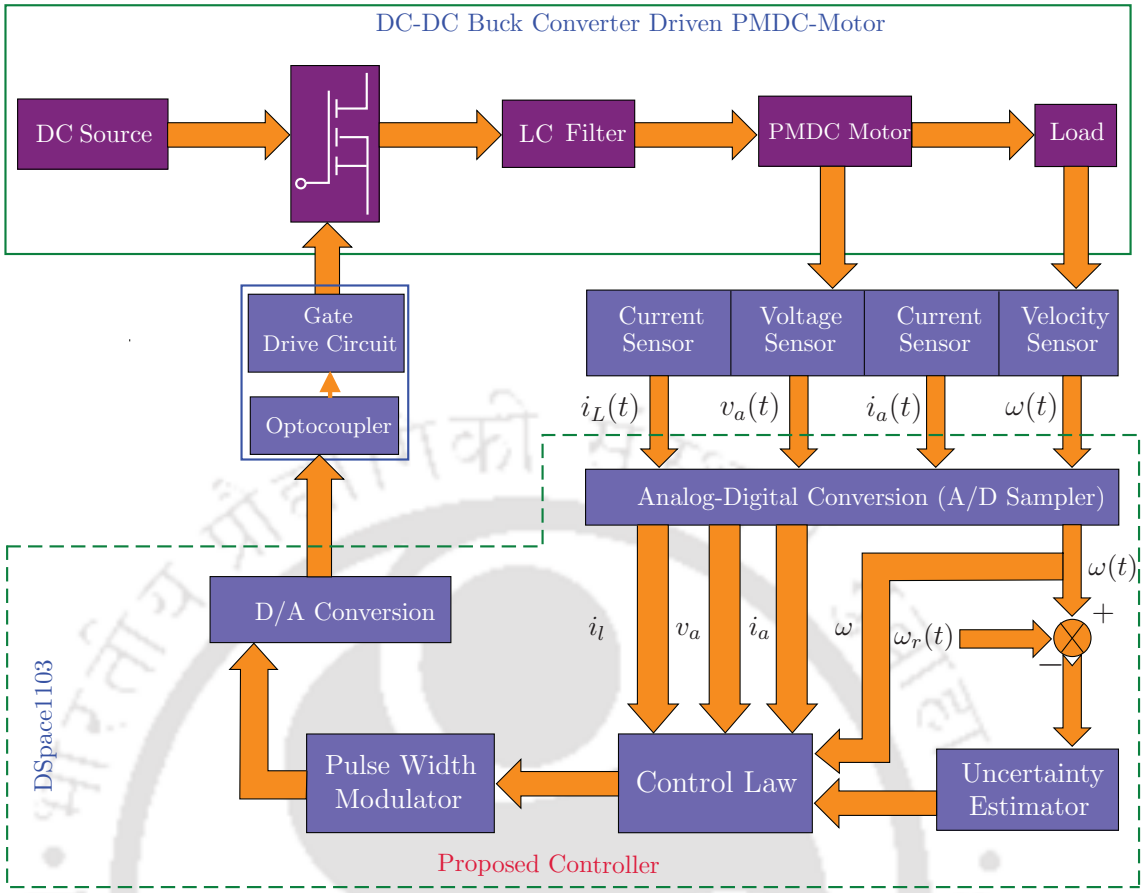

Figure 2.14: Functional block diagram representing the realization of the ABSC on DC-DC buck converter PMDC-motor combination.

Table 2.2: Specifications of DC-DC buck converter driven PMDC-Motor

System parameters	Rating
Power Converter Rating P	120W
Power Switch MOSFET S_w	IRFP460 (500V/18A)
Power Diode D	6A4 MIC
Switching frequency f_s	20kHz
Supply DC voltage E	$26V$
PMDC Motor	$\frac{1}{3}$HP, 24V
Nominal Load Torque τ_L	0.012Nm
Armature Resistance R_a	2.5Ω
Armature Inductance L_a	$176mH$
Viscous Friction Coefficient B	$2.401e^{-6}N-ms$
Moment of Inertia J	$3.9108e^{-6}Kg.m^2$
Buck Inductor L	$20mH$, 10A Reactor 195M10
DC Capacitor C	$220\mu F, 450V$
Back Electromotive Force Constant K_e	0.0145 Vs/rad
Torque Constant K_t	0.0105 N-m/A
Resistor Load R	20Ω
Reference Angular Velocity ω_r	$52.3rad/s$

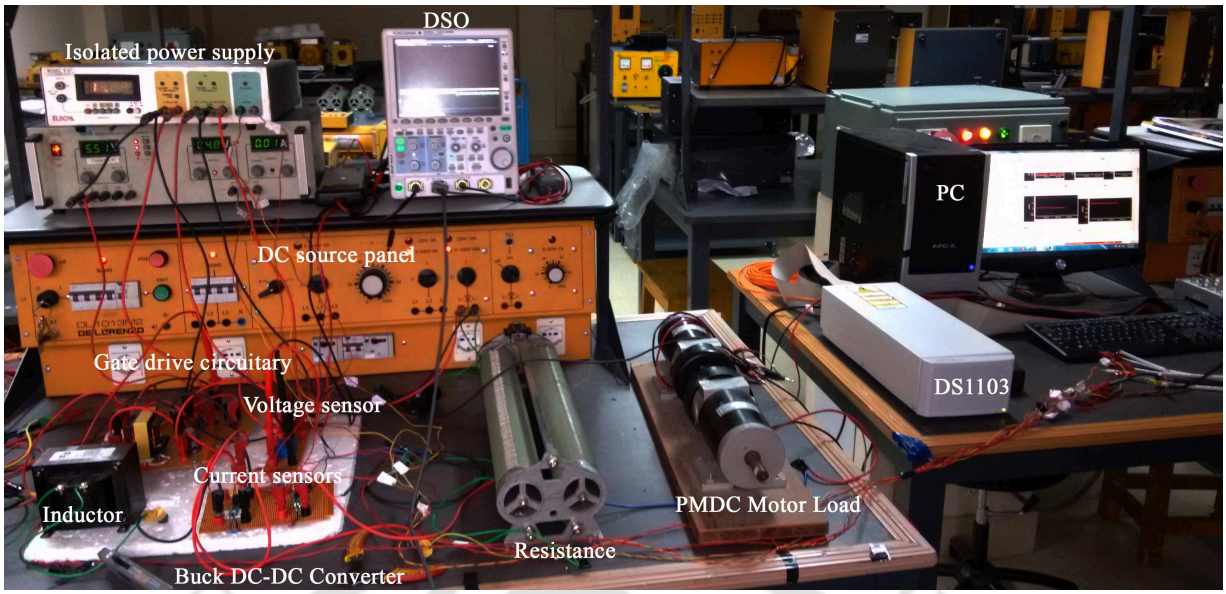

Figure 2.15: Experimental set-up of cascaded DC-DC buck converter-PMDC motor combination

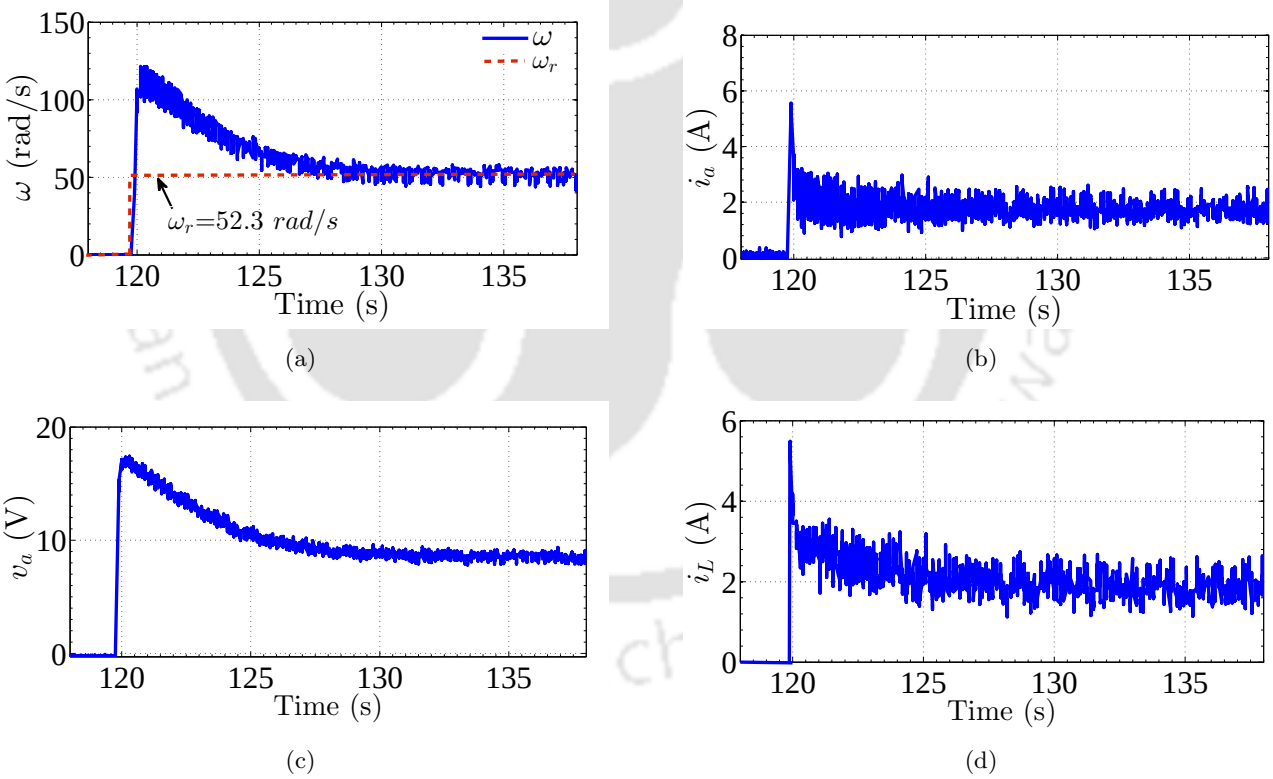

Figure 2.16: Start-up response under ABSC scheme.

Test 1: A step change in ω_r from 0 - 52.3 rad/s (0 - 500 rpm).

Test 2: A step change in τ_L from nominal 0.01 Nm to 0.063 Nm and vice-versa.

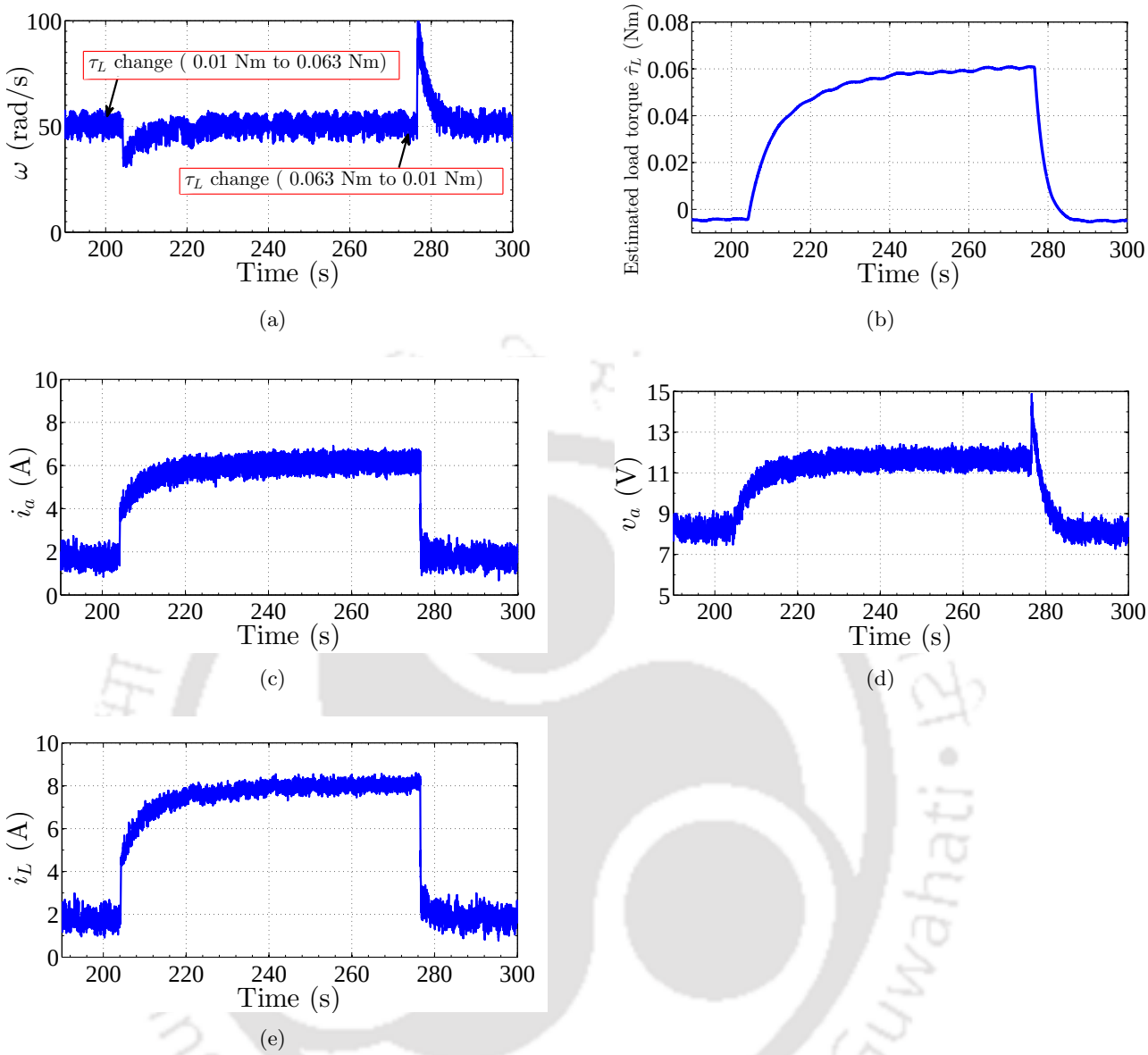

Figure 2.17: Control response under ABSC scheme for sudden changes in load torque τ_L from nominal 0.01 Nm to 0.063 Nm and vice-versa.

Test 3: A step change in ω_r from 52.3 - 104.7 rad/s (500 - 1000 rpm).

A discussion on the results obtained under the above tests performed experimentally are elucidated below.

Test 1: Step change in ω_r from 0 - 52.3 rad/s (0 - 500 rpm):

The start-up response of DC-DC buck converter PMDC-motor combination under the action of ABSC is shown in Figure 2.16. It can be observed that the angular velocity of PMDC-motor tracks the desired velocity with an overshoot of more than 100% and reaches ω_r in $7s$. Meanwhile the peak-to-peak ripple in the angular velocity $\Delta\omega$ under this nominal condition is found to be $9rad/s$. The profiles of other system states are also provided in Figure 2.16.

Test 2: Step change in τ_L from nominal 0.01 Nm to 0.063 Nm and vice-versa:
To evaluate the effectiveness of the ABSC, the DC-DC buck converter driven PMDC-motor is subjected to a sudden decrease in the load torque from nominal 0.01Nm to 0.063Nm and again decreased from perturbed value of 0.063Nm to nominal 0.01Nm. Figure 2.17 shows that the adaptation mechanism is successful in estimating the unknown profile of load torque and is able to track the constant speed of 52.3rad/s (500 rpm) well within 8s. The corresponding plot of load estimation torque $\hat{\tau}_L$ along with behavior of other system states are also provided in Figure 2.17.

Test 3: Step change in ω_r from 52.3 - 104.7 rad/s (500 - 1000 rpm):
Next, the performance of the adaptive backstepping control for angular velocity control of DC-DC buck converter fed PMDC-motor to a step change in ω_r from $52.3 rad/s$ to $104.7 rad/s$ is investigated and the responses are plotted in Figure 2.18 (a). From Figure 2.18 (a) it is found that the ABSC scheme is able to track a new set value of reference velocity in approximately $5s$.

Test 4: Step change in ω_r from 52.3 - 31.4 rad/s (500 - 300 rpm):
Lastly, the proposed ABSC is evaluated on DC-DC buck converter driven PMDC-motor for a sudden angular velocity tracking from $52.3 rad/s$ to $31.4 rad/s$. The response obtained is recorded in Figure 2.18 (b). It is observed that ABSC scheme tracks the new reference velocity of $31.4 rad/s$ in $4s$.

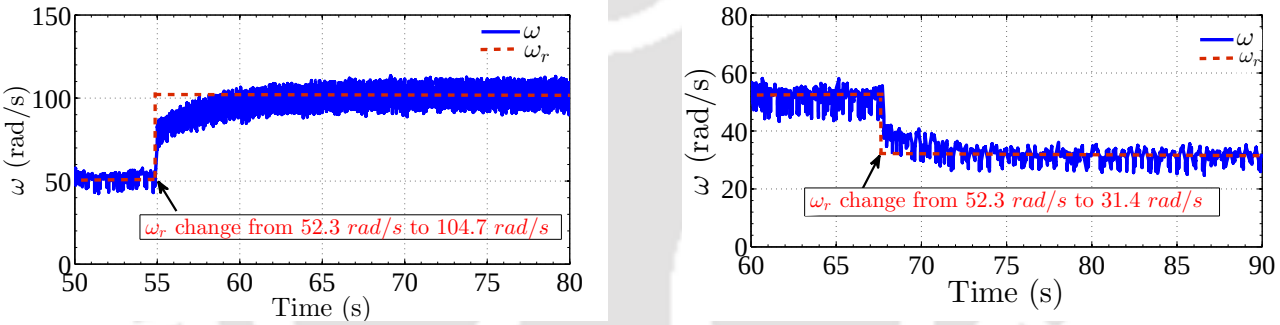

Figure 2.18: Angular velocity tracking under ABSC scheme: (a) from 52.3 rad/s to 104.7 rad/s and (b) from 52.3 rad/s to 31.4 rad/s.

2.5 Summary

In this chapter, an adaptive control strategy integrated with backstepping control mechanism is developed for the output voltage regulation in DC-DC buck converter system feeding resistive load. A detailed design of the adaptive backstepping control (ABSC) scheme, followed by subsequent proof of closed loop stability by Lyapunov stability criterion is presented. The efficacy of proposed ABSC scheme is evaluated under wide range of perturbations in the load resistance, input voltage and reference voltage. A detailed discussion on the practical implementation aspects of the proposed controller is furnished. Further, the usefulness of ABSC is established on the developed experimental prototype in the laboratory. In furtherance, the issue of angular velocity control in DC-DC buck converter driven PMDC-motor load is addressed through the ABSC scheme. The performance is

evaluated experimentally under wide range of perturbations in the load torque and the reference trajectories. This investigation reveals that the ABSC method bears a promising potential in delivering an appreciable estimation of the varying unknown load. It is also noteworthy that the ABSC scheme exhibits robustness against a wide range of disturbances, in addition to successfully tracking the reference output with satisfactory performance.

3

Neuro-Adaptive Backstepping Control of DC-DC Buck Converters

Contents

3.1 Introduction

In the previous chapter it is observed that, though the estimation of unknown varying load is successful with adaptive backstepping control, yet the adaptation process is slow. This causes a degraded transient output performance during both start-up and load change. From the seminal works of Ge *et* al. [86], it is a well established fact that neural networks are universal approximators of unknown functions. Motivated by this fact, in this chapter an attempt has been made to investigate and design intelligent control techniques based on orthogonal polynomial based neural networks. At first, the adaptive backstepping methodology is integrated with Chebyshev neural network (CNN). A rigorous stability and transient performance analysis have been provided to give an insight to the tuning of controller parameters. The advantage of the CNN based approximation of the unknown load, in comparison to other neural network schemes lies in the fact that it offers faster convergence and thereby making it well suited for applications in online adaptation problems. Moreover in CNN, computational burden is less. The proposed Chebyshev neural network based ABSC scheme is compared with radial basis function neural network (RBFNN) based ABSC and conventional ABSC, which demonstrates superiority in the proposed CNN-ABSC method. A Hermite neural network (HNN) based ABSC is next proposed for a quicker and closer estimation of unknown load parameters. This HNN-ABSC scheme offers much faster rejection of load perturbations, compared to the CNN-ABSC. Relevant simulation and experimental studies are presented supporting the claims.

3.2 Chebyshev Neural Network (CNN) based Uncertainty Estimation

Exploiting the universal function approximation property of neural networks, a single layer Chebyshev neural network is successfully used to solve the function approximation problem. A brief description about Chebyshev polynomials [87] is provided below.

Let us consider an infinite dimensional function space $\mathscr{F}$ and an approximation space or subspace $\mathscr{A}$, meaning that $\mathscr{A} \subseteq \mathscr{F}$ along with the measure $\|f - f^*\|$ signifying the deviation of the approximation f^* in $\mathscr{A}$ from the actual function f in $\mathscr{F}$. Therefore from Weierstrass's Theorem [87], any function f in $\mathscr{C}[a,b] \subseteq \mathscr{F}$ and for any given $\epsilon > 0$, $\exists$ a polynomial p_n for sufficiently large n such that $\|f - p_n\|_\infty < \epsilon$. The same holds for $\|f - p_n\|_p < \epsilon$ for $p \geq 1$. Now, our attention is focussed to the case of best $\mathscr{L}_2$ polynomial approximation p_n^* in $\mathscr{A}$ of a function f in the function space $\mathscr{F}$. In other words, it reduces to a problem of least square approximation and hence can be stated as below.

Let us find a polynomial approximation $p_n^*(x)$ to the function $f(x)$, such that,

$$\|f(x) - p_n^*(x)\|_2 \leq \|f(x) - p_n(x)\|_2 \quad \forall p_n(x) \in \mathscr{A} \text{ and } x \in [a,b].$$

Initiation of the approximation procedure by the method of least squares firstly requires the function f in $\mathscr{F}$ to be represented as a linear combination of $(n+1)$ basis functions spanning the subspace $\mathscr{A} \subseteq \mathscr{F}$ also known as the Hilbert space. Therefore, considering $\mathscr{A}$ as a finite dimensional subspace spanned by $(n+1)$ polynomial bases $\{\phi_i\}_{i=0}^n$, the approximated function p_n belonging to $\mathscr{A}$ can be

written as,

$$p_n(x) = \sum_{i=0}^{n} w_i \phi_i = \mathbf{W^T \Phi}(x), \quad w_i \in \mathbb{R} \tag{3.1}$$

where, $\mathbf{W} = [w_0 \;\; w_1 \dots w_i \dots w_n]^T$ and $\mathbf{\Phi}(x) = [\phi_0(x) \;\; \phi_1(x) \dots \phi_i(x) \dots \phi_n(x)]^T$. Now the aim is to find w_i, such that $\|f - p_n\|_2$ is minimized. Hence defining $E(w_0, w_1, w_2, ...w_n) = \int_a^b (f(x) - p_n(x))^2 dx$, a necessary condition for E to have a minimum is,

$$\frac{\partial E}{\partial w_i} = 0 \tag{3.2}$$

$$0 = -2 \int_a^b (f(x) - p_n(x)) \frac{\partial p_n(x)}{\partial w_i} dx \tag{3.3}$$

$$0 = -2 \int_a^b (f(x) - p_n(x)) \phi_i(x) dx. \tag{3.4}$$

Hence the above equalities yield the following condition,

$$\int_a^b f(x)\phi_i(x)dx = \int_a^b p_n \phi_i(x)dx = \int_a^b \sum_{j=0}^{n} w_j \phi_j(x)\phi_i(x)dx = \sum_{j=0}^{n} w_j \int_a^b \phi_j(x)\phi_i(x)dx. \tag{3.5}$$

For ease of understanding, the mathematical pre-requisites pertaining to function spaces are provided subsequently as Definition 1, Lemma 1 and Lemma 2.

Definition 1. *Given an interval (a,b) and a weight function $\omega(x)$ which is positive in (a,b), a weighted Sobolev space [88] $\mathscr{L}^2_\omega(a,b)$ is defined as,*

$$\mathscr{L}^2_\omega(a,b) := \{f(x) : \int_a^b f^2(x)\omega(x)dx < \infty\} \tag{3.6}$$

with the inner product defined as $\langle f, g\rangle_w := \int_a^b f(x)g(x)\omega(x)dx$.

Remark 2. *Weighted Sobolev space is a function space which is a vector space endowed with an inner product and a norm given as $\|f\|_{\mathscr{L}^2_\omega} := \langle f, f\rangle_\omega^{1/2} < \infty$. It can also be termed as a weighted Hilbert space, but usage of Sobolev space is much more general to encompass a large class of functions (not only smooth functions but also piecewise continuous functions).*

Lemma 1. *The best $\mathscr{L}_2$ polynomial approximation p_n^* of degree n to a given $\mathscr{L}_2$ integrable function $f(x)$ is unique and is characterized by the property that $\langle f - p_n^*, p_n\rangle$=0 for any other polynomial p_n of degree n.*

Proof: Please refer to work in [87]. □

A corollary can be derived from the above Lemma 1, given as Lemma 2.

Lemma 2. *The best $\mathscr{L}_2$ polynomial approximation p_n^* of degree n to $f(x)$ may be expressed in terms*

of the orthogonal polynomial family $\{\phi_i\}$ *in the form:*

$$p_n^* = \sum_{i=0}^{n} w_i \phi_i, \qquad w_i = \frac{\langle f, \phi_i \rangle}{\langle \phi_i, \phi_i \rangle}. \tag{3.7}$$

Proof: The above result can be proved as follows. For $k = 0, 1, \ldots, n$,

$$\begin{aligned} \langle f - p_n^*, \phi_k \rangle &= \langle f - \sum_{i=0}^{n} w_i \phi_i, \phi_k \rangle \qquad (3.8) \\ &= \langle f, \phi_k \rangle - \sum_{i=0}^{n} w_i \langle \phi_i, \phi_k \rangle \\ &= \langle f, \phi_k \rangle - w_k \langle \phi_k, \phi_k \rangle \\ &= 0 \quad \text{by definition of } w_k. \qquad (3.9) \end{aligned}$$

Now any polynomial p_n can be written as $p_n = \sum_{i=0}^{n} d_i \phi_i$, where d_i is the coefficient of the basis function ϕ_i and hence $\langle f - p_n^*, p_n \rangle = \sum_{i=0}^{n} d_i \langle f - p_n^*, \phi_i \rangle = 0$ can be derived from (3.9). Therefore p_n^* is proved to be the best approximation from Lemma 1.

The orthogonality property of Chebyshev polynomial makes it highly suitable to be used for function approximation. Chebyshev polynomials belong to the weighted Sobolev space $\mathscr{L}_\omega^2(a, b)$ with respect to the weight function, $w(x) = \dfrac{1}{\sqrt{1 - x^2}}$ and are given by the generating function $\phi_{n+1}(x) = 2x\phi_n(x) - \phi_{n-1}(x)$ with $\phi_0(x) = 1$ and $\phi_1(x) = x$. Now since Chebyshev polynomials are orthogonal they form a basis to span the space $\mathscr{L}_\omega^2 := \mathscr{A}$ or the approximation space known as the weighted Sobolev space. The orthogonal property can be shown as,

$$\langle \phi_i(x), \phi_j(x) \rangle = \int_{-1}^{1} \frac{\phi_i(x)\phi_j(x)}{\sqrt{1 - x^2}} dx \tag{3.10}$$

$$\langle \phi_i(x), \phi_j(x) \rangle = \begin{cases} 0 & i \neq j \\ \pi & i = j = 0 \\ \pi/2 & i = j \end{cases}. \tag{3.11}$$

It is found that the orthogonal property is surfaced in the process of finding the best $\mathscr{L}_2$ approximation of a function f with a polynomial p_n^* of degree n.

Suppose, it is needed to find a polynomial $p_n(x) \in \mathscr{A}$, such that it is the best approximation to the continuous function $f(x)$ in the interval [0,1]. It means that the requirement is to find $p^*(x)$ such that $\|f(x) - p^*(x)\|_2 \leq \|f(x) - p(x)\|_2$. Considering the basis of $\mathscr{A}$ as, $\{\phi_i\}_{i=0}^n$ given by $\phi_0 = 1$, $\phi_1 = x$, $\phi_2 = x^2, \ldots, \phi_n = x^n$, which is necessarily a polynomial regression problem,

$$\int_0^1 f(x)x^i dx = \sum_{j=o}^{n} w_j \int_0^1 x^j x^i = \sum_{j=o}^{n} w_j \int_0^1 x^{i+j} dx = \sum_{j=o}^{n} w_j \left[\frac{x^{i+j+1}}{i+j+1} \right]_0^1 = \sum_{j=o}^{n} \frac{w_j}{i+j+1}. \tag{3.12}$$

From (3.12), a matrix equation in n unknowns can be formulated as follows, and thereafter solved to

get the unknown parameters.

$$\underbrace{\begin{bmatrix} 1 & \frac{1}{2} & \dots & \frac{1}{n+1} \\ \frac{1}{2} & \frac{1}{3} & \dots & \frac{1}{n+2} \\ \vdots & \vdots & \ddots & \vdots \\ \frac{1}{n+1} & \frac{1}{n+2} & \dots & \frac{1}{2n+1} \end{bmatrix}}_{\mathbf{H}} \underbrace{\begin{bmatrix} w_0 \\ w_1 \\ \vdots \\ w_n \end{bmatrix}}_{\mathbf{W}} = \underbrace{\begin{bmatrix} \int_0^1 f(x)dx \\ \int_0^1 xf(x)dx \\ \vdots \\ \int_0^1 x^n f(x)dx \end{bmatrix}}_{\mathbf{y}} \tag{3.13}$$

where, $\mathbf{H}$ is called the Hilbert matrix and it is an ill-posed problem. The condition number of the matrix $\mathbf{H}$ goes on increasing as the degree of the polynomial $p_n^* \in \mathscr{A}$ is increased. However, $p_n^* \in \mathscr{A}$ was used in the best approximation of the function $f \in \mathscr{F}$. From Weierstrass Theorem [87], accuracy of approximation increases as n increases. Thereby, a better way to find $p_n^*(x)$ is necessary. Therefore, an orthogonal basis $\phi_i(x)$ is chosen such that $\int_a^b \phi_i(x)\phi_j(x)dx = 0$ for $i \neq j$. Then the condition for minimization of the performance index $\|f(x) - p_n^*(x)\|_2$ reduces to the following,

$$\int_a^b f(x)\phi_i(x)dx = w_i \int_a^b \phi_i^2(x)dx \quad \text{for } i = 0, 1, ...n. \tag{3.14}$$

Now w_i can be easily determined from (3.7). Moreover, any orthogonal set $\{\phi_i\}_{i=0}^n$ is always linearly independent and hence provides a basis for spanning $\mathscr{A}$ or an $(n+1)$- dimensional space. Now using Chebyshev polynomials as basis function set $\{\phi_i\}_{i=0}^n$ and utilizing the condition in (3.5) yields,

$$\int_0^1 f(x)\phi_i(x)dx = w_i \int_0^1 \phi_i^2(x)dx, \quad i = 0, 1, \dots, n \tag{3.15}$$

for $i = 0, 1, 2, \dots, n$. Thereby the matrix equations in n unknowns are found as

$$\underbrace{\begin{bmatrix} \int_0^1 \phi_0^2(x)dx & 0 & \dots & 0 \\ 0 & \int_0^1 \phi_1^2(x)dx & \dots & 0 \\ \vdots & \vdots & \ddots & \vdots \\ 0 & 0 & \dots & \int_0^1 \phi_n^2(x)dx \end{bmatrix}}_{\mathbf{H}} \underbrace{\begin{bmatrix} w_0 \\ w_1 \\ \vdots \\ w_n \end{bmatrix}}_{\mathbf{W}} = \underbrace{\begin{bmatrix} \int_0^1 f(x)\phi_0^2(x)dx \\ \int_0^1 f(x)\phi_1^2(x)dx \\ \vdots \\ \int_0^1 f(x)\phi_n^2(x)dx \end{bmatrix}}_{\mathbf{y}} \tag{3.16}$$

This results in significant reduction in the condition number of matrix $\mathbf{H}$, which implies that the problem (3.16) is well-posed and a proper solution $\mathbf{W}$ is possible respecting the minimization of the approximation error norm. Therefore, from the condition number aspect, the function approximation using Chebyshev polynomials as basis functions is better. Hence, the best $\mathscr{L}_2$ approximation using Chebyshev polynomials has been proved to minimize the square approximation error over $x \in [-1, 1]$. In this work, the method proposed for weight tuning in the approximation of the unknown function is formulated using an online learning based on Lyapunov function. In contrary to least square approximation problem, a Lyapunov based learning also minimizes the same performance index and hence both are equivalent. The relation between Lyapunov based learning and method of least square can be easily established mathematically, yielding the same result for optimal weights as in (3.7).

The overall closed loop stability guarantees the minimization of the Lyapunov function and therefore the obtained weights are essentially the best approximation of the unknown function. Moreover, the assurance of asymptotic stability guarantees high precision in approximation accuracy.
In contrast to radial basis function neural networks (RBFNN) the same least square based procedure yields the following:

$$\int_{-1}^{1} f(x)\phi_i(x)dx = \sum_{j=0}^{n} w_j \int_{-1}^{1} \phi_j(x)\phi_i(x)dx. \tag{3.17}$$

In RBFNN, the basis functions are chosen as, $\{\phi_i\}_{i=0}^{n} = \{exp(-\frac{x-\mu_i}{2\sigma^2})\}_{i=0}^{n}$, where μ and σ are the mean and standard deviation in Gaussian distribution. Substituting ϕ_i in (3.17), it is observed that the condition number is greater than in Chebyshev polynomial based neural network leading to an ill-posed problem with increasing number of neurons n, and thereby increasing the computation burden. Moreover, they are not orthogonal and hence the best approximation can not be achieved. Furthermore, Chebyshev polynomials are well known to economize power series. Therefore, a function can be approximated using lesser number of basis functions or neurons than in the RBFNN. Hence the computational complexity is highly reduced. Considering the above the Chebyshev Neural Networks (CNN) offer promising potential for application in unknown function approximation.

3.2.1 CNN based Adaptive Backstepping Control for DC-DC Buck Converters with Resistive Load

As the loading conditions in a DC-DC buck converters are highly uncertain, control action through conventional backstepping scheme alone is not sufficient and would result in a bounded yet degraded performance which is not desirable. Therefore in this section, a neural network with Chebyshev polynomials is used to estimate the unknown load parameter which is controlled by employing the ABSC method.

3.2.1.1 Controller Design

Referring to the DC-DC buck converter circuit presented in Section 2.3 and its dynamics defined in (2.41) -(2.42), the control design procedure using CNN based adaptive backstepping is summarized below:
Step 1. In (2.41), $\frac{x_1}{R}$ is treated as an unknown nonlinear function and it is approximated by using Chebyshev neural network as $\mathbf{W^{*T}\Phi}$ where $\mathbf{W}^*$ is the optimum weight vector and $\mathbf{\Phi}$ represents the Chebyshev polynomial basis vector which serves as the regressor matrix. Replacing $\frac{x_1}{R}$ in (2.41) with $\mathbf{W^{*T}\Phi}$ yields

$$\dot{x}_1 = -\frac{\mathbf{W^{*T}\Phi}}{C} + \frac{x_2}{C}. \tag{3.18}$$

Now (3.18) and (2.42) together define the buck converter dynamics, which is utilized in the design of the proposed CNN-ABSC scheme.

Step 2. Next, the error variables are defined as

$$z_1 = x_1 - v_r \tag{3.19}$$

$$z_2 = \frac{x_2}{C} - \alpha - \dot{v}_r \tag{3.20}$$

where v_r is the reference output voltage and α is the pseudo-control input considered to stabilize the first tracking error variable z_1.

Step 3. Using the dynamics of the error variable z_1, the pseudo-control input α is selected as

$$\alpha = -c_1 z_1 + \frac{\hat{\mathbf{W}}^{\mathbf{T}}\mathbf{\Phi}}{C} - z_2 \tag{3.21}$$

where c_1 is the controller gain and $\hat{\mathbf{W}}$ is the adaptively estimated weight vector. This leads to the development of the next error variable z_2 as

$$\dot{z}_2 = -\frac{x_1}{LC} - \sum_{k=1}^{2}\frac{\partial\alpha}{\partial x_k}\dot{x}_k - \sum_{k=0}^{1}\frac{\partial\alpha}{\partial {v_r}^{(k)}}{v_r}^{(k+1)} - \dot{\hat{\mathbf{W}}}^{\mathbf{T}}\frac{\partial\alpha}{\partial\hat{\mathbf{W}}^{\mathbf{T}}} + \frac{E}{LC}u - \ddot{v}_r \tag{3.22}$$

Thus, (3.22) provides the direction to formulate the actual control input u in such a way that it must stabilize the error z_2. Therefore, u is found to be

$$u = \frac{LC}{E}\Bigg(- z_1 - c_2 z_2 + \frac{x_1}{LC} + \frac{\partial\alpha}{\partial x_1}\left(\frac{x_2}{C}\right) - \frac{\partial\alpha}{\partial x_1}\left(\frac{\hat{\mathbf{W}}^{\mathbf{T}}\mathbf{\Phi}}{C}\right) + \sum_{k=0}^{1}\frac{\partial\alpha}{\partial {v_r}^{(k)}}{v_r}^{(k+1)} + \dot{\hat{\mathbf{W}}}^{\mathbf{T}}\frac{\partial\alpha}{\partial\hat{\mathbf{W}}^{\mathbf{T}}} + \ddot{v}_r + \frac{\partial\alpha}{\partial x_1}\mathbf{P}\vartheta_{\mathbf{2}}\Bigg) \tag{3.23}$$

where c_2 is the controller gain and $\vartheta_{\mathbf{2}} = \vartheta_{\mathbf{1}} + \frac{\partial\alpha}{\partial x_1}\frac{\mathbf{\Phi}}{C}z_2$ with $\vartheta_{\mathbf{1}} = -\frac{\mathbf{\Phi}}{C}z_1$. The definition and requirement of the functions $\vartheta_{\mathbf{i}}$ in the course of ABSC design has been explained in Chapter 2.

Step 4. Further, the neural network weight vector $\hat{\mathbf{W}}$ is updated online using the update law

$$\dot{\hat{\mathbf{W}}} = -\frac{\mathbf{P}\mathbf{\Phi}}{C}\left(z_1 - \frac{\partial\alpha}{\partial x_1}z_2\right) \tag{3.24}$$

where $\mathbf{P} > 0$ is a user defined diagonal matrix denoting the adaptive rate. This completes the design of the proposed CNN-ABSC for the DC-DC buck converter. Detailed stability proof of the proposed CNN-ABSC scheme is discussed in the next sub-section, which further clarifies the design procedure of the proposed control methodology. The block diagram representation of the proposed CNN-ABSC scheme for DC-DC buck converters is shown in Figure 3.1.

Remark 3. *A high value of* $\mathbf{P}$ *leads to fast adaptation and good transient performance. However, such a* $\mathbf{P}$ *may result in decreased stability margin of the buck converter system and hence should be chosen carefully. The positive gain constants* c_1 *and* c_2 *for the pseudo and actual control laws depend on the designer's choice. However, very high values of* c_1 *and* c_2 *are not recommended because these may lead to large overshoots.*

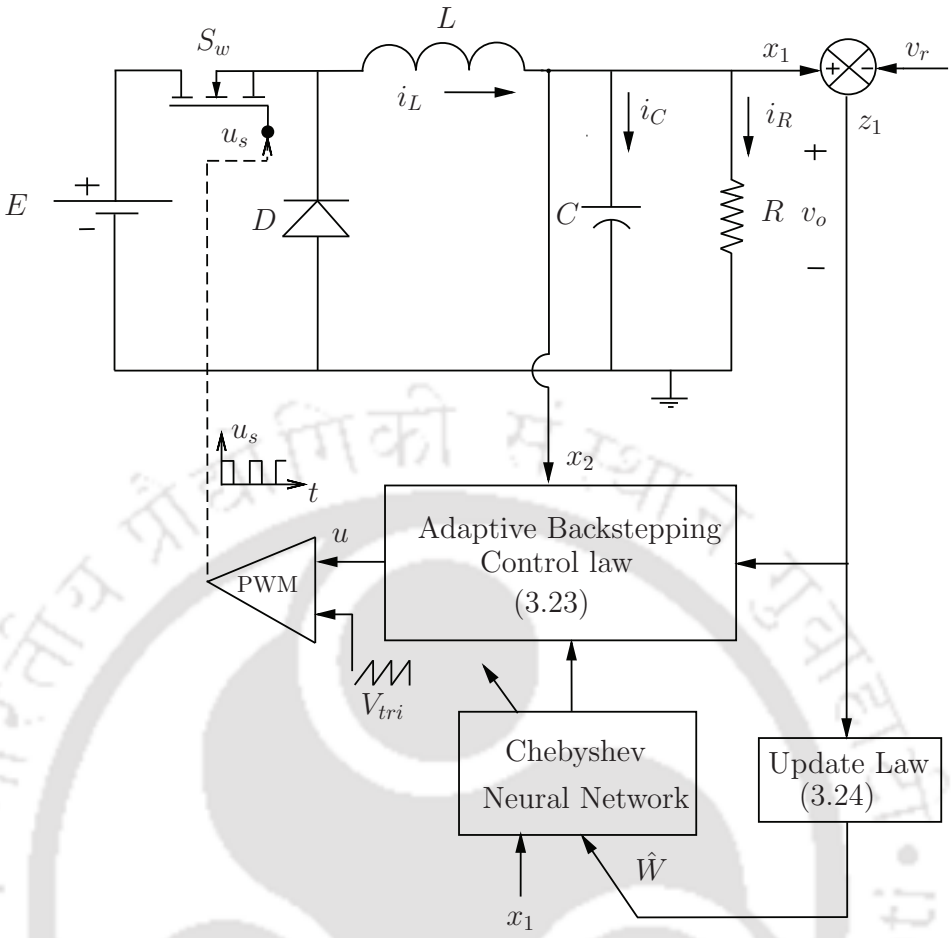

Figure 3.1: Schematic diagram of proposed CNN-ABSC scheme for DC-DC buck converters

3.2.1.2 Stability Analysis

In this section, asymptotic stability of the error variables z_1 and z_2 are established. The analysis is carried out in a stepwise procedure as follows. For the stabilization of z_1, the first Lyapunov function V_1 is taken as

$$V_1 = \frac{1}{2}z_1^2 + \frac{1}{2}\tilde{\mathbf{W}}^{\mathbf{T}}\mathbf{P}^{-\mathbf{1}}\tilde{\mathbf{W}} \tag{3.25}$$

where $\tilde{\mathbf{W}} = \mathbf{W}^* - \hat{\mathbf{W}} \Rightarrow \dot{\tilde{\mathbf{W}}} = \dot{\mathbf{W}}^* - \dot{\hat{\mathbf{W}}} = -\dot{\hat{\mathbf{W}}}$ since $\mathbf{W}^*$ is the optimum weight vector. Taking time derivative of (3.25) yields

$$\dot{V}_1 = z_1\dot{z}_1 - \tilde{\mathbf{W}}^{\mathbf{T}}\mathbf{P}^{-\mathbf{1}}\dot{\hat{\mathbf{W}}} \tag{3.26}$$

Using (3.18)-(3.21) in (3.26) yields,

$$\dot{V}_1 = z_1\Big(z_2 - c_1 z_1 - \frac{\tilde{\mathbf{W}}^{\mathbf{T}}\mathbf{\Phi}}{C}\Big) + \tilde{\mathbf{W}}^{\mathbf{T}}\mathbf{P}^{-\mathbf{1}}\dot{\hat{\mathbf{W}}}. \tag{3.27}$$

To avoid overparameterization, $\dot{\hat{\mathbf{W}}} = -\frac{\mathbf{P}\boldsymbol{\Phi}z_1}{C}$ is not used as the adaptation law. Instead, a special function $\vartheta_\mathbf{1} := -\frac{\mathbf{P}\boldsymbol{\Phi}z_1}{C}$ is defined, known as the first tuning function. Such a substitution results in,

$$\dot{V}_1 = -c_1 {z_1}^2 + \tilde{\mathbf{W}}^\mathbf{T}(\vartheta_\mathbf{1} - \mathbf{P^{-1}}\dot{\hat{\mathbf{W}}}) + z_1 z_2. \tag{3.28}$$

To establish the stability of z_2 requires defining another Lyapunov function V_2 as

$$V_2 = \frac{1}{2}z_2^2. \tag{3.29}$$

Taking the time derivative of V_2 and using (3.22) yields,

$$\dot{V}_2 = z_2\Big(-\frac{x_1}{LC} - \sum_{k=1}^{2}\frac{\partial\alpha}{\partial x_k}\dot{x}_k - \sum_{k=0}^{1}\frac{\partial\alpha}{\partial {v_r}^{(k)}}{v_r}^{(k+1)} - \dot{\hat{\mathbf{W}}}^\mathbf{T}\frac{\partial\alpha}{\partial\hat{\mathbf{W}}^\mathbf{T}} + \frac{E}{LC}u - \ddot{v}_r\Big). \tag{3.30}$$

On substitution of u from (3.23) leads to

$$\dot{V}_2 = -c_2 {z_2}^2 - z_1 z_2 + \tilde{\mathbf{W}}^\mathbf{T}\frac{\partial\alpha}{\partial x_1}\boldsymbol{\Phi}z_2 + \frac{\partial\alpha}{\partial\hat{\mathbf{W}}^\mathbf{T}}(\mathbf{P}\vartheta_\mathbf{2} - \dot{\hat{\mathbf{W}}}). \tag{3.31}$$

Now to show the closed loop stability of the converter under the action of the control law (3.23) and the adaption law (3.24), the total Lyapunov function as V is considered as

$$\begin{aligned} V &= V_1 + V_2 \\ &= \frac{1}{2}\mathbf{z}^\mathbf{T}\mathbf{z} + \frac{1}{2}\tilde{\mathbf{W}}^\mathbf{T}\mathbf{P^{-1}}\tilde{\mathbf{W}} \end{aligned} \tag{3.32}$$

where $\mathbf{z} = [z_1 \;\; z_2]^T$. To show that V is positive definite, it is needed to confirm that $V = 0 \Leftrightarrow \mathbf{z} = 0 \Rightarrow z_1 = z_2 = 0$ and $\tilde{\mathbf{W}} = 0$. By defining $\xi = [\mathbf{z} \;\; \tilde{\mathbf{W}}]^T$ and $\mathbf{P^{-1}} = diag(\gamma_1^{-1}, \gamma_2^{-1}, \ldots, \gamma_5^{-1})$, let us assume that $\exists\ \xi \neq 0$ such that $\xi^\mathbf{T}\left[\begin{array}{c|c} \mathbf{I_2} & 0 \\ \hline 0 & \mathbf{P^{-1}} \end{array}\right]\xi = 0$. Considering $\mathbf{L} = \left[\begin{array}{c|c} \mathbf{I_2} & 0 \\ \hline 0 & \mathbf{P^{-1}} \end{array}\right]$ it is observed that $\mathbf{L}$ is a positive definite matrix and hence $V = 0$ only when $\xi = 0$ which is a contradiction and therefore the origin is the only equilibrium point. Hence V is positive definite. Now to prove that V is radially unbounded, the following expression is considered

$$\frac{\|\xi^\mathbf{T}\mathbf{L}\;\xi\|_2}{\|\xi\|_2^2} \leq \frac{\|\xi_2^2\|\|\mathbf{L}\|}{\|\xi\|_2^2} \leq \|\mathbf{L}\| < \infty.$$

Now let $\|\xi^\mathbf{T}\mathbf{L}\;\xi\|_\mathbf{2} \to c$ as $\|\xi\|_\mathbf{2} \to \infty$ where c is a constant

$$\Rightarrow \frac{\|\xi^\mathbf{T}\mathbf{L}\;\xi\|_2}{\|\xi\|_2^2} \leq \frac{c}{\|\xi\|_2^2} \to 0 \;\text{ as }\; \|\xi\|_2 \to \infty.$$

But this is a contradiction and therefore it is established that the Lyapunov function $\xi^\mathbf{T}\mathbf{L}\;\xi$ is radially unbounded. Hence, it is proved that the total Lyapunov function V is positive definite and radially unbounded. Next, taking the time derivative of the total Lyapunov function (3.32) and substituting

from (3.28), (3.31) and (3.24) yields

$$\dot{V} \leq -c_1 z_1^2 - c_2 z_2^2 \leq -\begin{bmatrix} z_1 & z_2 \end{bmatrix} \begin{bmatrix} c_1 & 0 \\ 0 & c_2 \end{bmatrix} \begin{bmatrix} z_1 \\ z_2 \end{bmatrix} \tag{3.33}$$

Hence, $\dot{V}$ is negative semi-definite but proving asymptotic stability of $\mathbf{z}$ requires $\dot{V} = 0 \Leftrightarrow \mathbf{z} = 0$. Now from (3.33), it is found that since $c_1, c_2 > 0$, the matrix involving c_1 and c_2 is positive definite. Therefore $\dot{V} = 0$ is attained only when $\mathbf{z} = 0$. Hence it is concluded that $\dot{V}$ is negative definite or $\dot{V} < 0$. Therefore, the origin $z_1 = 0$ and $z_2 = 0$ is the only positively invariant set. Therefore, by LaSalle's theorem [41], the origin is globally asymptotically stable.

3.2.1.3 Transient Performance Analysis

In order to start the analysis of transients in the event of frequent load changes, two norms $\mathscr{L}_{2[a,b]}$ and $\mathscr{L}_{\infty[a,b]}$ involving $f(t)$ are considered below.

$$\|f(t)\|_{2[a,b]} = \Big(\int_a^b \|f(t)\|^2 dt\Big)^{\frac{1}{2}} \tag{3.34}$$

$$\|f(t)\|_{\infty[a,b]} = \sup_{t\in[a,b]} |f(t)|. \tag{3.35}$$

It is assumed that there are finite number of time instances T_k, where load changes occur. In order to analyze the transient performance, the total Lyapunov function V during the interval $[T_{k-1}, T_k)$ is defined as V_{k-1} given by

$$V_{k-1} = \frac{1}{2}\mathbf{z^T z} + \frac{1}{2}\tilde{\mathbf{W}}^{\mathbf{T}}\mathbf{P^{-1}}\tilde{\mathbf{W}} \tag{3.36}$$

and from the design and stability analysis in (3.33) it is found that

$$\dot{V}_{k-1} \leq -\sum_{i=1}^{2} c_i z_i^2 \leq 0 \tag{3.37}$$

where $k = 0, 1, ..., \infty$. Now the transient performance analysis is described by evaluating $\mathscr{L}_{2[T_{k-1},t_k]}$ and $\mathscr{L}_{\infty[T_{k-1},t_k]}$ of the output tracking error $z_1(t)$, where $t_k \in (T_{k-1}, T_k)$ with $T_0 = 0$ and $T_\infty = \infty$. Therefore from (3.37), it follows that

$$\begin{aligned} \|z_1(t)\|^2_{2[T_{k-1},t_k]} &= \int_{T_{k-1}}^{t_k} z_1^2(t)dt \leq -\frac{1}{c_1}\int_{T_{k-1}}^{t_k} \dot{V}_{k-1}(t)dt \\ &= \frac{1}{c_1}[V_{k-1}(T_{k-1}) - V_{k-1}(t_k)] \leq \frac{1}{c_1}V_{k-1}(T_{k-1}) \end{aligned} \tag{3.38}$$

and further,

$$z_1^2(t) \leq 2V_{k-1}(t) \leq 2V_{k-1}(T_{k-1}) \qquad t \in [T_{k-1}, T_k) \tag{3.39}$$

Defining $\|\tilde{\mathbf{W}}(T_{k-1})\|^2_{\mathbf{P}^{-1}} = \tilde{\mathbf{W}}^{\mathbf{T}}(T_{k-1})\mathbf{P}^{-1}\tilde{\mathbf{W}}(T_{k-1})$ and using (3.38) and (3.39), yields

$$\|z_1(t)\|_{2[T_{k-1},t_k]} \leq \frac{1}{\sqrt{2c_1}}\Big[\mathbf{z^T z}(T_{k-1}) + \|\tilde{\mathbf{W}}^{\mathbf{T}}(T_{k-1})\|^2_{P^{-1}}\Big]^{\frac{1}{2}} \tag{3.40}$$

$$\|z_1(t)\|_{\infty[T_{k-1},t_k]} \leq \left[\mathbf{z^T z}(T_{k-1}) + \|\tilde{\mathbf{W}}^{\mathbf{T}}(T_{k-1})\|^2_{\mathbf{P}^{-1}}\right]^{\frac{1}{2}}. \tag{3.41}$$

From the above expressions it can be derived that the transient performance can be improved by increasing c_1 and $\mathbf{P}$. However, very large values of c_1 and $\mathbf{P}$ may improve the transient performance during $[T_{k-1}, T_k)$ but will increase the $\mathscr{L}_2$ and $\mathscr{L}_\infty$ norm of $z_1(t)$ for the next interval $[T_k, T_{k+1})$. It may result in higher overshoots which is undesirable. Hence, c_1 and $\mathbf{P}$ values should be chosen judiciously.

3.2.1.4 Simulation Results and Discussion

The proposed CNN-ABSC scheme is simulated on a digital platform using Matlab software with a step size of $50\mu s$. The buck converter parameters selected are as follows: $E = 25V$, $L = 59mH$, $C = 220\mu F$ $R = 20\Omega$, $v_r = 10V$ and $f_s = 20KHz$. The number of neurons in CNN is $n = 5$, adaptation rate matrix $\mathbf{P} = diag(\{\gamma_i\}_{i=1}^5)$, where $\gamma_i = 9 \times 10^{-5}$ and controller gains are $c_1 = 2200$, $c_2 = 15$. The required number of neurons n and stabilizing gains c_1, c_2 along with adaptation rate matrix $\mathbf{P}$ are carefully chosen to yield a satisfactory transient and steady state performances for both output voltage and inductor current. Taking into account the extreme practical conditions, the nature of uncertainties considered in this thesis are sudden changes in the nominal values of system parameters R, E and v_r. Performance of the proposed CNN-ABSC is evaluated under a wide range of operating points by subjecting the buck converter system to the following situations: 1) load resistance change, 2) input voltage change and 3) reference output voltage change. The measurement specifications in terms of rise time, settling time, peak over/under shoots in the magnitude of the output voltage are carefully studied and reported.

The proposed control scheme demands instantaneous information about both the converter states x_1 and x_2 to be fed into the controller in order to produce the control signal u as described in (3.23). The control signal generated is continuous in nature and acts as a modulating signal to the PWM block. Hereinafter, the PWM generator compares the signal u with the fixed frequency sawtooth carrier waveform V_{tri}, generating gate pulses to operate the switch S_w. During the entire process, the controller is assumed to have no knowledge about the loading conditions. Hence, the role of the proposed Chebyshev polynomial based neural network becomes significant in adaptively estimating the accurate value of the unknown and uncertain load resistance in the least possible time. The updated information of load parameter R greatly helps the conventional backstepping procedure in generating appropriate control action to compensate accurately for the uncertain load.

Further, the efficacy of the proposed CNN-ABSC is compared with those of the radial basis function neural network (RBFNN) based adaptive backstepping control and the conventional adaptive backstepping control (ABSC) procedure. It is to be noted that all these three methods utilize online leaning mechanism. Moreover, for the sake of fair comparison the computations are carried out under identical conditions of simulation study.

The nonlinear function approximations during start-up by means of RBFNN based adaptive backstepping control, conventional adaptive backstepping control and the proposed CNN-ABSC scheme are given in Figure 3.2 (a). During start-up, the RBFNN based adaptive backstepping control acts slow and estimates the unknown load in $0.45s$. On the other hand, the conventional adaptive back-

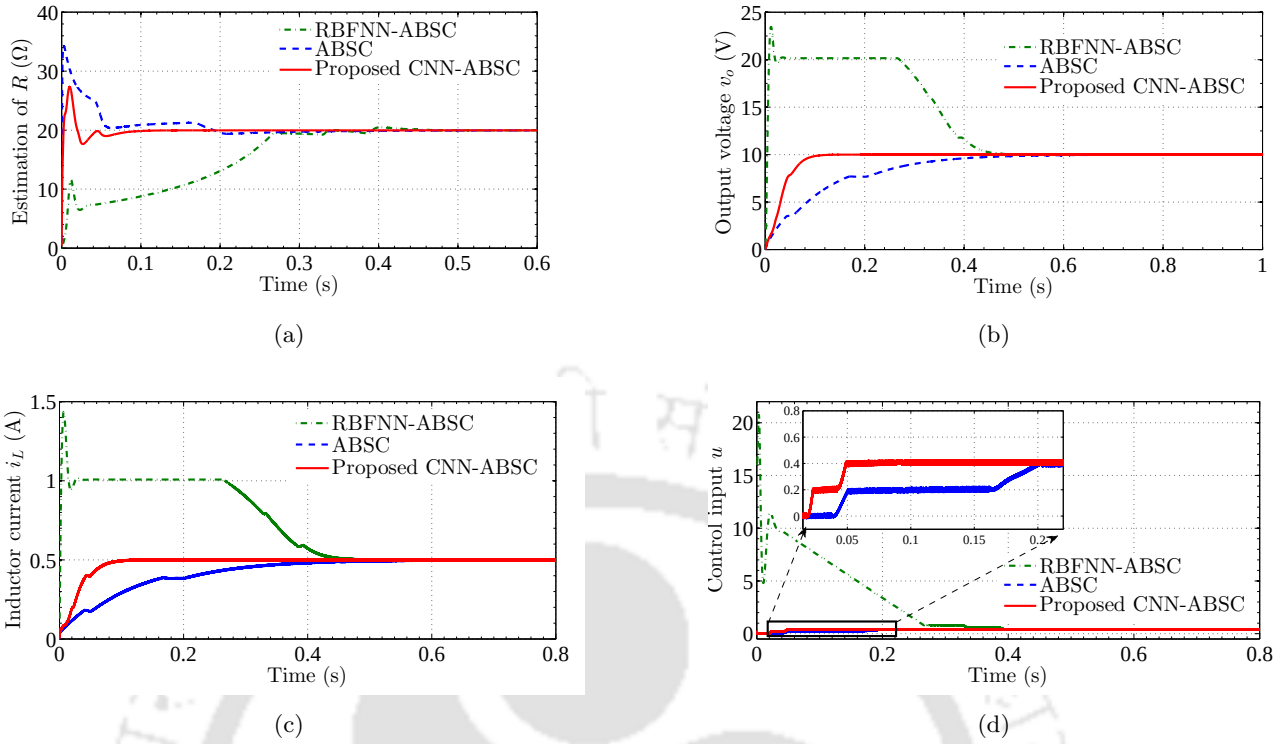

Figure 3.2: Simulation response curves of DC-DC buck converter during start-up: (a) estimation of load R, (b) output voltage, (c) inductor current and (d) control input.

Table 3.1: Performance of load resistance estimation during start-up

Response	Controller	Performance	
		$P_o(\%)$	$t_s(s)$
Estimation	RBFNN-ABSC	–	0.45
	ABSC	70	0.38
	Proposed CNN-ABSC	37.5	0.09

stepping control mechanism yields a larger overshoot, amounting to 70% while estimating the same. In addition, the conventional adaptive backstepping control takes $0.38s$ to converge to the desired value of 20Ω. In contrary, the proposed CNN-ABSC is quick in approximating the unknown load parameter well within $0.09s$ and offers approximately 50% lesser overshoot in comparison to the conventional adaptive backstepping control scheme. The time taken by the proposed CNN-ABSC in estimation is almost 1/5 times lesser than the time required in conventional adaptive backstepping control. A summary of performance indices during start-up, in terms of peak overshoot (P_o) and settling time (t_s) is given in Table 3.1 for ease of comparison. The subsequent dynamic responses obtained for output voltage and inductor current are shown in Figure 3.2 (b) and Figure 3.2 (c) respectively. The RBFNN based adaptive backstepping control method takes larger time to learn and tune the neural network weights. As a result the output voltage v_o converges to the desired reference voltage $10V$ in $0.47s$, as observed in Figure 3.2 (b). The RBFNN-ABSC produces an extremely high initial peak of 135%

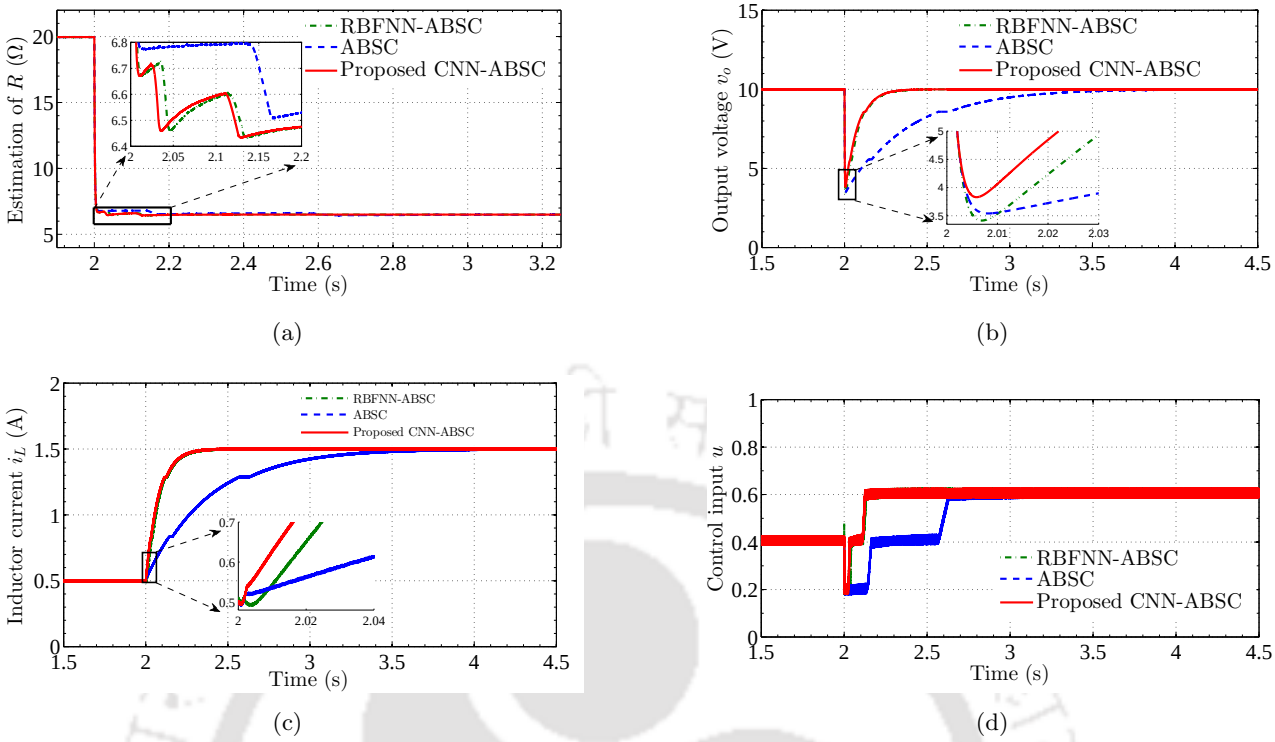

Figure 3.3: Simulation response curves of DC-DC buck converter during step change in load resistance R from 20Ω to 6.66Ω at $t = 2s$: (a) estimation of R, (b) output voltage, (c) inductor current and (d) control input.

in the v_o before settling to desired output voltage. The behavior of inductor current can be found in Figure 3.2 (c). Overshoot upto $1.5A$ against desired current of $0.5A$, besides 100% higher current existing for more than $0.25s$ is not admissible in real time. The average control input u generated by all the three methods are presented in Figure 3.2 (d). It is known that the gate pulses are generated by the PWM block only when $u \in [0, 1]$. Hence, RBFNN-ABSC generates pulse pattern lately due to its slow learning. Therefore, such a transient response of v_o and i_L by RBFNN-ABSC is intolerable and may severely damage the device. On the other hand, the conventional ABSC performs with a settling time of $0.48s$ for both v_o and i_L, but with no overshoot. In contrary, the proposed CNN-ABSC offers fast learning and reaches the desired set-point in $0.09s$ with absolutely no overshoot and steady state error. The corresponding i_L plot in the case of CNN-ABSC shows a smooth curve during start-up making it suitable for real-time use.

Table 3.2: Performance of output voltage for step change in load resistance from 20Ω to 6.666Ω

Response	**Controller**	**Performance**	
		$P_u(\%)$	$t_s(s)$
Output voltage	RBFNN-ABSC	59.5	0.1
	ABSC	63.5	0.42
	Proposed CNN-ABSC	60.1	0.08

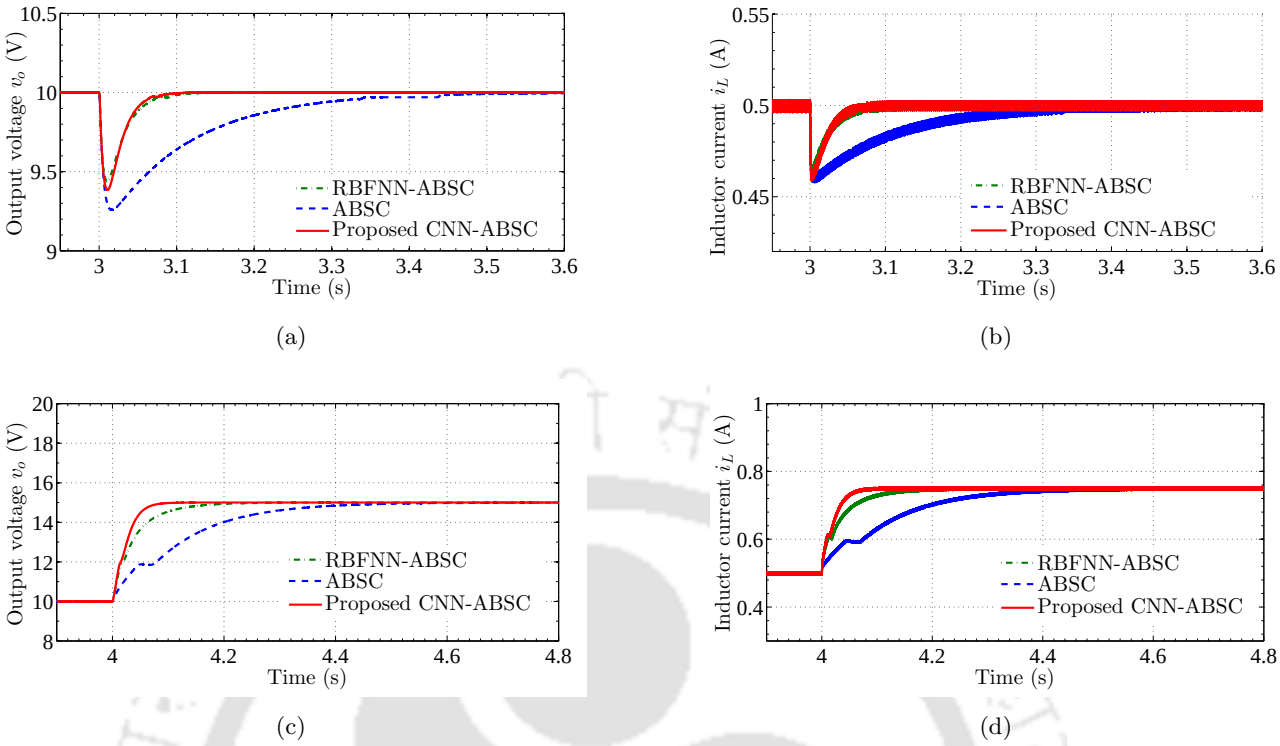

Figure 3.4: Simulation response curves v_o and i_L of DC-DC buck converter during a step change in: (a)-(b) input voltage E from $25V$ to $17V$ at $t = 3s$ and (c)-(d) reference voltage v_r at $t = 4s$.

In order to investigate the efficiency of the proposed CNN-ABSC technique over wide range of operating points, the DC-DC buck converter system is subjected to sudden change in the load resistance. The magnitude of load resistance R is changed from 20Ω to 6.66Ω which amounts to 66.66% change from its nominal value. During the occurrence of such large mismatched uncertainty, the performance of the RBFNN-ABSC, conventional ABSC and proposed CNN-ABSC can be found in Figure 3.3. It can be observed in Figure 3.3 (a) that the approximation of load is faster in the proposed method followed by RBFNN-ABSC and conventional ABSC. Consequently the v_o and i_L profiles also demonstrate an improvement with the proposed CNN-ABSC scheme as depicted in Figure 3.3 (b)-3.3 (c). Closer examination of performance measure of v_o profile given in Table 3.2 reveals a faster response by the proposed CNN-ABSC in terms of settling time (t_s). The peak undershoot (P_u) in the case of CNN-ABSC is lower than that of ABSC, but a little higher than that of RBFNN-ABSC. The control signal generated during this study is given in Figure 3.3 (d). Further, the integral of absolute error (IAE) of load estimation error has been evaluated for time $0 - 4.5s$, including both start-up and load change phase and the obtained measurements are tabulated in Table 3.3, which clearly indicate the supremacy of proposed control.

Further, in order to test the immunity of the proposed CNN-ABSC scheme towards matched uncertainty, the DC-DC buck converter is subjected to a step change in the magnitude of input DC voltage E from nominal $25V$ to $17V$ at $t = 3s$. The responses of v_o and i_L under such a change are

Table 3.3: IAE for time $0 - 4.5s$ for start-up and load disturbance

RBFNN-ABSC	ABSC	Proposed CNN-ABSC
3.0281	1.0401	0.6606

plotted in Figures 3.4 (a)-3.4 (b). The conventional ABSC rejects the uncertainty in $0.5s$, whereas RBFNN-ABSC and proposed CNN-ABSC are quite faster to counteract and compensate such a disturbance. Lastly, for examining the tracking performance of the proposed control, the value of reference output voltage v_r is subjected to a sudden change in its magnitude level. Figures 3.4 (c)- 3.4 (d) show the plots depicting the behavior of output voltage and inductor current i_L respectively under such a condition. At time $t = 4s$, a step change in v_r is given to the DC-DC buck converter to track the output voltage from $10V$ to $15V$. Conventional ABSC and RBFNN-ABSC procedure are found to track the new reference trajectory in $0.65s$ and $0.25s$ respectively. On the contrary, the proposed CNN-ABSC successfully tracks the new set-point in about $0.07s$. The corresponding inductor current plot also witnesses a faster adaptation under proposed CNN-ABSC as shown in Fig. 3.4 (d). Thus the results obtained under start-up, load change, input voltage change and reference voltage change clearly demonstrate the effectiveness of the proposed CNN-ABSC method in fast and smooth tracking of desired output voltage and satisfactory inductor current, indicating its suitability in real-time applications to DC-DC buck converters.

3.2.1.5 Experimental Results and Discussion

To realize the closed loop control action on the DC-DC buck converter, the experimental studies are conducted using the laboratory set-up shown in Figure 2.9 in Section 2.3.4.1 (Chapter 2) with equipments and components described therein. The parameters used in the experiment include an inductor $L = 59mH$ with an inductive resistance $r_L = 4.54\Omega$, capacitor $C = 220\mu F$, nominal duty ratio $k = 0.4$, desired output voltage $v_r = 10V$, nominal input DC voltage $E = 25V$ and nominal load resistance $R = 20\Omega$. To study the response of the proposed CNN-ABSC under reference voltage change, the DC-DC buck converter is subjected to change in reference tracking signal from nominal $10V$ to $15V$. The results obtained by using the conventional ABSC scheme and the proposed CNN-ABSC scheme are shown in Figure 3.5 (a) and Figure 3.5 (b) respectively. It is found in these figures that the proposed CNN-ABSC method takes $1s$ to track the new trajectory of $15V$ whereas the ABSC method takes $3.6s$ to do the same.

The performance of the proposed CNN-ABSC is evaluated on the experimental platform by injecting large amount of uncertainty at the load end. The load resistance is suddenly changed from 20Ω to 10Ω and vice-versa, as a consequence of which the load current is perturbed from $0.5A$ to $1.0A$ and again from $1.0A$ to $0.5A$. The performance exhibited by the conventional ABSC scheme and proposed CNN-ABSC scheme are shown in Figure 3.5 (c) and Figure 3.5 (d) respectively. It is observed from Figure 3.5 (c) and Figure 3.5 (d) that during loading, the proposed CNN-ABSC method takes $1.8s$ to track the set $10V$ output voltage whereas the conventional ABSC method takes $7s$ to track that

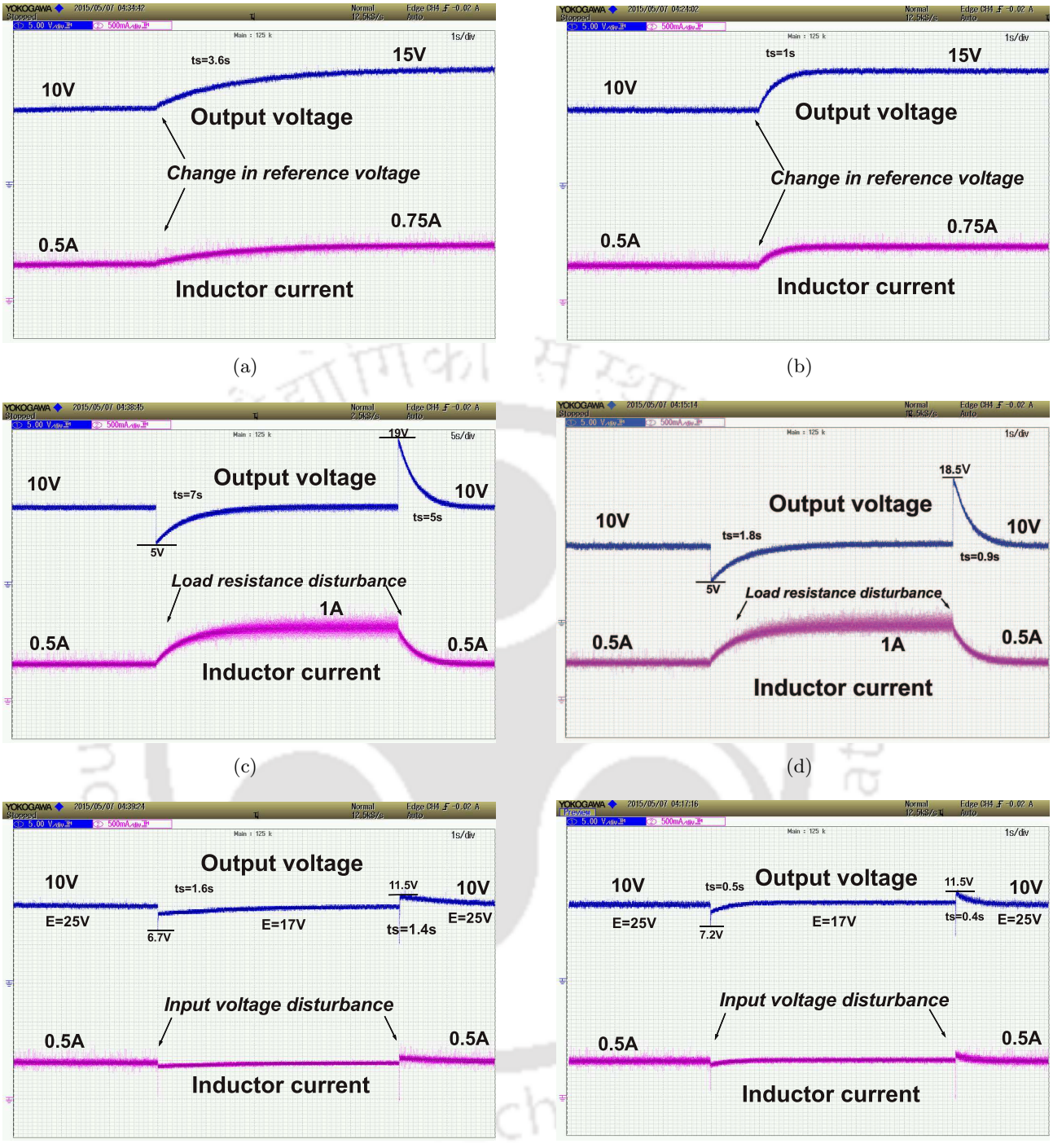

Figure 3.5: Experimental response curves of DC-DC buck converter: (a) under v_r change from $10V$ to $15V$ with ABSC scheme (scale: x-axis; time (1s/div), y-axis: voltage (5V/div), current (500mA/div)), (b) under v_r change from $10V$ to $15V$ with the proposed CNN-ABSC scheme (scale: x-axis; time (1s/div), y-axis: voltage (5V/div), current (500mA/div)), (c) under R change from 20Ω to 10Ω and vice-versa, with ABSC scheme (scale: x-axis; time (5s/div), y-axis: voltage (5V/div), current (500mA/div)), (d) under R change from 20Ω to 10Ω and vice-versa (scale: x-axis; time (1s/div), y-axis: voltage (5V/div), current (500mA/div)), with the proposed CNN-ABSC scheme, (e) under E change from $25V$ to $17V$ and vice-versa, with ABSC scheme (scale: x-axis; time (1s/div), y-axis: voltage (5V/div), current (500mA/div)) and (f) under E change from $25V$ to $17V$ and vice-versa, with the proposed CNN-ABSC scheme (scale: x-axis; time (1s/div), y-axis: voltage (5V/div), current (500mA/div)).

desired voltage. Similarly, during unloading the proposed method takes merely $0.9s$ to track the set $10V$ of output voltage whereas the conventional ABSC method takes $5s$ to track that desired voltage. Besides peak-to-peak ripple in v_o is observed to be $0.4V$ under CNN-ABSC in comparison to $0.68V$ under ABSC method.

For studying effectiveness of the proposed CNN-ABSC scheme under changes in the input voltage, a disturbance mechanism is created in the input supply by connecting a 900Ω resistance in parallel to the supply and using as a potential divider circuit. The two different input levels are realized with the help of single pole double throw (SPDT) switch. Change in input voltage E is made from nominal $25V$ to $17V$ and vice-versa. The performance of both the techniques are presented in Figure 3.5 (e) and Figure 3.5 (f). It is clearly observed that the proposed CNN-ABSC scheme is robust and has better tracking time of $0.5s$ in comparison to $1.6s$ taken by conventional ABSC scheme during input voltage reduction. Similarly, during input voltage rise, the proposed scheme is robust and has better tracking time of $0.4s$ in comparison to $1.4s$ in ABSC.

Remark 4. *To study the closeness of results in simulation and experiments, the following Table 3.4 is presented by comparing Figure 3.3(b) and Figure 3.5(d), wherein the buck converter system is subjected to load resistance perturbation from nominal 20Ω to 10Ω.*

Table 3.4: Comparison of proposed CNN-ABSC method in simulation and hardware during load disturbance from 20Ω to 10Ω

Performance metric	**Simulation**	**Hardware**
Peak undershoot, P_u (%)	60.1	50
Settling time t_s (s)	0.08	1.8

3.2.2 CNN based Adaptive Backstepping Control of DC-DC Buck Converter Driven PMDC-Motor

In reference to the DC-DC buck converter driven PMDC motor described in Section 2.4.1, a neuro-adaptive control using Chebyshev neural network is proposed for the angular velocity control. The design of Chebyshev neural network based adaptive backstepping control method is discussed next.

3.2.2.1 Controller Design

In this subsection, the proposed control scheme is discussed along with the closed loop stability analysis of the overall control structure. The control design is based on backstepping procedure augmented with adaptive Chebyshev neural network (CNN) for angular velocity tracking. The design methodology involves a step by step procedure to obtain the final control law u by selection of appropriate state functions as intermediate virtual-control signals, in order to perform the task of stabilizing lower $(n-1)$-th order subsystems of a full n-th order system. The neural network is used for approximating the unknown nonlinear profile of the load torque τ_L.

The inherent properties of CNN [87], where the Chebyshev polynomial acts as the basis function, are found to be effective in dealing with the approximation problems of nonlinear functions. As discussed

previously in Section 3.2, the advantages of CNN can be enumerated as follows. (1) The orthogonality property of Chebyshev polynomials is the main feature which is utilized to get the best approximation of an unknown function. (2) The condition number using RBFNN is greater than that obtained using CNN, leading to ill-posed function approximation problems with increasing number of neurons n. Hence, the computational burden in CNN is lesser compared to that in RBFNN. As such, a function can be approximated using lesser number of basis functions or neurons using CNN. Therefore, the application of online learning based CNN in the control of electrical drives is well justified. In the following text, the necessary preliminaries of CNN are discussed for a clear understanding of the proposed control.

From the Stone-Weierstrass Theorem [87], for a $y \subset \Omega_y$, any unknown nonlinear function $f(y)$ can be approximated as,

$$f(y) = \mathbf{W^T \Phi}(y) \tag{3.42}$$

under a given compact set $\Omega_y \subset \mathbb{R}$. Here, $\mathbf{W} = [w_0 \ w_1 \dots w_i \dots w_p]^T$ is the optimum weight vector and $\mathbf{\Phi}(y)$ is the regressor with its elements being the Chebyshev polynomial basis functions and $\mathbf{\Phi}(y) = [\phi_0(y) \ \ \phi_1(y) \dots \phi_i(y) \dots \phi_p(y)]^T$. Also,

$$\phi_{i+1}(y) = 2y\phi_i(y) - \phi_{i-1}(y)$$

where i denotes the dimension of the Chebyshev polynomial. Then there exists an ideal weight vector such that the neural network can closely approximate $f(y)$. In general, Chebyshev polynomials $\phi_i(\xi)$ are defined in $\xi \in [-1, 1]$. However, in practice ξ may not always be confined in the closed interval $[-1, 1]$. Therefore, using a nonlinear transformation $y = \mathcal{T}(\xi) = \tanh(\xi)$, Chebyshev polynomials can be defined for any range of $\xi \in \mathbb{R}$ ensuring $y \in [-1, 1]$. Hence, in order to proceed with the control design, the unknown load torque τ_L is estimated as $\tau_L = \mathbf{W^T \Phi}(\omega)$ with the weight vector $\mathbf{W}$ being estimated online. Adopting the backstepping control [69] methodology, the states of the system are defined as $x_1 = \omega$, $x_2 = i_a$, $x_3 = v_a$ and $x_4 = i_L$. Thereafter, in order to initiate with control design, let us define the operator $\mathcal{D}_y(\cdot) := \partial(\cdot)/\partial y$, $f(y)^{(r)}$ as the $r-$th time derivative of $f(y)$ and the tracking error variables as,

$$\left.\begin{aligned} z_1 &= x_1 - \omega_r \\ z_2 &= \left(\frac{K_t}{J}\right) x_2 - \alpha_1 \\ z_3 &= \left(\frac{K_t}{JL_a}\right) x_3 - \alpha_2 \\ z_4 &= \left(\frac{K_t}{JCL_a}\right) x_4 - \alpha_3 \end{aligned}\right\}. \tag{3.43}$$

These tracking error variables in (3.43) are subsequently stabilized utilizing the virtual control inputs α_i $(i = 1,\ 2,\ 3)$, as

$$\alpha_1 = -c_1 z_1 + (B/J)x_1 + (\hat{\mathbf{W}}^{\mathbf{T}}\mathbf{\Phi}/J) + \omega_r^{(1)} \tag{3.44}$$

$$\alpha_2 = -z_1 - c_2 z_2 + \left(\frac{K_t R_a}{JL_a}\right) x_2 + \left(\frac{K_t K_e}{JL_a}\right) x_1 + \mathcal{D}_{x_1}(\alpha_1)\left[\left(\frac{K_t}{J}\right) x_2 - \left(\frac{B}{J}\right) x_1\right]$$
$$+ \mathcal{D}_{x_1}(\alpha_1)\frac{\hat{\mathbf{W}}^{\mathbf{T}}\mathbf{\Phi}}{J} + \sum_{k=0}^{1} \mathcal{D}_{\omega_r^{(k)}}(\alpha_1)\omega_r^{(k+1)} + \mathcal{D}_{\hat{\mathbf{W}}^{\mathbf{T}}}(\alpha_1)\mathbf{\Gamma}\vartheta_{\mathbf{2}} \tag{3.45}$$

$$\alpha_3 = -z_2 - c_3 z_3 + \left(\frac{K_t}{JL_a C}\right) x_2 + \left(\frac{K_t}{JL_a CR}\right) x_3 + \mathcal{D}_{x_1}(\alpha_2)\left[\left(\frac{K_t}{J}\right) x_2 - \left(\frac{B}{J}\right) x_1\right]$$
$$+ \mathcal{D}_{x_1}(\alpha_2)\frac{\hat{\mathbf{W}}^{\mathbf{T}}\mathbf{\Phi}}{J} + \mathcal{D}_{x_2}(\alpha_2)\dot{x}_2 + \mathcal{D}_{\hat{\mathbf{W}}^{\mathbf{T}}}(\alpha_2)\mathbf{\Gamma}\vartheta_{\mathbf{3}} + \sum_{k=0}^{2} \mathcal{D}_{\omega_r^{(k)}}(\alpha_2)\omega_r^{(k+1)} - \mathcal{D}_{\hat{\mathbf{W}}^{\mathbf{T}}}(\alpha_1)\mathbf{\Gamma}\mathcal{D}_{x_1}(\alpha_2)\frac{\mathbf{\Phi}}{J} z_2. \tag{3.46}$$

In the above mentioned virtual control laws α_i, the terms $\mathbf{\Gamma}$ and ϑ_i denote the adaptive rate parameter and adaptive tuning functions, respectively. The recursive relation among tuning functions ϑ_i is defined by $\vartheta_i = \vartheta_{i-1} + w_i z_i$, wherein, $w_1 := -\Phi/J$, $w_2 := \mathcal{D}_{x_1}(\alpha_1)\frac{\Phi}{J}$ and $w_3 := \mathcal{D}_{x_1}(\alpha_2)\frac{\Phi}{J}$. Since the optimal weight vector required for the estimation of the nonlinear uncertain load torque τ_L is unknown, an online Lyapunov based adaptive learning strategy is developed to yield the optimal weight vector to be used in (3.42) yielding a close approximation of the uncertain load torque denoted as $\hat{\tau}_L$. This optimal weight vector estimate $\hat{\mathbf{W}}(\mathbf{t})$ is given by

$$\hat{\mathbf{W}}(\mathbf{t}) = \hat{\mathbf{W}}(t_0) - \frac{\mathbf{\Gamma}}{J}\int_{t_0}^{t} \mathbf{\Phi}(x_1(\nu))(z_1(\nu) - \mathcal{D}_{x_1}(\alpha_1)z_2(\nu) - \mathcal{D}_{x_1}(\alpha_2)z_3(\nu) - \mathcal{D}_{x_1}(\alpha_3)z_4(\nu))d\nu. \tag{3.47}$$

Remark 5. *The virtual control derivatives $\dot{\alpha}_i$ in backstepping are derived analytically since α_i is designed in such a manner that they are continuously differentiable. This is in accordance with the conventional backstepping procedure and the reader is referred to [52].*

Finally, the overall control input $u(t)$ satisfying the Lyapunov criterion of closed loop stability of the tracking error dynamics derived from (3.43) is given by,

$$u(t) = \frac{JCLL_a}{K_t E}\left[-z_3 - c_4 z_4 + \left(\frac{K_t}{JCLL_a}\right) x_3 + \left(\frac{K_t}{JL_a C}\right) x_2 + \left(\frac{K_t}{JL_a CR}\right) x_3\right.$$
$$+ \mathcal{D}_{x_1}(\alpha_3)\left[\left(\frac{K_t}{J}\right) x_2 - \left(\frac{B}{J}\right) x_1\right] + \sum_{j=2}^{3} \mathcal{D}_{x_j}(\alpha_3)\dot{x}_j + \sum_{k=0}^{3} \mathcal{D}_{\omega_r{}^{(k)}}(\alpha_2)\omega_r^{(k+1)} + \mathcal{D}_{\hat{\mathbf{W}}^{\mathbf{T}}}(\alpha_3)\mathbf{\Gamma}\vartheta_{\mathbf{4}}$$
$$\left. + \mathcal{D}_{x_1}(\alpha_3)\frac{\hat{\mathbf{W}}^{\mathbf{T}}\mathbf{\Phi}}{J} - \sum_{k=2}^{3} z_k \mathcal{D}_{\hat{\mathbf{W}}^T}(\alpha_{k-1})\mathbf{\Gamma}\mathcal{D}_{x_1}(\alpha_3)\frac{\mathbf{\Phi}}{J}\right] \tag{3.48}$$

The detailed procedure of the proposed control design is inherently embedded in the stability proofs and will be clear while conducting the stability analysis of the proposed CNN-ABSC scheme. The proposed control scheme for angular velocity tracking in the system described is schematically represented in Figure 3.6.

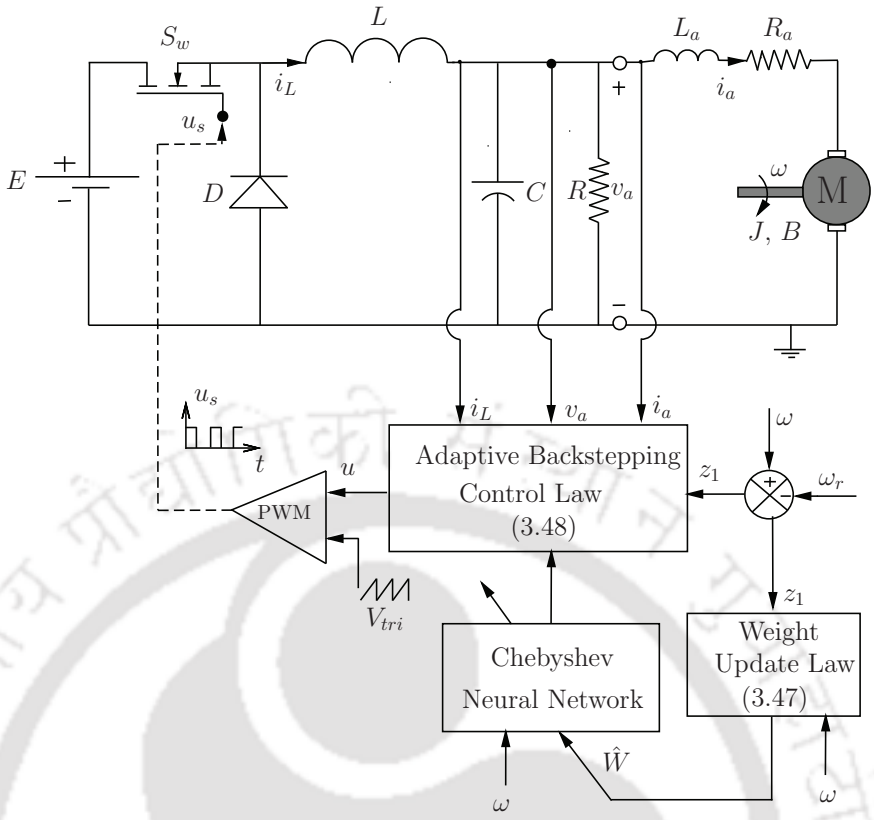

Figure 3.6: Schematic diagram of the proposed CNN-ABSC scheme for angular velocity control of DC-DC buck converter driven PMDC motor.

3.2.2.2 Stability Analysis

The stability analysis starts with the formulation of the closed loop DC-DC buck converter fed PMDC motor system under the action of the proposed controller. It is then followed by the application of Lyapunov stability criterion to infer the stability properties of the speed tracking error dynamics. The stability results of the proposed control algorithm are summarized in Theorem 1.

Theorem 1. *Considering the cascaded dynamics of DC-DC buck converter-PMDC motor combination* (2.62)*, the control law* $u(t)$ *in* (3.48) *along with the CNN weight updation law in* (3.47) *ensures a bounded estimation of the uncertain varying load torque* τ_L *which subsequently guarantees asymptotic angular speed tracking, meaning that* $\lim_{t\to\infty}(x_1 - \omega_r) = 0$*. Therefore, the largest invariant set in which the closed loop trajectories finally reside is given by,*

$$\mathcal{M} = \{(\mathbf{z},\ \tilde{\mathbf{W}}) \in \mathbb{R}^9 : \mathbf{z} = \mathbf{0}, \tilde{\mathbf{W}}^{\mathbf{T}}\mathbf{\Phi}(x_1^*) = 0\} = \{(\mathbf{x},\ \tilde{\mathbf{W}}) \in \mathbb{R}^9 : \mathbf{x} = \mathbf{x}^*, \tilde{\mathbf{W}}^{\mathbf{T}}\mathbf{\Phi}(x_1^*) = 0\}.$$

Further, the proposed controller assures the closed-loop system to be asymptotically stable at all instances of sudden variation in load torque τ_L*. The term* x_1^* *denotes the reference speed trajectory* ω_r*,* $\mathbf{z} = [z_1\ z_2\ z_3\ z_4]^T$ *defines the tracking error variables with* $\tilde{\mathbf{W}}$ *as the weight estimation error and* $\mathbf{x} = [x_1\ x_2\ x_3\ x_4]^T$ *denotes the state vector.*

Proof. In order to investigate the closed loop stability of the DC-DC buck converter fed PMDC motor system under the action of the proposed controller, let us first define the tracking error dynamics derived from (3.43) as follows,

$$\dot{z}_1 = -\left(\frac{B}{J}\right)x_1 - \left(\frac{\mathbf{W^T\Phi}}{J}\right) + z_2 + \alpha_1 + \omega_r^{(1)} \tag{3.49}$$

$$\dot{z}_2 = -\left(\frac{K_tK_e}{JL_a}\right)x_1 - \left(\frac{K_tR_a}{JL_a}\right)x_2 + z_3 + \alpha_2 - \mathcal{D}_{x_1}(\alpha_1)\dot{x}_1 - \sum_{k=0}^{1}\mathcal{D}_{\omega_r^{(k)}}(\alpha_1)\omega_r^{(k+1)} - \mathcal{D}_{\hat{\mathbf{W}}^\mathbf{T}}(\alpha_1)\dot{\hat{\mathbf{W}}} \tag{3.50}$$

$$\dot{z}_3 = -\left(\frac{K_t}{JL_aC}\right)x_2 - \left(\frac{K_t}{JL_aCR}\right)x_3 + z_4 + \alpha_3 - \sum_{j=1}^{2}\mathcal{D}_{x_j}(\alpha_2)\dot{x}_j - \sum_{k=0}^{2}\mathcal{D}_{\omega_r^{(k)}}(\alpha_2)\omega_r^{(k+1)} - \mathcal{D}_{\hat{\mathbf{W}}^\mathbf{T}}(\alpha_2)\dot{\hat{\mathbf{W}}} \tag{3.51}$$

$$\dot{z}_4 = -\left(\frac{K_t}{JCLL_a}\right)x_3 + \left(\frac{K_tE}{JCLL_a}\right)u(t) - \sum_{j=1}^{3}\mathcal{D}_{x_j}(\alpha_3)\dot{x}_j - \sum_{k=0}^{3}\mathcal{D}_{\omega_r{}^{(k)}}(\alpha_3)\omega_r^{(k+1)} - \mathcal{D}_{\hat{\mathbf{W}}^T}(\alpha_3)\dot{\hat{\mathbf{W}}}. \tag{3.52}$$

Substituting the virtual control laws defined in (3.44)-(3.46) and the control input $u(t)$ from (3.48) into (3.49)-(3.52), the tracking error dynamics can be redefined as,

$$\begin{bmatrix}\dot{z}_1\\ \dot{z}_2\\ \dot{z}_3\\ \dot{z}_4\end{bmatrix} = \underbrace{\begin{bmatrix}-c_1 & 1 & 0 & 0\\ -1 & -c_2 & 1+\sigma_{23} & \sigma_{24}\\ 0 & -1-\sigma_{23} & -c_3 & 1+\sigma_{34}\\ 0 & -\sigma_{24} & -1-\sigma_{34} & -c_4\end{bmatrix}}_{\mathcal{A}(\mathbf{z},\hat{\mathbf{W}})}\begin{bmatrix}z_1\\ z_2\\ z_3\\ z_4\end{bmatrix} + \tilde{\mathbf{W}}^\mathbf{T}\underbrace{\begin{bmatrix}-\frac{\Phi}{J}\\ \mathcal{D}_{x_1}(\alpha_1)\frac{\Phi}{J}\\ \mathcal{D}_{x_1}(\alpha_2)\frac{\Phi}{J}\\ \mathcal{D}_{x_1}(\alpha_3)\frac{\Phi}{J}\end{bmatrix}}_{\mathcal{R}_\mathbf{1}(\mathbf{z},\hat{\mathbf{W}})} + \underbrace{\begin{bmatrix}0\\ \mathcal{D}_{\hat{W}^T}(\alpha_1)\\ \mathcal{D}_{\hat{W}^T}(\alpha_2)\\ \mathcal{D}_{\hat{W}^T}(\alpha_3)\end{bmatrix}}_{\mathcal{R}_\mathbf{2}(\mathbf{z},\hat{\mathbf{W}})}(\mathbf{\Gamma}\vartheta_\mathbf{4} - \dot{\hat{\mathbf{W}}}) \tag{3.53}$$

where, $\sigma_{ij} = -\frac{\partial\alpha_{i-1}}{\partial\hat{\mathbf{W}}^\mathbf{T}}\mathbf{\Gamma}w_j$. To investigate the stability of (3.53), let us define $\mathbf{z} = [z_1\ z_2\ z_3\ z_4]^T$ and consider a positive definite, continuously differentiable Lyapunov function $V : \mathcal{D} \subseteq \mathbb{R}^4\times\mathbb{R}^5\times[0,\infty) \longrightarrow \mathbb{R}_+$ as in (3.54) and let $\mathfrak{B}_l$ denote a ball of radius l.

$$V(\mathbf{z},\tilde{\mathbf{W}},t) := \frac{1}{2}\mathbf{z^T P z} + \frac{1}{2}\tilde{\mathbf{W}}^\mathbf{T}\mathbf{\Gamma^{-1}}\tilde{\mathbf{W}} \tag{3.54}$$

where $\mathbf{P}$, $\mathbf{\Gamma}^{-1} > 0$. This implies that, there exist class $\mathcal{K}$ functions $\beta_1(\cdot)$ and $\beta_2(\cdot)$ defined on $[0,\ r]$,

where $\mathfrak{B}_r \subset \mathcal{D} \subseteq \mathbb{R}^4 \times \mathbb{R}^5$, such that,

$$\beta_1(\|\upsilon\|) \leq V(\mathbf{z}, \tilde{\mathbf{W}}, t) \leq \beta_2(\|\upsilon\|) \quad \forall \upsilon \in \mathfrak{B}_r \tag{3.55}$$

where $\upsilon = [\mathbf{z(t)}, \tilde{\mathbf{W}}(\mathbf{t})]^T \in \mathbb{R}^9$. Now, taking the time derivative of $V(\mathbf{z}, \tilde{\mathbf{W}}, t)$ yields,

$$\dot{V}(\mathbf{z}, \tilde{\mathbf{W}}, t) = \frac{\partial V(\mathbf{z}, \tilde{\mathbf{W}}, t)}{\partial t} + \frac{\partial V(\mathbf{z}, \tilde{\mathbf{W}}, t)}{\partial \mathbf{z}}\dot{\mathbf{z}} + \frac{\partial V(\mathbf{z}, \tilde{\mathbf{W}}, t)}{\partial \tilde{\mathbf{W}}}\dot{\tilde{\mathbf{W}}} \tag{3.56}$$

$$= \frac{1}{2}(\mathbf{z^T P \dot{z}} + \dot{\mathbf{z}}^\mathbf{T}\mathbf{P z}) + \frac{1}{2}(\tilde{\mathbf{W}}^\mathbf{T}\mathbf{\Gamma^{-1}}\dot{\tilde{\mathbf{W}}} + \dot{\tilde{\mathbf{W}}}^\mathbf{T}\mathbf{\Gamma^{-1}}\tilde{\mathbf{W}}) \tag{3.57}$$

$$= \frac{1}{2}\mathbf{z^T}\Big(\mathbf{P}\mathcal{A} + \mathcal{A}^\mathbf{T}\mathbf{P}\Big)\mathbf{z} + \tilde{\mathbf{W}}^\mathbf{T}\mathcal{R}_\mathbf{1}\mathbf{P z} + \mathcal{R}_\mathbf{2}(\mathbf{\Gamma}\vartheta_\mathbf{4} - \dot{\hat{\mathbf{W}}})\mathbf{P z} - \tilde{\mathbf{W}}^\mathbf{T}\mathbf{\Gamma^{-1}}\dot{\tilde{\mathbf{W}}}. \tag{3.58}$$

Considering $\mathbf{P} = \mathbf{I}_{4\times4}$ and the adaptation rate matrix $\mathbf{\Gamma^{-1}}$, both satisfying to be positive definite symmetric (PDS) matrices yield,

$$\begin{aligned}\dot{V} &= \frac{1}{2}\mathbf{z^T}(\mathcal{A} + \mathcal{A}^\mathbf{T})\mathbf{z} + \tilde{\mathbf{W}}^\mathbf{T}\mathcal{R}_\mathbf{1}^\mathbf{T}\mathbf{z} + \mathcal{R}_\mathbf{2}(\mathbf{\Gamma}\vartheta_\mathbf{4} - \dot{\hat{\mathbf{W}}})\mathbf{z} - \tilde{\mathbf{W}}^\mathbf{T}\mathbf{\Gamma^{-1}}\dot{\tilde{\mathbf{W}}} \\ &= -\mathbf{z^T Q z} + \tilde{\mathbf{W}}^\mathbf{T}\mathcal{R}_\mathbf{1}^\mathbf{T}\mathbf{z} + \mathcal{R}_\mathbf{2}(\mathbf{\Gamma}\vartheta_\mathbf{4} - \dot{\hat{\mathbf{W}}})\mathbf{z} - \tilde{\mathbf{W}}^\mathbf{T}\mathbf{\Gamma^{-1}}(\mathbf{\Gamma}\vartheta_\mathbf{4}).\end{aligned}$$

The tuning function $\vartheta_\mathbf{4}$ is found as,

$$\vartheta_\mathbf{4} = \vartheta_\mathbf{1} + \vartheta_\mathbf{2} + \mathcal{D}_{x_1}(\alpha_2)\frac{\mathbf{\Phi}}{J}z_3 + \mathcal{D}_{x_1}(\alpha_3)\frac{\mathbf{\Phi}}{J}z_4. \tag{3.59}$$

Substitution of $\dot{\hat{\mathbf{W}}} = \mathbf{\Gamma}\vartheta_\mathbf{4}$ in the immediate equation of $\dot{V}$ yields,

$$\dot{V}(\mathbf{z}, \tilde{\mathbf{W}}, t) = -\mathbf{z^T Q z} \leq 0 \quad \forall t \geq 0, \upsilon \in \mathbb{R}^9. \tag{3.60}$$

The inequality (3.60) is derived using (3.47) and the fact that $\mathbf{Q} = -(\mathcal{A} + \mathcal{A}^\mathbf{T})/2 = diag(c_1, c_2, c_3, c_4)$ is also PDS on account of $c_1,\ c_2,\ c_3,\ c_4 > 0$. This proves that there exist two class $\mathcal{K}$ functions β_3 and β_4 on $[0,\ a]$, where $\mathfrak{B}_a \subset \mathcal{D} \subseteq \mathbb{R}^4$ such that,

$$\underbrace{-\lambda_{max}(\mathbf{Q})\|\mathbf{z}\|^\mathbf{2}}_{-\beta_3(\|\mathbf{z}\|)} \leq \dot{V} \leq \underbrace{-\lambda_{min}(\mathbf{Q})\|\mathbf{z}\|^\mathbf{2}}_{\beta_4(\|\mathbf{z}\|)} \quad \forall \mathbf{z} \in \mathfrak{B}_a \subset \mathfrak{B}_r. \tag{3.61}$$

Therefore, the only compact invariant set outside which $\dot{V}(\mathbf{z}, \tilde{\mathbf{W}}, t)$ is negative definite is defined as, $\mathscr{S}_1 := \Big\{\mathbf{z} \in \mathbb{R}^4 : \dot{V}(\mathbf{z}, \tilde{\mathbf{W}}, t) = 0 \Rightarrow \mathbf{z} = \mathbf{0}\Big\}$. From LaSalle's Invariance Theorem [41], it follows that $\upsilon := [\mathbf{z}\ \tilde{\mathbf{W}}]^T \in \mathbb{R}^9$ converges to the largest invariant set $\mathcal{M} \subset \mathscr{S}_1$. On this invariant set, $\mathbf{z} = \mathbf{0}$ and $\dot{\mathbf{z}} = \mathbf{0}$. Substituting $\mathbf{z} = \mathbf{0}$ and $\dot{\mathbf{z}} = \mathbf{0}$ in (3.53) yields $\dot{\tilde{\mathbf{W}}} = \mathbf{0}$ and $\tilde{\mathbf{W}}^\mathbf{T}\mathbf{\Phi} = 0$, $\forall(\mathbf{z}, \hat{\mathbf{W}}) \in \mathcal{M}$. Since $z_1 = x_1 - \omega_r$ then $x_1 = \omega_r = x_1^*$ and $(\mathbf{W} - \hat{\mathbf{W}})^\mathbf{T}\mathbf{\Phi}(x_1^*) = 0$ is satisfied on $\mathcal{M}$. Thus, the largest invariant set $\mathcal{M} \subset \mathscr{S}_1$ is given by $\mathcal{M} = \{(\mathbf{z},\ \tilde{\mathbf{W}}) \in \mathbb{R}^9 : \mathbf{z} = \mathbf{0}, \tilde{\mathbf{W}}^\mathbf{T}\mathbf{\Phi}(x_1^*) = 0\} = \{(\mathbf{x},\ \tilde{\mathbf{W}}) \in \mathbb{R}^9 : \mathbf{x} = \mathbf{x}^*, \tilde{\mathbf{W}}^\mathbf{T}\mathbf{\Phi}(x_1^*) = 0\}$. This proves convergence of $(\mathbf{z}, \tilde{\mathbf{W}})$ to $\mathcal{M}$ implying $\mathbf{x} \to \mathbf{x}^*$ as $t \to \infty$.
Since the Lyapunov function $V(\mathbf{z}, \tilde{\mathbf{W}}, t)$ is radially unbounded with respect to υ and $V(t) \to 0$ as $t \to \infty$, the function $V(\mathbf{z}, \tilde{\mathbf{W}}, t)$ satisfies to be a $\mathcal{KL}_\infty$ function over $[0,\ \infty)$, that is on $\mathfrak{B}_\infty$. Further,

it is found that $\lim_{t\to\infty}\beta_4(\|\mathbf{z}\|)=0$. Hence, invoking LaSalle-Yoshizawa Theorem [41] the overall system (3.53) under the action of the proposed controller is globally asymptotically stable and the region of attraction is given by $\mathscr{S}_2 := \{\upsilon \in \mathfrak{B}_\infty \backslash \mathcal{M} : \dot{V} < 0\}$, which as per global invariant set theorem includes all initial conditions spanning the entire $\mathfrak{B}_\infty \subseteq \mathcal{D} \subset \mathbb{R}^4 \times \mathbb{R}^5$ as $r \to \infty$. Hence, $\mathbf{x} = \mathbf{x}^*$ is proved to be globally asymptotically stable implying boundedness of $\hat{\mathbf{W}}$. Alternatively, the stability can also be inferred from the signal convergence lemma. The negative definiteness of $\dot{V}$ implies $\mathbf{z} \in \mathcal{L}_2 \cap \mathcal{L}_\infty$ and $\dot{\mathbf{z}} \in \mathcal{L}_\infty$ which further proves that $\lim_{t\to\infty}\mathbf{z(t)}=0$. However, the analysis is not yet complete. Now it has to be proved that the stability results derived in the preceding text hold in the event of uncertain load changes occurring at abrupt unknown time instances t_1, t_2, ..., t_s. Therefore, let us define the Lyapunov function $V_s(t) : \mathcal{T}_s \to \mathbb{R}_+$ for each $\mathcal{T}_s := [t_s, t_{s+1})$ as,

$$V_s = \frac{1}{2}\mathbf{z^T z} + \frac{1}{2}\tilde{\mathbf{W}}^{\mathbf{T}}\mathbf{\Gamma^{-1}}\tilde{\mathbf{W}}. \tag{3.62}$$

It is evident from (3.60) that $\dot{V}_s \leq 0$. This in turn proves that V_s is positive definite and is monotone decreasing in $\mathcal{T}_s$. The piecewise continuity of V_s at various sub domains $[t_s, t_{s+1})$ can be shown using the continuity criteria for monotone functions. Therefore, from the monotonic decreasing property of V_s, it can be concluded that for $t_s < t_{s+1}$, $V_s(t_s^+) = V_s(t_s) \geq V_s(t_{s+1}^-)$. During start-up, that is in the interval $\mathcal{T}_0$, $V_0(t_0^+) = V_0(t_0) \geq V_0(t_1^-)$ and since $V_0(t_0)$ is finite, it can be inferred that $\mathbf{z} \in \mathcal{L}_2 \cap \mathcal{L}_\infty$ and $\dot{\mathbf{z}} \in \mathcal{L}_\infty$. Now let us consider the time interval $\mathcal{T}_1$ during which load change occurs and accommodated by the controller. For $\mathcal{T}_1$, $V_1(t_1^+) \leq 2V_0(t_1^-) + \delta V_1$. Similarly, $V_{s+1}(t_{s+1}^+) \leq 2V_s(t_{s+1}^-) + \delta V_{s+1}$ can be deduced. The term δV_{s+1} is finite and results from the jumps in the adaptive parameter $\tilde{\mathbf{W}}(\mathbf{t})$ in the event of load changes. Hence $V_{s+1}(t_{s+1}^+)$ is bounded in $\mathcal{T}_{s+1}$ if $V_s(t_{s+1}^-)$ is bounded on $\mathcal{T}_s$. To explain further, it is known that $V_{s+1}(t_{s+1}^+) \leq 2V_s(t_{s+1}^-) + \delta V_{s+1} \leq 4V_{s-1}(t_s^-) + 2\delta V_s + \delta V_{s+1}$. Proceeding with such an iterative procedure yields $V_{s+1}(t_{s+1}) \leq \Lambda V_0(t_0) + \Upsilon$ for $t \in [t_{s+1}, \infty)$, where $\Lambda > 0$ and $\Upsilon > 0$ denote generic positive constants. Since $V_0(t_0)$ is bounded, the closed loop signal boundedness at each time interval between the onset of load change and its subsequent accommodation, is guaranteed. This completes the proof. □

3.2.2.3 Transient Performance Analysis

In this section, the $\mathcal{L}_2$ and $\mathcal{L}_\infty$ transient performance bounds of the tracking error $\mathbf{z(t)}$ are calculated. Before proceeding, let us first define $\mathcal{L}_2$ norm as

$$\|\mathbf{z(t)}\|_{2[t_1,t_2]} = \left(\int_{t_1}^{t_2} |\mathbf{z(t)}|^2 dt\right) \tag{3.63}$$

and $\mathcal{L}_\infty$ norms as,

$$\|\mathbf{z(t)}\|_{\infty[t_1,t_2]} = \sup_{t\in[t_1,t_2]} |\mathbf{z(t)}| \tag{3.64}$$

A general bound on the transient performance of the output is derived which encompasses the start up transient response as well as the transients encountered at instances of frequent load changes. From (3.60), the negative definiteness of $\dot{V}_s$ is proved, which implies that during the time interval $\mathcal{T}_s$ with

$T_s \in (t_s, t_{s+1})$,

$$\|\mathbf{z(t)}\|^2_{2[t_s,T_s]} = \int_{t_s}^{T_s} |\mathbf{z(t)}|^2 dt \leq -\frac{1}{\lambda_{min}(\mathbf{Q})} \int_{t_s}^{T_s} \dot{V}_s(t) dt$$

where $\lambda_{min}(\cdot)$, $\lambda_{max}(\cdot)$ denote the minimum and maximum eigen values of their arguments.

$$= -\frac{1}{\lambda_{min}(\mathbf{Q})}[V_s(T_s) - V_s(t_s)] \leq \frac{1}{\lambda_{min}(\mathbf{Q})} V_s(t_s). \tag{3.65}$$

Now defining $\mathbf{\Gamma} = \gamma \mathbf{I}_{5\times 5}$ yields,

$$\begin{aligned} \|\mathbf{z(t)}\|_{2[t_s,T_s]} &\leq \frac{1}{\sqrt{2\lambda_{min}(\mathbf{Q})}} \Big(\|\mathbf{z}(t_s)\|^2 + \frac{\|\tilde{\mathbf{W}}(t_s)\|^2}{\gamma} \Big)^{\frac{1}{2}} \\ &\leq \frac{\|\mathbf{z}(t_s)\|}{\sqrt{2\lambda_{min}(\mathbf{Q})}} + \frac{\|\tilde{\mathbf{W}}(t_s)\|}{\sqrt{2\gamma\lambda_{min}(\mathbf{Q})}}. \end{aligned} \tag{3.66}$$

Similarly, using the fact that $\mathbf{z}(t)^2 \leq 2V_s(t) \leq 2V_s(t_s)$, the $\mathcal{L}_\infty$ bound on the tracking error can be found as,

$$\begin{aligned} \|\mathbf{z}(t)\|_{\infty[t_s,T_s]} &\leq \Big(\|\mathbf{z(t_s)}\|^2 + \frac{1}{\gamma} \|\tilde{\mathbf{W}}(t_s)\|^2 \Big)^{\frac{1}{2}} \\ \|\mathbf{z}(t)\|_{\infty[t_s,T_s]} &\leq \|\mathbf{z(t_s)}\| + \frac{1}{\sqrt{\gamma}} \|\tilde{\mathbf{W}}(t_s)\|. \end{aligned} \tag{3.67}$$

From the above inequalities (3.66) and (3.67), it can be well inferred that an increase in the virtual control gains and the adaptation rate γ result in improved output transients. Very large values of virtual control gain and γ may improve the transient response during $[t_{s-1}, t_s)$ significantly while increasing the $\mathcal{L}_2$ and $\mathcal{L}_\infty$ of the output tracking error $z_1(t)$ following the immediate next interval $[t_s, t_{s+1})$ when load change occurs. This results in high output overshoots at such instances of load change and may sometimes lead to instability as well, which is not desirable. Hence, the virtual control gain and the adaptation rate γ must be chosen judiciously so as to circumvent such consequences while faithfully achieving the control objective.

3.2.2.4 Experimental Results and Discussion

Experimental studies are carried out in laboratory set-up as shown in Figure 2.15 in Section 2.4.4 (Chapter 2). The specifications of the experimental set-up and the parameters associated with the proposed controller are given in Table 2.2. The stabilizing gains of the controller are chosen suitably to obtain a satisfactory response. The gains selected are: $c_1 = 1 \times 10^7$, $c_2 = 1 \times 10^4$, $c_3 = 1 \times 10^2$ and $c_4 = 1 \times 10^2$. Besides, the adaptation rate $\mathbf{P}$=diag$(\{\gamma_i\}_{i=1}^5)$ where $\gamma_i = 1.1 \times 10^{-9}$ is chosen.
The system of DC-DC buck converter fed PMDC-motor is studied for the following experimental case studies.
Case Study I: A step change in ω_r from 0rad/s to 52.3rad/s $(0 - 500\text{rpm})$.
Case Study II: A step change in τ_L from nominal $0.01Nm$ to $0.063Nm$ and vice-versa.

Case Study III: A step change in ω_r from 52.3rad/s to 104.7rad/s ($500 - 1000$rpm).
Case Study IV: A step change in ω_r from 52.3rad/s to 31.4rad/s ($500 - 300$rpm).
The results obtained by using the proposed controller are compared against the results of conventional adaptive backstepping control (ABSC) technique. The aforementioned case studies are discussed in details in the succeeding text.
Case Study I: The nominal value of angular velocity is set to 52.3rad/s which amounts to 500 revolutions per minute (rpm). Figure 3.7 (a)-(e) show the tracking performance of angular velocity ω along with plots of i_a, v_a, i_L and switching signal u_s under the action of ABSC method. It can be observed that angular velocity exhibits high overshoot besides taking $9s$ to converge to the desired value of 52.3rad/s. The performance of the proposed CNN-ABSC method is shown in Figure 3.7 (f)-(j). From these Figures it is clear that the peak overshoot during startup is reduced by 20% and also the time taken to reach to the nominal ω is significantly reduced to $1.4s$. In addition, it is also observed that the peak-to-peak ripple in angular velocity $\Delta\omega$ is $8.8rad/s$, whereas in ABSC method $\Delta\omega$ is found to be $9rad/s$.

Case Study II: An exact knowledge of the varying load torque is essential for effective tracking and control of angular velocity of the PMDC motor. Therefore, by utilizing an online adaptation mechanism for accurate estimation of the uncertain load torque, this test is carried out. Figure 3.8 shows the results containing angular velocity ω, online estimation of unknown load torque τ_L, i_a, v_a and i_L for sudden load torque variation from nominal value of $0.01Nm$ to $0.063Nm$ for both the conventional ABSC scheme and the proposed CNN-ABSC scheme. The conventional ABSC scheme results in a decrease in angular velocity ω from the desired 52.3rad/s and reaches to 31.4rad/s and takes further $12.5s$ to track the nominal value. Next, when the load torque is reduced from $0.063Nm$ to nominal $0.01Nm$, the ABSC scheme reaches the desired level of ω in 9s. However, from Figure 3.8 (f) it is evident that the proposed CNN-ABSC method results in a reduction in angular velocity to 32.3rad/s and settles within a time of $3s$ to reach the nominal value. Similarly, when the load torque is reduced to $0.01Nm$, the proposed scheme quickly tracks the desired level within $1.5s$. For quick summary of the results Table 3.5 is provided.

Table 3.5: Performance of angular velocity tracking under load torque disturbance

τ_L change	Controller	Settling time (s)
0.01Nm to 0.063Nm	ABSC	$12.5s$
	Proposed CNN-ABSC	$3\ s$
0.063Nm to 0.01Nm	ABSC	$9s$
	Proposed CNN-ABSC	$1.5s$

Case Study III: The cascaded combination of DC-DC buck converter PMDC-motor drive is subjected to sudden change in the angular velocity from 52.3rad/s to 104.7rad/s which amounts to change in speed from nominal 500rpm to 1000rpm. The relevant plots can be found in Figure 3.9. It is observed from these plots that the conventional ABSC technique takes nearly $7.8s$ to track the desired value

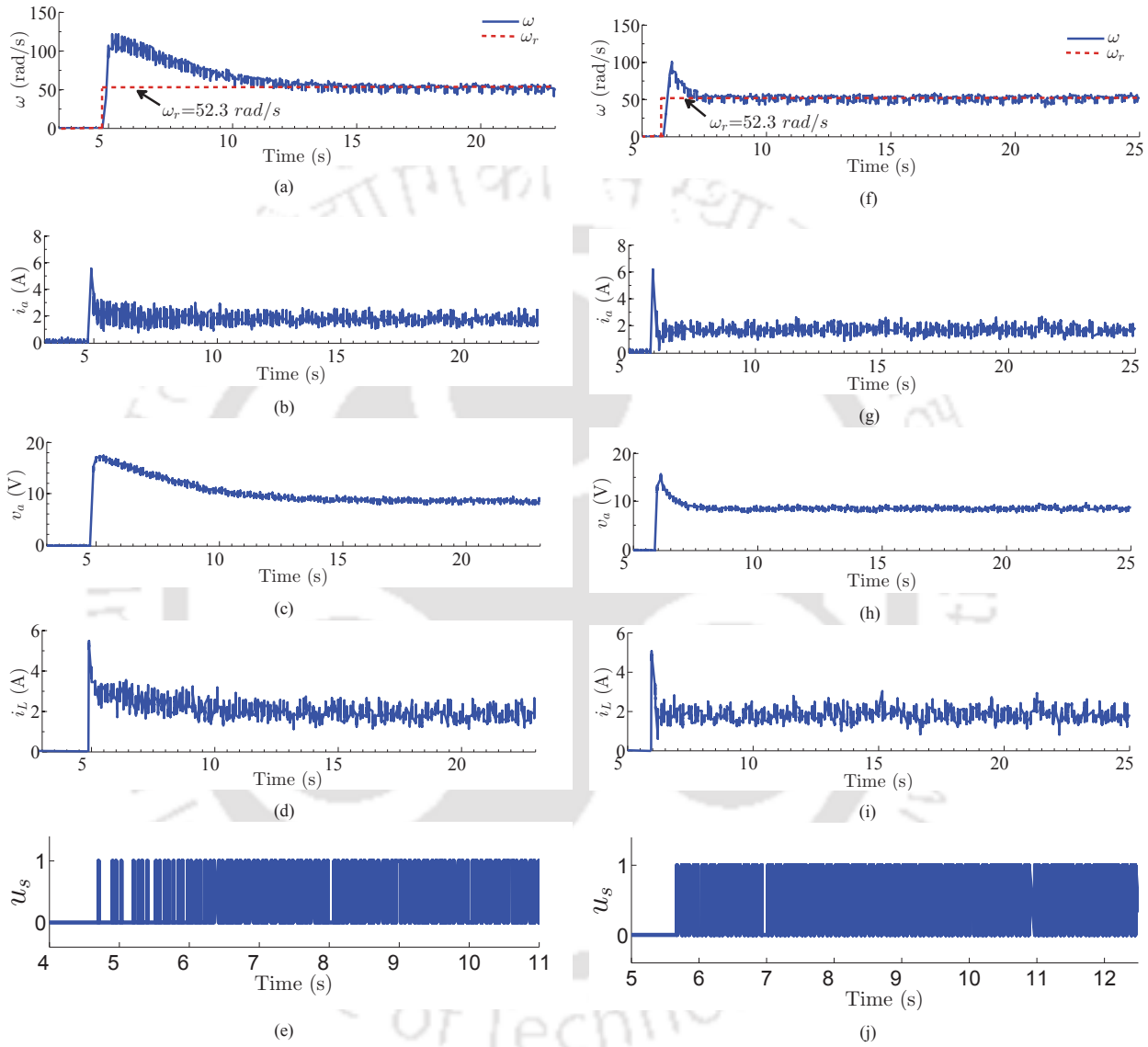

Figure 3.7: Start-up response under ABSC scheme: (a)-(e) and proposed CNN-ABSC scheme: (f)-(j).

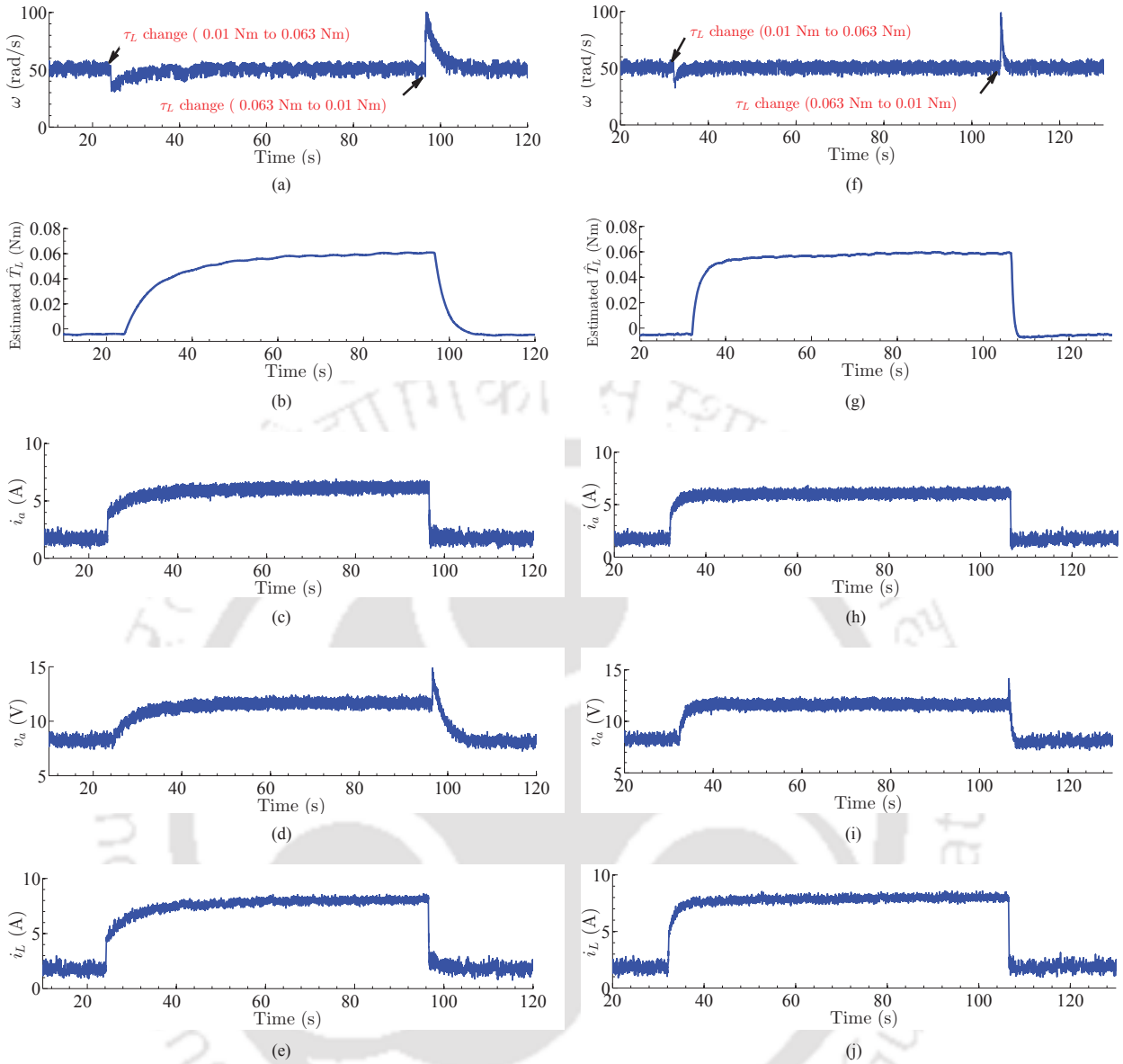

Figure 3.8: Control response under ABSC scheme: (a)-(e) and proposed CNN-ABSC scheme (f)-(j), for sudden changes in load torque τ_L from nominal $0.01Nm$ to $0.063Nm$ and vice-versa.

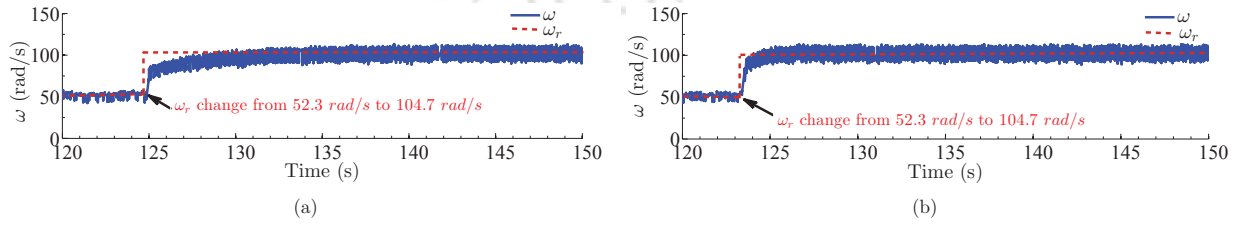

Figure 3.9: Angular velocity tracking from 52.3rad/s to 104.7rad/s under (a) ABSC scheme; (b) proposed CNN-ABSC scheme.

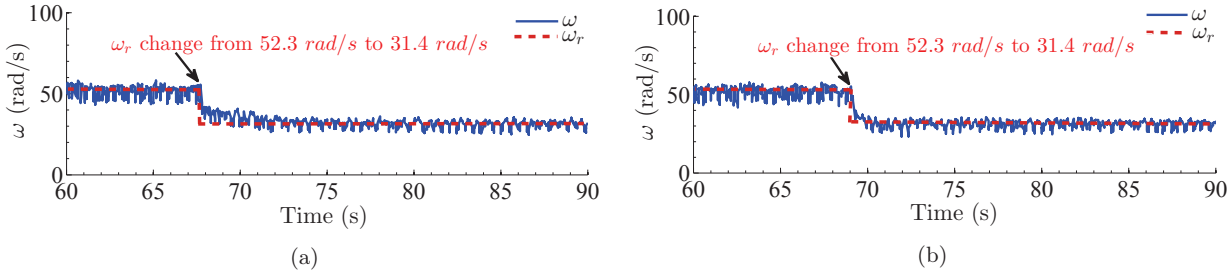

Figure 3.10: Angular velocity tracking from 52.3rad/s to 31.4rad/s under (a) ABSC scheme and (b) proposed CNN-ABSC scheme.

whereas the proposed CNN-ABSC method takes 2.8s to reach the new set point of 104.7rad/s.
Case Study IV: Lastly, to evaluate the behavior of the PMDC-motor in the event of a sudden change in the reference angular velocity from the nominal value to a lower value, the reference w_r is changed from 52.3rad/s to 31.4rad/s and the corresponding responses obtained from the ABSC and the proposed CNN-ABSC are presented in Figure 3.10 (a) and Figure 3.10 (b) respectively. The ABSC tracks the desired velocity in 4s, whereas the proposed control attains the same objective in a time period of 2s. It is clear from the above plots that the proposed CNN-ABSC scheme is quick in responding to desired angular velocity requirements in much lesser time in contrast to the conventional ABSC scheme.

3.3 Hermite Neural Network (HNN) based Uncertainty Estimation

Similar to Chebyshev neural networks (CNN), recursive Hermite polynomial can also be utilized to construct single layer neural networks for unknown function approximation offering several advantages. Firstly, other polynomials such as Legendre polynomials, Chebyshev polynomials and Laguerre polynomials [89] also share the orthogonal property as Hermite polynomials. However, the input range for such polynomials is restricted to the interval $[-1, 1]$. The constraint on the input space in such polynomial based neural networks is undesirable as it would limit the representational capability of the network. On the other hand, representing any unknown function to a high degree of accuracy utilizing Hermite polynomial basis functions does not require the input range to be restricted to a particular interval $[-1, 1]$. Instead any unknown function within its domain $[-\infty,\ \infty]$ can be represented using Hermite polynomial neural networks. Therefore compared to CNN, apart from both being computationally simple, HNN can be utilized for estimation of a larger class of functions. Other beneficial attributes of HNNs when integrated with a control strategy are based on inferences drawn from extensive investigations to follow in the sequel and hence beyond the scope of this section.
The Hermite neural network [89, 90] is explained below. Thereafter it is proposed to be utilized as an estimator to be integrated with a backstepping control technique to arrive at the final control law. Hermite polynomials are recursive orthogonal polynomials which satisfy the recurrence formula, given by (3.68):

$$H_{r+1}(x_1) = x_1 H_r(x_1) - r H_{r-1}(x_1). \tag{3.68}$$

The terms $H_r(x_1),\ r = 0, \ldots, (\rho-1)$ denote the set of Hermite polynomials with $H_0 = 1$, $H_1(x_1) = x_1$ and ρ defines the dimension of the function space in which the unknown function is estimated. Now, in the context of its application to control design in DC-DC buck converters, Hermite neural network (HNN) with online training is constructed to estimate the varying uncertain load resistance R. From (2.41) the unknown function to be estimated is given by $f(\cdot) = x_1/R$. Therefore, using function approximation properties and Stone Weierstrass Theorem, the unknown function can be approximated to an acceptable accuracy as $f(\cdot) = \mathbf{W^*}^{\mathbf{T}}\mathbf{\Phi}(x_1)$ with $\mathbf{W^*} = [w_1^*\ w_2^*\ w_3^* \ldots w_\rho^*]^T$ as the optimal weight vector and

$$\mathbf{\Phi}(x_1) = [H_0(x_1)\ H_1(x_1)\ \ldots\ H_{\rho-1}(x_1)]^T \tag{3.69}$$

as the vector of the basis set spanning the function space wherein the unknown function is approximated.

Nevertheless, the weights w_i^* must be chosen close to their optimal values to obtain an accurate estimate of the unknown function. With no knowledge of the function to be estimated, it is difficult to arrive at the set of such optimal weights which would yield an approximation with high degree of accuracy. Hence, a Lyapunov based weight learning law is formulated using the output tracking error information resulting in an adaptive Hermite neural network to yield a close approximation of the unknown function. Hereafter, this bounded estimation of the uncertain unknown function $f(x_1)$ is fed to the backstepping controller for subsequent cancellations to attain asymptotic stability of the tracking error dynamics.

3.3.1 HNN based Adaptive Backstepping Control of DC-DC Buck Converters with Resistive Load

3.3.1.1 Control and Update Law

Following the controller design procedure of CNN-adaptive backstepping control (ABSC) for DC-DC buck converter, as explained in previous Section 3.2.1, the following results are obtained.
Replacing the unknown load x_1/R term in (2.41) with $\mathbf{W^*}^{\mathbf{T}}\mathbf{\Phi}$, where $\mathbf{\Phi}$ is given in (3.69) and incorporating in the adaptive backstepping control structure, the following control law can be derived:

$$u = \frac{LC}{E}\Bigg(- z_1 - c_2 z_2 + \frac{x_1}{LC} + \frac{\partial \alpha}{\partial x_1}\left(\frac{x_2}{C}\right) - \frac{\partial \alpha}{\partial x_1}\left(\frac{\mathbf{\hat{W}^T\Phi}}{C}\right) + \sum_{k=0}^{1}\frac{\partial \alpha}{\partial {v_r}^{(k)}}{v_r}^{(k+1)} + \mathbf{\dot{\hat{W}}^T}\frac{\partial \alpha}{\partial \mathbf{\hat{W}^T}} + \ddot{v}_r + \frac{\partial \alpha}{\partial x_1}\mathbf{P\vartheta_2}\Bigg) \tag{3.70}$$

and weight update law is found as

$$\mathbf{\dot{\hat{W}}} = -\frac{\mathbf{P\Phi}}{C}\left(z_1 - \frac{\partial \alpha}{\partial x_1}z_2\right) \tag{3.71}$$

where $\mathbf{P} > 0$ is a user defined diagonal matrix symbolizing the adaptive rate and $\mathbf{\Phi}$ is defined in (3.69). The proposed HNN-ABSC scheme for DC-DC buck converters is shown in Figure 3.11.

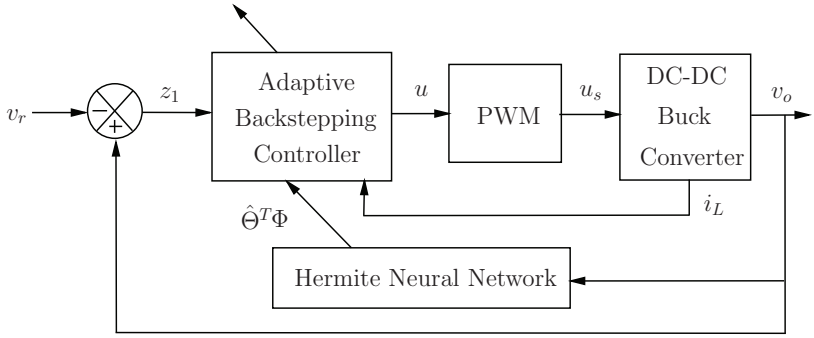

Figure 3.11: Block diagram of the proposed HNN-ABSC scheme for DC-DC buck converters

3.3.1.2 Simulation Results and Discussions

In order to study the performance of the proposed Hermite neural network based adaptive backstepping control (HNN-ABSC), the closed loop DC-DC buck converter is simulated on Matlab tool with a step size of $50\mu s$. The DC-DC buck converter parameters are slected as follows: $E = 25V$, $L = 59mH$, $C = 220\mu F$, $R = 20\Omega$, $v_r = 10V$ and $f_s = 20KHz$. The number of neurons in Hermite neural network $n = 5$, adaptation rate matrix $\mathbf{P} = diag(\{\gamma_i\}_{i=1}^{5})$, where $\gamma_i = 9 \times 10^{-5}$ and controller gains are $c_1 = 2200$, $c_2 = 15$. Further, the proposed control method is compared with the CNN-ABSC method [91]. The tests conducted are as follows.

Case 1. Start-up response (0-10V):

The responses v_o and i_L, obtained during the converter start-up are shown in Figure 3.12 (a)-(b) and the estimates of the load resistance R are provided in Figure 3.12 (e). The results suggest a quicker estimation of load resistance R leading to a faster transient response during start-up under the proposed HNN-ABSC method in $0.046s$ in contrast to CNN-ABSC method.

Case 2. Load resistance change:

The effectiveness of proposed control is evaluated by subjecting the DC-DC buck converter to load resistance change. Load resistance R is suddenly changed from 20Ω to 10Ω. The dynamic response exhibited is given in Figure 3.12 (c)-(d). Besides, the computed estimates of R during load current change are also presented in Figure 3.12 (f). It can be easily inferred from the results that under load change the HNN-ABSC is more effective and yields in better output response.

Case 3. Input voltage disturbance:

Further, the influence of disturbance in input voltage is studied by suddenly reducing the supply voltage E from $25V$ to $17V$. The results are provided in Figure 3.13 (a)-(b), which demonstrate that the HNN-ABSC is faster in responding to the change in supply voltage then the CNN-ABSC.

Case 4. Reference voltage tracking:

At last, tracking performance during set-point change is investigated by suddenly varying reference voltage v_r from $10V$ to $15V$. The results are shown in Figure 3.13 (c)-(d). Results obtained above are tabulated in Table 3.6 and Table 3.7 for quick performance assessment. From the tabular results, a fast and superior control action by the proposed HNN-ABSC method in comparison to CNN-ABSC [91]

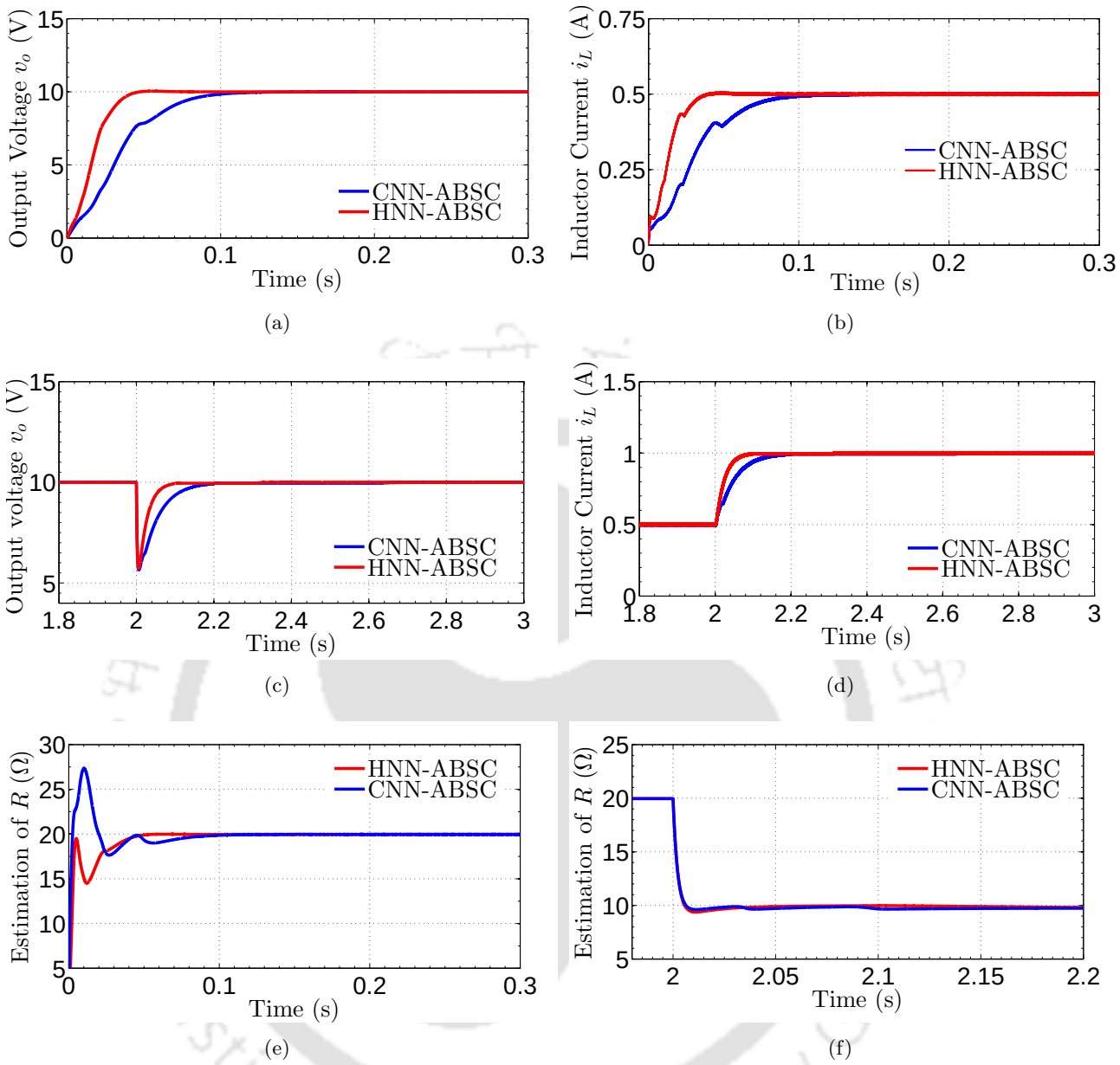

Figure 3.12: Simulation response curves of DC-DC buck converter during: (a)-(b) start-up and (c)-(d) load resistance change from 20Ω to 10Ω. Estimation of load profile during (e) start-up and (f) load change from 20Ω to 10Ω.

is evident.

Remark 6. *An attempt has been made to show the efficacy of proposed control methods with the PID controller. The gains of PID controller obtained by using Zeigler-Nichols method are* $k_p = 3.6$, $k_i = 0.001$ *and* $k_d = 0.00025$. *The result has been shown in Figure 3.15. It is to be noted that, though PID controller attains a faster convergence, it produces a peak-overshoot of* 50% *which is not acceptable. Further, the impact of PID controller in terms of transient performance will be significant during experimentation.*

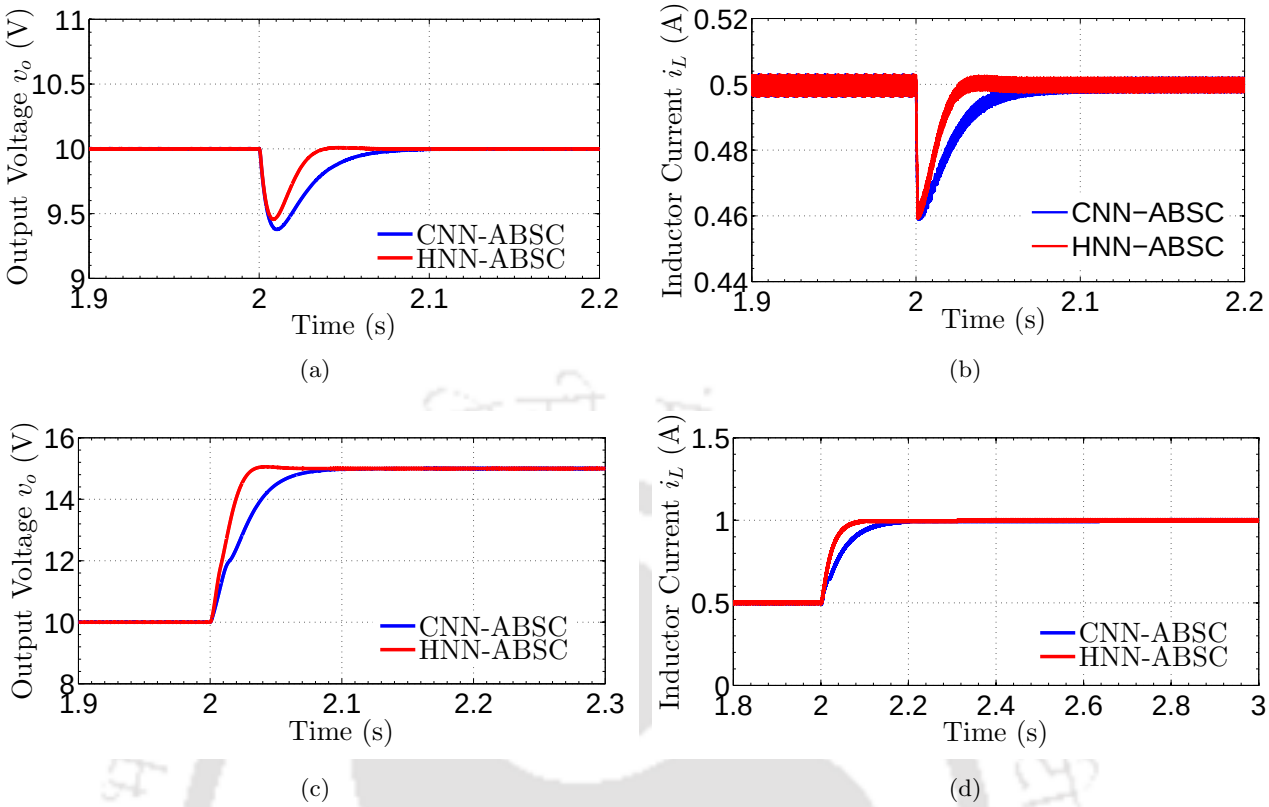

Figure 3.13: Simulation response curves of DC-DC buck converter during: (a)-(b) input voltage E change from $25V$ to $17V$ and (c)-(d) reference voltage v_r change from $10V$ to $15V$.

3.3.1.3 Experimental Results and Discussions

The proposed HNN based adaptive backstepping control is evaluated on an experimental prototype of DC-DC buck converter as discussed in Chapter 2. The start-up response is shown in Figure 3.14 (a). The output voltage v_o and inductor current i_L respond quickly to the reference command and reach the desired levels of $10V$ and $0.5A$ in 0.038s. Besides, the peak-to-peak ripple in v_o under HNN-ABSC method is observed to be 0.62V. Next the sensitivity of v_o is evaluated under a varying load current from $0.5A$ to $1A$ and vice-versa as shown in Figure 3.14 (b). The corresponding changes in gate pulses of power switch S_w are also presented for clarity. Next, the efficiency of the proposed control is tested by subjecting the converter to a step change in supply voltage from $25V$ to $17V$ and

Table 3.6: Performance during start-up and reference voltage change

Response	**Controller**	**Start-up** $v_r = 0V \longrightarrow 10V$	**Reference voltage change** $v_r = 10V \longrightarrow 15V$
		t_s (s)	t_s (s)
Output voltage	CNN-ABSC	0.09	0.07
	HNN-ABSC	**0.046**	**0.04**

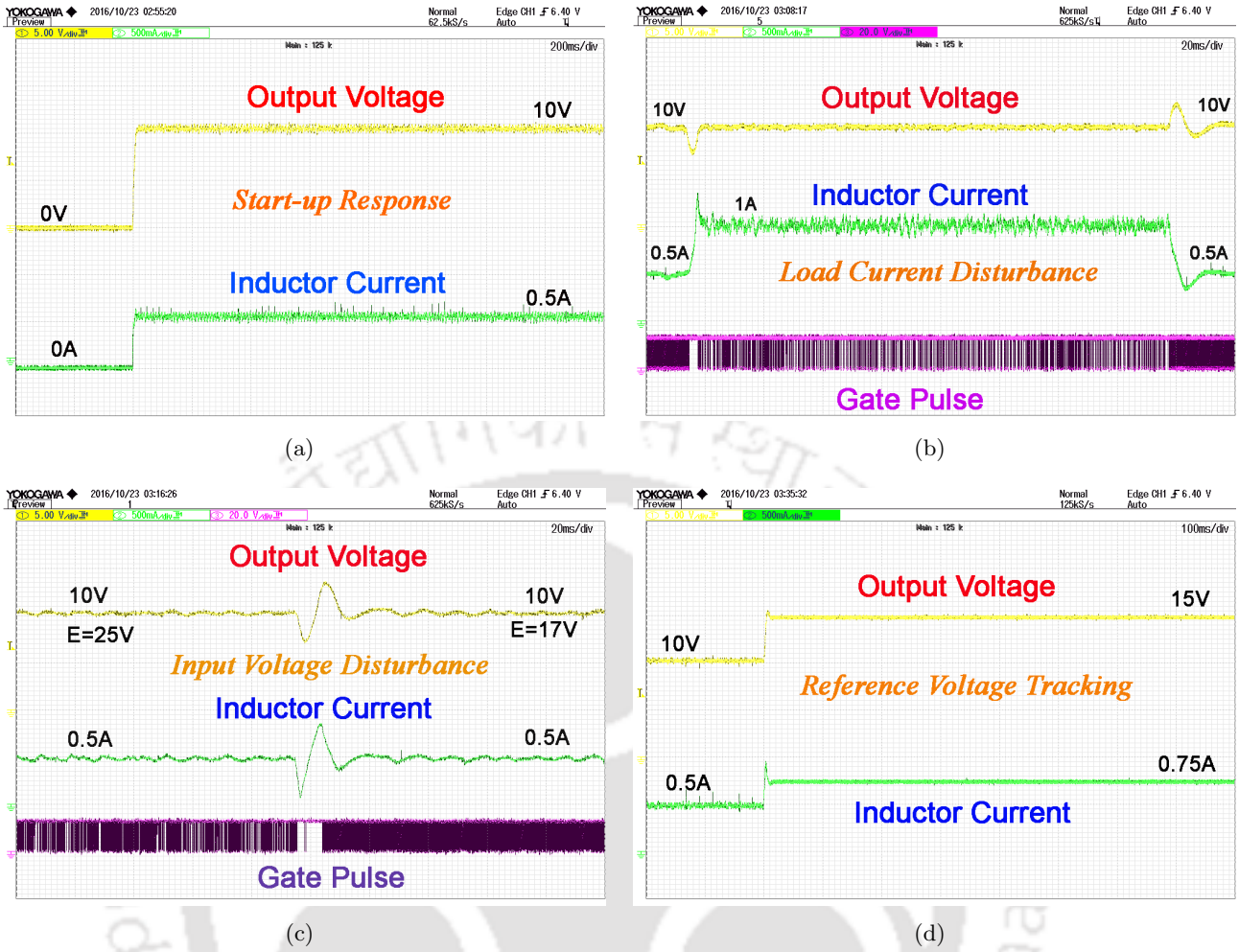

Figure 3.14: Experimental response of DC-DC buck converter under the action of proposed HNN-ABSC control: (a) start-up response for $v_r = 10V$, (scale: x-axis, time: 1 unit=200ms/div and y-axis, voltage: 1 unit=5.0V/div, current: 1 unit=500mA/div), (b) response under load resistance R change from 20Ω to 10Ω and vice-versa, (scale: x-axis, time: 1 unit=20ms/div and y-axis, voltage: 1 unit=5.0V/div, current: 1 unit=500mA/div, Gate pulse 1unit=20V/div), (c) input voltage E disturbance from 25V to 17V, (scale: x-axis, time: 1 unit=20ms/div and y-axis, voltage: 1 unit=5.0V/div, current: 1 unit=500mA/div, Gate pulse 1unit=20V/div) and (d) reference output voltage v_r tracking from $10V$ to $15V$, (scale: x-axis, time: 1 unit=100ms/div and y-axis, voltage: 1 unit=5.0V/div, current: 1 unit=500mA/div).

the corresponding response is shown in Figure 3.14 (c). Due to effective action of the controller, v_o tracks back the set-point of $10V$ in $0.052s$. At the end, rapidness in tracking a varying set-point is recorded in Figure 3.14 (d). It is noted that the due to fast adaptability of the proposed HNN-ABSC, v_o attains desired $15V$ set-point in $0.033s$.

Remark 7. *To study the closeness of results in simulation and experiments, the following Table 3.8 is presented by comparing Figure 3.12(c) and Figure 3.14(b), wherein the buck converter system is subjected to load resistance perturbation from nominal 20Ω to 10Ω.*

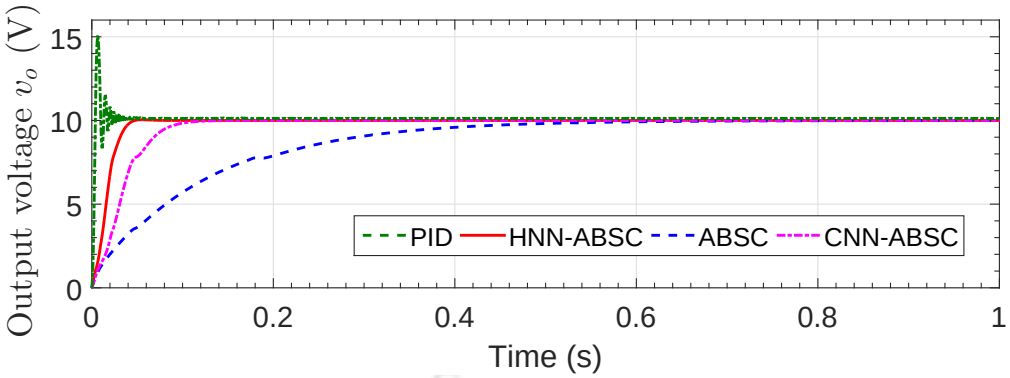

Figure 3.15: Output voltage profile during start-up.

Table 3.7: Transient performance during load resistance change and input voltage disturbance

Response	**Controller**	**Load Resistance change** $R = 20\Omega \rightarrow 10\Omega$		**Input Voltage Disturbance** $E = 25V \rightarrow 17V$	
		P_u (%)	t_s (s)	P_u (%)	t_s (s)
Output voltage	CNN-ABSC	45	0.2	6.8	0.1
	HNN-ABSC	**43**	**0.1**	**5.8**	**0.05**

Table 3.8: Comparison of proposed HNN-ABSC method in simulation and hardware during load disturbance from 20Ω to 10Ω

Performance metric	**Simulation**	**Hardware**
Peak undershoot, P_u *(%)*	45	43
Settling time t_s *(s)*	0.09	0.1

3.3.2 HNN based Adaptive Backstepping Control of DC-DC Buck Converter Driven PMDC-Motor

In a similar manner, the HNN is used to estimate the load torque online in the angular velocity control problem of DC-DC buck converter PMDC-motor system. The HNN is integrated with adaptive backstepping control to yield the proposed HNN-adaptive backstepping control.

3.3.2.1 Control and Update Law

Similar to previous sections, the weight update $\hat{\mathbf{W}}(\mathbf{t})$ and control law $u(t)$ can be deduced as given in (3.72) and (3.73) respectively.

$$\hat{\mathbf{W}}(\mathbf{t}) = \hat{\mathbf{W}}(\mathbf{t_0}) - \frac{\mathbf{\Gamma}}{J}\int_{t_0}^{t} \Phi(x_1(\nu))(z_1(\nu) - \mathcal{D}_{x_1}(\alpha_1)z_2(\nu) - \mathcal{D}_{x_1}(\alpha_2)z_3(\nu) - \mathcal{D}_{x_1}(\alpha_3)z_4(\nu))d\nu \quad (3.72)$$

where Φ is defined in (3.69). The following expression gives the required control input $u(t)$ as,

$$u(t) = \frac{JCLL_a}{K_tE}\left[-z_3 - c_4z_4 + \left(\frac{K_t}{JCLL_a}\right)x_3 + \left(\frac{K_t}{JL_aC}\right)x_2 + \left(\frac{K_t}{JL_aCR}\right)x_3 + \mathcal{D}_{x_1}(\alpha_3)\left[\left(\frac{K_t}{J}\right)x_2 - \left(\frac{B}{J}\right)x_1\right] + \sum_{j=2}^{3}\mathcal{D}_{x_j}(\alpha_3)\dot{x}_j + \sum_{k=0}^{3}\mathcal{D}_{\omega_r{}^{(k)}}(\alpha_2)\omega_r^{(k+1)} + \mathcal{D}_{\hat{\mathbf{W}}^{\mathbf{T}}}(\alpha_3)\mathbf{\Gamma}\vartheta_{\mathbf{4}} + \mathcal{D}_{x_1}(\alpha_3)\frac{\hat{\mathbf{W}}^{\mathbf{T}}\mathbf{\Phi}}{J} - \sum_{k=2}^{3}z_k\mathcal{D}_{\hat{\mathbf{W}}^T}(\alpha_{k-1})\mathbf{\Gamma}\mathcal{D}_{x_1}(\alpha_3)\frac{\mathbf{\Phi}}{J}\right] \tag{3.73}$$

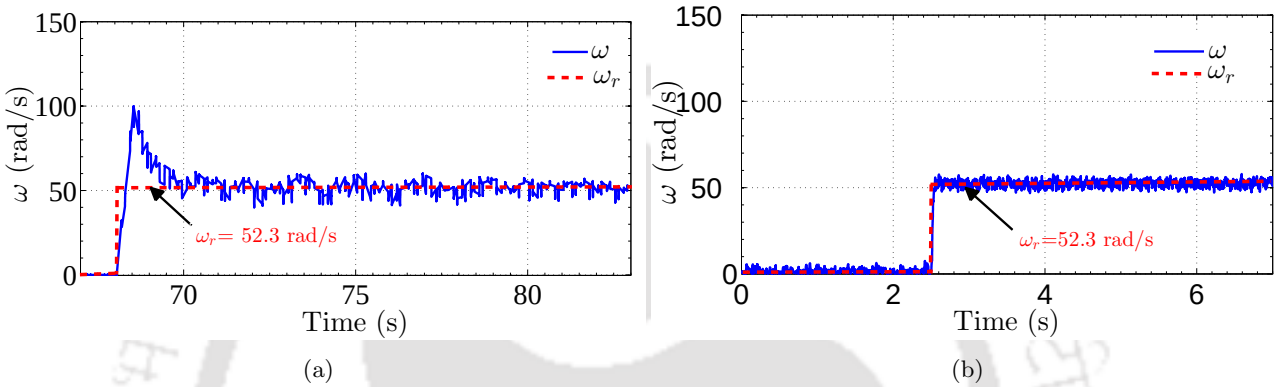

Figure 3.16: Experimental response curves of angular velocity during start-up for $\omega_r = 52.3rad/s$: (a) CNN-ABSC and (b) HNN-ABSC.

3.3.2.2 Experimental Results and Discussion

Real time investigation is conducted on a DC-DC buck converter driven PMDC-motor to evaluate the effectiveness of the proposed the HNN-adaptive backstepping control technique. The results obtained are provided in Figures 3.16-3.18. The results are plotted under start-up response, load torque disturbance and change in the reference angular velocity. Further, the strength of the proposed HNN-ABSC method is evaluated by comparing the results with Chebyshev neural network based adaptive backstepping control (CNN-ABSC) technique discussed previously under identical conditions. From Figures 3.16 (a)-(b) it is evident that the HNN-ABSC method yields satisfactory and fast response during start-up without yielding peak overshoots. Moreover, the time taken to settle to the desired velocity is $0.3s$ by HNN-ABSC in contrast to $6s$ by CNN-ABSC, besides yielding $6.8rad/s$ peak-to-peak ripple in ω. In Figures 3.17 it can be seen that a load change from $0.01Nm$ to $0.063Nm$ and vice-versa causes minor impact on the angular velocity under the action of the proposed HNN-ABSC as shown in 3.17 (b). However, in case of CNN-ABSC the velocity response yields significant undershoot and overshoot during loading and unloading as shown in Figure 3.17 (a). The corresponding estimation of unknown load torque during load change under both CNN-ABSC and HNN-ABSC are plotted in Figures 3.17 (c)-3.17 (d). The changes in armature current i_a are also plotted in Figures 3.17 (e)-3.17 (f). At last, the performance under reference angular velocity change is also evident from Figures 3.18

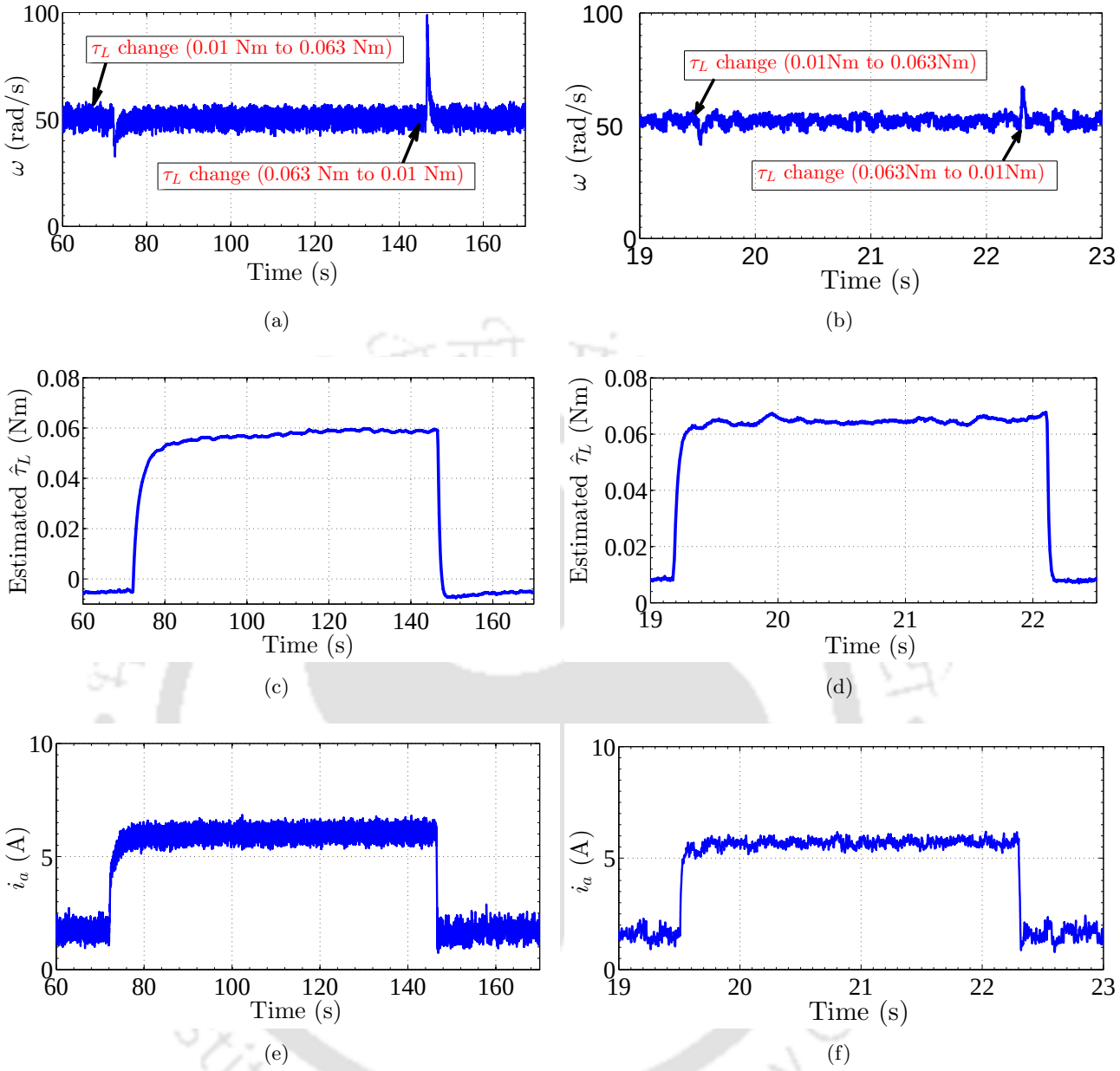

Figure 3.17: Experimental response curves during sudden change in load torque τ_L from $0.01Nm$ to $0.063Nm$ and vice-versa: (a) angular velocity under CNN-ABSC, (b) angular velocity under HNN-ABSC, (c) estimated load torque under CNN-ABSC, (d) estimated load torque under HNN-ABSC, (e) armature current under CNN-ABSC and (f) armature current under HNN-ABSC.

(a)-(b). From all these results it can be clearly visualized that the proposed HNN-ABSC outperforms earlier proposed CNN-ABSC in transient performance, under varying conditions in load, input voltage, reference voltage and load torque.

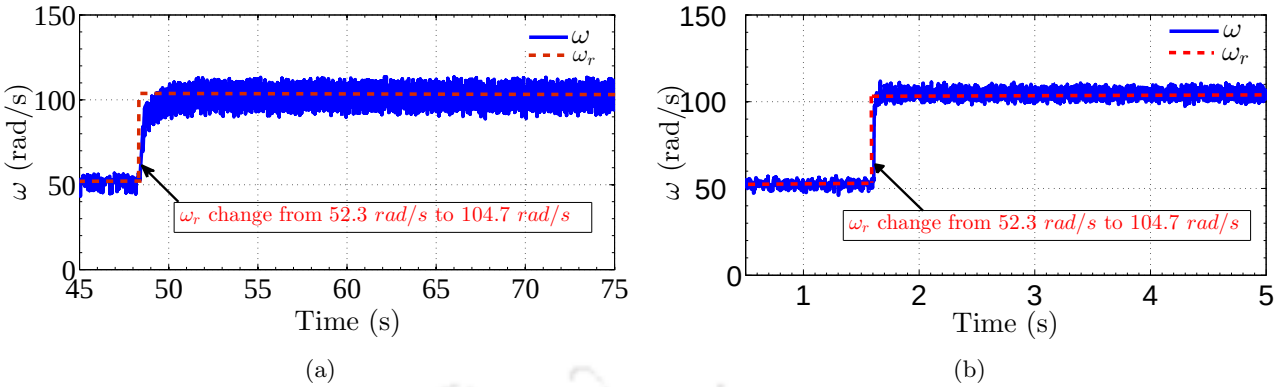

Figure 3.18: Experimental response curves of angular velocity during reference angular velocity change from $\omega_r = 52.3 rad/s$ to $\omega_r = 104.7 rad/s$): (a) CNN-ABSC and (b) HNN-ABSC.

3.4 Summary

This chapter proposes two neuro-adaptive backstepping control methodologies for the transient performance improvement in the output state. At first, a single functional layer Chebyshev neural network (CNN) based adaptive backstepping control method is proposed for the output voltage regulation of DC-DC buck converters feeding resistive load. Here, the Chebyshev polynomial based neural network is used for approximating the unknown varying load resistance. The proposed controller design followed by its stability analysis is supplemented with transient performance analysis. Extensive numerical simulations have been carried out to examine the performance of the proposed CNN-ABSC scheme. A comparative evaluation with radial basis function neural network (RBFNN) based adaptive backstepping control and the conventional adaptive backstepping control mechanism developed in the previous chapter is undertaken. It is observed that the RBFNN based adaptive backstepping control provides a satisfactory response in the steady state, but initially takes larger learning time to tune the neural network weights. As a consequence, there exist a significant overshoot and long time delay during start-up while responding to the desired tracking requirement. On the contrary, the conventional adaptive backstepping control provides a smoother but slow regulation of output voltage. However, the proposed CNN-ABSC method offers a superior transient and steady state performance, owing to its fast estimation of the unknown varying load. The proposed control has been validated by experimental investigation. The experimental results demonstrate that the proposed control is successful in faithfully obtaining a much faster and more accurate estimation of the unknown load resistance even in hardware platform, in comparison to conventional adaptive backstepping technique. In addition, the proposed CNN-ABSC scheme is found to be robust against input voltage changes. Further, this CNN-ABSC method is extended for controlling a DC-DC buck converter driven PMDC motor for angular velocity tracking. The performance of the proposed CNN-ABSC is validated experimentally by subjecting the PMDC-motor system to a wide change in load torque. The results obtained are compared against conventional adaptive backstepping control technique developed in the previous chapter, under identical conditions of experimental study. The results suggest the practical

applicability and robustness of the proposed intelligent control method in successful rejection of load torque uncertainties, in addition to offering better transient performance than the conventional adaptive backstepping control scheme.

Next, the adaptation mechanism is improved by developing a Hermite neural network (HNN) based uncertainty compensation scheme in the framework of adaptive backstepping control, similar on the lines of CNN based controller design. The performance of this HNN-ABSC method is investigated in both simulation and experimental platforms under wide operating range. Quickness in tracking the desired output during start-up and reference voltage change, robustness against load and input voltage fluctuations are established by comparing the performance of HNN based ABSC with the CNN based ABSC in the DC-DC buck converter control task. The HNN-adaptive backstepping control is further extended for angular velocity tracking in DC-DC buck converter fed PMDC-motor. The experiments reveal a significant improvement in the transient performance during start-up and reference voltage tracking without yielding overshoot under the action of HNN-adaptive backstepping control over CNN based one. Furthermore, the supremacy of the HNN based estimation of unknown load torque is also established by its efficient rejection of load perturbations, thereby guaranteeing an improved transient response in angular velocity tracking.

4

Finite Time Exact Compensation of Uncertainties in DC-DC Buck Converters

Contents

4.1 Introduction

It is well known that DC-DC buck converters are inevitably prone to parametric, non-parametric, matched and mismatched perturbations due to uncertain variations in load and circuit parameters. As mentioned earlier, these uncertainties result in a degraded output voltage tracking which is undesirable. The backstepping control (BSC) [41] method proves to be a promising technique in achieving an acceptable transient performance. Here, the trajectory initialization and large virtual control gains selected in the initial design phase maintain satisfactory transient performance. However, since variations in the load, input voltage and system parameters are unanticipated and unknown in time, trajectory initialization is not very feasible. Besides, it has been proved mathematically [92] that the high virtual control gains in the initial phase might result in improved start-up response but degrades post perturbation transients. Lately, as an alternative to neural network based adaptive control, the disturbance observer based control [93–96] has emerged as an attractive way to tackle the uncertainties encountered during system operation and to subsequently achieve an improved performance. However, majority of such works in the recent past considers the disturbance to be bounded and slowly varying with respect to time. On the contrary, implementation of disturbance observer based control to compensate state dependent uncertainties is non trivial and has very limited literature. Extended state observer (ESO) [97] based estimation of lumped uncertainty is found to be a simple method for observing unmeasured states and uncertainties. The requirement of minimum knowledge about the system dynamics is one of the salient features of ESO. Recently, model free active disturbance rejection control (ADRC) [98], [99] techniques have also been proposed yielding satisfactory nominal performance while reducing the effect of unknown external disturbances and modeling imperfections. The significant strength of ADRC lies in its ability to estimate the unknown disturbance and reject the same in the closed loop system without compromising on the nominal control performance [100]. Since the performance of output voltage tracking in DC-DC buck converters is largely influenced by matched and mismatched uncertainties, hence it is necessary to use accurate values of load resistance, input voltage and plant parameters in the controller design to achieve a high precision output voltage tracking. In view of the same, a disturbance observer based controller seems to be an appropriate choice to achieve a robust output voltage tracking with an improved transient performance.

Taking into account the aforementioned issues, a control methodology is proposed in the context of DC-DC buck converters, wherein an exact disturbance observer with finite time convergence is integrated with backstepping control to yield a faithful output voltage tracking while compensating the lumped uncertainties in finite time. Some of the general attributes of the method proposed in this work are as follows; (1) time bound exact estimation of the uncertainty; (2) applicability to a large class of nonlinear uncertain systems affected by matched and mismatched uncertainties which may not be linearly parameterized; (3) unlike conventional adaptive backstepping control strategies [52,91], the proposed scheme does not need persistence of excitation condition for convergence of estimation. Conventional adaptive backstepping control design procedure requires the uncertainties to be linearly parameterized wherein the signals in the regressor matrix are known and bounded. Therefore, for parameter convergence to their true values, the regressor matrix must be persistently exciting (PE). On the contrary, the proposed finite time observer based backstepping control (FTOBSC) method

does not necessarily require the uncertainties to be linearly parameterized and hence no PE condition is required; (4) unlike SMC based approaches [72, 101–103] applied to DC-DC buck converters, the proposed control offers comparatively superior transient and steady state performances while being completely immune to mismatched uncertainties. In contrast to [72], the requirement of measuring units has been minimal in the proposed control structure without effecting the performance; (5) relative to neuro-adaptive control schemes for DC-DC buck converters [91,104], the proposed methodology exhibits a simple structure offering ease in implementation, finite time estimation of matched and mismatched uncertainties and reduced computational burden; and (6) real-time applicability of the proposed control to DC-DC buck converters has been investigated through extensive experimental study under wide variations in load and input voltage. The obtained results support theoretical claims and prove the superiority of the proposed method over relevant existing methods intended for similar applications.

4.2 Proposed Controller Design

Let us revisit the DC-DC buck converter circuit in Figure 2.1. In state space, the dynamics of the averaged DC-DC buck converter model in CCM [71, 72] are written as

$$\left.\begin{aligned} \dot{x}_1 &= -\frac{x_1}{RC} + \frac{x_2}{C} \\ \dot{x}_2 &= -\frac{x_1}{L} + \frac{uE}{L} \end{aligned}\right\} \tag{4.1}$$

where x_1 and x_2 are the states representing output voltage v_o and inductor current i_L. Further, u is the averaged control input to be designed. The schematic diagram of the proposed finite time exact compensation based backstepping controller for DC-DC buck converter is shown in Figure 4.1. The proposed controller utilizes two finite time disturbance observers to estimate the lumped uncertainties encountered in each of the voltage and uncertainty tracking dynamics, exactly in finite time. Thereafter, these estimates are fed to a nominal backstepping controller resulting in subsequent compensation of such external uncertainties besides maintaining a superior nominal tracking performance.

4.2.1 Backstepping Control

Backstepping control [39–41] is a systematic design procedure to arrive at the final control law with stability guaranteed in the sense of Lyapunov. The design procedure is provided below.
The tracking error variables z_1 and z_2 are defined as

$$\left.\begin{aligned} z_1 &= x_1 - v_r \\ z_2 &= \tfrac{x_2}{C} - \alpha \end{aligned}\right\} \tag{4.2}$$

where v_r is the reference output voltage and α is the pseudo-control input to stabilize the z_1-subsystem. In (4.1), let us consider that there is a change in load resistance R and input voltage E by $dR = R - R_0$ and $dE = E - E_0$ respectively, with R_0 and E_0 being the nominal values. Thus incorporating load

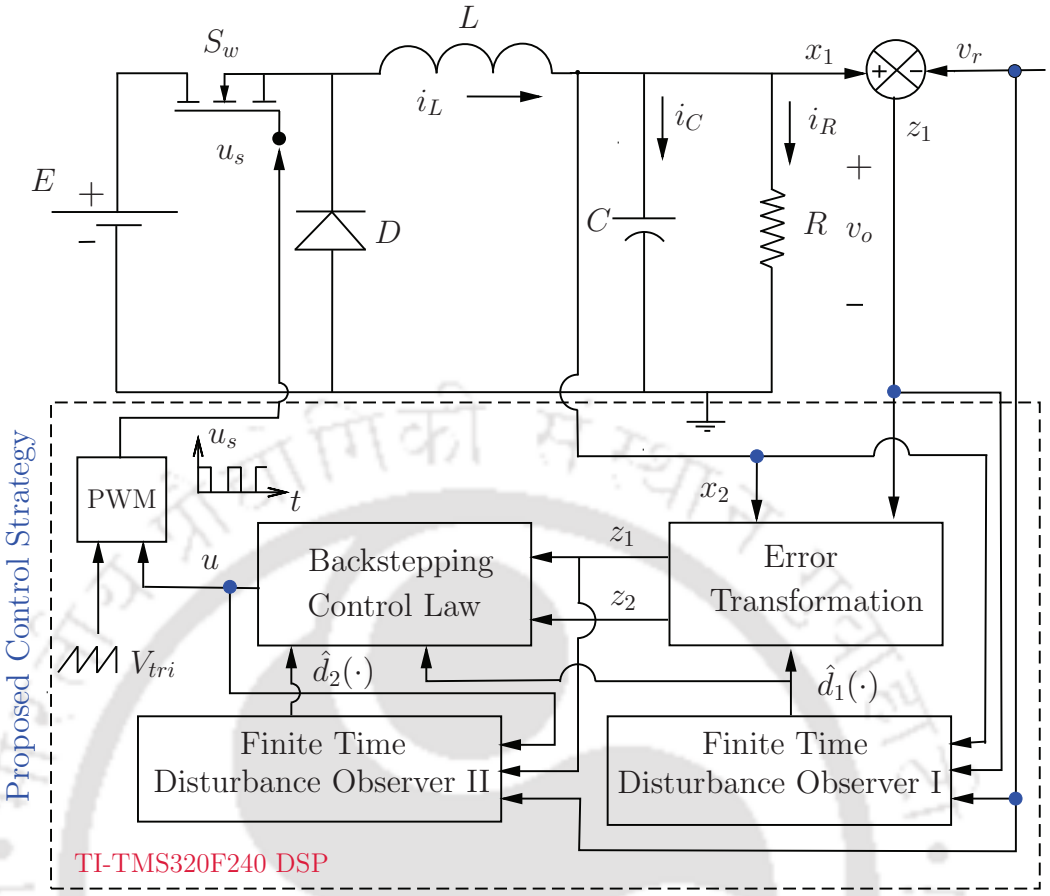

Figure 4.1: Proposed finite time observer based backstepping control (FTOBSC) strategy

and input voltage changes into the DC-DC buck converter model (4.1) yields,

$$\left.\begin{aligned} \dot{x}_1 &= -\frac{x_1}{R_0 C} + \frac{x_2}{C} + d_1 \\ \dot{x}_2 &= -\frac{x_1}{L} + \frac{uE_0}{L} + d_2 \end{aligned}\right\} \tag{4.3}$$

where, $d_1 := \left(-\frac{1}{RC} + \frac{1}{R_0 C}\right) x_1$ and $d_2 := \frac{u}{L}(E - E_0)$. Now, taking the first time derivatives of error variables z_1 and z_2 and using (4.2) and (4.3) gives,

$$\left.\begin{aligned} \dot{z}_1 &= -\tfrac{x_1}{R_0 C} + \tfrac{x_2}{C} + d_1 - \dot{v}_r \\ \dot{z}_2 &= -\tfrac{x_1}{LC} + \tfrac{uE_0}{LC} + \bar{d}_2 - \dot{\alpha} \end{aligned}\right\} \tag{4.4}$$

where d_1 is a lumped uncertainty influencing the z_1 error dynamics. It represents the perturbation arising due to changes occurring in R. Similarly, $\bar{d}_2$ represents the lumped uncertainty taking into account the changes occurring in input voltage E, defined as $\bar{d}_2 = d_2/C$. The virtual control input α

for stabilizing the voltage error subsystem (z_1-dynamics) is given by,

$$\alpha = \frac{x_1}{R_0 C} + \dot{v}_r - \hat{d}_1 - c_1 z_1 \tag{4.5}$$

and the actual control law u to stabilize the z_2-subsystem in (4.4) is obtained as,

$$u = \frac{LC}{E_0}\Big(\frac{x_1}{LC} - \hat{\bar{d}}_2 - c_2 z_2 - z_1 + \dot{\alpha}\Big) \tag{4.6}$$

where $c_1,\ c_2 > 0$ are the controller gain parameters, states x_1 and x_2 are the measured output voltage and inductor current of the converter. Further, $\hat{d}_1(\cdot)$ and $\hat{\bar{d}}_2(\cdot)$ are the estimates of d_1 and $\bar{d}_2$, obtained from the finite time disturbance observers. Herein, through the estimation of unknown lumped uncertainties d_1, $\bar{d}_2$ and thereafter feeding these estimates to the controller for subsequent cancellations, the compensation for the changes in load resistance, inductance, capacitance and input voltage are ensured while achieving a faithful output voltage tracking. In addition, $\dot{d}_1$ and $\dot{\bar{d}}_2$ are assumed to be at-least once continuously differentiable. The finite time disturbance observer design is explained in the following subsection.

4.2.1.1 Finite Time Disturbance Observer Design for Buck Converter

In order to find an exact estimation of the unknown lumped uncertainties d_1 and $\bar{d}_2$, a finite time disturbance observer is employed. This would yield an enhanced output transient performance besides achieving a finite time compensation in the event of intrinsic and extrinsic disturbances. Therefore, in a similar manner as discussed in the previous section and also explained in [105–107], the design of finite time disturbance observer is followed by the derivation of its error dynamics and subsequent finite time stability analysis. Following Appendix A.1, the finite time disturbance observer for the z_1 tracking error dynamics is given by

$$\left.\begin{aligned} \dot{\xi}_{11} &= -\tfrac{\lambda_1}{\varepsilon}|\xi_{11} - z_1|^{\frac{1}{2}}\mathrm{sgn}(\xi_{11} - z_1) - \tfrac{x_1}{RC} + \tfrac{x_2}{C} - \dot{v}_r + \xi_{12} \\ \dot{\xi}_{12} &= -\tfrac{\lambda_2}{2\varepsilon^2}\mathrm{sgn}(\xi_{12} - \upsilon_1) \\ \upsilon_1 &= -\tfrac{\lambda_1}{\varepsilon}|\xi_{11} - z_1|^{\frac{1}{2}}\mathrm{sgn}(\xi_{11} - z_1) + \xi_{12} \end{aligned}\right\} \tag{4.7}$$

and the disturbance observer dynamics for the z_2 subsystem are described as

$$\left.\begin{aligned} \dot{\xi}_{21} &= -\tfrac{\bar{\lambda}_1}{\varepsilon}|\xi_{21} - z_2|^{\frac{1}{2}}\mathrm{sgn}(\xi_{21} - z_2) - \tfrac{x_1}{LC} + \tfrac{uE}{LC} + \xi_{22} \\ \dot{\xi}_{22} &= -\tfrac{\bar{\lambda}_2}{2\varepsilon^2}\mathrm{sgn}(\xi_{22} - \upsilon_2) \\ \upsilon_2 &= -\tfrac{\bar{\lambda}_1}{\varepsilon}|\xi_{21} - z_2|^{\frac{1}{2}}\mathrm{sgn}(\xi_{21} - z_2) + \xi_{22} \end{aligned}\right\} \tag{4.8}$$

where ξ_{11} and ξ_{21} denote the estimates of z_1 and z_2 respectively. The observer variables ξ_{12} and ξ_{22} represent the lumped disturbance estimates $\hat{d}_1$ and $\hat{\bar{d}}_2$ respectively. The terms $\lambda_1, \bar{\lambda}_1, \lambda_2, \bar{\lambda}_2$ are the observer gains and $\varepsilon > 0$ is a small number close to zero. In subsequent analysis, a bound on ε will be found so as to achieve a finite time convergence of the observer error dynamics to the origin.

4.3 Stability Analysis

Prior to the stability analysis concerning the closed loop system under the action of the proposed controller, an input to state property of the system with respect to the bounded variations in load and input voltage is investigated. This would eventually enable to arrive upon necessary conditions required for control design offering nominal performance recovery with finite time uncertainty estimation. Therefore, the analysis commences with the proof of boundedness of system state trajectories as follows.

4.3.1 Boundedness of System Trajectories

Firstly, let us consider a Lyapunov function $V : \mathbb{R}^2 \times [0, \infty) \to \mathbb{R}_+$ as $(\mathbf{z}, t) \mapsto \mathbf{z^T z}$. Thereafter, taking the first time derivative of V and using the control law in (4.6) without the estimates of the lumped uncertainty d_1 and d_2 yields,

$$\dot{V} = z_1(-c_1 z_1 + z_2 + d_1) + z_2 \dot{z}_2 \tag{4.9}$$

$$= -c_1 z_1^2 - c_2 z_2^2 + z_1 d_1 + z_2 d_2. \tag{4.10}$$

Now the uncertainties $d_1(x_1, t)$, $\bar{d}_2(u, t)$ satisfy the following inequality. Firstly, $d_1 \leq L_1\|x_1\| \leq L_1(\|\mathbf{z}\| + |v_r|)$ and $d_2 \leq L_2\|u\|$, where $L_1 = \max\{\frac{\partial d_1}{\partial \mathbf{x}}\}$, $L_2 = \max\{\frac{\partial d_2}{\partial u}\}$ are positive constants. Using the preceding inequalities and Peter Paul inequality [41] with L_1 factor yields

$$\dot{V} \leq -c_1 z_1^2 - c_2 z_2^2 + L_1 \frac{z_1^2}{2} + \frac{\|\mathbf{z}\|^2}{2L_1} + L_1|v_r|\|\mathbf{z}\| + z_2 L_2\|u\|$$

$$\leq -c_0\|\mathbf{z}\|^2 + \frac{\|\mathbf{z}\|^2}{2L_1} + L_1|v_r|\|\mathbf{z}\| + L_2\|\mathbf{z}\|\|u\| \tag{4.11}$$

$$\leq -\left(c_0 - \frac{1}{2L_1}\right)\|\mathbf{z}\|^2 + L_1|v_r|\|\mathbf{z}\| + L_2\|u\|\|\mathbf{z}\| \tag{4.12}$$

$$\dot{V} \leq -k^*\|\mathbf{z}\|^2 + (L_1|v_r| + L_2\|u\|)\|\mathbf{z}\|$$

$$\leq -\frac{k^*}{2}\|\mathbf{z}\|^2 - \|\mathbf{z}\|\left(k^*\frac{\|\mathbf{z}\|}{2} - L_1|v_r| - L_2\|u\|\right) \tag{4.13}$$

where $k^* = \left(c_0 - \frac{1}{2L_1}\right)$. The above inequality implies the negative definiteness of $\dot{V}$ if $\|\mathbf{z}\| > 2(L_1|v_r| + L_2\|u\|)/k^*$ with $c_0 := \min\{c_1 - L_1/2, c_2\}$. Now, from a practical engineering point of view, the assumption $\|u\| < \bar{u}_0$ and $\|\dot{u}\| < \bar{u}_1$ are justified, where $\bar{u}_0$ and $\bar{u}_1$ are the upper bounds. Further, the reference trajectory v_r and its derivatives belong to the compact set $D_{v_r} \in D_x$, where D_x is the domain of attraction of the nominal controlled system. Hence the error state vector $\|\mathbf{z}\|$ is bounded and resides in compact set Ω_z defined as $\{\mathbf{z} \in \mathbb{R}^2 : \|\mathbf{z}\| \leq 2(L_1|v_r| + L_2\|u\|)/k^*\}$. Therefore, the initial conditions must reside within the compact set $\Omega_z^\epsilon := \{\mathbf{z} \in \mathbb{R}^2 | \|\mathbf{z}\| \leq 2\epsilon\,(L_1|v_r| + L_2\|u\|/k^*)\,, 0 \leq \epsilon < 1\} \subset \Omega_\mathbf{z}$. Owing to positive invariance of the set $\Omega_\mathbf{z}$, all error trajectories starting inside compact set $\Omega_\mathbf{z}^\epsilon$ will never leave $\Omega_\mathbf{z}$. Thus, if $\mathbf{z} \in \Omega_\mathbf{z}^\epsilon$, it follows that $\mathbf{x} \in \Omega_x \in D_x$ and the lumped uncertainties $d_1(\mathbf{x}, t)$ and $d_2(\mathbf{x}, t)$ are uniformly piecewise continuous and bounded.

4.3.2 Observer Stability Analysis

Now, proceeding with the observer error dynamics, let us define $\tilde{\xi}_{i1} = \xi_{i1} - z_i$ and $\tilde{\xi}_{i2} = \xi_{i2} - d_i(\cdot)$. Hence, the error dynamics are given by,

$$\left.\begin{aligned} \dot{\tilde{\xi}}_{i1} &= -\tfrac{\lambda_1}{\varepsilon}|\tilde{\xi}_{i1}|^{\frac{1}{2}}\mathrm{sgn}(\tilde{\xi}_{i1}) + \tilde{\xi}_{i2} \\ \dot{\tilde{\xi}}_{i2} &= -\tfrac{\lambda_2}{2\varepsilon^2}\mathrm{sgn}(|\tilde{\xi}_{i1}|^{\frac{1}{2}}\mathrm{sgn}(\tilde{\xi}_{i1})) + \dot{d}_i(\cdot) \end{aligned}\right\} \tag{4.14}$$

where $i = 1, 2$ in (4.14) represent the observer error dynamics for z_1 and z_2 subsystems respectively. Now, the finite time stability analysis of the observer error dynamics in (4.14) is carried out in Theorem 2 below.

Theorem 2. *Considering the observer error dynamics given by* (4.14) *and assuming that the disturbance d_i is at least once continuously differentiable, the resulting observer error variables $\tilde{\xi}_{i1}$ and $\tilde{\xi}_{i2}$ converge to the origin in a finite time provided the gain $\frac{\lambda_2}{2\varepsilon^2} > \sup\{\dot{d}_i(.)\} = \mathcal{L} > 0$, yielding $\hat{d}_i(\cdot) = \xi_{i2}$.*

Proof: To analyze the finite time stability of the observer error dynamics (4.14), the degree of homogeneity of the associated vector fields must be first sought for, followed by the proof of asymptotic stability of the observer error variables. Applying a homogeneity transformation $T_r : (t,\ \tilde{\xi}_{i1}) \longmapsto (rt,\ r^{3-i}\tilde{\xi}_{i1})$, with $i = 1, 2$ to the observer error dynamics yields the degree of homogeneity of the associated vector fields to be $-1 < 0$. Therefore, as a final step to ascertain the stability of the observer, let us consider a strict Lyapunov function $V_0 : \mathbb{R}^2 \setminus \{0\} \times [0, \infty) \to \mathbb{R}_+$ as $(\zeta, t) \mapsto \zeta^{\mathbf{T}}\mathbf{P}\zeta$, where, $\zeta = [\zeta_1\ \zeta_2]^T = [\lceil\tilde{\xi}_{i1}\rfloor^{1/2}\ \tilde{\xi}_{i2}]^T$ and $\lceil\tilde{\xi}_{i1}\rfloor^{\nu} := |\tilde{\xi}_{i1}|^{\nu}\mathrm{sgn}(\tilde{\xi}_{i1})$. The first time derivative of ζ is given by,

$$\dot{\zeta} = \begin{bmatrix} \frac{1}{2}|\tilde{\xi}_{i1}|^{-1/2}\dot{\tilde{\xi}}_{i1} \\ \dot{\tilde{\xi}}_{i2} \end{bmatrix} = \begin{bmatrix} \frac{1}{2}|\tilde{\xi}_{i1}|^{-1/2}(-\frac{\lambda_1}{\varepsilon}\lceil\tilde{\xi}_{i1}\rfloor^{\frac{1}{2}} + \tilde{\xi}_{i2}) \\ -\frac{\lambda_2}{2\varepsilon^2}\mathrm{sgn}(\tilde{\xi}_{i2} - \dot{\tilde{\xi}}_{i2}) + \dot{d}_i(\cdot) \end{bmatrix} \tag{4.15}$$

$$= |\tilde{\xi}_{i1}|^{-1/2}\begin{bmatrix} -\frac{\lambda_1}{2\varepsilon} & \frac{1}{2} \\ -(\frac{\lambda_2}{2\varepsilon^2} - \dot{d}_i(\cdot)\mathrm{sgn}(\tilde{\xi}_{i1})) & 0 \end{bmatrix}\begin{bmatrix} \lceil\tilde{\xi}_{i1}\rfloor^{1/2} \\ \tilde{\xi}_{i2} \end{bmatrix}.$$

As argued in [108], using the fact that $\sup\{\dot{d}_i(.)\} = \mathcal{L}$ (justified in Section 4.3.1) yields

$$\dot{\zeta} \leq |\tilde{\xi}_{i1}|^{-1/2}\underbrace{\begin{bmatrix} -\frac{\lambda_1}{2\varepsilon} & \frac{1}{2} \\ -(\frac{\lambda_2}{2\varepsilon^2} - \mathcal{L}) & 0 \end{bmatrix}}_{\mathbf{A}}\begin{bmatrix} \lceil\tilde{\xi}_{i1}\rfloor^{1/2} \\ \tilde{\xi}_{i2} \end{bmatrix}. \tag{4.16}$$

Hence the first time derivative of the Lyapunov function candidate V_0 can be written as,

$$\dot{V}_0 \leq |\tilde{\xi}_{i1}|^{-1/2}\zeta^{\mathbf{T}}(\mathbf{A}^{\mathbf{T}}\mathbf{P} + \mathbf{P}\mathbf{A})\zeta \leq -|\tilde{\xi}_{i1}|^{-1/2}\zeta^{\mathbf{T}}\mathbf{Q}\zeta \leq 0. \tag{4.17}$$

The above equality is derived from the fact that the matrix $\mathbf{A}$ is Hurwitz and $\mathbf{P}$ is a positive definite symmetric matrix satisfying the Lyapunov criterion given by, $\mathbf{A}^{\mathbf{T}}\mathbf{P} + \mathbf{P}\mathbf{A} = -\mathbf{Q}$ with $\mathbf{Q} > 0$. However, the matrix $\mathbf{A}$ is guaranteed to be Hurwitz if and only if the observer gain $\dfrac{\lambda_2}{2\varepsilon^2} > \sup(\dot{d}_i(.)(t)) = \mathcal{L}$ and

$\frac{\lambda_1}{\varepsilon} > 0$. Now, from Rayleigh principle [41], $|\tilde{\xi}_{i1}|^{1/2} \leq \lceil \tilde{\xi}_{i1} \rfloor^{1/2} \leq \|\zeta\|_2 < \beta_{min}^{-1/2}(\mathbf{P}) V_0^{1/2}$. Then $\dot{V}_0$ can be represented as,

$$\begin{aligned}
\dot{V}_0 &\leq -|\tilde{\xi}_{i1}|^{-1/2} \beta_{min}(\mathbf{Q}) \|\zeta\|_2 \\
&\leq -\beta_{min}^{1/2}(\mathbf{P}) V_0^{-1/2} \beta_{min}(\mathbf{Q}) \|\zeta\|_2 \qquad (4.18) \\
&\leq -\frac{\beta_{min}^{1/2}(\mathbf{P}) \beta_{min}(\mathbf{Q})}{\beta_{max}(\mathbf{P})} V_0^{1/2} \leq -\gamma V_0^{1/2} \qquad (4.19)
\end{aligned}$$

where $\gamma = \frac{\beta_{min}^{1/2}(\mathbf{P}) \beta_{min}(\mathbf{Q})}{\beta_{max}(\mathbf{P})}$, $\beta_{max}(\cdot)$ and $\beta_{min}(\cdot)$ denote the maximum and minimum eigen values of a square matrix. Since the transformed error dynamics ζ is continuous, it follows that ζ decays to zero in finite time, which in turn implies that the observer error variables $\tilde{\xi}_{i1}$ and $\tilde{\xi}_{i2}$ converge to the origin in finite time. Therefore, using Theorem 2.1 in [106], and from (4.19), the observer error dynamics are inferred to be finite time stable. This completes the proof.□

Let us consider, $V_0(t_0) = V_0(0)$, and the final convergence time T satisfying $V_0(T) = 0$ due to negative definiteness of $\dot{V}_0(t)$. From (4.18) it follows that,

$$\begin{aligned}
&\dot{V}_0 + \gamma V_0^{1/2} \leq 0 \\
\Rightarrow &\int_{V_0(0)}^{V_0(T)} \frac{dV_0}{V_0^{1/2}} \leq -\gamma(T - 0) \\
\Rightarrow &2(V_0(T)^{1/2} - V_0(0)^{1/2}) \leq -\gamma T.
\end{aligned}$$

As $V_0(T) = 0$, it is substituted in the above inequality, to get closed form expression for the convergence time T in terms of initial conditions and observer gains as defined below.

$$T \leq \frac{2V_0(0)^{1/2}}{\gamma} \qquad (4.20)$$

Therefore, (4.20) reflects that the relevant parameter influencing the finite time convergence is the bound on the convergence time given by T. On the contrary, such closed form definition of the upper bound on the convergence time for any arbitrary initial condition is not possible in case of asymptotic (exponentially converging) observers.

Hereinafter the exactness in the estimation of disturbance using the disturbance observer featuring finite time convergence is proved. The results have been summarized in Theorem 3.

Theorem 3. *The disturbance observer* (4.7)-(4.8) *yields an exact estimation of the disturbance provided that it is at least once continuously differentiable, i.e* $\sup\{\dot{d}_i\}$ *is available. This implies that at steady state, the exact ultimate bound on the observer error variables is given by* $\tilde{\xi}_{i1} = 0$ *and* $\tilde{\xi}_{i2} = 0$.

Proof: In order to proceed with the proof, the procedure of finding ultimate bounds presented in [109] is followed. Considering the observer error dynamics in (4.7), using a particular diffeomorphism, it has to be transformed to a more suitable form for ease of analysis. Utilizing the diffeomorphism $[\psi_{i1},\ \psi_{i2}]^T = [|\tilde{\xi}_{i1}|^{\frac{1}{2}} \text{sgn}(\tilde{\xi}_{i1}),\ \varepsilon \tilde{\xi}_{i2}]^T$ and $\bar{D}_i = \frac{D_i}{\psi_{i1}{}'(\tilde{\xi}_{i1})}$, where $D_i = \dot{d}_i(\cdot)$, the transformed observer

error (4.7)-(4.8) dynamics are obtained as,

$$\begin{bmatrix} \dot{\psi}_{i1} \\ \dot{\psi}_{i2} \end{bmatrix} = \frac{\psi'_{i1}(\tilde{\xi}_{i1})}{\varepsilon} \Bigg\{ \underbrace{\begin{bmatrix} -\lambda_1 & 1 \\ -\lambda_2 & 0 \end{bmatrix}}_{\mathbf{F}} \begin{bmatrix} \psi_1 \\ \psi_2 \end{bmatrix} + \varepsilon^2 \underbrace{\begin{bmatrix} 0 \\ 1 \end{bmatrix}}_{\mathbf{G}} \bar{D}_i \Bigg\}. \tag{4.21}$$

Let us now consider the auxiliary dynamics as,

$$\begin{bmatrix} \dot{\psi}_{i1} \\ \dot{\psi}_{i2} \end{bmatrix} = \begin{bmatrix} -\lambda_1 & 1 \\ -\lambda_2 & 0 \end{bmatrix} \begin{bmatrix} \psi_1 \\ \psi_2 \end{bmatrix} + \varepsilon^2 \begin{bmatrix} 0 \\ 1 \end{bmatrix} \bar{D}_i. \tag{4.22}$$

From Filippov's Theorem 3 of Chapter 2 in [110], it is inferred that the dynamics described in (4.21) and (4.22) have the same trajectories provided the function $\frac{\psi'_{i1}}{\varepsilon}$ is positive definite. Now the analysis of disturbance estimation error is carried out using the auxiliary dynamics in (4.22). Finally, the original estimation error can be obtained using the expression of ψ_{i1} in a formal change of co-ordinates in (4.22). Now, using the concept of linear system theory and Lemma 1 mentioned in [109], the ultimate bound on the estimation error is derived as $|\psi_{ik}| \leq \varepsilon^2 \{\mathcal{F}\}_k \|\bar{D}_i\|_\infty$ where,

$$\mathcal{F} = \begin{bmatrix} \mathcal{F}_1 \\ \mathcal{F}_2 \end{bmatrix} = \int_0^\infty |e^{\mathbf{F}\tau}\mathbf{G}| d\tau. \tag{4.23}$$

Using the fact that $\|D_i\|_\infty < K$ where $K > 0$ and with the change of co-ordinates to obtain the original estimation error yields

$$\left.\begin{aligned} 2\varepsilon^2 |\tilde{\xi}_{11}|^{\frac{1}{2}} \mathcal{F}_1 K = |\tilde{\xi}_{11}|^{\frac{1}{2}} \mathrm{sgn}(\tilde{\xi}_{11}) \\ |\tilde{\xi}_{11}|^{\frac{1}{2}} (2\varepsilon^2 \mathcal{F}_1 K - 1) = 0 \end{aligned}\right\}. \tag{4.24}$$

Solving (4.24) yields that if $\varepsilon^2 < \frac{1}{2}\mathcal{F}_1 K$, the estimation error $\tilde{\xi}_{i1}$ exactly converges to zero. Similarly, the ultimate bound on the disturbance estimation error $\tilde{\xi}_{i2}$ can be found using the relation $\tilde{\psi}_{i2} \leq 2\varepsilon^2 \mathcal{F}_2 K |\tilde{\xi}_{i1}|^{\frac{1}{2}}$, implying $\tilde{\xi}_{i2} = 0$. Therefore, it is proved that the finite time disturbance observer (4.7) and (4.8) achieves an exact estimation of state and disturbances.

4.3.3 Closed-loop Stability Analysis

By using the Lyapunov stability criteria, closed loop signal boundedness of the overall controlled system in the event of sudden input and load variation is investigated. The result is summarized in Theorem 4 as follows.

Theorem 4. *Considering the DC-DC buck converter system* (4.1) *affected by load variations and input changes in addition to parametric uncertainties, the controller given by* (4.6) *ensures asymptotic output voltage tracking. Subsequently, the closed loop trajectories finally reside at the most within a maximal set* $\mathscr{S}^*$ *in the neighborhood of the origin and are ultimately bounded in the set* $\mathscr{S}$*, where* $\mathscr{S}^* \subseteq \mathscr{S}$ *is defined as* $\mathscr{S}^* := \{\mathbf{z} \in \mathbb{R}^2 \mid \|\mathbf{z}\|_2 < (\|\tilde{d}_1\|_\infty^2 + \|\tilde{d}_2\|_\infty^2)^{\frac{1}{2}}/\min\{c_1, c_2\}\}$ *and* $\mathscr{S} := \{\mathbf{z} \in \mathbb{R}^2 \mid \|\mathbf{z}\|_2 \leq \beta_{max}^{\frac{1}{2}}(M)(\|\tilde{d}_1\|_\infty^2 + \|\tilde{d}_2\|_\infty^2)^{\frac{1}{2}}\}$ *and ultimately converge to the origin. Here* $\beta_{max}(\mathbf{M})$ *denotes the maximum eigen value of the user defined matrix* $\mathbf{M} \in \mathbb{R}^{2\times 2}$ *whose elements are given as* $a_{11} = 1/c_1^2, a_{12} = a_{21} = 1/c_1^2 c_2, a_{22} = (c_1^2 + 1)/c_1^2 c_2^2$ *and* $c_1, c_2 > 0$ *are the controller gains.*

Proof: The objective is to prove the asymptotic stability of the error variables z_1 and z_2 defined in (4.4). The proof follows in a systematic way by considering stepwise procedure as discussed below. For notational convenience and easy interpretation of terms in the theorem, the disturbance estimation error is defined as $\tilde{\mathbf{d}} = [\tilde{d}_1\ \tilde{d}_2]^T = [\{\tilde{\xi}_{i2}\}_{i=1}^2]^T$. The error dynamics of z_1 and z_2 in (4.4) can be rewritten by substituting the virtual control law α and the actual control input u from (4.5) and (4.6) to yield

$$\begin{bmatrix} \dot{z}_1 \\ \dot{z}_2 \end{bmatrix} = \underbrace{\begin{bmatrix} -c_1 & 1 \\ -1 & -c_2 \end{bmatrix}}_{\mathcal{A}} \begin{bmatrix} z_1 \\ z_2 \end{bmatrix} + \underbrace{\begin{bmatrix} 1 & 0 \\ 0 & 1 \end{bmatrix}}_{\mathcal{B}} \underbrace{\begin{bmatrix} \tilde{d}_1(\cdot) \\ \tilde{d}_2(\cdot) \end{bmatrix}}_{\tilde{\mathbf{d}}(\cdot)}. \tag{4.25}$$

Let us define $\mathbf{z} := [z_1\ z_2]^T$ and consider a positive definite continuously differentiable Lyapunov function $V : \mathbb{R}^2 \times [0, \infty) \to \mathbb{R}_+$, where

$$V(z,t) = \frac{1}{2}\mathbf{z^T}\mathcal{P}\mathbf{z} \tag{4.26}$$

Here $\mathcal{P}$ is a positive definite symmetric matrix satisfying the Lyapunov criterion. Now, taking the time derivative of $V(\cdot)$ and using (4.25) yields,

$$\begin{aligned} \dot{V}(\mathbf{z},t) &= \frac{1}{2}(\mathbf{z^T}\mathcal{P}\dot{\mathbf{z}} + \dot{\mathbf{z}}^\mathbf{T}\mathcal{P}\mathbf{z}) \\ &= \frac{1}{2}(\mathbf{z^T}\mathcal{P}(\mathcal{A}\mathbf{z} + \mathcal{B}\tilde{\mathbf{d}}(\cdot)) + (\mathbf{z^T}\mathcal{A}^\mathbf{T} + \tilde{\mathbf{d}}^\mathbf{T}(\cdot)\mathcal{B}^\mathbf{T})\mathcal{P}\mathbf{z}) \\ &= \frac{1}{2}z^T(\mathcal{A}^\mathbf{T}\mathcal{P} + \mathcal{P}\mathcal{A})\mathbf{z} + \mathbf{z^T}\mathcal{P}\mathcal{B}\tilde{\mathbf{d}}(\cdot) = -\frac{1}{2}\mathbf{z^T}\mathcal{Q}\mathbf{z} + \mathbf{z^T}\tilde{\mathbf{d}}(\cdot). \end{aligned} \tag{4.27}$$

Here (4.27) is derived using the fact that $-\mathcal{Q} = (\mathcal{P}\mathcal{A} + \mathcal{A}^\mathbf{T}\mathcal{P})$ and $\mathcal{P} = I_{2\times 2}$. Now for $\dot{V}(\cdot)$ to be negative definite, the condition to be satisfied is $\mathbf{z^T}\mathcal{Q}\mathbf{z} > \mathbf{2z^T}\tilde{\mathbf{d}}(\cdot)$, which implies that $\|\mathbf{z}\|_2 > \frac{2}{\lambda_{max}(\mathbf{Q})}\|\tilde{\mathbf{d}}(\cdot)\|_\infty$. Therefore, it can be concluded that the largest positively invariant compact set in which the trajectories finally reside is given by $\mathscr{S}^*$, defined as

$$\mathscr{S}^* := \{\mathbf{z} \in \mathbb{R}^2 |\ \|\mathbf{z}\|_2 < (\|\tilde{d}_1\|_\infty^2 + \|\tilde{d}_2\|_\infty^2)^{1/2}/\max\{c_1, c_2\}\}. \tag{4.28}$$

However, the derived bounding set $\mathscr{S}^*$ of the trajectories is a very crude approximation and does not reflect the ultimate bound on the trajectories under the proposed control. Therefore, the ultimate bound on the error variables z_1 and z_2 can be found from (4.25) using Lemma 1 presented in [109]. The error dynamics in (4.25) is represented as a linear time invariant system with bounded disturbance estimation errors $\tilde{d}_1$ and $\tilde{d}_2$. Hence, the ultimate bound is found as, $|z_i| \leq \mathcal{F}_{i1}\|\tilde{d}_1\|_\infty + \mathcal{F}_{i2}\|\tilde{d}_2\|_\infty,\ i = 1, 2$. The term $\mathcal{F}_{ij}$ is calculated as $\mathcal{F}_{ij} = \int_0^\infty \{e^{\mathcal{A}\tau}\mathcal{B}_j\}_i d\tau$, where $\mathcal{B}_j$ denotes the j^{th} column of the $\mathcal{B}$ matrix. The matrix $\bar{\mathcal{F}}$ is defined as

$$\begin{aligned} \bar{\mathcal{F}} &:= \begin{bmatrix} \mathcal{F}_{11} & \mathcal{F}_{12} \\ \mathcal{F}_{21} & \mathcal{F}_{22} \end{bmatrix} \\ &= \begin{bmatrix} \int_0^\infty e^{-c_1\tau}d\tau & \frac{1}{c_2-c_1}\int_0^\infty (e^{-c_1\tau} - e^{-c_2\tau})d\tau \\ 0 & \int_0^\infty e^{-c_2\tau}d\tau \end{bmatrix}. \end{aligned} \tag{4.29}$$

Therefore, using the matrix $\bar{\mathcal{F}}$ in (4.29) the ultimate bounds are given by,

$$\left.\begin{array}{c} |z_1| \leq \frac{1}{c_1}\|\tilde{d}_1\|_\infty + \frac{1}{c_1 c_2}\|\tilde{d}_2\|_\infty \\ |z_2| \leq \frac{1}{c_2}\|\tilde{d}_2\|_\infty \end{array}\right\}. \tag{4.30}$$

The set inside which the trajectories ultimately reside is given by $\mathscr{S} \supseteq \mathscr{S}^*$ defined as

$$\mathscr{S} := \{\mathbf{z} \in \mathbb{R}^2 \mid \ \|\mathbf{z}\|_2 \leq \beta_{max}^{1/2}(\mathbf{M})(\|\tilde{d}_1\|_\infty^2 + \|\tilde{d}_2\|_\infty^2)^{\frac{1}{2}}\} \tag{4.31}$$

where β_{max} denotes the largest eigen value of the matrix $\mathbf{M}$ given by,

$$\mathbf{M} = \begin{bmatrix} \frac{1}{c_1^2} & \frac{1}{c_1^2 c_2} \\ \frac{1}{c_1^2 c_2} & \frac{c_1^2+1}{c_1^2 c_2^2} \end{bmatrix}.$$

The above sets can be made smaller by proper adjustments of controller parameters c_1 and c_2 yielding an enhanced tracking performance. Therefore, ultimately a bounded system tracking error existence in a very close vicinity of the origin is proved.

4.4 Simulation Results and Discussion

To investigate the effectiveness of the proposed finite time observer based backstepping control (FTOBSC) for DC-DC buck converter, a simulation study is conducted using Matlab-Simulink tool. The robustness of the proposed FTOBSC scheme is evaluated under adaptive backstepping (ABSC) and neural network based ABSC method as given in following subsections.

Comparison with adaptive backstepping control method

The proposed FTOBSC scheme is compared with the adaptive backstepping control (ABSC) presented in Chapter 2 under identical conditions of simulation study. The following tests are undertaken using the parameters described in Table 4.1 for all the simulation studies.

Table 4.1: Specifications

System parameters	Rating	Controller parameters	Value
Supply DC voltage, E	25V	Observer gain, λ_1, $\bar{\lambda}_1$, ε	100, 100, 0.1
Filter Inductance, L	59mH	Observer gain, λ_2, $\bar{\lambda}_2$, ε	2, 2, 0.1
Inductor resistance, r_L	4.54Ω	Backstepping gain, c_1	280
Filter capacitance, C	220μF	Backstepping gain, c_2	1.5
Nominal load, R	20Ω	Sample rate	25μs
Reference voltage, v_r	10V	Switching frequency, f_s	20kHz

Test 1- Start-up response: The start-up transients of the output voltage v_o and inductor current i_L in response to a reference voltage $v_r = 10V$ are shown in Figure 4.2 (a) and 4.2 (b) respectively. The ABSC technique exhibits an oscillatory behavior while settling to the desired reference in 130ms. In contrast, the proposed scheme results in a quicker action, besides yielding a smooth response in

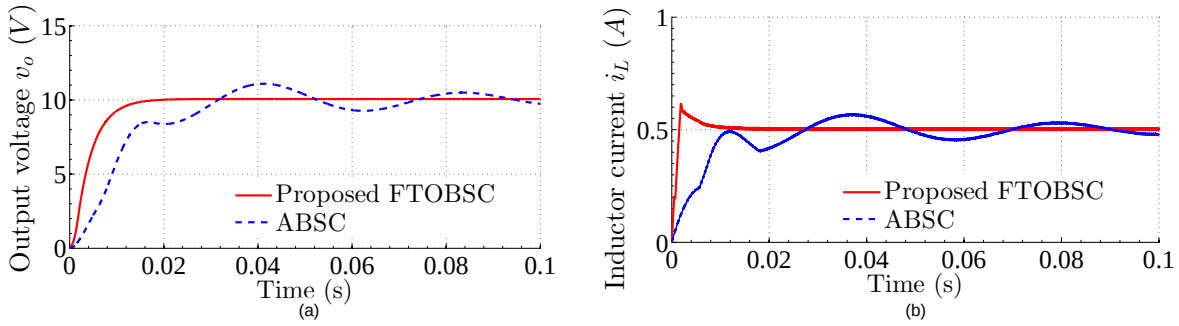

Figure 4.2: Simulated response curves of DC-DC buck converter system during start up: (a) output voltage v_o and (b) inductor current i_L.

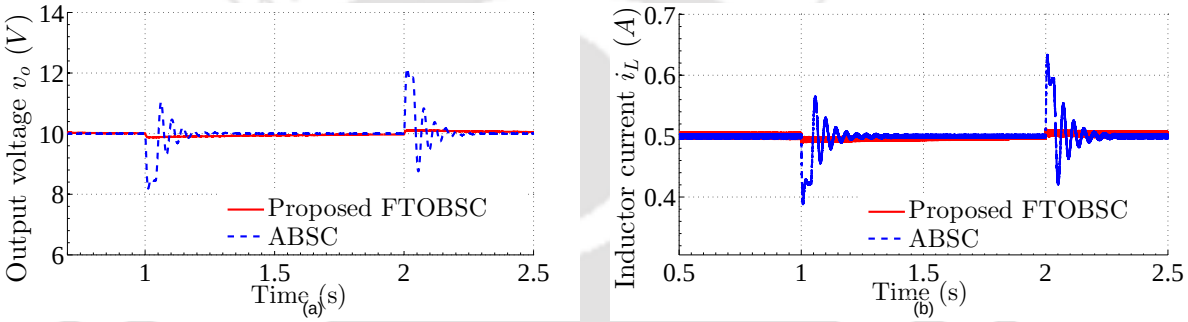

Figure 4.3: Simulated response curves of DC-DC buck converter system during step change in input voltage E from $25V$ to $17V$ at $t = 1s$ and vice-versa at $t = 2s$: (a) output voltage v_o and (b) inductor current i_L.

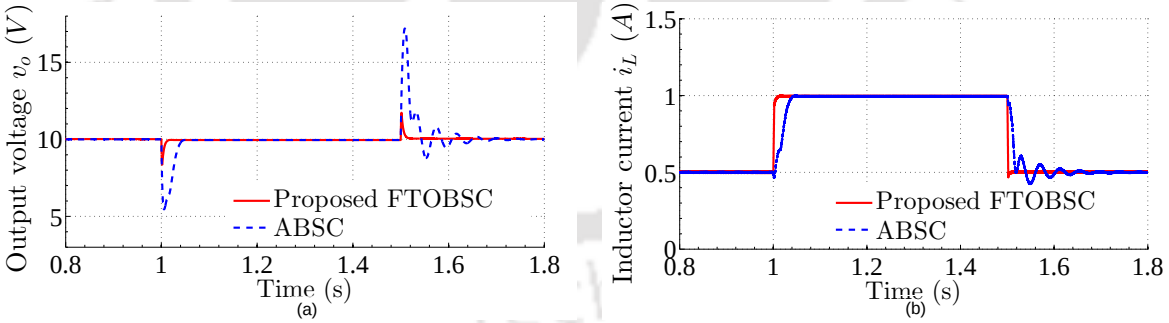

Figure 4.4: Simulated response curves of DC-DC buck converter system during a step change in load resistance R from 20Ω to 10Ω at $t = 1s$ and vice-versa at $t = 1.5s$: (a) output voltage v_o and (b) inductor current i_L.

achieving the required set-point in less than $20ms$. The corresponding plot of i_L shows the out-performance of the proposed FTOBSC method over the ABSC by yielding a faster response.

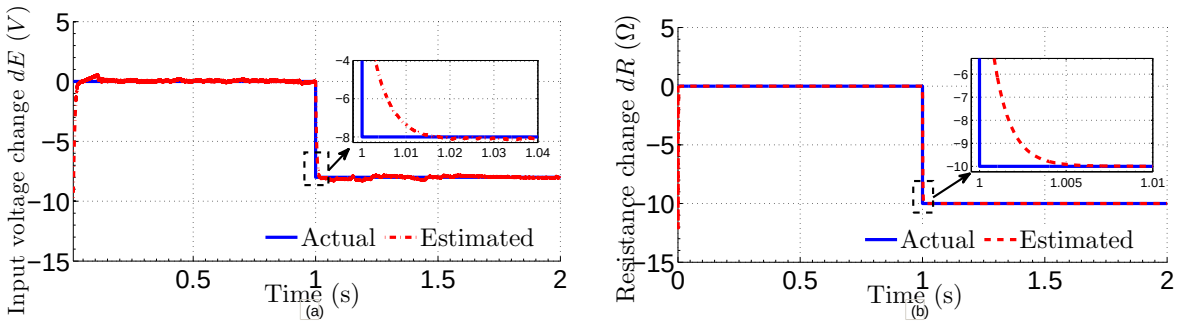

Figure 4.5: Simulation response curves of uncertainty estimation during; (a) input voltage E change from $25V$ to $17V$ at $t = 1s$ and (b) load resistance R change from 20 Ω to 10Ω at $t = 1s$.

Test 2-Robustness towards matched uncertainty: The next test is to examine the performance of the proposed FTOBSC scheme under matched uncertainty conditions. The DC input voltage E is perturbed from $25V$ to $17V$ and vice-versa, amounting to 32% step change in matched uncertainty. Figures 4.3 (a) and 4.3 (b) depict the responses under the ABSC and the proposed FTOBSC method. ABSC results in oscillations when the supply voltage is suddenly reduced and tracking to the desired voltage level is achieved with 12% peak undershoot and settling time of $180ms$. Further, during increase in E from $17V$ to $25V$, a 20% peak overshoot is produced with $200ms$ to converge to the nominal value under the ABSC scheme. In contrary, the proposed methodology produces an insensitive behavior under both the input change conditions, yielding no undershoot/overshoot. The corresponding unperturbed response of i_L with the proposed control can be observed in Figure 4.3 (b). These results clearly indicate that the proposed scheme outperforms the ABSC scheme when operated under matched uncertainties.

Test 3-Robustness towards mismatched uncertainty: Often the DC-DC converters are influenced by uncertainties not satisfying the matching condition. Hence to test the response of the proposed control under mismatched uncertainties, a loading and an unloading test are conducted on the DC-DC buck converter. Figures 4.4 (a) and 4.4 (b) show the responses of v_o and i_L, obtained during the loading and unloading tests respectively. During loading, the load resistance R is suddenly decreased from the nominal value of 20Ω to 10Ω amounting to 50% change, at time $t = 1s$. It can be observed from Figure 4.4 (a) that the ABSC produces large undershoot of 45%, besides taking $50ms$ in settling to the reference value. Similarly, during the unloading test, the load resistance R is suddenly increased from 10Ω to 20Ω at time $t = 1.5s$, leading to a high peak overshoot of 70% in v_o. Besides, oscillations are produced till final voltage convergence in $0.7s$. In contrast, the proposed scheme yields an undershoot of 20% during the loading test with settling time of $18ms$. Similarly, during unloading test, the proposed method provides a much lesser peak overshoot of 18% and moreover, exhibits smooth transients while settling in $16ms$. The corresponding plots of inductor current for both ABSC and the proposed scheme can be found in Figure 4.4 (b) which suggests that the proposed scheme is successful in producing a better i_L response compared to ABSC scheme.

Further, the uncertainty estimation performance in the proposed controller is demonstrated by presenting the plots of estimated input voltage change dE and estimated load resistance change dR in

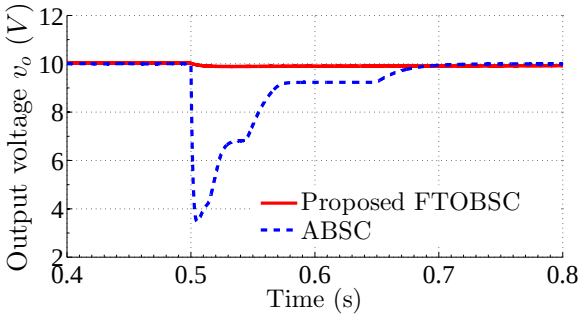

Figure 4.6: Simulation response curve for DC-DC buck converter system for output voltage v_o during simultaneous step change in load resistance R from 20Ω to 10Ω and input voltage E from $25V$ to $17V$.

Figure 4.5 (a) and Figure 4.5 (b) respectively, obtained for subsequent compensation using the controller. It is evident that dE and dR are compensated in $18ms$ and $5ms$ respectively.

Test 4-Robustness against simultaneous application of matched and mismatched uncertainties: In real-time situations, many a times the DC-DC converters encounter both matched and mismatched uncertainties at the same time. Hence, the effectiveness of the proposed control is also evaluated under this case. A sudden change in load resistance R from 20Ω to 10Ω and input voltage E from $25V$ to $17V$ at time $t = 0.5s$ is made and the resulting response in v_o is shown in Figure 4.6. Figure 4.6 shows that the ABSC scheme generates a large undershoot of 65% while taking $0.18s$ to track the reference voltage of $10V$. In contrast, the proposed control method yields an unperturbed and satisfactory dynamic response, indicating the potential of the proposed strategy.

Remark 8. *A fact has to be remarked upon that there is still no quantitative measure nor any explicit relationship between the virtual control gains (c_1, c_2) and the performance of tracking error available in literature. However, choice of these parameters is guided through the transient performance bounds as mentioned in Krstic* et al. *[52]. The transient performance of the output voltage tracking error in both $\mathcal{L}_2$ and $\mathcal{L}_\infty$ sense can be improved by increasing c_1. However, such an increase improves the initial output transient response but at the same time induces a cumulative increment in $\mathcal{L}_2$ norm of the output at each successive instants of uncertain load change. This leads to increased magnitude of output overshoot/undershoot at instances of load and input variations, which is undesirable. Further, increment in c_1 also may increase the magnitude of inductor current. Hence, a compromise has to be reached [111]. For the sake of choosing these free parameters, an illustration on how the choice of c_1 effects the $\mathcal{L}_2$ performance of the tracking error is presented. The parameter c_1 is varied by setting its values at $100, 280, 500$ and 800 with c_2 fixed at 1.5. The tracking error with different c_1 are compared in Figures 4.7 (a)-(b). It is evident from the figures that the $\mathcal{L}_2$ norm of the output decreases initially before the load change as c_1 increases. However, at the same time, it is observed that the magnitude of current increases (at start up) as c_1 increases. Further, if c_1 is fixed and c_2 is increased, the inductor current spike during transients increases significantly and may go beyond an acceptable value thereby damaging the converter. In view of the aforementioned arguments and illustrations, it is concluded that the gain parameters have to be chosen judiciously so as to maintain a trade-off between the output voltage and inductor current performance.*

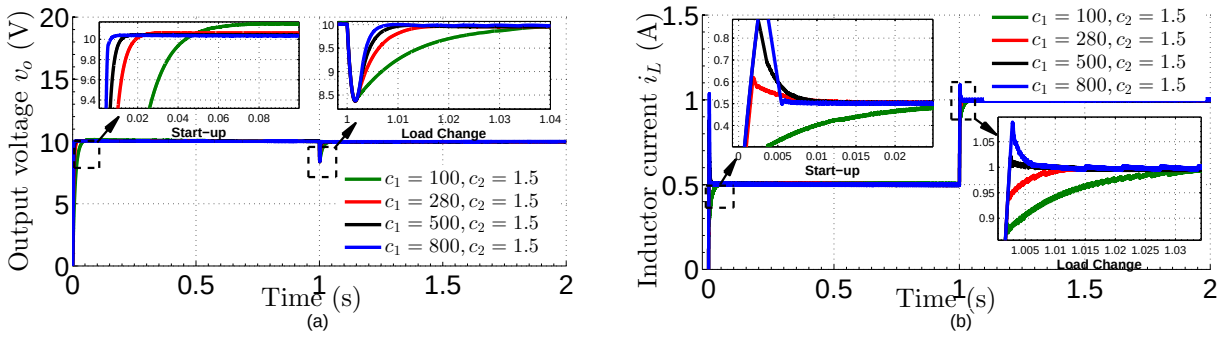

Figure 4.7: Simulated response curves of proposed FTOBSC scheme under start-up and load change ($R \rightarrow 20\Omega$ to 10Ω) at $t = 1s$ for different controller gains; (a) output voltage and (b) inductor current.

Remark 9. *To study the closeness of results in simulation and experiments, the following Table 4.2 is presented by comparing Figure 4.4(a) and Figure 4.9(e), wherein the buck converter system is subjected to load resistance perturbation from nominal 20Ω to 10Ω.*

Table 4.2: Comparison of proposed FTOBSC in simulation and hardware during load disturbance from 20Ω to 10Ω

Performance metric	**Simulation**	**Hardware**
Peak undershoot, P_u (%)	20	45
Settling time t_s (s)	0.018	0.085

Comparison with neural network based adaptive backstepping control:

The performance of the proposed control is further evaluated with that of Chebyshev neural network

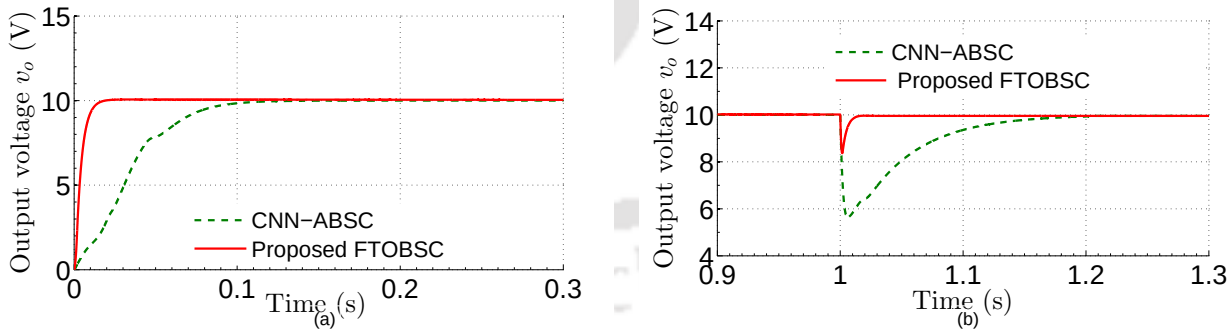

Figure 4.8: Comparison of simulation response of DC-DC buck converter system: (a) output voltage v_o during start up and (b) output voltage v_o during a step change in load resistance R from 20Ω to 10Ω at $t = 1s$.

(CNN) based adaptive backstepping control [91] discussed in Chapter 3. For fairness of comparison, the converter parameter values and simulation environment have been kept similar for the two cases. It must be noted that in [91], authors have shown that the CNN-adaptive backstepping control is superior in performance compared to traditional Radial basis function neural network (RBFNN)-adaptive

backstepping control when applied to DC-DC buck converter system. The output voltage during start-up and load resistance change under proposed and CNN-adaptive backstepping control [91] have been presented in Figure 4.8 (a) and Figure 4.8 (b) respectively. It is evident from Figure 4.8 (a) that the CNN-adaptive backstepping control is able to track the desired reference voltage of $10V$ in nearly $100ms$ and the proposed control attains desired $10V$ in $20ms$ only. Similarly it is observed in Figure 4.8 (b) that during 50% change in R, the voltage drops down to $5.5V$ and $8.3V$ under the CNN-ABSC and the proposed FTOBSC method respectively. Further, the CNN-ABSC and the proposed FTOBSC scheme require $200ms$ and $20ms$ respectively to settle to the reference voltage.

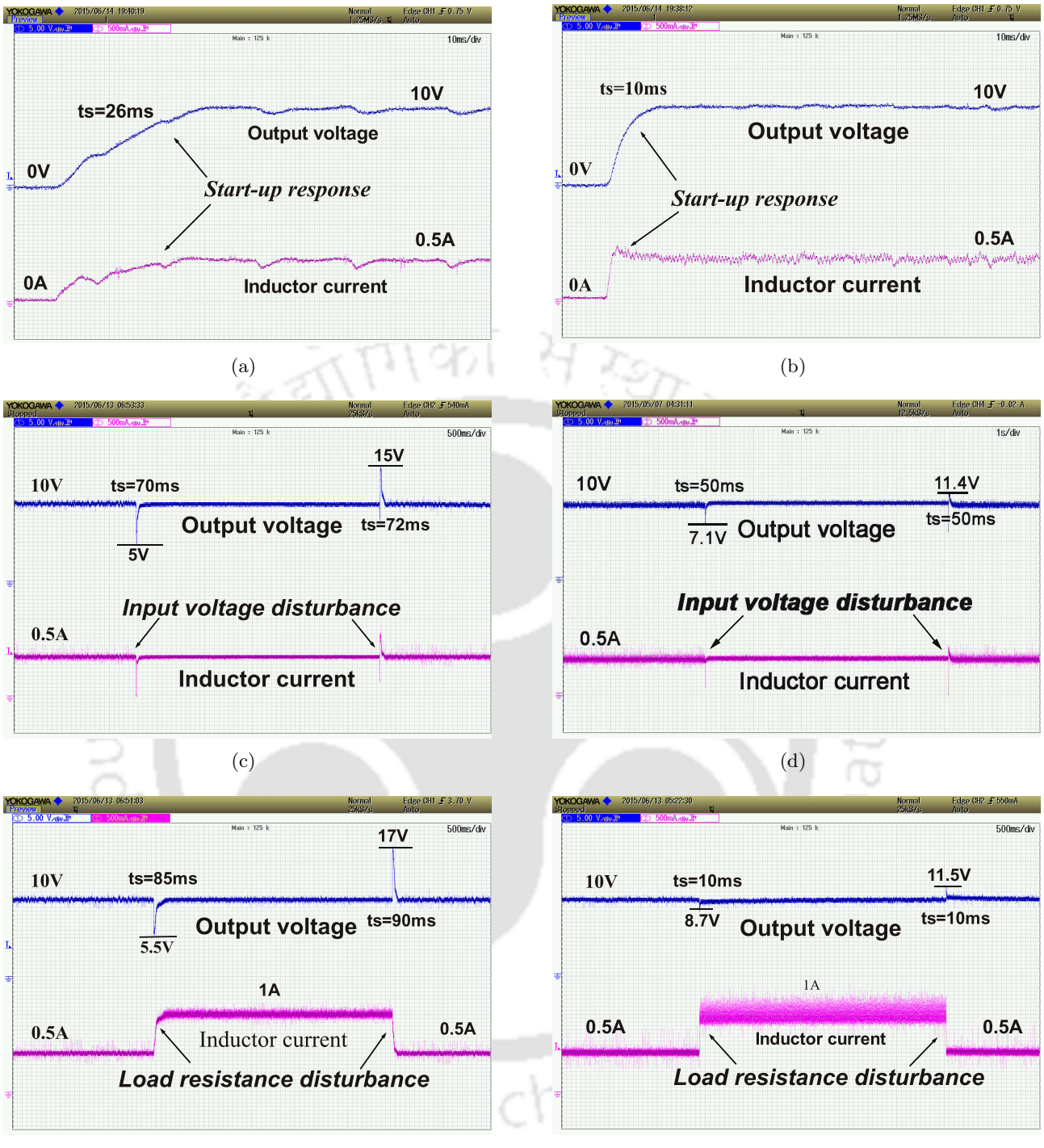

Figure 4.9: Experimental response curves of DC-DC buck converter system: (a) ABSC: output voltage v_o and inductor current i_L during start up (scale: x-axis; time (10ms/div), y-axis; voltage (5V/div) and current (500mA/div)), (b) proposed FTOBSC scheme: output voltage v_o and inductor current i_L during start up (scale: x-axis; time (10ms/div), y-axis; voltage (5V/div) and current (500mA/div)), (c) ABSC: output voltage v_o and inductor current i_L during a step change in input voltage E from $25V$ to $17V$ and vice-versa (scale: x-axis; time (500ms/div), y-axis; voltage (5V/div) and current (500mA/div)), (d) proposed FTOBSC scheme: output voltage v_o and inductor current i_L during a step change in input voltage E from $25V$ to $17V$ and vice-versa (scale: x-axis; time (1s/div), y-axis; voltage (5V/div) and current (500mA/div)), (e) ABSC: output voltage v_o and inductor current i_L during a step change in load resistance R from 20Ω to 10Ω and vice-versa (scale: x-axis; time (500ms/div), y-axis; voltage (5V/div) and current (500mA/div)) and (f) proposed FTOBSC scheme: output voltage v_o and inductor current i_L during a step change in load resistance R from 20Ω to 10Ω and vice-versa (scale: x-axis; time (500ms/div), y-axis; voltage (5V/div) and current (500mA/div)).

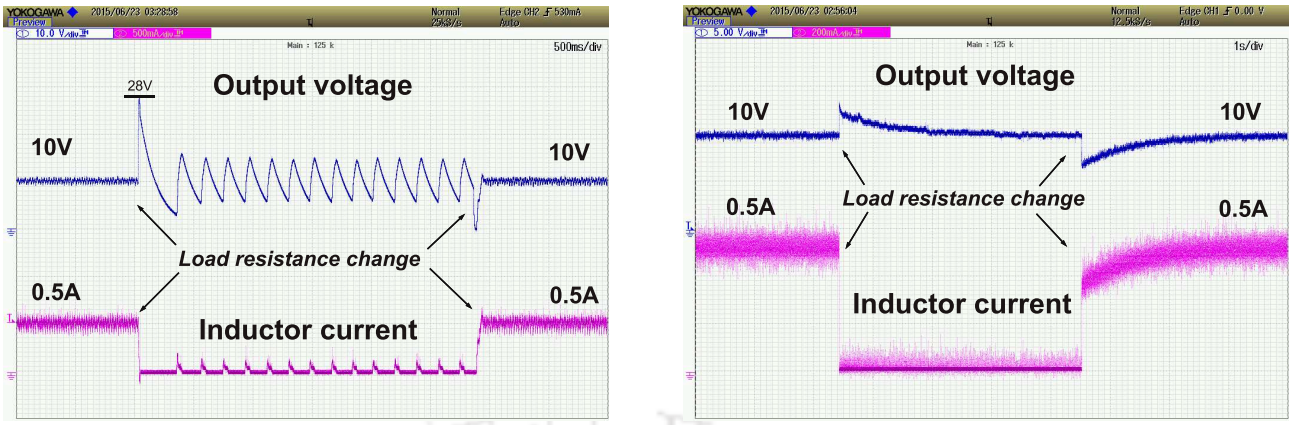

(a) (b)

Figure 4.10: Experimental response curves of DC-DC buck converter system during heavy loading with R change from nominal 20Ω to 800Ω: (a) ABSC scheme and (b) proposed FTOBSC scheme.

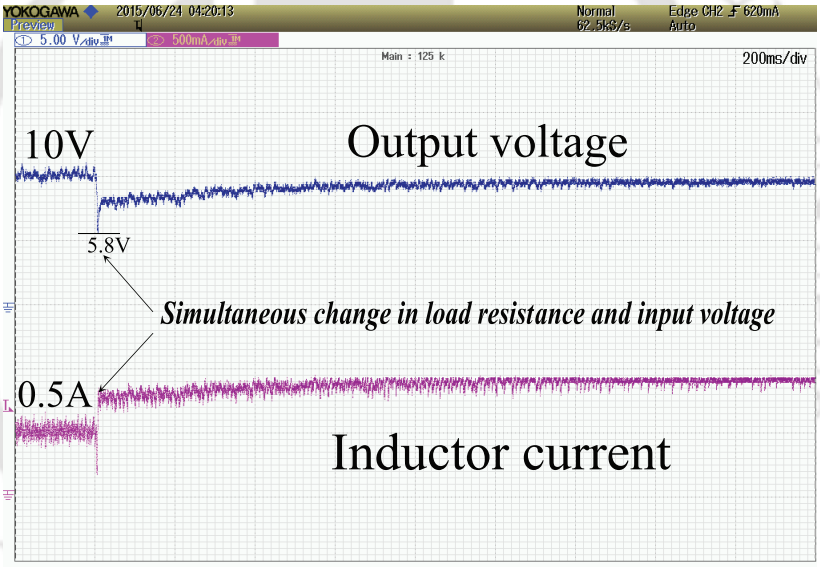

Figure 4.11: Experimental response curves of proposed FTOBSC scheme for DC-DC buck converter system for output voltage v_o during simultaneous step change in load resistance R from 20Ω to 10Ω and input voltage E from $25V$ to $17V$ (scale: x-axis; time (200ms/div), y-axis; voltage (5V/div) and current (500mA/div)).

4.5 Experimental Results and Discussion

Experimental investigation is conducted to evaluate the effectiveness of the ABSC and the proposed FTOBSC scheme under identical conditions of simulation study mentioned in Section 4.4. Figure 4.9 (a) and 4.9 (b) demonstrate the start-up performances of ABSC and the proposed control respectively. Figure 4.9 (a) shows that the ABSC takes nearly $26ms$ to settle to the desired reference voltage of $10V$. The non-smooth profile of both the system states under the action of ABSC is its limitation. In contrast, the proposed control yields smoother responses for both v_o and i_L and takes a small time

of $10ms$ to reach the reference output voltage. Moreover, it must be observed that the peak-to-peak ripple in v_o under proposed method is 0.5V, in contrast to 0.7V in case of ABSC method.

The DC-DC buck converter is investigated for a matched uncertainty condition by suddenly changing the supply voltage E from nominal $25V$ to $17V$ and vice-versa. The responses obtained with ABSC and the proposed control are shown in Figure 4.9 (c) and 4.9 (d). Figure 4.9 (c) shows that ABSC brings an undershoot of 50% while taking time of $70ms$ to reject the input voltage uncertainty. Similarly, when the input supply is brought back from $17V$ to $25V$, the ABSC results in an overshoot of 50% and settles to the desired value in $72ms$. In contrary, the proposed control results in a relatively lesser undershoot of 29% and settling time of $50ms$ during supply voltage decrease. During the supply increase, the proposed method produces 14% peak overshoot and needs $50ms$ to converge to the reference $10V$.

Next, to check robustness under mismatched uncertainty conditions, the DC-DC buck converter is subjected to change in resistance R from 20Ω to 10Ω and vice-versa. Figure 4.9 (e) and 4.9 (f) show the responses under ABSC and proposed scheme respectively. ABSC produces an undershoot of 45% in v_o and settles in $85ms$. During unloading condition, v_o suffers a high overshoot of 70% and takes $90ms$ time to settle to the set-point. On the other hand, Figure 4.9 (f) shows that the proposed FTOBSC method yields relatively smaller peak undershoot/overshoot, along with faster settlement. During loading it produces 13% undershoot and requires $10ms$ settling time and during unloading condition it yields almost the same performance. The performance measures under start-up, matched and mismatched perturbations have been summarized in Table 4.3. It is evident from Table 4.3 that the transient performance indices like peak overshoot/undershoot and settling time are significantly lower in the case of the proposed FTOBSC method compared to the ABSC method. Another noteworthy feature of the proposed FTOBSC method is its ability to contain the peak-to-peak ripple voltage (Δv_o) in the output to an extremely low value. As is observed in Table 4.3, the proposed FTOBSC produces only $0.35V$ as peak-to-peak ripple voltage (Δv_o) whereas in the ABSC, Δv_o is significantly high amounting to $1.2V$. The response of the propose control scheme under heavy loading with R change from nominal 20Ω to 800Ω and vice-versa is shown in Fig. 4.10. It is evident from Figure 4.10 (a) that the conventional ABSC scheme performs poorly exhibiting high oscillations in the output voltage v_o besides producing large overshoot and undershoot. In contrary, the proposed control method is found to be robust as observed in Figure 4.10 (b). This exhibits the wide applicability range of the proposed FTOBSC method on DC-DC buck converters.

Further, in order to test the usefulness of the proposed method under simultaneous application of matched and mismatched uncertainties on the DC-DC buck converter system, experimental study is conducted for the same magnitude of disturbance as discussed in Section 4.4 and results are shown in Fig. 4.11. The ABSC scheme fails to handle simultaneous disturbances and leads to shutting down of the DC-DC buck converter. In contrast, the proposed method rejects both load change and input voltage change effectively and recovers the nominal condition within $0.5s$ as observed in Figure 4.11. During this time the inductor current i_L also shows a satisfactory response.

Table 4.3: Experimental results of output voltage performance under ABSC and proposed FTOBSC method

Method	Start-up Response		Variation in E 25V⇌17V		Variation in R 20Ω ⇌10Ω	
	t_s(s)	$\triangle v_o$(V)	t_s (s)	M_p%	t_s (s)	M_p%
ABSC	0.026	1.2	0.070	50*	0.085	45*
			0.072	50	0.090	70
Proposed FTOBSC	0.01	0.35	0.05	29*	0.010	13*
			0.05	14	0.010	15

t_s-Settling time, $\triangle v_o$-Peak-to-peak ripple output voltage, ∗Undershoot %

Remark 10. *The proposed control design for the DC-DC buck converter may have many prominent and sensitive power source applications like in wireless sensor networks, radio-frequency identification, GPS, advanced datacom systems, point-of-load converters in servers, solar PV, quad-copters and other similar systems which demand high performance [112, 113]. For instance, when a system undergoes a transition from its deep sleep mode to active mode, a fast supply voltage with rapid load current switching capability are important to achieve lower latency. Hence, this necessitates the requirement of high performance DC-DC buck converter with faster dynamic responses in both reference tracking and load transients. Therefore, real-time applicability of the proposed control in the context of DC-DC buck converters can be inferred.*

4.6 Summary

A new uncertainty estimation based backstepping controller is proposed for DC-DC buck converters supplying resistive loads. The proposed control uses dual finite time observers for uncertainty estimation integrated with a backstepping control technique. Such an observer is used to exactly estimate the input voltage change and load resistance change as a lumped uncertainty in finite time. The approach followed permits faster computation of unknown disturbances and thus helps in obtaining a quick and consistent dynamical response under wide operating range. A rigorous mathematical proof for stability of the observer and the controller is presented, besides analyzing estimation correctness. Further, the proposed control scheme is compared with the conventional adaptive backstepping control under identical conditions of both simulation and experimental studies. The results obtained confirm that both the simulation and experimental findings are in good agreement. The proposed control is found to withstand wide variation in load and input voltage not only individually, but also under their simultaneous occurrence, without compromising on the desired output voltage tracking. In addition, the efficiency of the proposed control is also established by comparing the results of conventional adaptive backstepping control and Chebyshev neural networks based adaptive backstepping control methods proposed in Chapter 2 and Chapter 3 respectively. The results exhibit a faster transient and better steady state performance in the output voltage.

5

Finite Time Current Observer Based Adaptive Backstepping Control of DC-DC Buck Converters

Contents

5.1 Introduction

In order to improve the tracking performance of DC-DC buck converters, most of the modern control methods rely on the knowledge of inductor current, while formulating the final control law. Usually, an inner current loop is used to shape the input current waveform besides using an external voltage loop for the output voltage regulation [114, 115]. Designing the inner current loop requires a precise knowledge about the inductor current. The current is generally measured using Hall-effect based current sensor. However, the current sensor suffers from the following issues: 1) the remnant flux introduces a time varying DC bias into the control loop; 2) a high degree of sensitivity to the measurement noise results in an imprecise current measurement (although low-pass filters can be used, they add time delay and subsequently deteriorate the stability margin); 3) additional circuitry of the current sensor contributes to power loss; 4) high cost of current sensor substantially increases the overall cost of the controller; 5) current sensor when exposed to high temperatures and high current surges, faces potential threat of overheating eventually leading to its failure. Other devices available to measure the current include resistive current sensor and current transformer (CT). The resistive current sensor demands a precise and noise-free differential amplifier for the effective action. Moreover, it increases power loss in the circuit. Hence, such methods are not viable for use in high power applications. On the contrary, the CT method of current sensing is popular in the industry, but the placement of CT in series increases the inductive path leading to high voltage spikes during switching transients. In addition, CTs need to be reset for the magnetizing inductance under every switching cycle, which may impose a restriction on the upper limit of the duty ratio in DC-DC buck converters. Considering the aforementioned challenges, current sensorless control techniques are encouraged to provide a cleaner, inexpensive and noise-free estimation of the inductor current. Such controllers proposed in the literature use an observer to reconstruct the original current state from the output voltage information. It is noteworthy that due to a rapid growth in the computational capacity of present day DSP and FPGA boards, the matter of high computational burden should not be considered as a serious concern.

Since the estimation techniques demand an exact system model, in [116] an almost accurate converter model was used for current estimation. Nevertheless, the control strategy is complex to be implemented. In [117], the proposed current observer is computationally simple and less sensitive to changes occurring in the input voltage. However, the error in current estimation here is high on account of non-consideration of parasitic parameters. Later, an extended-Kalman-filter based observer [118] was used to estimate the inductor current and improve the estimation accuracy. In [119], the current estimation is found to be closer to the actual profile of inductor current due to consideration of possible parasitic parameters. However, the proposed method requires an auxiliary circuitry for switching voltage sampling. Further, the compensation of such parametric variations depends largely on the load conditions, which are otherwise unknown and difficult to estimate. Lately, in [120] the authors proposed a sensorless-control design utilizing a sampled-data based reduced order observer, instead of conventional full-order observers for estimation of current dynamics. The work successfully demonstrated the current sensorless control of DC-DC buck converters in real-time.

In the context of adaptive backstepping control design presented in this work, the output voltage

of the DC-DC buck converter is controlled by an appropriate current variable corresponding to the control law. The robustness of the output voltage under load uncertainties is ensured by choice of an appropriate inductor current variable acting as the virtual control input. Therefore, an enhanced transient performance in the output voltage at the instances of load changes can be ensured if the current can be correctly estimated during load change, in least possible time. Further, the output voltage performance depends on how promptly the controller responds to such uncertainties by generating the desired current, which thereby controls the voltage, to guarantee an asymptotically stable output voltage tracking. Hence, resorting to a current sensorless control necessitates designing an observer which is accurate or rather exact and fast enough in estimating the inductor current signal. This would surely help in rendering a prompt controller action consequently yielding an efficient and robust voltage tracking with satisfactory transient and steady state behaviour.

As discussed above, the accuracy and fast convergence of current observer error are the two important aspects to be dealt with. This is due to the fact that if the observer does not estimate the current quickly and correctly, it will result in degraded post load change transient performance of the output voltage with persisting steady state error. With this motivation, high gain observers with asymptotic stability emerge to be a good choice to achieve a close to accurate estimation within very short time. However, there are some issues encountered in high gain observers with asymptotic stability which restrict their application to the concerned problem and these are listed below.

(i) Peaking affect which may lead to overall closed loop system instability

(ii) No guarantee on exactness of estimation

(iii) Noise amplification with high observer gains, which is highly undesirable as the signal to be estimated gets corrupt with this high noise. Further, the current signal to be observed must be a slowly varying signal, so as to allow the observer to converge asymptotically in sufficiently lower time. This way, an estimation of a high frequency current signal can lead to steady state error, due to rise in the L_2 bounds of the current error in the estimation. This leads to a an inaccurate control signal generation, which will subsequently result in output performance degradation.

Therefore, usage of a finite time current observer is essential for exactness in the estimation, boundedness of estimation in presence of noise (very small bound) and no peaking affect. Further, it is proved in this work that the estimation is exact and negative homogeneity combined with the asymptotic stability (not exponential stability) implies a finite time stable origin.

As discussed in Chapter 2, Section 2.3, the DC-DC Buck converter dynamics are represented in state space form as

$$\dot{x}_1 = -\frac{x_1}{RC} + \frac{x_2}{C} \tag{5.1}$$

$$\dot{x}_2 = -\frac{x_1}{L} + \frac{uE}{L} \tag{5.2}$$

where $u \in \mathbb{Z}_+ = \{0, 1\}$ is the control signal denoting the opening and closing operation of switch S_w. The objective is to obtain a faithful tracking of output voltage v_o, besides ensuring a satisfactory transient behavior.

5.2 Proposed Controller Design

The proposed control integrates the finite time current observer with an adaptive backstepping control (FTCO-ABSC) mechanism for a current sensorless control.

5.2.1 Adaptive Backstepping Control (ABSC)

Briefly, the steps involved are recalled below:

Step 1: The term $\frac{x_1}{R}$ in (5.1) is assumed to be an unknown function. It is estimated by framing an updation law to yield $\Theta^{*T}\Phi$ where Θ^* is the optimum weight and Φ is the regressor. Replacing $\frac{x_1}{R}$ in (5.1) with $\Theta^{*T}\Phi$ yields

$$\dot{x}_1 = -\frac{\Theta^{*T}\Phi}{C} + \frac{x_2}{C}. \tag{5.3}$$

Now, (5.3) and (5.2) define the dynamics of the DC-DC buck converter which will be utilized in control design.

Step 2: The error variables are defined as

$$\left.\begin{aligned} z_1 &= x_1 - v_r \\ z_2 &= \tfrac{\hat{x}_2}{C} - \alpha \end{aligned}\right\} \tag{5.4}$$

where $\hat{x}_2$ is the estimated inductor current obtained by using finite time current observer discussed in the next subsection and v_r is the reference output voltage.

Step 3: Using the output voltage dynamics in (5.3), the z_1-dynamics is stabilized using a virtual-control input α as,

$$\alpha = -c_1 z_1 + \frac{\hat{\Theta}^T\Phi}{C} + \dot{v}_r \tag{5.5}$$

where $c_1 > 0$ is the controller gain and $\hat{\Theta}^T\Phi$ is the adaptive estimate of unknown function $\frac{x_1}{R}$. Moreover, $\tilde{\Theta} = \Theta^* - \hat{\Theta}$. Subsequently, the next error z_2 can be rewritten as

$$\dot{z}_2 = \frac{\dot{\tilde{\xi}}_2}{C} - \frac{x_1}{LC} - \sum_{k=1}^{2}\frac{\partial\alpha}{\partial x_k}\dot{x}_k - \sum_{k=0}^{1}\frac{\partial\alpha}{\partial {v_r}^{(k)}}{v_r}^{(k+1)} - \dot{\hat{\Theta}}^T\frac{\partial\alpha}{\partial\hat{\Theta}^T} + \frac{E}{LC}u \tag{5.6}$$

where $\tilde{\xi}_2 = \tilde{x}_2 = \hat{x}_2 - x_2$ is the error in current state estimation. Appropriate selection of control law u to stabilize z_2 is to be guided properly. Hence, u is found from (5.6) as

$$\begin{aligned} u = &\frac{LC}{E}\left(-z_1 - c_2 z_2 + \frac{x_1}{LC} + \frac{\partial\alpha}{\partial x_1}\left(\frac{x_2}{C}\right) - \frac{\partial\alpha}{\partial x_1}\left(\frac{\hat{\Theta}^T\Phi}{C}\right) + \sum_{k=0}^{1}\frac{\partial\alpha}{\partial {v_r}^{(k)}}{v_r}^{(k+1)}\right. \\ &\left. + \dot{\hat{\Theta}}^T\frac{\partial\alpha}{\partial\hat{\Theta}^T} + \ddot{v}_r + \frac{\partial\alpha}{\partial x_1}\gamma\vartheta_2\right) \end{aligned} \tag{5.7}$$

where $c_2 > 0$ defines the controller gain, γ is the adaptation rate and ϑ_2 is a tuning function described as $\vartheta_2 = -\frac{\Phi}{C}z_1 + \frac{\partial\alpha}{\partial x_1}\frac{\Phi}{C}z_2$.

Step 4: Further, to find the optimal weight required for estimation of the uncertain term $\frac{x_1}{R}$, an online Lyapunov based adaptive learning law is formulated to yield a close approximation. The optimum

weight vector estimate $\hat{\Theta}(t)$ as explained in (2.50) is given by

$$\hat{\Theta}(t) = \hat{\Theta}(t_0) - \gamma \int_{t_0}^{t} \frac{\Phi(x_1(\nu))}{C} \left(z_1(\nu) - \frac{\partial \alpha}{\partial x_1} z_2(\nu) \right) d\nu. \tag{5.8}$$

where $\gamma > 0$ is the adaption rate. In order to compute the control law u in (5.7) precisely, the exact knowledge of system states is essential. Hence, the proposed methodology proposes the control strategy with a minimal usage of sensing units. The inductor current state x_2 is reconstructed from the finite time current observer.

Remark 11. *The choice of adaptation gain parameter γ is crucial in order to attain a fast and satisfactory dynamic response of the output voltage state of the converter. A high value of γ results in a faster adaptation and enhanced transient response. However, a very high value of γ also results in a decreased stability margin of DC-DC buck converter system. Therefore, it is recommended to judiciously prescribe the value of γ in such a way that a desired and satisfactory control response is achieved, besides preserving a safe stability margin.*

5.2.2 Finite Time Current Observer (FTCO)

Following the design philosophy in Section A.1, herein a finite time current estimator is presented. The idea is to consider the unknown current as a disturbance rather than a state variable. Hence, the proposed current observer design utilizes only the voltage tracking error dynamics instead of considering the full dynamics of the buck converter. This would render computational simplicity and enhance output transient performance by reconstructing the inductor current under both nominal and perturbed situations. Hence, its applicability to the control design problem of DC-DC buck converters is well suited. The current observer is designed followed by the finite time stability analysis. The dynamics of the proposed finite time current observer (FTCO) is given as,

$$\left.\begin{aligned} \dot{\xi}_1 &= -\tfrac{\lambda_1}{\varepsilon} |\xi_1 - x_1|^{\frac{1}{2}} \mathrm{sgn}(\xi_1 - x_1) - \tfrac{\hat{\Theta}^T \Phi}{C} + \tfrac{\xi_2}{C} \\ \dot{\xi}_2 &= -\tfrac{\lambda_2}{2\varepsilon^2} \mathrm{sgn}(\xi_2 - \upsilon_1) \\ \upsilon_1 &= -\tfrac{\lambda_1}{\varepsilon} |\xi_1 - x_1|^{\frac{1}{2}} \mathrm{sgn}(\xi_1 - x_1) + \tfrac{\xi_2}{C} \end{aligned}\right\} \tag{5.9}$$

where ξ_1 and ξ_2 denote the estimates of x_1 and x_2 respectively. The terms λ_1, λ_2 are the observer gains and $\varepsilon > 0$ is a small number close to zero. In subsequent analysis, a bound on ε will be found so as to achieve a finite time convergence of the observer error to the origin. Proceeding further, let us define $\Delta(x_1,\ t) = x_2$, $\tilde{\xi}_1 = \xi_1 - x_1$ and $\tilde{\xi}_2 = \xi_2 - \Delta(\cdot)$. Hence, the error dynamics are written as,

$$\left.\begin{aligned} \dot{\tilde{\xi}}_1 &= -\tfrac{\lambda_1}{\varepsilon} |\tilde{\xi}_1|^{\frac{1}{2}} \mathrm{sgn}(\tilde{\xi}_1) + \tilde{\xi}_2 \\ \dot{\tilde{\xi}}_2 &= -\tfrac{\lambda_2}{2\varepsilon^2} \mathrm{sgn}(|\tilde{\xi}_1|^{\frac{1}{2}} \mathrm{sgn}(\tilde{\xi}_1)) + \dot{\Delta}(\cdot) \end{aligned}\right\}. \tag{5.10}$$

Next, the finite time stability of the observer error dynamics described in (5.10) is stated in Theorem 5 below.

Theorem 5. *Considering the finite time current observer error dynamics given by* (5.10) *and assuming that the disturbance $\Delta(x_1, t)$ is at least once continuously differentiable, the resulting observer*

error variables $\tilde{\xi}_1$ *and* $\tilde{\xi}_2$ *converge to the origin in finite time provided the gain* $\frac{\lambda_2}{2\varepsilon^2} > \sup\{\dot{\Delta}(.)\} = \mathcal{L}$, $\mathcal{L} > 0$ *yielding* $\hat{\Delta}(\cdot) = \xi_2$.

Proof: For analyzing the finite time stability of observer error dynamics in (5.10), the degree of homogeneity of the vector fields associated must be obtained first. Applying a homogeneity transformation $T_r : (t,\ \tilde{\xi}_1) \longmapsto (rt,\ r^{3-i}\tilde{\xi}_1)$ to the observer error dynamics yields the degree of homogeneity of the associated vector fields to be $-1 < 0$. Therefore, as a next step, to ensure the finite time stability of the observer, let us consider a Lyapunov function $V_0 = \zeta^{\mathbf{T}}\mathbf{P}\zeta$, where, $\zeta = [\zeta_1\ \zeta_2]^T = [\lceil\tilde{\xi}_1\rfloor^{1/2}\ \tilde{\xi}_2]^T$ and $\lceil\tilde{\xi}_1\rfloor^{\nu} = |\tilde{\xi}_1|^{\nu}\mathrm{sgn}(\tilde{\xi}_1)$. The first time derivative of ζ is given by,

$$\begin{aligned}\dot{\zeta} &= \begin{bmatrix} \frac{1}{2}|\tilde{\xi}_1|^{-1/2}\dot{\tilde{\xi}}_1 \\ \dot{\tilde{\xi}}_2 \end{bmatrix} = \begin{bmatrix} \frac{1}{2}|\tilde{\xi}_1|^{-1/2}(-\frac{\lambda_1}{\varepsilon}\lceil\tilde{\xi}_1\rfloor^{\frac{1}{2}} + \tilde{\xi}_2) \\ -\frac{\lambda_2}{2\varepsilon^2}\mathrm{sgn}(\tilde{\xi}_2 - \dot{\tilde{\xi}}_2) + \dot{\Delta}(\cdot) \end{bmatrix} \\ &= \begin{bmatrix} \frac{1}{2}|\tilde{\xi}_1|^{-1/2}(-\frac{\lambda_1}{\varepsilon}\lceil\tilde{\xi}_1\rfloor^{\frac{1}{2}} + \tilde{\xi}_2) \\ -\frac{\lambda_2}{2\varepsilon^2}\mathrm{sgn}(\frac{\lambda_1}{\varepsilon}\lceil\tilde{\xi}_1\rfloor^{\frac{1}{2}}) + \dot{\Delta}(\cdot) \end{bmatrix} \end{aligned} \tag{5.11}$$

$$\begin{aligned} &= \frac{1}{2}|\tilde{\xi}_1|^{-1/2}\begin{bmatrix} -\frac{\lambda_1}{\varepsilon}\lceil\tilde{\xi}_1\rfloor^{1/2} + \tilde{\xi}_2 \\ -2\frac{\lambda_2}{2\varepsilon^2}\lceil\tilde{\xi}_1\rfloor^{1/2} + 2\dot{\Delta}(\cdot)|\tilde{\xi}_1|^{1/2} \end{bmatrix} \\ &= \frac{1}{2}|\tilde{\xi}_1|^{-1/2}\begin{bmatrix} -\frac{\lambda_1}{\varepsilon}\lceil\tilde{\xi}_1\rfloor^{1/2} + \tilde{\xi}_2 \\ -(\frac{\lambda_2}{\varepsilon^2}\lceil\tilde{\xi}_1\rfloor^{1/2} - \dot{\Delta}(\cdot)\mathrm{sgn}(\tilde{\xi}_1))\lceil\tilde{\xi}_1\rfloor^{1/2} \end{bmatrix} \end{aligned} \tag{5.12}$$

$$= |\tilde{\xi}_1|^{-1/2}\begin{bmatrix} \frac{2\lambda_1}{\varepsilon} & \frac{1}{2} \\ -(\frac{\lambda_2}{2\varepsilon^2} - \dot{\Delta}(\cdot)\mathrm{sgn}(\tilde{\xi}_1)) & 0 \end{bmatrix}\begin{bmatrix} \lceil\tilde{\xi}_1\rfloor^{1/2} \\ \tilde{\xi}_2 \end{bmatrix}.$$

As argued in [108], using the fact that $\sup\{\dot{\Delta}(.)\} = \mathcal{L}$, gives

$$\begin{aligned} &= |\tilde{\xi}_1|^{-1/2}\underbrace{\begin{bmatrix} \frac{2\lambda_1}{\varepsilon} & \frac{1}{2} \\ -(\frac{\lambda_2}{2\varepsilon^2} - \mathcal{L}) & 0 \end{bmatrix}}_{\mathbf{A}}\begin{bmatrix} \lceil\tilde{\xi}_1\rfloor^{1/2} \\ \tilde{\xi}_2 \end{bmatrix} \\ &= |\tilde{\xi}_1|^{1/2}\mathbf{A}\zeta. \end{aligned} \tag{5.13}$$

Thereby the first time derivative of V_0 can be written as,

$$\dot{V}_0 = |\tilde{\xi}_1|^{-1/2}\zeta^{\mathbf{T}}(\mathbf{A}^{\mathbf{T}}\mathbf{P} + \mathbf{P}\mathbf{A})\zeta = -|\tilde{\xi}_1|^{-1/2}\zeta^{\mathbf{T}}\mathbf{Q}\zeta < 0 \tag{5.14}$$

It can be noted that (5.14) above is satisfactory because the matrix $\mathbf{A}$ is Hurwitz and the matrix $\mathbf{P}$ is a positive definite symmetric matrix satisfying the Lyapunov criterion given by $\mathbf{A}^{\mathbf{T}}\mathbf{P} + \mathbf{P}\mathbf{A} = -\mathbf{Q}$ with $\mathbf{Q} > \mathbf{0}$. The matrix $\mathbf{A}$ is guaranteed to be Hurwitz if and only if the observer gain $\frac{\lambda_2}{2\varepsilon^2} > \sup(\dot{\Delta}(.)) = \mathcal{L}$ and $\frac{\lambda_1}{\varepsilon} > 0$. Using Rayleigh principle [41], $|\tilde{\xi}_1|^{1/2} \leq \lceil\tilde{\xi}_1\rfloor^{1/2} \leq \|\zeta\|_2 < \beta_{min}^{-1/2}(\mathbf{P})V_0^{1/2}$ and then $\dot{V}_0$ can

be rewritten as,

$$\dot{V}_0 \leq -|\tilde{\xi}_1|^{-1/2}\beta_{min}(\mathbf{Q})\|\zeta\|_2$$
$$\leq -\beta_{min}^{1/2}(\mathbf{P})V_0^{-1/2}\beta_{min}(\mathbf{Q})\|\zeta\|_2 \tag{5.15}$$
$$\leq -\frac{\beta_{min}^{1/2}(\mathbf{P})\beta_{min}(\mathbf{Q})}{\beta_{max}(\mathbf{P})}V_0^{1/2} \leq -\mathbf{\Gamma}V_0^{1/2} \tag{5.16}$$

where the term $\Gamma = \dfrac{\beta_{min}^{1/2}(\mathbf{P})\beta_{min}(\mathbf{Q})}{\beta_{max}(\mathbf{P})}$ is the observer gain parameter and $\beta_{max}(\cdot)$ and $\beta_{min}(\cdot)$ denote the maximum and minimum eigen values of a square matrix. Though the transformation ζ is continuous, it follows that ζ reduces to zero in finite time which means that the observer error variables $\tilde{\xi}_1$ and $\tilde{\xi}_2$ converge to the origin in finite time. Further, (5.16) can be solved to obtain an explicit expression describing the maximum finite time required for the estimation error to converge to the origin.

Let us consider, $V_0(t_0) = V_0(0)$, and the final convergence time T satisfying $V_0(T) = 0$ due to negative definiteness of $\dot{V}_0(t)$ and proceed as follows.

$$\dot{V}_0 + \Gamma V_0^{1/2} \leq 0$$
$$\Rightarrow \int_{V_0(0)}^{V_0(T)} \frac{dV_0}{V_0^{1/2}} \leq -\Gamma(T-0)$$
$$\Rightarrow 2(V_0(T)^{1/2} - V_0(0)^{1/2}) \leq -\Gamma T.$$

As $V_0(T) = 0$, it is substituted in the above inequality to get closed form expression for the convergence time T in terms of initial conditions and observer gains as defined below.

$$T \leq \frac{2V_0(0)^{1/2}}{\Gamma} \tag{5.17}$$

Therefore, (5.17) reflects that the relevant parameter influencing the finite time convergence is the bound on the convergence time given by T.

Using Theorem 2.1 given in [106], the observer error dynamics are inferred to be finite time stable from (5.16) . This completes the proof. □.

Next, to justify the exactness in the estimation of inductor current using the proposed current observer, the results have been summarized as Theorem 6.

Theorem 6. *The current observer given in* (5.9) *yields an exact estimation of the current provided that it is at least once continuously differentiable, i.e* $\sup\{\dot{\Delta}\}$ *exists. This means that at steady state, the exact ultimate bound on the observer error variables is given by* $\tilde{\xi}_1 = 0$ *and* $\tilde{\xi}_2 = 0$.

Proof: Following the procedure of finding the ultimate bounds presented in [109], the observer error dynamics described in (5.10) are now considered and using a specific diffeomorphism, error dynamics have to be transformed to a more suitable form to make the analysis convenient. Utilizing the diffeomorphism $[\psi_1,\ \psi_2]^T = [|\tilde{\xi}_1|^{\frac{1}{2}}\text{sgn}(\tilde{\xi}_1),\ \varepsilon\tilde{\xi}_2]^T$ and $\bar{D} = \frac{D}{\psi_1{}'(\tilde{\xi}_1)}$, where $D_i = \dot{\Delta}(\cdot)$, the transformed

dynamics are obtained as

$$\begin{bmatrix} \dot{\psi}_1 \\ \dot{\psi}_2 \end{bmatrix} = \frac{\psi'(\tilde{\xi}_1)}{\varepsilon}\left\{ \underbrace{\begin{bmatrix} -\lambda_1 & 1 \\ -\lambda_2 & 0 \end{bmatrix}}_{\mathbf{F}} \begin{bmatrix} \psi_1 \\ \psi_2 \end{bmatrix} + \varepsilon^2 \underbrace{\begin{bmatrix} 0 \\ 1 \end{bmatrix}}_{\mathbf{G}} \bar{D} \right\}. \tag{5.18}$$

Now let us consider the auxiliary dynamics as,

$$\begin{bmatrix} \dot{\psi}_1 \\ \dot{\psi}_2 \end{bmatrix} = \begin{bmatrix} -\lambda_1 & 1 \\ -\lambda_2 & 0 \end{bmatrix} \begin{bmatrix} \psi_1 \\ \psi_2 \end{bmatrix} + \varepsilon^2 \begin{bmatrix} 0 \\ 1 \end{bmatrix} \bar{D}. \tag{5.19}$$

As given in [110], it is understood that the dynamics described in (5.18) and (5.19) follow the same trajectories, in case $\frac{\psi_1'}{\varepsilon}$ is a positive definite function. Hence, analysis of current estimation error using the auxiliary dynamics in (5.19) is now carried out. Finally, the original estimation error can be obtained using (5.19). Next, using the concept of linear control theory and Lemma 1 mentioned in [109], the ultimate bound on the estimation error is derived as $|\psi_k| \leq \varepsilon^2 \{\mathcal{F}\}_k \|\bar{D}\|_\infty$, where,

$$\mathcal{F} = \begin{bmatrix} \mathcal{F}_1 \\ \mathcal{F}_2 \end{bmatrix} = \int_0^\infty |e^{\mathbf{F}\tau}\mathbf{G}| d\tau \tag{5.20}$$

Since $\|\bar{D}\|_\infty < K$ with the change of co-ordinates, the original estimation error can be obtained as

$$\left.\begin{array}{c} 2\varepsilon^2 |\tilde{\xi}_1|^{\frac{1}{2}} \mathcal{F}_1 K = |\tilde{\xi}_1|^{\frac{1}{2}} \mathrm{sgn}(\tilde{\xi}_1) \\ |\tilde{\xi}_1|^{\frac{1}{2}} (2\varepsilon^2 \mathcal{F}_1 K - 1) = 0 \end{array}\right\}. \tag{5.21}$$

By solving (5.21), it is found that if $\varepsilon^2 < \frac{1}{2}\mathcal{F}_1 K$, the estimation error $\tilde{\xi}_1$ exactly converges to zero. Similarly, the ultimate bound on the current estimation error $\tilde{\xi}_2$ can be found using the relation, $\tilde{\psi}_2 \leq 2\varepsilon^2 \mathcal{F}_2 K |\tilde{\xi}_1|^{\frac{1}{2}}$, implying $\tilde{\xi}_2 = 0$. Therefore, it is proved that the finite time current observer (5.9) achieves an exact estimation of the current state. □

5.3 Stability Analysis

Lyapunov stability criterion is studied for the closed loop signal boundedness of the overall converter system under the action of the proposed control. The result has been summarized in Theorem 7 as follows.

Theorem 7. *For the DC-DC buck converter* (5.3)-(5.2) *affected by different types of uncertainties, the control law in* (5.7) *achieves an asymptotic output voltage tracking. The closed loop trajectories reside finally within a small maximal set* $\mathscr{S}^*$ *in the vicinity of the origin and are ultimately bounded in the set* $\mathbb{S}$*, where* $\mathscr{S}^* \subseteq \mathbb{S}$ *and are defined as* $\mathscr{S}^* := \{\mathbf{z} \in \mathbb{R}^2 \mid \|\mathbf{z}\|_2 < (\|\dot{\tilde{\xi}}_2/C\|_\infty)/\min\{c_1, c_2\}\}$ *and* $\mathbb{S} := \{(z_1, z_2) \in \mathbb{R}^2 | \|\mathbf{z}\|_2^2 \leq \beta_{max}(\mathbf{M})(\|\tilde{\Theta}^T/C\|_\infty^2 + \|\dot{\tilde{\xi}}_2/C\|_\infty^2)\}$*, where* $\beta_{max}(\mathbf{M})$ *denotes the maximum eigen value of the user defined matrix* $\mathbf{M} \in \mathbb{R}^{2\times 2}$ *whose elements are given as* $a_{11} = 1/c_1^2, a_{12} = a_{21} = 1/c_1^2 c_2, a_{22} = (c_1^2+1)/c_1^2 c_2^2$ *and* $c_1, c_2 > 0$ *are the controller gains.*

Proof: The asymptotic stability of the error variables z_1 and z_2 defined in (5.4) are proved here. The proof is carried out in a systematic manner by considering a stepwise procedure as discussed

below.

The controller error dynamics of z_1 and z_2 in (5.4) can be rewritten by substituting the virtual control law α and the actual control input u from (5.5) and (5.7) respectively to yield,

$$\begin{bmatrix} \dot{z}_1 \\ \dot{z}_2 \end{bmatrix} = \underbrace{\begin{bmatrix} -c_1 & 1 \\ -1 & -c_2 \end{bmatrix}}_{\mathcal{A}} \begin{bmatrix} z_1 \\ z_2 \end{bmatrix} + \underbrace{\begin{bmatrix} -1 \\ \frac{\partial \alpha}{\partial x_1} \end{bmatrix}}_{\mathcal{B}_1} \frac{\tilde{\Theta}^T \Phi}{C} + \underbrace{\begin{bmatrix} 0 \\ 1 \end{bmatrix}}_{\mathcal{B}_2} \frac{\dot{\tilde{\xi}}_2}{C}. \tag{5.22}$$

Let us define $\mathbf{z} := [z_1 \ z_2]^T$ and consider a positive definite continuously differentiable Lyapunov function $V : \mathbb{R}^2 \times [0, \infty) \rightarrow \mathbb{R}_+$ defined as

$$V = \frac{1}{2}\mathbf{z^T}\mathcal{P}\mathbf{z} + \frac{1}{2\gamma}\tilde{\Theta}^T\tilde{\Theta} \tag{5.23}$$

where $\mathcal{P}$ is a positive definite symmetric matrix satisfying the Lyapunov criterion. Now, taking the time derivative of $V(\cdot)$ yields,

$$\begin{aligned} \dot{V}(z,t) &= \frac{1}{2}\mathbf{z^T}\mathcal{P}\mathcal{A} + \frac{1}{2}z^T\mathcal{P}\mathcal{B_1}\frac{\tilde{\Theta}^T\Phi}{C} + \frac{1}{2}\mathbf{z^T}\mathcal{P}\mathcal{B_2}\frac{\dot{\tilde{\xi}}_2}{C} + \frac{1}{2}\mathbf{z^T}\mathcal{A^T}\mathcal{P}\mathbf{z} + \frac{1}{2}\Big(\frac{\tilde{\Theta}^T\Phi}{C}\Big)^T\mathcal{B_2^T}\mathcal{P}\mathbf{z} - \frac{\tilde{\Theta}^T\dot{\tilde{\Theta}}}{\gamma} \\ &= \frac{1}{2}(\mathcal{P}\mathcal{A} + \mathcal{A^T}\mathcal{P})\mathbf{z} + \mathbf{z^T}\mathcal{P}\mathcal{B_1}\frac{\tilde{\Theta}^T\Phi}{C} + \mathbf{z^T}\mathcal{P}\mathcal{B_2}\frac{\dot{\tilde{\xi}}_2}{C} - \frac{\tilde{\Theta}^T\dot{\tilde{\Theta}}}{\gamma} \\ &\leq -\frac{1}{2}\mathbf{z^T}\mathcal{Q}\mathbf{z} + \|\mathcal{P}\mathcal{B_2}\|\|\dot{\tilde{\xi}}_2/C\| \ \|\mathbf{z}\| \end{aligned} \tag{5.24}$$

where $\mathcal{Q}$ is positive definite symmetric matrix. For $\dot{V}$ to be negative definite, $\|\mathbf{z}\|_2 > \frac{2}{\lambda_{min}(\mathbf{Q})}\Big\|\frac{\dot{\tilde{\xi}}_2}{C}\Big\|_\infty$ which implies that the trajectories firstly enter $\|\mathbf{z}\|_2 \leq \frac{2}{\lambda_{min}(\mathbf{Q})}\Big\|\frac{\dot{\tilde{\xi}}_2}{C}\Big\|_\infty$ and finally converge to the set very close to the origin given by $\|\mathbf{z}\|_2 < \frac{2\|\dot{\tilde{\xi}}_2\|_\infty}{\lambda_{min}(\mathbf{Q})C}$. However, the derived invariant set does not set the ultimate or actual bounds on the closed loop trajectories. Therefore, using Lemma 1 stated in [109], the actual bounds of z_1 and z_2 can be found. Formulating the tracking error dynamics as a linear time invariant uncertain system with bounded current estimation error derivative $\dot{\tilde{\xi}}_2$ and load estimation error as in (5.22), the bound can be found as, $|z_i| \leq \mathcal{F}_{i1}\|\tilde{\Theta}/C\|_\infty + \mathcal{F}_{i2}\|\dot{\tilde{\xi}}_2/C\|_\infty$, where $i = 1, 2$ and $j = 1, 2$. Further, $\mathcal{F}_{ij}$ can be evaluated as $\mathcal{F}_{ij} = \int_0^\infty \{e^{\mathcal{A}\tau}\mathcal{B}_j\}_i d\tau$, where $\mathcal{B_j}$ is the distribution matrix of the j^{th} perturbation. Further, the matrix $\mathcal{F}$ is calculated as

$$\mathcal{F} = \begin{bmatrix} \frac{1}{c_1} & \frac{1}{c_1 c_2} \\ 0 & \frac{1}{c_2} \end{bmatrix}. \tag{5.25}$$

Therefore, the actual bounds on the closed loop trajectories are found to be

$$\left.\begin{aligned} |z_1| \leq \tfrac{1}{c_1}\|\tilde{\Theta}^T/C\|_\infty + \tfrac{1}{c_1 c_2}\|\dot{\tilde{\xi}}_2/C\|_\infty \\ |z_2| \leq \tfrac{1}{c_2}\|\dot{\tilde{\xi}}_2/C\|_\infty \end{aligned}\right\}. \tag{5.26}$$

Hence, the actual bounding set in which the error variables z_1 and z_2 reside at steady state is given

by $\mathbb{S}$ defined as

$$\mathbb{S} := \{(z_1, z_2) \in \mathbb{R}^2 | \|\mathbf{z}\|_2^2 \leq \beta_{max}(\mathbf{M})(\|\tilde{\Theta}^T/C\|_\infty^2 + \|\dot{\tilde{\xi}}_2/C\|_\infty^2)\} \tag{5.27}$$

where $\beta_{max}(\mathbf{M})$ is the largest eigen value of the matrix $\mathbf{M}$ which is given by

$$\mathbf{M} = \begin{bmatrix} \frac{1}{c_1^2} & \frac{1}{c_1^2 c_2} \\ \frac{1}{c_1^2 c_2} & \frac{1+c_1^2}{c_1^2 c_2^2} \end{bmatrix}. \tag{5.28}$$

The schematic diagram of the proposed finite time current observer based adaptive backstepping control (FTCO-ABSC) scheme is shown in Figure 5.1.

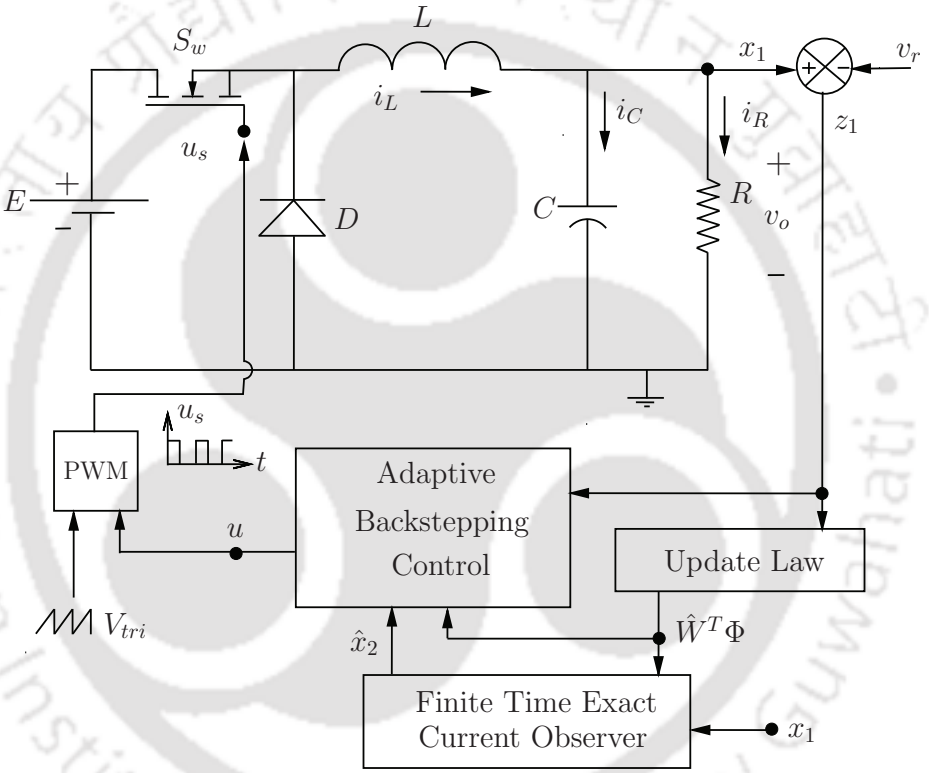

Figure 5.1: Schematic diagram of proposed FTCO-ABSC scheme for DC-DC buck converters

5.4 Experimental Results and Discussion

In order to investigate the performance of the proposed FTCO-ABSC scheme, a prototype of DC-DC buck converter as discussed in subsection 2.3.4 of Chapter 2, equipped with the closed loop control is made with following specification. Supply DC voltage $E = 25V$, filter inductor, $L = 59mH$, inductor resistance $r_L = 4.54\Omega$, capacitor $C = 220\mu F, 450V$ rating, nominal load resistance $R = 20\Omega$, reference output voltage $v_r = 10V$ and switching frequency $f_s = 20kHz$. Further the selected controller parameters are adaptive gain $\gamma = 9 \times 10^{-5}$, observer rate $\lambda_1 = 0.05$, $\lambda_2 = 0.5$, observer parameter

$\varepsilon = 0.05$ and backstepping gains $c_1 = 6000$, $c_2 = 20$. To investigate the performance and robustness, the proposed control scheme is applied to the DC-DC buck converter system under different test conditions as described below. The proposed FTCO-ABSC is also evaluated against conventional adaptive backstepping control (ABSC) procedure [91] under identical experimental conditions. The tests conducted are the following:

Test 1: Step change in reference voltage from $0 - 10V$

The transient performance of output voltage v_o and inductor current i_L in response to the reference voltage $v_r = 10V$ during start-up are evaluated in Figure 5.2. Figure 5.2 (a) demonstrates the responses of converter states under ABSC control. The output voltage takes $28ms$ to reach the desired reference, besides suffering from $2V$ peak-to-peak ripple voltage in the steady state. The corresponding response of i_L can be observed in Figure 5.2 (a). In the contrary, the proposed FTCO-ABSC in Figure 5.2 (b) provides a quick start-up within $15ms$ and a clean output voltage profile with negligible ripple. However, the inductor current shows a peak in initial phase while reaching the nominal current of $0.5A$. Also, it must be noted that the peak-to-peak ripple in the output v_o under the action of proposed FTCO-ABSC method is $0.3V$, in contrast to $0.7V$ ripple offered by ABSC scheme.

Test 2: Sudden change in input voltage E **from** $25V$ **to** $17V$ **and vice-versa**.

The effectiveness of the proposed control under a matched uncertainty is examined in this test. After the steady state is reached, the DC-DC buck converter is exposed to a sudden source voltage change scenario. The input voltage E is suddenly perturbed from the nominal $25V$ to $17V$ and vice-versa, amounting to 32% input voltage disturbance. The performances of v_o and i_L under ABSC in response to source voltage change are shown in Figure 5.2 (c). The result shows that during the input change from $25V$ to $17V$, the conventional ABSC yields a large undershoot of 50% and reaches $5V$ level. The time taken to reject input disturbance is observed to be $70ms$. Similarly, the change of input voltage from 17 V to nominal $25V$ produces a 50% overshoot with a settling time of $70ms$ while tracking the set $10V$ reference voltage. Corresponding inductor current exhibits high undershoot and overshoot. On the other hand, the performance of the proposed FTCO-ABSC strategy in 5.2 (d) is satisfactory and yields no undershoot and overshoot. Subsequently, the inductor current exhibits a cleaner profile.

Test 3: Sudden change in load resistance R **from** 20Ω **to** 10Ω **and vice-versa.**

The robustness of the proposed control is next investigated under widely varying load conditions. Figure 5.3 (a) and 5.3 (b) reveal the converter response for the loading test, under which R changes from 20Ω to 10Ω, amounting to 50% change. The ABSC method produces an undershoot of 45% in v_o and reaches the level of $5.5V$. In addition, the time recorded to reject such a mismatched uncertainty is noted to be $85ms$. Similarly, during the unloading test, R changes from 10Ω to 20Ω. The ABSC shows a high overshoot of $17V$, accounting to a 70% peak and convergence time of $90ms$. Interestingly, under the proposed FTCO-ABSC scheme, the output voltage demonstrates a robust and accurate immediate tracking of desired reference voltage. The response obtained in the proposed method is devoid of any overshoot and undershoot during both loading and unloading conditions. Subsequently, the inductor current response in also found to be satisfactory.

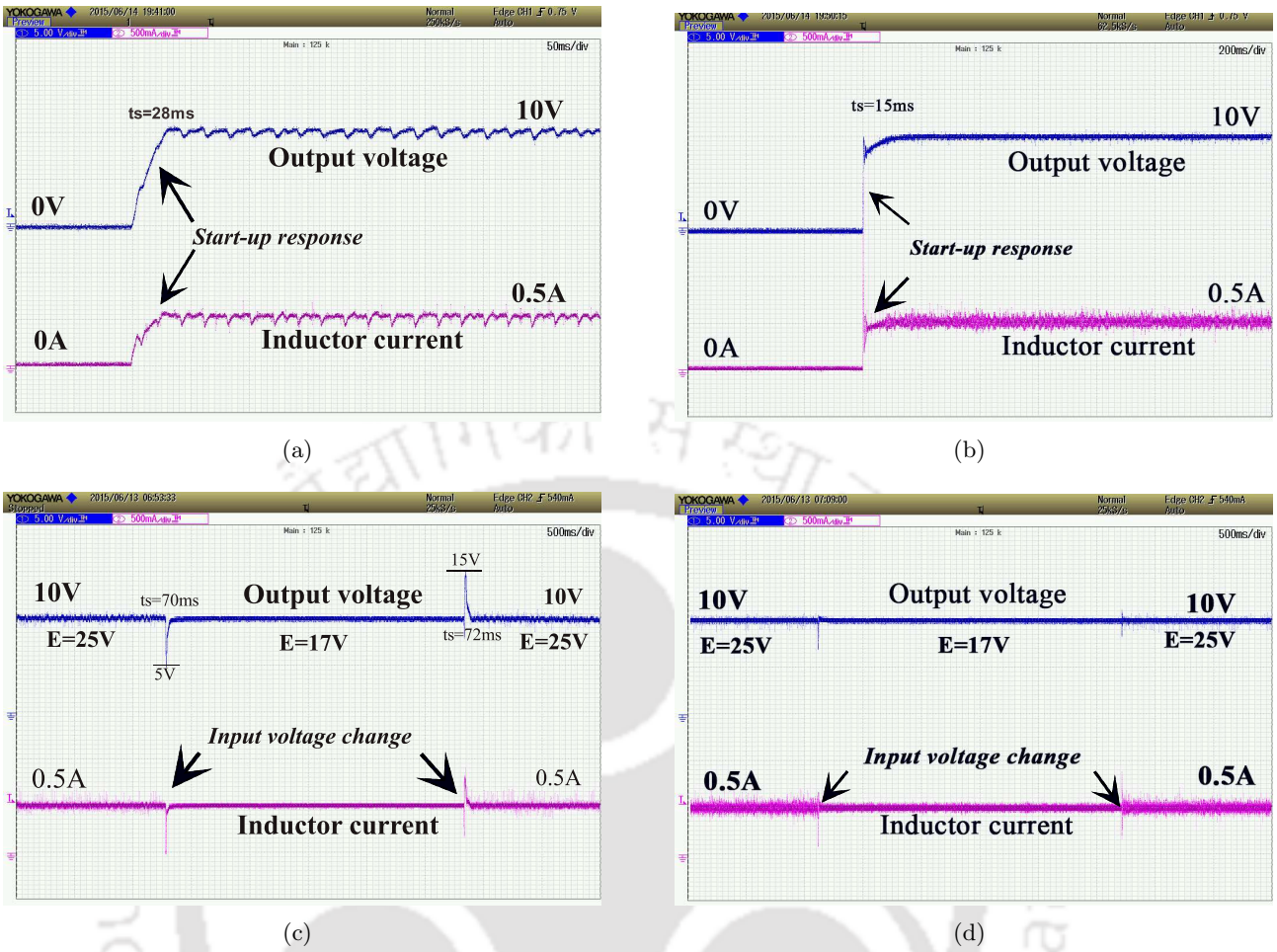

Figure 5.2: Experimental response curves of DC-DC buck converter: (a) ABSC: output voltage v_o and inductor current i_L during start up (scale: x-axis; time (50ms/div), y-axis; voltage (5V/div) and current (500mA/div)), (b) proposed FTCO-ABSC: output voltage v_o and inductor current i_L during start up (scale: x-axis; time (200ms/div), y-axis; voltage (5V/div) and current (500mA/div)), (c) ABSC: output voltage v_o and inductor current i_L during a step change in input voltage, E from $25V$ to $17V$ and vice-versa (scale: x-axis; time (500ms/div), y-axis; voltage (5V/div) and current (500mA/div)) and (d) proposed FTCO-ABSC: output voltage v_o and inductor current i_L during a step change in input voltage E from $25V$ to $17V$ and vice-versa (scale: x-axis; time (500ms/div), y-axis; voltage (5V/div) and current (500mA/div)).

Remark 12. *In Figure 5.2 (a), the output voltage profile under the operation of ABSC exhibits oscillations with peak to peak ripple of 0.85V across the desired 10V output. These oscillations may be due to sensor noise.*

Test 4: **Reference voltage change from** $10V - 15V$.

Lastly, to investigate the response speed of the proposed control algorithm, v_r is suddenly changed from nominal $10V$ to 15. The transient response obtained with ABSC mechanism is shown in Figure 5.3 (c). Initially the ABSC response is observed to be faster. However, it takes nearly $200ms$ time to converge to the new reference voltage of $15V$. On the contrary, the proposed control in Figure 5.3 (d) yields a rapid response of v_o in $5ms$. The inductor current dynamics show an overshoot during the trajectory change.

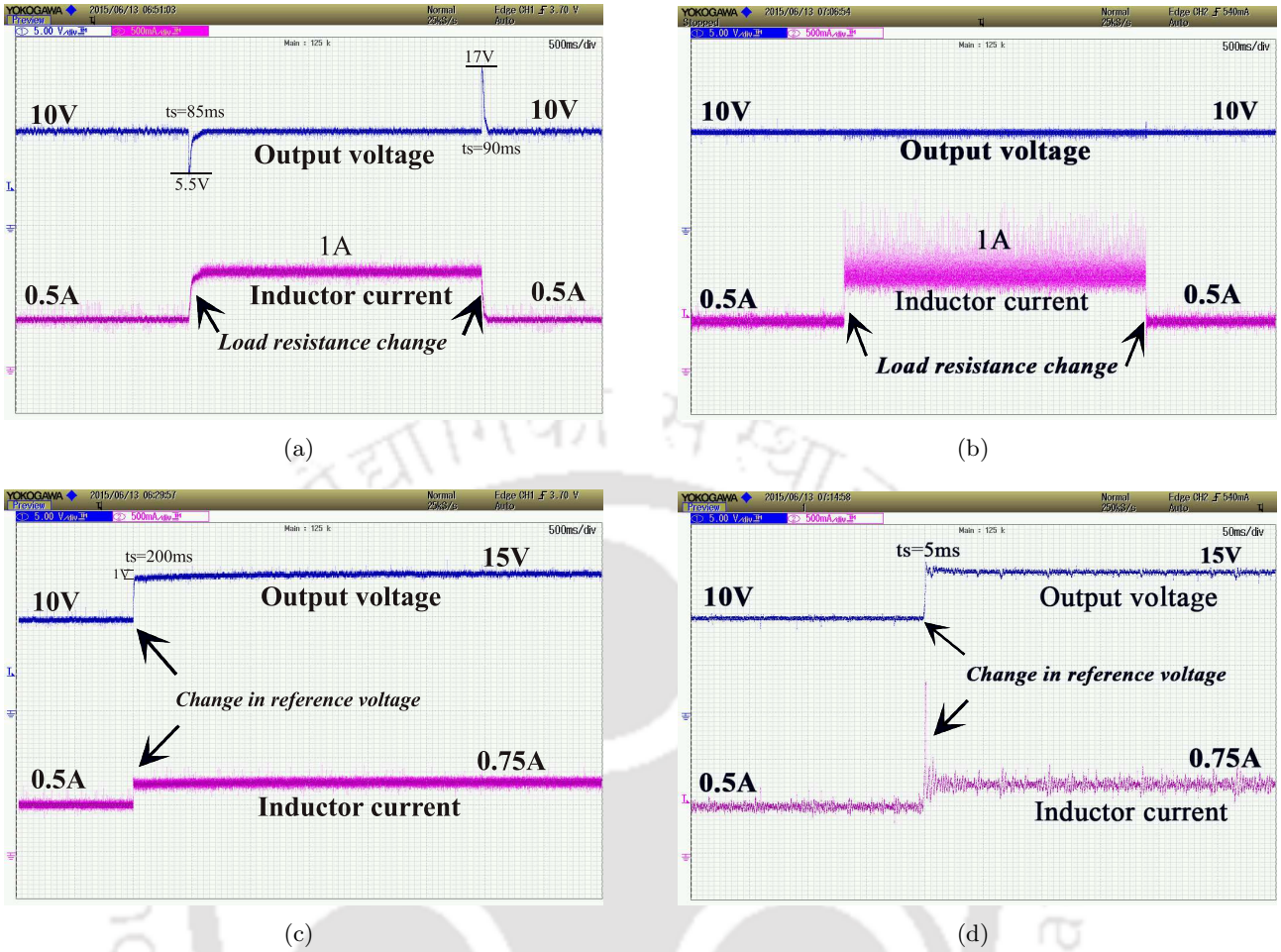

Figure 5.3: Experimental response curves of DC-DC buck converter: (a) ABSC: output voltage v_o and inductor current i_L during a step change in load resistance R from 20Ω to 10Ω and vice-versa (scale: x-axis; time (500ms/div), y-axis; voltage (5V/div) and current (500mA/div)), (b) proposed FTCO-ABSC: output voltage v_o and inductor current i_L during a step change in load resistance R from 20Ω to 10Ω and vice-versa (scale: x-axis; time (500ms/div), y-axis; voltage (5V/div) and current (500mA/div)), (c) ABSC: output voltage v_o and inductor current i_L during a step change in v_r from $10V$ to $15V$ (scale: x-axis; time (500ms/div), y-axis; voltage (5V/div) and current (500mA/div)) and (d) proposed FTCO-ABSC: output voltage v_o and inductor current i_L during a step change in v_r from $10V$ to $15V$ (scale: x-axis; time (50ms/div), y-axis; voltage (5V/div) and current (500mA/div)).

The experiments investigated have shown that the proposed FTCO-ABSC strategy is capable to provide a strict output voltage regulation for a wide range of perturbations under both matched and mismatched conditions. The spikes produced in the inductor current profile during reference voltage change are a result of dependency of error variables z_1 and z_2 on the derivative of current estimation error $\tilde{\xi}_2$ and the same may be tolerated by slight increase in the power handling capability of the converter.

5.5 Summary

A novel control methodology that enables a stable and robust trajectory tracking of the output voltage in DC-DC buck converters for widely varying source voltage and load resistance change is proposed in this work. The proposed control utilizes the adaptive backstepping procedure, besides observing the inductor current using a finite time observer. The finite time convergence of inductor current is validated mathematically. Stability analysis of the overall closed loop DC-DC buck converter system is established. Experimental investigation is conducted under widely varying input as well as load and reference voltage changes. The results are evaluated against the conventional adaptive backstepping control method. The results shown indicate that the proposed FTCO-ABSC scheme is successful in estimating the unknown current which promises potential for realizing a current sensorless controller.

6

Conclusions and Scope for Future Work

Contents

In this chapter, the conclusions drawn on the basis of the research work undertaken in this thesis are presented. Further, the scope for future research is also outlined.

6.1 Conclusions

The thesis is aimed towards the design, analysis and realization of a few backstepping based adaptive control strategies in the context of DC-DC buck converters. The primary focus throughout the thesis has been on the improvement of transient performance in DC-DC buck converters in the event of unknown and unanticipated uncertainties. Large changes in converter system parameters lead to unacceptable transients, eventually causing damage to the converter components, which is undesirable. Hence, in this thesis, a few adaptive control methodologies have been designed.
It is evident that the performance of modern controllers primarily depends on the accuracy of system model and exact parameter values. Nevertheless, correct knowledge of system parameters and exact system representation are very difficult in real time scenarios. Hence, adaptive control emerges as a powerful tool for controller design in uncertain systems. These controllers are capable of identifying the system accurately and in addition provide a superior transient performance compared to robust controllers in unanticipated adverse conditions. Therefore, in this thesis, online parameter estimation based backstepping control methodology is developed for DC-DC buck converters. An adaptive backstepping control (ABSC) method is firstly designed and developed for DC-DC buck converters. The varying load is estimated first for delivering the expected output response using the framework of backstepping control. The developed method is experimentally evaluated on DC-DC buck converter feeding an unknown resistive load and then applied to a PMDC-motor load under widely varying unknown load conditions. This method is found to be reasonably successful in achieving desired control objectives at wide range of operating points, however at the cost of slow start-up response and high peaks in the output state in the event of step disturbances in the load. In the next chapter, two neural network based online estimation methodologies are proposed for estimating the unknown load. Firstly, exploiting the orthogonal property of Chebyshev polynomials, a single functional layer Chebyshev neural network (CNN) integrated with ABSC is proposed. This method yields a much closer and faster approximation of the unknown load compared to conventional adaptive backstepping control. The proposed CNN-ABSC method is evaluated for the DC-DC buck converter system feeding both resistive and PMDC-motor loads. The obtained results confirm a superior performance of CNN-ABSC over conventional ABSC during transients. Moreover, it is also established that the proposed CNN-ABSC method outperforms the radial basis function neural network (RBFNN) based ABSC method by providing a faster estimation of load uncertainty. However, in the all three methods of ABSC, RBFNN-ABSC and proposed CNN-ABSC, not much improvement is observed in mitigating peak overshoot/undershoot during transients. A Hermite polynomial based neural network for online learning is explored next. Besides retaining the merits of orthogonality and accuracy of unknown function approximation, Hermite polynomials relax the restriction on the range on input signal. The proposed Hermite neural network (HNN) based ABSC is tested in both numerical and experimental platforms on DC-DC buck converters with resistive and PMDC-motor loads. The study reveals a significant improvement in the transient performance offered by HNN-ABSC in contrast to CNN-ABSC,

featuring much lesser peak overshoots during start-up and sudden load changes. In addition, it is also observed that the proposed HNN-ABSC yields an appreciable steady state response by reducing ripple in the output state.

Although the neural network based estimation strategies offer a reasonably closer estimation than the conventional ABSC method, yet the exactness in estimation cannot be guaranteed. The neural network based estimation techniques at the most result in a bounded estimation error or rather an asymptotic convergence of estimation error. Hence, a time bound exact estimation of uncertainties is highly essential to ensure a robust tracking performance. In this direction, a dual finite time exact disturbance observer based backstepping control method is proposed for DC-DC buck converters. Although the buck converter dynamics largely depend on the information of varying load, yet the accurate knowledge of other converter parameters like input voltage, inductor and capacitor values is necessary for good transient performance of the output state. The finite time exact estimation of lumped uncertainties and their subsequent compensation result in efficient tracking of output voltage under sudden and concurrent change in load and input uncertainties.

Finally, in the last chapter the control design problem of DC-DC buck converter is revisited from the perspective of developing a sensorless adaptive control scheme. A finite time current observer methodology is developed to dispense with the use of current sensors in real-time. The proposed current sensorless control scheme uses disturbance observer technique to yield a smooth and clean control signal. The results obtained confirm that under the action of the proposed control scheme, the output voltage response is improved under both start-up and load transients and yields no peak overshoot/undershoot during input and load disturbances. However, the inductor current exhibits peak overshoots under such an action.

Scope for Future Work

Future possible directions which are worthy to be explored are suggested below.

- Design and analysis of orthogonal polynomial based neuro-adaptive control for output voltage regulation in other types of DC-DC converters such as boost and buck-boost.
- Extension of finite time disturbance observer based backstepping control methodology in angular velocity tracking of DC-DC buck converter driven PMDC-motor.
- Extension of finite time disturbance observer based control methodology for boost and buck-boost converters.
- Further, a finite time current estimation based sensorless adaptive control technique can be explored for boost and buck-boost converters.

A

Appendix

Contents

A.1 A prelude to the finite time disturbance observer design philosophy

Prior to the disturbance observer design, it would be interesting to have a prologue, explaining how the finite time stability notions in dynamical systems translate to arriving at solutions to disturbance estimation problems. Herein, instead of a qualitative explanation, the philosophy behind the design of disturbance observer featuring finite time convergence is mathematically elucidated. Such a procedure happens to be intuitively appealing and ensures a lucid understanding of the underlying ideology.
Let us start with a fundamental problem of designing a control input u for a perturbed scalar integrating system given by,

$$\dot{x} = u + d, \tag{A.1.1}$$

where d represents the perturbation input and is at least $\mathcal{C}^1$, i.e, $\sup\{|d|\} = \ell_1,\ \sup\{|\dot{d}|\} = \ell_2$. The design of the control input u is aimed at achieving a finite time stable (FTS) origin. It is well known from the definition of FTS [106] that if $\exists$ a Lyapunov function $V(\cdot) : \mathbb{R} \setminus \{0\} \times \mathbb{R}_+ \to \mathbb{R}_+$ and the closed loop system satisfies the inequality $\dot{V} \leq -cV^{\mu}$, $0 < \mu < 1$, the system trajectory $x(t)$ converges to the origin in finite time. As a benchmark example illustrating FTS, let us consider the dynamics as given below,

$$\dot{x} = -k_1|x|^{\mu}\text{sign}(x) \tag{A.1.2}$$

which has a finite time stable origin and has the following solution:

$$x(t) = \begin{cases} f(t, x(t_0)) & \text{if } \ 0 \leq t \leq \frac{|x(t_0)|^{1-\mu}}{k_1(1-\mu)} \\ 0 & \text{if } \ t > \frac{|x(t_0)|^{1-\mu}}{k_1(1-\mu)} \end{cases} \tag{A.1.3}$$

where, $f(t, x(t_0)) = \text{sign}(x(t_0))(|x(t_0)|^{1-\mu} - tk_1(1-\mu))^{\frac{1}{1-\mu}}$. The FTS of $x(t) = 0$ is obvious from its solution in (A.1.3) and also from the fact that it satisfies the Lyapunov stability criterion for FTS with $V(x,t) = |x|$. Now, comparing the benchmark example (A.1.2) and the control design problem considered in (A.1.1), a simple observation reveals that both the systems have same trajectories $x(t)$ with $u(t) = -k_1|x|^{\mu}\text{sign}(x)$ and $d = 0$. On contrary, FTS of $x(t) = 0$ cannot be guaranteed by this choice of $u(t)$ when $d \neq 0$. Instead, an ultimately bounded solution $x(t)$ is reached which is upper bounded by the bound on d which can be reduced by increasing the gain k_1. Nevertheless, such a procedure of gain increment would achieve $x(t) = 0$ if and only if $k_1 \to \infty$, which is not viable and has other adverse implications on system solutions. As an alternative, with an aim to achieve $x(t) = 0$ without substantially increasing the proportional gain factor k_1, an integral term is introduced in the control law as,

$$u(t) = -k_1|x|^{\mu}\text{sign}(x) - k_2 \int_{t_0}^{t} \psi(x(\sigma))d\sigma. \tag{A.1.4}$$

At this point of discussion, the integrand function $\psi(x(\sigma))$ is not known. However, a suitable choice of $\psi(\cdot)$ is eventually arrived at through mathematical arguments to follow in the sequel. Such a choice of $\psi(\cdot)$ would not only reduce the ultimate bound of the solution trajectories $x(t)$ but also render $x(t) = 0$ in finite time.

The most immediate choice of the function $\psi(\cdot)$ would be $\psi = x(t)$. Now, the question arises as to whether $\psi = x(t)$ would yield FTS for $x(t) = 0$. Investigation of stability properties of the system (A.1.1) driven by the control input (A.1.4) with the immediate choice of ψ is necessary to arrive at any conclusion in this regard. Therefore, with the choice of $V = |x|$, and taking its first time derivative yields,

$$\begin{aligned}\dot{V} &\leq -k_1 V^{\mu} - k_2 \left(\int_{t_0}^{t} |x(\sigma)| d\sigma \right) + d\text{sign}(x) \\ &\leq -k_1 V^{\mu} - k_2 \left(\int_{t_0}^{t} V d\sigma \right) + d\text{sign}(x) \qquad \text{(A.1.5)} \\ &\leq -k_2 \left(\int_{t_0}^{t} V d\sigma \right) + d\text{sign}(x) \qquad \text{(A.1.6)}\end{aligned}$$

Differentiating again with respect to time yields

$$\ddot{V} \leq -k_2 V(t) + (|\dot{d}| + k_2 V(t_0)) \leq -k_2 V(t) + (\ell_2 + k_2 V(t_0)). \qquad \text{(A.1.7)}$$

The solution of this inequality is given by,

$$V(t) \leq \frac{\dot{V}(t_0)}{k_2} \sin(k_2 t) + V(t_0) \cos(k_2 t) + \frac{\ell_2 + k_2 V(t_0)}{k_2} \qquad \text{(A.1.8)}$$

The solution (A.1.8) reveals that $x(t)$ is ultimately bounded with the bounding set being a function of $\sup\{|\dot{d}|\}$. Though the convergence rate of signal $x(t)$ is enhanced, the signal $x(t)$ eventually oscillates around the ultimate bound instead of converging to the origin in finite time. Therefore, the first choice of $\psi = x(t)$ is not suitable for the intended control objective.

Hence, the next choice of $\psi(\cdot)$ is based on the following arguments which fortunately happen to satisfy the criteria for FTS for $x(t) = 0$ in the perturbed scalar integrator dynamics (A.1.4). The inequality for $\dot{V}$ is derived from the previous choice of the Lyapunov function as,

$$\begin{aligned}\dot{V} &\leq -k_1 V^{\mu} - k_2 \left(\int_{t_0}^{t} \psi(\sigma) d\sigma \right) + d\text{sign}(x) \\ &\leq -k_1 V^{\mu} - k_2 \left(\int_{t_0}^{t} \psi(\sigma) d\sigma \right) \text{sign}(x) + |d|. \qquad \text{(A.1.9)}\end{aligned}$$

To ensure negative definiteness of $\dot{V}$ in the immediate inequality derived above, the following condition should be satisfied,

$$|d| \leq k_2 \left(\int_{t_0}^{t} \psi(\sigma) d\sigma \right) \text{sign}(x). \qquad \text{(A.1.10)}$$

From the concepts of real analysis, the inequality in (A.1.10) holds true if and only if,

$$k_2 \psi(\sigma) \text{sign}(x) - |\dot{d}| \geq 0 \qquad \text{(A.1.11)}$$

The choice of $\psi(\cdot)$ in the above inequality (A.1.11) is analogous to the problem of reaching law design in the first order sliding mode control design. The gain in such a reaching law should be chosen greater than or equal to the upper bound of the matched uncertainty. Translating such concepts into the design of ψ in (A.1.11) ultimately leads to selection of $\psi = \text{sign}(x)$ resulting in the inequality

$(k_2 - \sup\{|\dot{d}|\}) \geq 0$. Expression for $\dot{V}$ with this choice of $\psi = \text{sign}(x)$ will now be revisited and the stability properties of the closed loop system (A.1.1) under the action of the control input (A.1.4) will be explored. It is very obvious by now that the second choice of $\psi(\cdot)$ satisfying the inequality $(k_2 - \sup\{|\dot{d}|\}) \geq 0$ yields,

$$\dot{V} + k_1 V^{\mu} \leq 0. \tag{A.1.12}$$

Hence, from (A.1.12), it is proved that the perturbed scalar system (A.1.1) has a finite time stable origin with the control input designed as $u(t) = -k_1|x|^{\mu}\text{sign}(x) - k_2 \int_{t_0}^{t} \text{sign}(x(\sigma))d\sigma$.
Now, this concept is exploited to solve disturbance estimation problem. Let us consider an auxiliary state variable $v(t) = k_2 \int_{t_0}^{t} \text{sign}(x(\sigma))d\sigma$. Therefore, the perturbed integrator dynamics (A.1.1) becomes,

$$\dot{x} = -k_1|x|^{\mu}\text{sign}(x) - v + d \tag{A.1.13}$$

In this case, the signal $x(t)$ will converge to the origin in finite time and so does $\dot{x}(t)$ with the following implication. Substituting $x(t) = \dot{x}(t) = 0$ in (A.1.13), results in $(-v + d) = 0 \Longrightarrow v = d$. Therefore, apart form achieving FTS for $x = 0$, the control law also provides us with an exact estimate of $d(t)$, denoted as $\hat{d}(t)$ where,

$$\hat{d}(t) = v(t) = k_2 \int_{t_0}^{t} \text{sign}(x(\sigma))d\sigma \tag{A.1.14}$$

where, $\hat{d}(t)$ denotes the estimate of the unknown disturbance estimated with the help of the auxiliary design variable $v(t)$. Thus, defining the disturbance estimation error as $\tilde{d}(t) = d(t) - v(t)$, ultimately leads to a FTS second order system given by,

$$\dot{x} = -k_1|x|^{\mu}\text{sign}(x) + \tilde{d} \tag{A.1.15}$$

$$\dot{\tilde{d}} = -k_2\text{sign}(k_1|x|^{\mu}\text{sign}(x)) + \dot{d}(t) \tag{A.1.16}$$

under the choice of $k_2 \geq \sup\{|\dot{d}(t)|\}$. Here, it is noted that the disturbance $d(t)$ is observed in finite time by the auxiliary variable $v(t)$ in consequence to the FTS of $x(t) = 0$ from any initial conditions. In other words, the disturbance $d(t)$ is estimated by utilizing the behaviorial information from the perturbed integrator (A.1.1), characterized by $x(t)$. Hence, the set of equations in (A.1.15)-(A.1.16) defines a disturbance observer with finite time convergence obtained by using the system information extracted from the signal $x(t)$. As a corollary, it can be well extended to the design of disturbance estimators using only observation error information. Defining $x(t)$ as the actual measurement while $\hat{x}$ being the observed value of $x(t)$, the observation error is denoted by $\tilde{x}(t) := x(t) - \hat{x}(t)$. Replacing $x(t)$ in (A.1.15) by $\tilde{x}(t)$ yields,

$$\dot{\tilde{x}} = -k_1|\tilde{x}|^{\mu}\text{sign}(\tilde{x}) + \tilde{d} \tag{A.1.17}$$

$$\dot{\tilde{d}} = -k_2\text{sign}(k_1|\tilde{x}|^{\mu}\text{sign}(\tilde{x})) + \dot{d}(t) \tag{A.1.18}$$

with the observation error $\tilde{x}$ and the disturbance estimation error $\tilde{d}$ obviously converging to zero in finite time. Therefore, using the observer error dynamics (A.1.17)-(A.1.18), it is very straightforward to construct an observer which would rapidly and exactly estimate the disturbance $d(t)$ in the perturbed

integrator dynamics (A.1.1). Finally, the disturbance observer for the dynamics (A.1.1) is designed as,

$$\dot{\hat{x}} = -k_1|x - \hat{x}|^{\mu}\text{sign}(x - \hat{x}) + \hat{d} + u \tag{A.1.19}$$

$$\dot{\hat{d}} = -k_2\text{sign}(k_1|x - \hat{x}|^{\mu}\text{sign}(x - \hat{x})). \tag{A.1.20}$$

The state $\hat{d}(t)$ in (A.1.19) gives the estimate of the disturbance $d(t)$ to be fed to the controller for subsequent compensation. The disturbance observer derived here is different from the conventional linear disturbance observers and nonlinear disturbance observers (NDO) [121]. The design procedure is an outcome of clear logical reasoning unified with relevant mathematical procedures and arguments lending simplicity compared to other conventional disturbance observers with wide applicability. Ultimately, the disturbance estimator designed in this section is named as "*finite time disturbance observer*" (FTDO) ascribed to finite time convergence of the disturbance estimation error.

References

[1] M. H. Rashid, *Power Electronics: Circuits, Devices and Applications*, 3^{rd} ed. Pearson Publications, 2003.

[2] Rong-Jong Wai, Wen-Hung Wang and Chung-You Lin, "High-Performance Stand-Alone Photovoltaic Generation System," *IEEE Transactions on Industrial Electronics*, vol. 55, no. 1, pp. 240–250, Jan 2008.

[3] Rong-Jong Wai and Rou-Yong Duan, "High-efficiency power conversion for low power fuel cell generation system," *IEEE Transactions on Power Electronics*, vol. 20, no. 4, pp. 847–856, July 2005.

[4] Jaw-Kuen Shiau, Der-Ming Ma, Pin-Ying Yang, Geng-Feng Wang and Jhij Hua Gong, "Design of a Solar Power Management System for an Experimental UAV," *IEEE Transactions on Aerospace and Electronic Systems*, vol. 45, no. 4, pp. 1350–1360, Oct 2009.

[5] H. C. Chang and C. M. Liaw, "An integrated driving/charging switched reluctance motor drive using three-phase power module," *IEEE Transactions on Industrial Electronics*, vol. 58, no. 5, pp. 1763–1775, 2011.

[6] Ned Mohan, Tore M. Undeland and William P. Robbins, *Power Electronics: Converters, Applications and Design*, 3rd ed. John Wiley and Sons, Inc, 2003.

[7] H. El Fadil, F. Giri, O. El Magueri and F. Z. Chaoui, "Control of DC-DC power converters in the presence of coil magnetic saturation," *Control Engineering Practice*, vol. 17, no. 7, pp. 849 – 862, 2009.

[8] A. G. Perry, G. Feng, Y. F. Liu and P. C. Sen, "A design method for PI-like fuzzy logic controllers for DC-DC converter," *IEEE Transactions on Industrial Electronics*, vol. 54, no. 5, pp. 2688–2696, Oct 2007.

[9] L. Guo, J. Y. Hung and R. M. Nelms, "Evaluation of dsp-based PID and fuzzy controllers for DC-DC converters," *IEEE Transactions on Industrial Electronics*, vol. 56, no. 6, pp. 2237–2248, June 2009.

[10] B. Johansson and M. Lenells, "Possibilities of obtaining small-signal models of DC-DC power converters by means of system identification," in *Twenty-Second International Telecommunications Energy Conference*, 2000, pp. 65–75.

[11] M. Shirazi, J. Morroni, A. Dolgov, R. Zane and D. Maksimovic, "Integration of frequency response measurement capabilities in digital controllers for DC-DC converters," *IEEE Transactions on Power Electronics*, vol. 23, no. 5, pp. 2524–2535, 2008.

[12] B. Miao, R. Zane and D. Maksimovic, "System identification of power converters with digital control through cross-correlation methods," *IEEE Transactions on Power Electronics*, vol. 20, no. 5, pp. 1093–1099, 2005.

[13] Z. Zhao and A. Prodi, "Limit-cycle oscillations based auto-tuning system for digitally controlled DC-DC power supplies," *IEEE Transactions on Power Electronics*, vol. 22, no. 6, pp. 2211–2222, 2007.

[14] M. M. Peretz and S. Ben-Yaakov, "Time domain identification of PWM converters for digital controllers design," in *IEEE Power Electronics Specialists Conference*, 2007, pp. 809–813.

[15] A. Barkley and E. Santi, "Improved online identification of a DC-DC converter and its control loop gain using cross-correlation methods," *IEEE Transactions on Power Electronics*, vol. 24, no. 8, pp. 2021–2031, 2009.

[16] T. Roinila, M. Vilkko and T. Suntio, "Fast loop gain measurement of a switched-mode converter using a binary signal with a specified fourier amplitude spectrum," *IEEE Transactions on Power Electronics*, vol. 24, no. 12, pp. 2746–2755, 2009.

[17] A. Simpkins, "System identification: Theory for the user," *IEEE Robotics Automation Magazine*, vol. 19, no. 2, pp. 95–96, June 2012.

[18] Y. F. Liu, E. Meyer and X. Liu, "Recent developments in digital control strategies for DC/DC switching power converters," *IEEE Transactions on Power Electronics*, vol. 24, no. 11, pp. 2567–2577, 2009.

[19] L. Corradini, P. Mattavelli, W. Stefanutti and S. Saggini, "Simplified model reference-based autotuning for digitally controlled SMPS," *IEEE Transactions on Power Electronics*, vol. 23, no. 4, pp. 1956–1963, 2008.

[20] B. Miao, R. Zane and D. Maksimovic, "Automated digital controller design for switching converters," in 36^{th} *IEEE Power Electronics Specialists Conference*, 2005, pp. 2729–2735.

[21] R. A. Fisher, M. A., "On the mathematical foundations of theoretical statistics," *Philosophical Transactions of the Royal Society of London A: Mathematical, Physical and Engineering Sciences*, vol. 222, no. 594–604, pp. 309–368, 1922.

[22] K. Astrom, "Maximum likelihood and prediction error method," *Automatica*, vol. 16, no. 5, pp. 551–574, Sept. 1980.

[23] S. F. Schmidt, "The kalman filter - its recognition and development for aerospace applications," *Journal of Guidance, Control and Dynamics*, vol. 4, no. 1, pp. 4–7, 1981.

[24] A. Prodic and D. Maksimovic, "Design of a digital PID regulator based on look-up tables for control of high-frequency DC-DC converters," in *IEEE Workshop on Computers in Power Electronics*, 2002, pp. 18–22.

[25] Dingxin Shuai, Yunxiang Xie and Xiaogang Wang, "Optimal control of Buck converter by state feedback linearization," in 7^{th} *World Congress on Intelligent Control and Automation WCICA*, June 2008, pp. 2265–2270.

[26] Sira-Ramirez H., "Nonlinear P-I controller design for switch mode DC-to-DC power converters," *IEEE Transactions on Circuits and Systems*, vol. 38, no. 4, pp. 410–417, Apr 1991.

[27] Shuai Ding-xin, "State feedback exact linearization control of Buck-Boost converter," in *International Power Electronics and Application Conference and Exposition (PEAC)*, Nov 2014, pp. 1490–1494.

[28] Y. Duan and H. Jin, "Digital controller design for switchmode power converters," in *Fourteenth Annual Applied Power Electronics Conference and Exposition*, vol. 2, 1999, pp. 967–973.

[29] K. Sundareswaran and V.T. Sreedevi, "Boost converter controller design using queen bee assisted ga," *IEEE Transcations on Industrial Electronics*, vol. 56 (3), pp. 778–783, 2009.

[30] K. Sundareswaran, V. Devi, S. Sankar, P. Srininivasa, R. Nayak and S. Peddapati, "Feedback controller design for a boost converter through evolutionary algorithms," *IET Power Electronics*, vol. 7, no. 4, pp. 903–913, April 2014.

[31] R. Severns, *Modern DC-DC Switchmode Power Converter Circuits*, 1st ed. Springer, Netherlands, 1985.

[32] R. J. Wai, Y. F. Lin, and Y. K. Liu, "Design of adaptive fuzzy-neural-network control for a single-stage boost inverter," *IEEE Transactions on Power Electronics*, vol. 30, no. 12, pp. 7282–7298, 2015.

[33] G. E. Pitel and P. T. Krein, "Real-time system identification for load monitoring and transient handling of DC-DC supplies," in *IEEE Power Electronics Specialists Conference*, 2008, pp. 3807–3813.

[34] K. M. Smedley and S. Cuk, "One-cycle control of switching converters," *IEEE Transactions on Power Electronics*, vol. 10, no. 6, pp. 625–633, Nov 1995.

[35] V. I. Utkin, "Variable structure systems with sliding modes," *IEEE Transactions on Automatic Control*, vol. 22, no. 2, pp. 212–222, 1977.

[36] Vadim Utkin, "Sliding mode control of DC/DC converters," *Journal of the Franklin Institute*, vol. 350, no. 8, pp. 2146 – 2165, 2013.

[37] H. Y. Yih and C. W. Chun, "Optimal variable-structure controller for DC motor speed control," *IET Control Theory and Applications*, vol. 131, no. 6, pp. 233–237, November 1984.

[38] B. Rashidi, M. Esmaeilpour, and M. R. Homaeinezhad, "Precise angular speed control of permanent magnet DC motors in presence of high modeling uncertainties via sliding mode observer-based model reference adaptive algorithm," *Mechatronics*, vol. 28, pp. 79–95, 2015.

[39] R. Sepulchre, M. Jankovic and P.V. Kokotovic, *Constructive Nonlinear Control*. Springer-Verlag London, 1997.

[40] K. Ezal, Z. Pan, and P. V. Kokotovic, "Locally optimal and robust backstepping design," *IEEE Transactions on Automatic Control*, vol. 45, no. 2, pp. 260–271, Feb 2000.

[41] H. K. Khalil, *Nonlinear systems*, Third, Ed. Upper Saddle River, (N.J.): Prentice Hall, 1996.

[42] Kokotovic P.V., "The joy of feedback: nonlinear and adaptive," *IEEE Control Systems*, vol. 12, no. 3, pp. 7–17, June 1992.

[43] "Front matter," in *Neural Systems for Control*, O. Omidvar and D. L. Elliott, Eds. San Diego: Academic Press, 1997, pp. i – iii. [Online]. Available: http://www.sciencedirect.com/science/article/pii/B9780125264303500155

[44] Bor-Ren Lin, "Power converter control based on neural and fuzzy methods," *Electric Power Systems Research*, vol. 35, no. 3, pp. 193 – 206, 1995.

[45] Cetin Elmas, Omer Deperlioglu and Hasan Huseyin Sayan, "Adaptive fuzzy logic controller for DC-DC converters," *Expert Systems with Applications*, vol. 36, no. 2, pp. 1540 – 1548, 2009.

[46] J. Linares Flores, J. Reger, and H. Sira Ramirez, "Load torque estimation and passivity-based control of a boost-converter/DC-motor combination," *IEEE Transactions on Control Systems Technology*, vol. 18, no. 6, pp. 1398–1405, Nov 2010.

[47] R. Silva Ortigoza, V. Hernandez Guzman, M. Antonio Cruz, and D. Munoz Carrillo, "DC-DC buck power converter as a smooth starter for a DC motor based on a hierarchical control," *IEEE Transactions on Power Electronics*, vol. 30, no. 2, pp. 1076–1084, Feb 2015.

[48] M. Tumari, M. Saealal, M. Ghazali, and Y. Wahab, "H-infinity with pole placement constraint in LMI region for a buck-converter driven DC motor," in *Proc. IEEE International Conference on Power and Energy (PECon)*, Dec 2012, pp. 530–535.

[49] H. Sira Ramirez and M. Oliver Salazar, "On the robust control of buck-converter DC-motor combinations," *IEEE Transactions on Power Electronics*, vol. 28, no. 8, pp. 3912–3922, Aug 2013.

[50] S. Abe, T. Ninomiya, J. Yamamoto and T. Uematsu, "Transient response comparison of voltage mode and current mode control on output-inductorless two-stage DC-DC converter," in 30^{th} *Annual Conference of IEEE Industrial Electronics Society, IECON*, vol. 1, 2004, pp. 308–312.

[51] R. D. Middlebrook, "Topics in multiple-loop regulators and current-mode programming," in *IEEE Power Electronics Specialists Conference*, 1985, pp. 716–732.

[52] M. Krstić, I. Kanellakopoulos, and P. Kokotović, *Nonlinear and adaptive control design*, ser. Adaptive and learning systems for signal processing, communications, and control. Wiley, 1995.

[53] W. Sun, H. Gao, and O. Kaynak, "Adaptive backstepping control for active suspension systems with hard constraints," *IEEE/ASME Transactions on Mechatronics*, vol. 18, no. 3, pp. 1072–1079, June 2013.

[54] F. J. Lin, L. T. Teng, and P. H. Shieh, "Intelligent adaptive backstepping control system for magnetic levitation apparatus," *IEEE Transactions on Magnetics*, vol. 43, no. 5, pp. 2009–2018, May 2007.

[55] J. Zhou, C. Wen, and Y. Zhang, "Adaptive backstepping control of a class of uncertain nonlinear systems with unknown backlash-like hysteresis," *IEEE Transactions on Automatic Control*, vol. 49, no. 10, pp. 1751–1759, Oct 2004.

[56] Y. Zhang, C. Wen, and Y. C. Soh, "Adaptive backstepping control design for systems with unknown high-frequency gain," *IEEE Transactions on Automatic Control*, vol. 45, no. 12, pp. 2350–2354, Dec 2000.

[57] Salimi M., Soltani J. and Markadeh G.A., "A novel method on adaptive backstepping control of buck choppers," in *Proceedings of* 2^{nd} *Power Electronics, Drive Systems and Technologies Conference (PEDSTC)*, Feb 2011, pp. 562–567.

[58] McIntyre M.L., Schoen M. and Latham J., "Simplified adaptive backstepping control of buck DC-DC converter with unknown load," in 14^{th} *IEEE Workshop on Control and Modeling for Power Electronics (COMPEL)*, June 2013, pp. 1–7.

[59] Fan Liping, Yu Yazhou, Boshnakov K., "Adaptive backstepping based terminal sliding mode control for DC-DC convertor," in *Proc. International Conference on Computer Application and System Modeling (ICCASM)*, vol. 9, Oct 2010, pp. 323–327.

[60] Li-kui Yi, Jun Zhao and Dan Ma, "Adaptive Backstepping Sliding Mode Nonlinear Control for Buck DC/DC Switched Power Converter," in *IEEE International Conference on Control and Automation*, May 2007, pp. 1198–1201.

[61] Wei Zhou, Xudong Ye, "Adaptive control of parallel DC-DC buck converters with uncertain parameters," in 12^{th} *International Conference on Control Automation Robotics Vision (ICARCV)*, Dec 2012, pp. 737–740.

[62] El Fadil H., Giri F., Haloua M., Ouadi H., "Nonlinear and adaptive control of buck power converters," in *Proc.* 42^{nd} *IEEE Conference on Decision and Control*, vol. 5, Dec 2003, pp. 4475–4480.

[63] Zhou Wei, Liu Bao-bin, "Analysis and design of DC-DC buck converter with nonlinear adaptive control," in 7^{th} *International Conference on Computer Science Education (ICCSE)*, July 2012, pp. 1036–1038.

[64] Sira-Ramirez H., Rios-Bolivar M., Zinober A.S.I., "Adaptive input-output linearization for PWM regulation of DC-to-DC power converters," in *Proceedings of American Control Conference*, vol. 1, June 1995, pp. 81–85.

[65] J. Zhou and C. Wen, *Adaptive Backstepping Control of Uncertain Systems: Nonsmooth Nonlinearities, Interactions or Time-Variations*, ser. Lecture Notes in Control and Information Sciences. Springer Berlin Heidelberg, 2008.

[66] P. Kokotović, *Foundations of adaptive control*, ser. Lecture notes in control and information sciences. Springer-Verlag, 1991.

[67] G. Tao, *Adaptive Control Design and Analysis*, ser. Adaptive and Cognitive Dynamic Systems: Signal Processing, Learning, Communications and Control. Wiley, 2003.

[68] L. Behera and I. Kar, *Intelligent Systems and Control: Principles and Applications*. OUP India, 2009.

[69] Laxmidhar Behera, Indrani Kar, *Intelligent Control Systems: Principles and Applications*. Oxford University Press, 2009.

[70] Hebertt Sira-Ramrez and Ramn Silva-Ortigoza, *Control Design Techniques in Power Electronics Devices*. Springer, 2006.

[71] R. Ling, D. Maksimovic, and R. Leyva, "Second-order sliding-mode controlled synchronous buck DC-DC converter," *IEEE Transactions on Power Electronics*, vol. 31, no. 3, pp. 2539–2549, March 2016.

[72] H. Komurcugil, "Adaptive terminal sliding-mode control strategy for DC-DC buck converters," *ISA Transactions*, vol. 51, no. 6, pp. 673 – 681, 2012.

[73] M. A. Ahmed, R. M. T. R. Ismail, and M. S. Ramli, "Control strategies of buck converter driven DC motor: A comparative assessment," *Australian Journal of Basic and Applied Sciences*, vol. 4, no. 10, pp. 4893–4903, 2010.

[74] "Pre- and post-filtering approach to sensorless VSS speed control of a permanent magnet DC motor subject to hammerstein and wiener nonlinearities," *Control Engineering Practice*, vol. 21, no. 11, pp. 1577 – 1583, 2013.

[75] B. Rashidi, M. Esmaeilpour, and M. R. Homaeinezhad, "Precise angular speed control of permanent magnet DC motors in presence of high modeling uncertainties via sliding mode observer-based model reference adaptive algorithm," *Mechatronics*, vol. 28, pp. 79 – 95, 2015.

[76] J. Linares-Flores and H. Sira-Ramirez, "DC motor velocity control through a DC-to-DC power converter," in *Decision and Control, 2004. CDC. 43rd IEEE Conference on*, vol. 5, Dec 2004, pp. 5297–5302 Vol.5.

[77] A. M. Zaki, M. El-Bardini, F. Soliman, and M. M. Sharaf, "Embedded two level direct adaptive fuzzy controller for DC motor speed control," *Ain Shams Engineering Journal*, 2015.

[78] R. Raja Ismail, M. Ahmad, and M. Ramli, "Speed control of buck-converter driven DC motor using LQR and PI: A comparative assessment," in *Proc. International Conference on Information Management and Engineering*, April 2009.

[79] T. Orlowska Kowalska and K. Szabat, "Optimization of fuzzy-logic speed controller for DC drive system with elastic joints," *IEEE Transactions on Industry Applications*, vol. 40, no. 4, pp. 1138–1144, July 2004.

[80] Chun-Fei Hsu, "Intelligent total sliding-mode control with dead-zone parameter modification for a DC motor driver," *IET Control Theory Applications*, vol. 8, no. 11, pp. 916–926, July 2014.

[81] Y. Tipsuwan and S. Aiemchareon, "A neuro-fuzzy network-based controller for DC motor speed control," in *31st Annual Conference of IEEE on Industrial Electronics Society, IECON.*, Nov 2005, pp. 2433–2438.

[82] R. J. Wai and R. Muthusamy, "Design of fuzzy-neural-network-inherited backstepping control for robot manipulator including actuator dynamics," *IEEE Transactions on Fuzzy Systems*, vol. 22, no. 4, pp. 709–722, Aug 2014.

[83] R. Sureshkumar and S. Ganeshkumar, "Comparative study of Proportional Integral and Backstepping controller for Buck converter," in *Proceedings of IEEE International Conference on Emerging Trends in Electrical and Computer Technology*, 2011, pp. 375–379.

[84] H. El Fadil and F. Giri, "Accounting of DC-DC power converter dynamics in DC motor velocity adaptive control," in *Proc. IEEE International Conference on Control Applications*, Oct 2006, pp. 3157–3162.

[85] C. Lanping, M. Zhenghua, and D. Soulin, "Adaptive speed controller design based on backstepping for DC motor system with parameter uncertainties," in *Proc. IEEE International Conference on Intelligent Computing*, vol. 2, Nov 2009, pp. 140–144.

[86] S. S. Ge, C. C. Hang, T. H. Lee, and T. Zhang, *Stable Adaptive Neural Network Control*, 1st ed. Springer Publishing Company, Incorporated, 2010.

[87] J.C. Mason, David C. Handscomb, *Chebyshev Polynomials*. Florida: Chapman & Hall, CRC Press, 2003.

[88] H. Brezis, *Functional Analysis, Sobolev Spaces and Partial Differential Equations*. Springer-Verlag New York, 2011.

[89] Koornwinder, Tom H.; Wong, Roderick S. C.; Koekoek, Roelof; Swarttouw, Ren F. , *Orthogonal Polynomials*, ser. NIST Handbook of Mathematical Functions. Cambridge University Press, 2010.

[90] M. Fedoryuk, *Hermite functions*, ser. Encyclopedia of Mathematics. Springer, 2001.

[91] T. K. Nizami and C. Mahanta, "An intelligent adaptive control of DC-DC buck converters," *Journal of the Franklin Institute*, vol. 353, no. 12, pp. 2588 – 2613, 2016.

[92] A. Chakravarty and C. Mahanta, "Actuator fault-tolerant control (FTC) design with post-fault transient improvement for application to aircraft control," *International Journal of Robust and Nonlinear Control*, 2015.

[93] A. Zolotas, "Disturbance observer based control: Methods and applications," *IEEE Control Systems*, vol. 35, no. 3, pp. 55–57, June 2015.

[94] L. Xiaoquan, L. Heyun, and H. Junlin, "Load disturbance observer-based control method for sensorless PMSM drive," *IET Electric Power Applications*, vol. 10, no. 8, pp. 735–743, 2016.

[95] W. H. Chen, J. Yang, L. Guo, and S. Li, "Disturbance observer based control and related methods: An overview," *IEEE Transactions on Industrial Electronics*, vol. 63, no. 2, pp. 1083–1095, Feb 2016.

[96] W.-H. Chen, "Disturbance observer based control for nonlinear systems," *IEEE/ASME Transactions on Mechatronics*, vol. 9, no. 4, pp. 706–710, Dec 2004.

[97] B.-Z. Guo and Z. liang Zhao, "On the convergence of an extended state observer for nonlinear systems with uncertainty," *Systems & Control Letters*, vol. 60, no. 6, pp. 420–430, 2011.

[98] J. Han, "From PID to active disturbance rejection control," *IEEE Transactions on Industrial Electronics*, vol. 56, no. 3, pp. 900–906, March 2009.

[99] Zhi-Liang Zhao and Bao-Zhu Guo, "On convergence of nonlinear active disturbance rejection control for MIMO systems," in *31st Chinese Control Conference*, July 2012, pp. 434–441.

[100] L. Guo and W.-H. Chen, "Disturbance attenuation and rejection for systems with nonlinearity via DOBC approach," *International Journal of Robust and Nonlinear Control*, vol. 15, no. 3, pp. 109–125, 2005.

[101] J. Wang, S. Li, J. Yang, B. Wu, and Q. Li, "Extended state observer-based sliding mode control for pwm-based DC-DC buck power converter systems with mismatched disturbances," *IET Control Theory Applications*, vol. 9, no. 4, pp. 579–586, 2015.

[102] H. Komurcugil, "Non-singular terminal sliding-mode control of DC-DC buck converters," *Control Engineering Practice*, vol. 21, no. 3, pp. 321 – 332, 2013.

[103] V. Utkin, "Sliding mode control of DC/DC converters," *Journal of the Franklin Institute*, vol. 350, no. 8, pp. 2146 – 2165, 2013.

[104] Indrani Kar, Laxmidhar Behera, "Direct adaptive neural control for affine nonlinear systems ," *Applied Soft Computing*, vol. 9, no. 2, pp. 756 – 764, March 2009.

[105] I. Yuri B. Shtessel and Arie Levant, "Smooth second-order sliding modes: Missile guidance application," *Automatica*, vol. 43, no. 8, pp. 1470 – 1476, 2007.

[106] S. P. Bhat and D. S. Bernstein, "Geometric homogeneity with applications to finite-time stability," *Mathematics of Control, Signals and Systems*, vol. 17, no. 2, pp. 101–127, 2005.

[107] T. R. Oliveira, A. Estrada, and L. M. Fridman, "Global and exact HOSM differentiator with dynamic gains for output-feedback sliding mode control," *Automatica*, vol. 81, no. 7, pp. 156 – 163, 2017.

[108] J. A. Moreno and M. Osorio, "Strict lyapunov functions for the super-twisting algorithm," *IEEE Transactions on Automatic Control*, vol. 57, no. 4, pp. 1035–1040, April 2012.

[109] L. K. Vasiljevic and H. K. Khalil, "Error bounds in differentiation of noisy signals by high-gain observers," *Systems & Control Letters*, vol. 57, no. 10, pp. 856 – 862, 2008.

[110] A.F. Filippov, *Differential equations with discontinuous righthand sides*, 1st ed., ser. Mathematics and its Applications, F.M. Arscott, Ed. Springer Netherlands, 1998, vol. 18.

[111] W. Wang and C. Wen, "Adaptive actuator failure compensation control of uncertain nonlinear systems with guaranteed transient performance," *Automatica*, vol. 46, no. 12, pp. 2082 – 2091, 2010.

[112] J. J. Chen, Y. S. Hwang, J. H. Yu, Y. T. Ku, and C. C. Yu, "A low-EMI buck converter suitable for wireless sensor networks with spur-reduction techniques," *IEEE Sensors Journal*, vol. 16, no. 8, pp. 2588–2597, 2016.

[113] M. P. Chan and P. K. T. Mok, "Design and implementation of fully integrated digitally controlled current-mode buck converter," *IEEE Transactions on Circuits and Systems I: Regular Papers*, vol. 58, no. 8, pp. 1980–1991, Aug 2011.

[114] Silva Ortigoza R., Hernandez Guzman V.M., Antonio Cruz M. and Munoz Carrillo D., "DC/DC buck power converter as a smooth starter for a DC motor based on a hierarchical control," *IEEE Transactions on Power Electronics*, vol. 30, no. 2, pp. 1076–1084, Feb 2015.

[115] R. Saadi, M. Bahri, M.Y. Ayad, M. Becherif, O. Kraa and A. Aboubou, "Dual loop control of fuel cell source using non-isolated IBC-IDDB converter for hybrid vehicle applications," *Energy Procedia*, vol. 50, pp. 155 – 162, 2014.

[116] Midya, P., Krein, P.T. and Greuel, M.F., "Sensorless current mode control-an observer-based technique for DC-DC converters," *IEEE Transactions on Power Electronics*, vol. 16, no. 4, pp. 522–526, Jul 2001.

[117] P. Mattavelli, "Digital control of DC-DC boost converters with inductor current estimation," in *IEEE Conference on Applied Power Electronics Conference and Exposition*, vol. 1, 2004, pp. 74–80 Vol.1.

[118] Beccuti, A.G., Mariethoz, S., Cliquennois, S., Shu Wang and Morari, M., "Explicit model predictive control of DC-DC switched-mode power supplies with extended kalman filtering," *IEEE Transactions on Industrial Electronics*, vol. 56, no. 6, pp. 1864–1874, June 2009.

[119] Ying Qiu, Liu, H. and Xiyou Chen, "Digital average current-mode control of PWM DC-DC converters without current sensors," *IEEE Transactions on Industrial Electronics*, vol. 57, no. 5, pp. 1670–1677, May 2010.

[120] Chuanlin Zhang, Junxiao Wang, Shihua Li, Bin Wu and Chunjiang Qian, "Robust control for pwm-based DC-DC buck power converters with uncertainty via sampled-data output feedback," *IEEE Transactions on Power Electronics*, vol. 30, no. 1, pp. 504–515, Jan 2015.

[121] M. Chen, G. Tao, and B. Jiang, "Dynamic surface control using neural networks for a class of uncertain nonlinear systems with input saturation," *IEEE Transactions on Neural Networks and Learning Systems*, vol. 26, no. 9, pp. 2086–2097, Sept 2015.